UNIVERSITAT POLITÈCNICA DE CATALUNYA BARCELONATECH

Automatic hands-free visualization of a six degrees of freedom agent within a complex anatomical space

Martina Finocchiaro

Marie Skłodowska-Curie European Joint Doctorate School
Doctoral thesis in Biomedical Engineering

Automatic hands-free visualization of a six degrees of freedom agent within a complex anatomical space

Author: Martina Finocchiaro

Supervisors Universitat Politècnica de Catalunya:
Prof. Alicia Casals & Dr. Albert Hernansanz

Supervisors Scuola Superiore Sant'Anna:
Prof. Arianna Menciassi & Prof. Gastone Ciuti

Automatic Control Department
Universitat Politècnica de Catalunya
Barcelona, Spain

The BioRobotics Institute
Scuola Superiore Sant'Anna
Pontedera, Italy

Automatic Control Department
Universitat Politècnica de Catalunya
C/ Jordi Girona 1-3
UPC-Campus Nord
Building Omega
08034 Barcelona, Spain

The BioRobotics Institute
Scuola Superiore Sant'Anna
Viale Rinaldo Piaggio 34
56025 Pontedera, Italy

ATLAS Marie-Curie Training Network,
GA No 813782

Summary

Over the years, a continuous development of intraluminal procedures resulted in strong benefits for the patients. Reduced blood loss, lower risk of infections, diminished scaring impact and quicker recovery time are among the most valuable ones. However, these improvements imposed high mental and physical stress to the clinicians. In this context, the introduction of robotic technologies has resulted in notable improvements in terms of flexibility of the endoscopes and control stability, by designing multi-steerable snake like robots and endoscopic capsules. Robotic devices also introduced additional Degrees Of Freedom (DOF) to control, as well as sensing information to process, posing the basis for a new framework of human-robot interaction.

Therefore, in the context of intraluminal robotic surgery, the present research focuses on the human-robot interaction, aiming at investigating the optimal way to design Human Machine Interface (HMI) with multiple levels of assistance. Accordingly, a modular bio-engineering framework was designed and developed for the analysis, evaluation and comparison of different HMI for robot assisted endoluminal procedure (*i.e.*, colonoscopy). The main component of the framework is a virtual simulator of the robotic colonoscopy procedure, developed using the Simulation Open Framework Architecture (SOFA). The simulator, endowed with 3D models of colons reconstructed from real patients' Computerized Tomography (CT) scans, realistically reproduces the anatomy and its performance during the robotic medical procedure in terms of timings, visual rendering and mechanical behaviour. Its open design allows to measure several metrics correlated with the quality of the procedure (*e.g.*, force exerted on the intestinal walls, timings etc.) and of control (*e.g.,* smoothness of trajectory). Therefore, the different HMI can be used to control the robotic endoscope in the virtual simulator and tested with user studies involving the endoscopists. This framework also comprises the use of wearable sensors to measure the cognitive load of the users through physiological data when testing the HMI in the simulation environment. Finally, a set of questionnaires were designed to be filled by the subjects after the tests for measuring their perceived physical and mental stress, and their overall impression on the interfaces. The framework was tested for the first time by 42 clinicians with the goal of deriving the optimal device for tele-operated control of robotic colonoscopes. To this end, a preliminary survey was driven among 71 endoscopists to derive the main characteristics and configuration of the control device desired by the final users. Accordingly, two selected systems were compared with the framework:

an haptic serial-kinematic device and a standard videogame joypad.

This users' test represented a first case study for the validation of the framework allowing to compare different HMI and derive their optimal features. Nevertheless, being the framework highly modular and open, is meant to be applied for the testing of different aspects of the HMI, both software and hardware *e.g.*, types of feedback, control strategies *etc.* Indeed, the final goal of the framework, and more in general of the present thesis, is to extract insights, guidelines and metrics over the design of the next generation intraluminal robotic devices.

Finally, this manuscript shows other applications and contributions (also to different medical scenarios) of the knowledge acquired in the field of robotic devices and simulation for intraluminal procedures.

Acknowledgements

Part 1

This thesis is the documentation of 3.5 years of research conducted between Universitat Politècnica de Catalunya (UPC, Barcelona) and Scuola Superiore Sant'Anna (SSSA, Pisa). This work was supported by the ATLAS project, which has received funding from the European Union's Horizon 2020 research and innovation program under the Marie Sklodowska-Curie grant agreement No 813782.

This research work has been conducted under the attentive supervision of prof. Alicia Casals and Dr. Albert Hernansanz from UPC, and prof. Arianna Menciassi and prof. Gastone Ciuti from SSSA. The unique combination of support and supervision from these brilliant researchers and world-class experts in the field of medical robotics has had an invaluable impact on the quality of the work, and more in general, on my personal development as researcher. Therefore, I firstly thank my senior supervisors prof. Casals and prof. Menciassi for their constant availability and support, for their invaluable suggestions which reflect years of research experience, and for their leading example as successful women in robotics (unfortunately, still under represented and sometimes still discriminated).

Secondly, I deeply thank the two people that followed closely this project day-by-day: Albert (Dr. Hernansanz) and Gastone (Prof. Ciuti). They provided constant help, support and mentorship on daily basis, for both technical and strategic matters. They were able to be always there for me, even during pandemic times or during my multiple travels for secondments. I am grateful for the several discussions which pushed me to strive for the highest quality of research, for the encouragements and suggestions and for always considering and respecting my point of view (including the times we had different opinions). Doing so, as supervisors, they gave me the freedom I needed to do my own experiments, to be right and wrong, to fall and rise up, and eventually to become a better researcher. As a Ph.D. student, I could haven not asked for better supervisors.

Having the great luck of conducting my research within a Marie Curie project, I could benefit from the support of several senior and junior expert researchers. Therefore, I thank all the professors and researchers of the ATLAS project. In particular, I thank Manu (Prof. Emmanuel Van Der Poorten) and Gianni (Dr. Gianni Borghesan) for coordinating in an excellent way the ATLAS project, for pushing the collabora-

tions between the students, for organizing really interesting courses, journal clubs and *capita selecta* (together with the other ATLAS partners), for teaching us how to properly write deliverables (although we did not enjoy writing them), for their helpful suggestions and motivations. In addition, I thank all my colleagues and friends from the ATLAS project for sharing this amazing journey with me. I thank the C2 group (Thao, Sanat, Jorge, Chun-Feng) for all the integration sessions, demos, discussions, deliverables, papers on our robotic platform for urinary tract related procedures. I thank Ameya and Diego (Prof. Diego dell'Alba) for the nice collaboration on the colonosocpy simulator. Finally, I thank Dr. Hugo Talbot and all the SOFA team for the massive technical help in developing the colonoscopy simulation platform.

Furthermore, this thesis would have not be possible without the strong and fruitful collaboration with our medical partners. Therefore, an immense thanks goes to my medical collaborators Prof. Alberto Arezzo from A.O.U. Citta della Salute e della Scienza di Torino and Dr. Carlos Garner-Argente from Hospital de la Santa Creu i Sant Pau. The discussions with them are among the most precious ones since they gave me the point of view of the clinicians, final users of our robotic technology. Prof. Arezzo and Dr. Garner-Argente allowed me to conduct multiple days experiments in their hospitals, involving 42 doctors from their teams. This research project owes a lot to them.

In addition, I would like to thank all the labmates from both my universities. In particular, Angelo, Marcello, Giorgia, Xuyang, Yu, Neri, Tommaso, Marco, Arianna from the Healthcare Mechatronics Lab of SSSA, and Maria, Marienne, Narcis, Cristina and Shoreth from UPC. They added extra value to this experience by being colleagues and friends, and by inspiring, motivating, and supporting me with concrete help, scientific discussions and suggestions while having fun all together.

Finally, I thank all my M.Sc thesis students: Andrea, Sonia, Roberta, Clara, Vittoria and Vanessa. They practically contributed in different ways to this research. While teaching to them, I have learnt a lot. Thank you.

Part 2

I would like to say thanks to all my friends and relatives which, in a way or another, gave a contribution to this thesis and to my Ph.D. journey.

Per prima cosa, vorrei esprimere la mia immensa gratitudine ad Alberto per l' aiuto costante, solido, pratico e per il supporto morale che mi ha dato in questi anni. Grazie per aver celebrato ogni mio piccolo e grande successo e per essermi stato accanto nei momenti più difficili di questo percorso. Una parte del mio successo accademico lo devo anche a te!

Ringrazio la mia compagna di avventure Elisa, fisicamente lontana ma con il cuore sempre vicino, per aver condiviso con me tantissime esperienze, accademiche e non. Mi rende felice e orgogliosa vedere che ricercatrici siamo diventate!

Grazie anche al mio amico Francesco, brillante ricercatore di Chicago, a Marta, Laura e tutti i compagni di università e incredibili colleghi. Pisa è sempre casa grazie a loro!

Grazie ad Alice ed Eleonora, supporto immancabile, distanti ma vicine, amiche speciali.

Grazie agli amici di una vita Nicoletta, Alice, Alessandro e Matteo per esserci sempre stati, nonostante le distanze e le differenze. Dalla scelta della classe al liceo, alle lauree, specializzazioni, matrimoni e dottorati, sempre insieme.

Gracias a mis compañeros de pisos en Barcelona, Matteo, Valentina, Paolo, David, Oihane para compartir conmigo estos años de vida, y mi aventura en Barcelona: salidas, comidas, pandemia, lock-down, patinete, deporte, mudanzas, risas, trabajo, charlas, fiestas y mucho más. ¡En general, gracias a todos mis amigos en Barcelona por estos años increibles!

Infine grazie alla mia famiglia stupenda. Grazie alle mie sorelle, diversissime ma sempre presenti l'una per l'altra, orgogliose di tutti i risultati raggiunti che siano accademici, familiari o lavorativi. Grazie alle mie zie, che nonostante l'età sono sempre state curiose e attente alla mia ricerca, e hanno festeggiato con me tutti i miei successi. Grazie, ai miei genitori incredibili! Supporto e amore infinito, sempre capaci di aiutarmi, sostenermi e motivarmi nei momenti di bisogno. Sempre disposti a darmi tutto per poter realizzare i miei sogni senza mai giudicarmi. Questa tesi è un successo anche vostro!

Abbreviations

HMI	Human Machine Interface
MIS	Minimally Invasive Surgery
DOF	Degrees Of Freedom
UI	User Interface
ATLAS	AuTonomous IntraLuminAl Surgery
SOFA	Simulation Open Framework Architecture
UI	User Interface
GUI	Graphical User Interface
EPM	External Permanent Magnet
AR	Augmented reality
AI	Artificial Intelligence
GI	Gastro Intestinal
OR	Operating Room
EGD	Esophagogastroduodenoscopy
ERCP	Endoscopic Retrograde Cholangioppancreatography
VR	Virtual Reality
SLAM	Simultaneous Localization And Mapping
CT	Computerized Tomography
FEM	Finite Element Method
VJ	Video game Joypad
HD	Haptic Device

DRL Deep Reinforcement Learning

DVC Deep Visuomotor Control

MDP Markov Decision Process

PPO Proximal Policy Optimization

TLX Task Load Index

SSE Steady State Error

MCS Modular Colon Simulator

FBG Fiber Bragg Grating

EM Electromagnetic

LSL Lab Streaming Layer

ICC Intestinal Cells of Cajal

FSI Fluid-Structure Interaction

Contents

List of Figures

List of Tables

Introduction

Intraluminal procedures are a particularly challenging branch of MIS, relying on the steering of flexible instruments through fragile lumens or vessels. Robotics and Artificial intelligence have the potential to make a big impact in this field, contributing to the development of the next generation of autonomous intraluminal surgical devices. In this context, the European Marie Curie ATLAS project aims at investigating and developing smart and flexible robots able to autonomously propel inside anatomical structures. AuTonomous IntraLuminAl Surgery (ATLAS) is a Marie Curie European Joint Doctorate school that targets the training of 15 early stage researchers (*i.e.*, Ph.D. students) in the aforementioned medical robotic field. The program involves seven European universities (including Universitat Politècnica de Catalunya, Barcelona), and several partner organizations such as hospitals (*e.g.*, Hospital Vall d'Hebron, Barcelona), companies and research centers. This PhD project is part of the ATLAS framework, and is jointly pursued at Universitat Politècnica de Catalunya (Barcelona, Spain) and Scuola Superiore Sant'Anna (Pisa, Italy). In the context of intraluminal robotic surgery, the presented research focuses on the human-robot interaction, aiming at investigating and designing multi-level autonomy HMI. Hence, in order to extensively develop and explain the whole research process, the document has been organized in the following sections.

Firstly, the introductory part (part I) will give an overview of the background information useful to understand the context in which this research is being developed. In particular, this section will provide basic knowledge about standard intraluminal interventions and the opportunities opened by robotics in this field, with a closer focus on HMI. It will also provide a review on the state of the art of HMI for robotic assisted intraluminal procedures. Finally, the proposed aims and contributions of the thesis are listed and explained. With this regard, the scope of this project is oriented towards the investigation of new insights for the design of advanced high-level User Interface (UI) of robotic assisted intraluminal devices. In this context, the research will mainly focus on the development and testing of a bio-engineering framework for the evaluation of HMI for robot assisted endoluminal devices, *i.e., HMI evaluation framework*.

Secondly, in order to deal with the aims and sub-goals of this thesis, the methodology implemented are extensively presented in part II. Accordingly, both the design of *HMI evaluation framework* and its main component (*i.e.*, virtual simulator, metrics oriented to the evaluation of the HMI) are reported.

Thirdly, the experiments conducted are described in part III, including (1) an online survey run to derive the most desired features of controller devices for robotic colonoscopy, (2) the validation of the simulator and (3) a user-study testing two teleoperated modalities with the *HMI evaluation framework*. Herein, both the design of the experiments and the results are presented.

Lastly, part IV presents additional contributions and applications of the insights acquired for this research in other scenarios. In this final paragraph, each chapter is dedicated to a different work, which is a result of a collaboration with collegues from the ATLAS project, and from both Universitat Politècnica de Catalunya and Scuola Superiore Sant'Anna.

As a final remark, a conclusion paragraph is dedicated to give the reader a summary about the achievements reached during this PhD thesis. Herein, the results obtained are discussed and the future steps planned are outlined.

Part I

Literature Review and Theoretical Framework

CHAPTER 1

Background

Over the years, the technological advancement has led to the development of a set of new surgical techniques called MIS. MIS is associated with limited size incisions, reducing the patient trauma in terms of pain, blood losses, scar dimension, risk of infection and length of hospitalization [2]. However, these improvements came at the cost for the surgeons, resulting in steeper learning curves, higher mental stress and physical overloading [3–5].

1.1 Intraluminal procedures

MIS can be classified into extraluminal, transluminal and intraluminal procedures, based on the anatomical access point and on the surgical workspace [2] (See Figure 1.1).

Accordingly, in extraluminal interventions surgical scopes, usually rigid, are introduced into the body through small skin incisions. Whereas, in transluminal procedures, long flexible endoscopes are inserted through anatomical orifices (*i.e.*, mouth, anal sphincter, urethra, blood vessel), and an incision on the lumen (*i.e.*, tubular structure) boundaries is applied to access the targeted body cavity. Finally, intraluminal interventions, the least invasive, are characterized by the lack of any tissue incision. Therefore, referring to intraluminal intervention, the procedure is performed advancing an endoscope inside a lumen without violating its anatomical boundaries (Figure 1.1). In this case, the vision is provided by a camera placed on top of the scope or using external imaging tools such as X-ray fluoroscopy in intravascular interventions [2].

Most intraluminal procedures encompass three main clinical targets: gastrointestinal operation, ureteroscopy, and endovascular catheterization. The low invasiveness of endoluminal interventions is a great benefit from the patient prospective. However, the limited workspace, the unstable control of long flexible scopes and the loss of the direct view over the surgical scene, now mediated by a camera and a monitor, make the procedure harder to perform for the clinicians [6]. In addition, the poor ergonomics of the instruments currently used in the clinical practice (*i.e.*, colonoscope, gastroscope, ureteroscope) increases the mental and physical burden of the surgeons, having negative effects both on the health of the clinician and on the procedure's outcome [3, 4]. In this scenario, the use of robot assistance can help addressing the

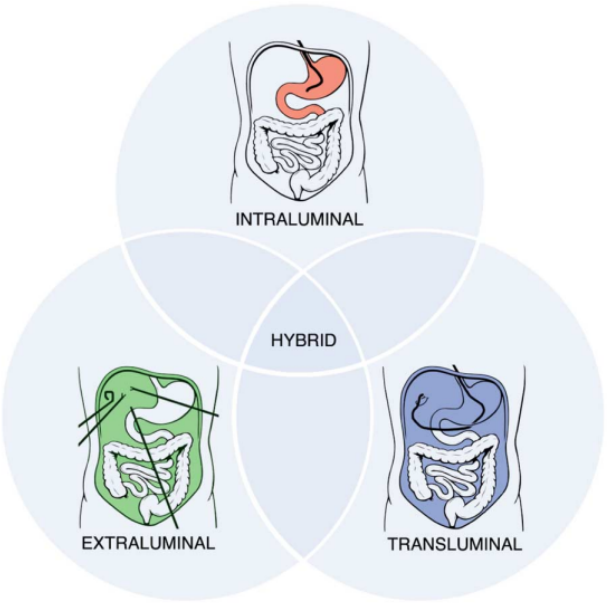

Figure 1.1. Classification of MIS procedures based on the anatomical access points and the surgical work-space. In intraluminal procedures the scope is advanced inside a lumen though an anatomical cavity. Whereas, transluminal interventions require the access and navigation of the scope though a natural orifice, followed by an incision of the luminal boundary to enter a body cavity (*e.g.*, abdomen). Finally, the extraluminal procedure allows the access of one or multiple scopes through a skin incision (*i.e.*, laparoscopy). Image courtesy of [2].

drawbacks related to MIS, increasing the stability and precision of the tools, and developing more supportive and user-friendly HMI.
Considering that this thesis mainly focuses on one intraluminal scenario, *i.e.,* colonoscopy, the following paragraph will describe more in details this procedure.

1.1.1 Colonoscopy

The colon is the final portion of the intestine, where water, nutrients and electrolytes from partially digested food are absorbed [7]. It is connected to the small intestine through the cecum and to the anus, through the rectum. A simplified diagram of the colon and its parts is shown in figure 1.2.

Colorectal cancer is the third most commonly diagnosed cancer worldwide, with an incidence of almost 2 million new cases only in 2018 [8]. Conventional colonoscopy represents the gold standard technique for the detection of cancer in the colon, which usually takes place when the patient presents some symptoms [9]. However, colorectal cancer can be prevented if the adenoma (*i.e.,* non-cancerous tumor) is detected and removed before it evolves into a carcinoma (*i.e.,* a cancerous tumor). This is possible by performing preventive examinations also on healthy subjects [9, 10]. During a colonoscopy, the colonoscope (*i.e.,* a long, passive flexible endoscope with a diameter of about 1 cm and a camera at the tool tip) is manually inserted through the anus and advanced along the colon. Once reached the cecum, the colonoscope is withdrawn

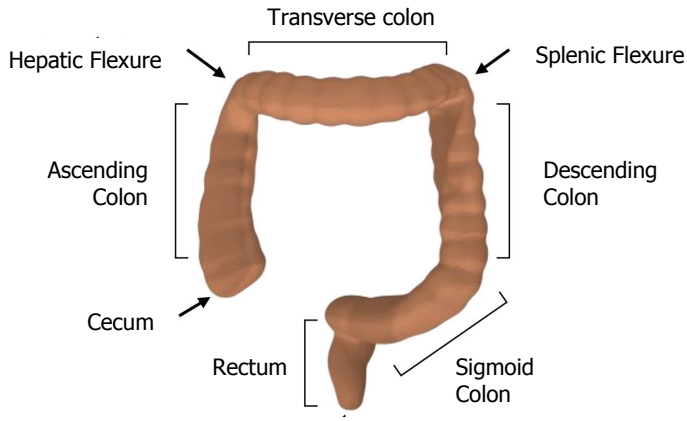

Figure 1.2. Simplified diagram of the large intestine and its parts.

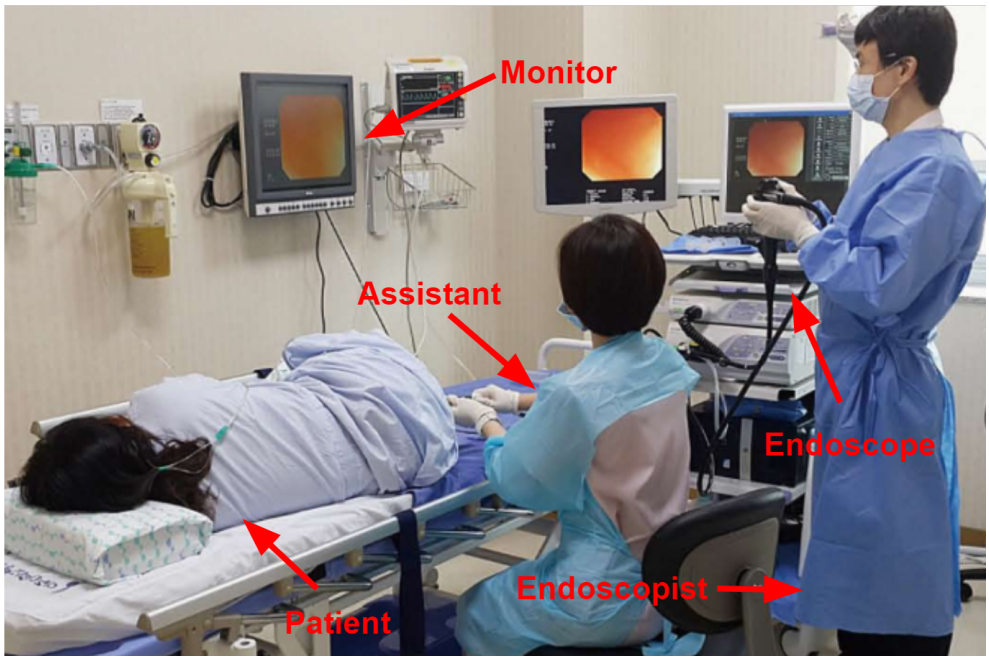

Figure 1.3. Example of intraluminal procedure scenario: colonoscopy. A flexible endoscope is guided inside the colon. The vision, mediated by a camera placed at the scope tool tip, is streamed on a monitor.

while visually inspecting the intestinal mucosa for the detection of any suspicious lesion [11]. The video recorded by the camera of the colonoscope is displayed on a

monitor, used by the doctors to orient the instrument inside the organ and to inspect the mucosa. Two wheels on the handler are used to deflect the active tip (the final portion of the endoscope of about 10 cm length) in two orthogonal directions (each deflection around ±90°). Special tools can be passed through the colonoscope to take biopsies, remove abnormalities, emit jets of water to clear the lens, and inflate/aspire air [11]. Figure 1.3 reproduces the intervention room scenario of colonoscopy, whereas figure 1.4 shows a colonoscope in details.

Figure 1.4. Standard colonoscope. A: Up deflection control; B: Down deflection control; C: Left deflection control; D: Right deflection control; E: Push forward and pull back.

1.2 Standard vs robot-assisted intraluminal procedures

In recent years, many research groups have focused on the development of robotic devices for intraluminal procedures, with the goal of enhancing flexibility and control stability. In this context, multi-steerable snake-like robots and capsule robots have been designed and thoroughly investigated as opposed to the standard passive

endoscope [12–17] (See examples of robotic assisted intraluminal devices in figure 1.5).

Figure 1.5. Examples of robotic endoscopic devices. A: Endoo platform, magnetic driven colonoscopy capsule [16]; B: The Neo guide multi-articulated snake-like endoscope for colonoscopy [12]; C: Magellan™ Robotic System flexible endovascular robotic endoscope (formerly Hansen Medical Inc. (Mountain View, CA, USA), acquired by Auris Health, Inc (Redwood City, CA, USA); D: Monarch™ Robotic assisted-bronchoscopy device by Auris Health, Inc (Redwood City, CA, USA) [18].

As previously mentioned, the endoscopes currently used in intraluminal procedures, such as colonoscopy or gastroscopy (*i.e.,* endoscopic exams to detect and potentially remove abnormalities in the upper gastrointestinal tract) are made by a long passive flexible shaft with an active tool tip. This tip can be deflected in two orthogonal directions by rotating two wheels located on the handler, at the end of the endoscope (see figure 1.4). Having a passive body, the scope makes multiple contacts with the lumen, during navigation. As a result, the contact friction increases, leading to looping formation, with the risk of breaking the organ' walls outside of the clinician's endoscopic field of view [11]. In addition, the creation of loops affects the control of the tool tip, modifying the transfer function between the handler wheels' rotation and the tool tip deflection. In this context, multi-articulated devices and capsule endoscopes have the potential to solve these problems, by changing the control paradigm [16]. Accordingly, replacing the passive shaft with an active multi-joints system would allow to have a control over the entire length of the endoscope, avoiding multiple contact. A step further is made by the endoscopic capsule, which would completely remove the shaft of the endoscope, carrying just a flexible tether including

the operative channels for the surgical tools and the water/air insufflation system. As a result, these innovative platforms extensively change the surgical paradigm, leaving space to the purposely design of a new set of high-level telemanipulation interfaces [6].

1.3 Human Machine Interfaces in robot-assisted intraluminal procedures

Besides the mechanical design of the surgical device, the interface used to maneuver the endoscope, together with the adopted control strategy and the quality of the feedbacks received during the interventions, have an important impact over the procedure outcome. Accordingly, all these factors can increase or decrease the difficulty of the tasks and are strictly connected to the users' physical and mental stress, influencing the final performances. The term UI or HMI commonly refer to the space of interaction between the user of a product and the product itself. In intraluminal procedures, the HMI includes all the equipment allowing the user (*i.e.*, clinician) interacting with the medical device (*i.e.*, endoscope), providing input through the tool handler, and receiving system output via a monitor (See figure 1.3). The goal of an HMI is generally to allow the user achieving an effective control over the machine and receive the inputs in order to facilitate the decisions' making process. Although there are no specific guidelines for the design of HMI, few metrics are commonly used for evaluating its quality. First, the hardware that mediates the interaction between the user and the machine is expected to be ergonomic. This means, that it needs to minimize the user physical stress by attenuating the discomfort and the risk of injury [4, 19]. Second, the device should be intuitive, providing a familiar interaction means to the user [20]. Finally, the HMI is expected to be user-friendly, that is easy-to-use and easy-to-learn. This feature is correlated with the complexity the HMI brings on the device, which in the worst cases, moves the focus of attention of the user from the object to control the interface itself. The more intuitive and user-friendly is the interface, the easier is the process of learning how to use it [21]. Based on this information, the quality of the HMI of standard intraluminal devices, such as the interface of the colonoscope, can be analyzed. Accordingly, current endoscopes present poor ergonomics, which was proved by many researchers to lead endoscopists experience wrist tendons inflammations, back pain, and neck discomfort as a result of their work activity [3, 4, 22]. In addition, the intrinsically non-intuitive mapping of the DOF between the handler and tool tip, makes the learning curve steeper, requiring more than 100 procedures to acquire competency [5]. These drawbacks increment even further due to the lack of any guidance or assistance. The introduction of robotics for intraluminal procedure has the potential to overcome the aforementioned issues, posing the basis of a new framework in terms of human-robot interaction and high-level telemanipulation control. However, a robotic solution would lead to a rise of the number of DOF to be controlled, as well as the sensing information that can be potentially provided to the user. For this reason, the whole concept of HMI must be re-thought. This

is particularly true because, following the recent advancements made in the field of artificial intelligence and automation, the HMI ceases to represent a unique control strategy, but has the potential to embed several levels of autonomy, shared control and assistive tasks.

It is possible to identify and list a set of characteristics which a robotic telemanipulation solution should be capable to provide, in order to support the clinician during the procedure:

- an ergonomic electromechanical interface requiring limited force to be maneuvered, and a more natural wrist pose with respect to the standard device controllers; these features will intrinsically decrease the clinician's risk of getting injured throughout the whole procedure;
- an intuitive mapping of the DOF between the master and the slave, aiming at increasing the surgeon's dexterity and manipulability;
- a user-centred and task-oriented Graphical User Interface (GUI) supporting the surgeons with specific tools (*e.g.*, guidance, suggestions, directions, *etc.*) depending on the phase and action in execution with haptic or visual cues; in this way, the information provided is maximized for each phase of the procedure, minimizing the surgeon's cognitive effort;
- a multilevel control autonomy system and HMI providing different levels of assistance and control to the clinicians and allowing them to focus on the most delicate tasks.

A summary of the main characteristics of the HMI, and its evaluation in a conventional endoscopy device, *i.e.*, the colonoscope, are provided in table 1.1.

Human Machine Interface (HMI)		Space of interaction between the user of a product and the product itself: equipment allowing the clinician to interact with the endoscope, providing inputs through the tool handler, and receiving outputs via a monitor or other means	
		Definition	**Standard colonoscope**
HMI characteristics	Intuitive	provide a familiar interaction means to the user: mapping the movements of the endoscope down to the controller, in a simple way that the users have experienced before	intrinsically non-intuitive mapping of the degrees of freedom (i.e. DOF) between the handler and tool tip
	User-friendly	easy-to-use and easy-to-learn: correlated with the complexity the UI brings on the device, which in the worst cases, moves the focus of the user from the object to control to the interface itself. The more intuitive and user-friendly is the interface, the easier is the process of learning how to use it	learning curve steep and lack of any guidance - requiring more than 100 procedures to acquire competency
	Ergonomic	hardware that mediates the interaction minimizes the user physical stress by attenuating the discomfort and the risk of injury	poor ergonomics - leading to wrist tendons inflammations, back and neck pain

Table 1.1. Definitions of HMI and its main characteristics, including its evaluation in the standard colonoscope

1.4 Levels of Autonomy in robot-assisted intraluminal procedures

As for driving vehicles [23], also the HMI of surgical robots can provide different levels of assistance and control to the clinician, switching from a fully manual control, to the automation of the whole procedure. Between manual and the autonomous control, there are potentially several layers of assisted functionalities. This means, for example, providing visual or force cues to guide the user during certain parts of the procedure. In this regard, *Yang et. al.* [24] identified six levels of assistance of surgical robotics (Figure 1.6):

0. **no autonomy** - the robot is manually tele-operated by the clinician and simply responds to commands;
1. **robot assistance** - the robot provides some physical guidance or virtual assistance while the clinician is fully in charge of the control over the system (*e.g.*, virtual fixtures);
2. **task autonomy** - the robot is autonomous for specific tasks started by the clinician, which can intervene if needed (*e.g.*, autonomous suturing);
3. **conditional autonomy** - the robot generates task strategies, and can perform them without close overlook by the user; however, it needs the approval of the clinician to start a strategy control or to select among the different strategies available;
4. **high autonomy** - the robot can take medical decisions but under the supervision of the clinicians;

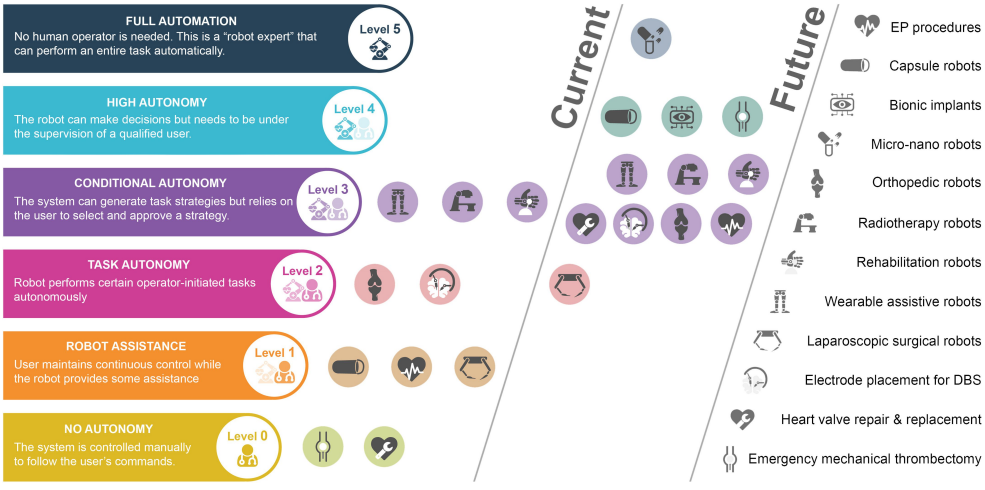

Figure 1.6. Classification of the levels of autonomy in medical robotics. Image from [25].

5. **fully autonomy** - the robot is the surgeon and no humans is needed in the loop.

The different levels of autonomy of a HMI are explored in this thesis in the chapters 9 and 10. In both cases, multiple level autonomy HMIs (up to level 4 of autonomy) are designed and tested respectively in the robotic colonoscopy and robotic ureteroscopy scenarios. Whereas, in chapter 8, two types of interface for teleoperated control of robotic endoscopes are tested for the robotic colonoscopy scenario, in this case in the "robot assistance" modality (level 1).

1.4.1 Levels of Autonomy in Robotic Colonoscopy

The classification of the different levels of autonomy in medical robotics can be tailored for the specific case of colonoscopy, as suggested by [15]. Considering the basic tasks of colonoscopy, *i.e.,* (1) navigation, (2) withdrawal examining the intestinal mucosa and (3) biopsy/removal of polyps, the different levels of autonomy can be defined as follow.

0. **No autonomy** (Direct robot control [15]) - The operator has direct control on the robot with a master console, without benefiting of any assistance. In the case, for instance, of magnetically controlled endoscopes, the operator would directly control the movements of the external permanent magnet [16], that allows to move the capsule inside the lumen. Therefore, no intelligent control, haptic feedback, augmented reality, movements constrain would be provided to the user.

1. **Robot assistance** (Intelligent teleoperation [15]) - The operator controls directly the final position of the colonoscope using a master console, benefiting of a simplified and smart control strategy. In the case of magnetic endoscopes, the robotic system will autonomously compute the movements of the external permanent magnet to have the robotic capsule reaching the point desired by the operator [15,26]. Therefore, the control would be more intuitive and easy for the user. In broader view, the robotic assistance would include any type of feedback and cues that can help the operator in the different tasks [27], *e.g.,* autonomous polyp detection [28,29] and classification, assistance in the navigation [30], *etc.*.

2. **Task Autonomy** - Semi-autonomous motion controlled by the clinician that needs to start the execution of the autonomous task, indicate the end target, and in same case waypoints of that motion. Examples of this type of tasks are movements of the colonoscope along predefined trajectories [31,32], autonomous retroflexion [33], autonomous intervention tasks (*e.g.,* biopsy) [34, 35], *etc.*. In terms of navigation, considering that the shape of the colon changes constantly, waypoints and end targets would need to be frequently updated by the clinician. According to [15], the features required to perform this task are the same as level 1, as the user remains in continuous control.

3. **Semi-autonomous navigation** - (Conditional Autonomy [15]) - the colonoscope is steered autonomously trough the lumen, thanks to computer vision techniques [27] or other methods [36]. The control strategy generated by the robotic system could be overridden by the operator which needs to constantly supervise the motion of the robot and approve its decision [15, 26, 37].

4. **High Autonomy** - The colonoscope autonomously perform a full colonoscopy under the supervision of an expert clinician. According to [27], deep learning based control will play a major role in achieving a fully autonomous navigation or polyp removal, including compensation for patient movements, *e.g.,* breathing.

5. **Full autonomy** - The colonoscopy is fully performed by a robot, and no expert operator is needed in the room.

As mentioned before, in chapter 8, two types of master console for teleoperated control of robotic colonoscopes are tested. In this case, the "robot assistance" modality (level 1) is applied, since the operator directly controls the movements of the endoscope tip with an intuitive control strategy. Indeed, in the experiments, the endoscope could be any type of robotic device, *e.g.,* magnetically controlled capsule or a snake-like robot. The user does not have to learn the specific control strategy of each robot, but can control directly the movements of the tip. The role of an assistive HMI is to allow the user to forget about the control strategy of the robot and focus on the real important aspects of the procedure (*i.e.,* diagnosis and treatment).

1.5 Conclusions

This chapter presents an overview on the specific medical context of this thesis, and more in general of the *ATLAS* project. In particular, section 1.3 provides the definitions of the desired characteristics of a HMI for robot-assisted intraluminal devices: *intuitiveness*, *ergonomy* and *user-friendliness*. This information, together with the analysis of the medical procedure, represent the basic knowledge for the definition of the metrics to track to evaluate the HMIs. This process will be described more in details in chapter 5. In addition, the information on the medical procedure, *i.e.,* colonoscopy, is used in this thesis, and in particular in chapter 4, 11, 12, to design the simulators of robotic colonoscopy.

The following chapter (chapter 2) will give an overview of the state-of-the-art HMIs for robot-assisted intralauminal procedures, exploring the different characteristics related to both hardware and software, including the different levels of autonomy.

CHAPTER 2

State of the Art

In the context of intraluminal procedures, the main components included in a HMI system are the physical controller and the GUI, showing the output of the camera together with any other useful visual cue. In addition to these modules, robotic devices can be enhanced with a force feedback system, auditory information and autonomous tasks. In the following chapter, a summary of the HMI designed for robot-assisted intraluminal interventions is presented.

2.1 Controllers for robotic teleoperation

Although there are few examples in the literature of robotic devices driven by controllers of standard endoscopes [12], many innovative intraluminal systems introduce new control interfaces. These include both the physical manipulator and the system used to map the DOF between the handler and the endoscope. In addition, the controller platform allows the user to perform extra tasks such as air/water insufflation, laser activation, surgical instruments manipulation. At present, various commercial systems are available for the tele-operated control, shown in figure 2.1. Among the most used interfaces, there is the Omega.x (Force dimensions, Nyon, Switzerland) family of haptic devices with parallel architecture [38] (Figure 2.1.5). These are high-precision 6-DOF force-feedback interfaces, also called haptic devices, which transmit digital information to the user through the sense of touch. Accordingly, the Flex Robotics System (Medrobotics, Raynham, MA, USA), a multiarticulated robot for GI endoscopic operations takes advantage of an Omega.3 device for maneuvering the endoscope [39, 40]. The same interface is adopted by the Magellan™ Robotic System [41] and the Sensei™ X2 Robotic System [42], both developed by Hansen Medical Inc (Mountain View, CA, USA) and later acquired by Auris Health, Inc. (Redwood City, CA, USA), respectively for intravascular interventions. In this case, an alternative control paradigm was provided to the user, including four buttons to drive the translation and tip deflection, and a wheel for rolling. Another commercial platform worth mentioning is the Monarch™ by Auris Health, Inc., used for bronchoscopy applications [18,43]. It is driven by a joypad, like those used for videogames (Figure 2.1.1). Furthermore, the buttons of the joypad are also used for implementing secondary tasks (*e.g.* irrigation, aspiration, *etc.*). A similar configuration is also adopted by the Ion robot (Intuitive Surgical, Inc., CA, USA) [44] and by the CorPath

GRX of the Corindus Vascular Inc. (Siemens Healthineers, Erlanger, Germany) [45]. Indeed, the Ion replaces the joypad with two spheres moved with two fingers (the indices of each hand). Whereas, the Corindus Vascular uses two hand cloches. In both configurations there is a decoupling of the controls (*i.e.,* insertion/retraction is controlled with one hand/finger, while the deflection with the other) and same type of inputs to control the endoscope (*i.e.* movements of two "levers").

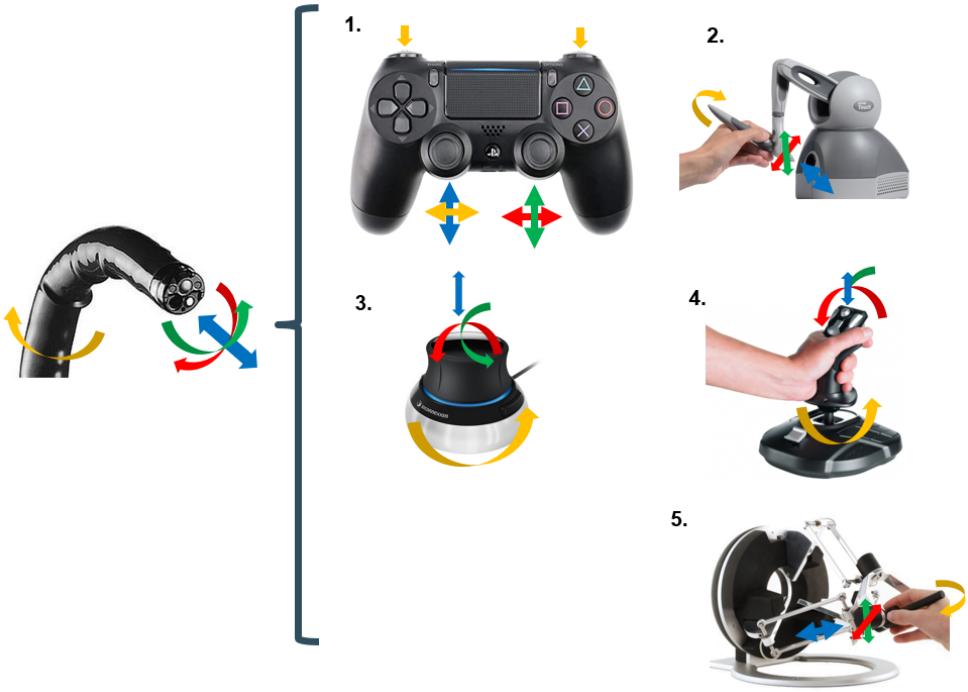

Figure 2.1. Commercial controllers driving robotic-assisted intraluminal devices. 1: videogame style joypad (*e.g.* DualShock® 4 controller of PlayStation® (Playstation, Tokyo, Japan); 2: haptic device with serial architecture (*e.g.* Touch™ (3D Systems, Rock Hill, South Carolina, USA))); 3: 3D mouse (*e.g.* SpaceMouse ® (3DConnexion, Munich, Germany); 4: hand joystick; 5: haptic device with parallel architecture (*e.g.* Omega x, Force dimensions, Nyon, Switzerland).

In addition to the mentioned devices, other manipulation systems include the 3D mouse (Figure 2.1.3) and the haptic device with serial architecture (Figure 2.1.2). The haptic device with serial architecture is used in a research context for magnetic driven capsule endoscopy. In particular, the Endoo system [16] uses the Touch™ device (3D System, Rock Hill, SC, USA), a 6-DOF manipulator providing haptic feedback. Whereas, a similar platform developed by [15], uses a joypad for driving the movement of the capsule. In these cases, the advancement and rotation of the

capsule is driven by the movements of an External Permanent Magnet (EPM), which is attached to a robotic arm. The EPM creates a magnetic link with one ore more magnets placed inside the capsule, driving its movements. This paradigm allows the miniaturized endoscope to deflect in two directions (*i.e.* pitch and yaw), and advance.

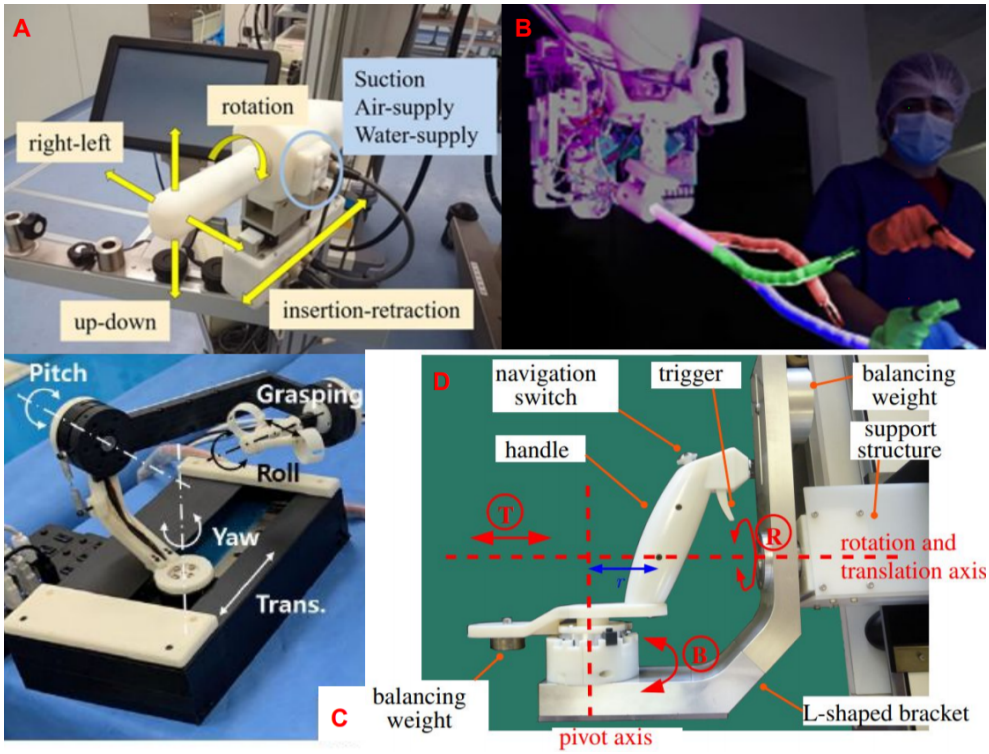

Figure 2.2. Customized controllers for robot assisted intraluminal interventions. A: RAFE [46]; B: i-2 Snake [13]; C: K-Flex [47]; D: STRAS [48].

Other robotic systems, developed in a research context, include custom-made controllers to better suit the design of the endoscope. Figure 2.2 shows few examples of these custom platforms. Among them, one interesting platform is the *K-flex* system, a GI endoscopic device with two attachable robotic arms for triangulation, including two 4-DOF controllers [47] (Figure 2.2.C). These controllers map the same movement of the hand (*i.e.*, translation, pitch, yaw, roll) onto the robotic arm, in an intuitive way. One of the two manipulators is used both for driving the attachable arm and the main endoscope, switching the control with a pedal. The *STRAS* platform presents similar controllers, but they allow to control two extra DOF in translation [48] (Figure 2.2.D). In addition, the main endoscope is moved by two 2-DOF finger joysticks placed on top of each handler. A different system is implemented in the *i-2 snake* platform, a snake-

like robotic endoscope designed for the gastrointestinal interventions [13] (Figure 2.2.A). In this case, the controller is a hand-held gripper with 6-DOF electromagnetic markers, which track the movements of the hand of the surgeons in the free 3D space. A recent work shows the design of a multimodal master console for the control of flexible endoscopes [49]. This system plans the use of an interface pedals driven for controlling the main endoscope movements. In addition, two Omega.3 devices are used for driving the two robotic arms attached to the main shaft for triangulation.

Finally, another set of advanced controllers were developed to drive standard endoscopes in a more efficient way, with respect to the usual one. These systems come with an electromechanical interface, which is adapted to the standard devices. An example is the *Teleflex* system, which allows to move a colonoscope using the previously mentioned Touch™ haptic device [50]. The same application has the *EOR 3* [51], which maps the rotation of a cylindrical hand manipulator with the roll of the endoscope, and the deflection of a finger joystick with the one of the tool tip. This system also provides force feedback. A similar project is the *RAFE*, a cylindrical 4-DOF hand manipulator for the control of the colonoscope movements [46] (Figure 2.2.A). Whereas, in the ureteroscopy scenario, the *Avicenna* platform was developed to drive any standard uretoscopes using two hand-joysticks and a wheel for fine adjustment of the deflection [52]. Recent studies also enabled the movement of an endoscope through gaze control, measured with eye-tracking device. This framework allows moving the endoscope whenever the user directs the gaze away from the center of the screen [53].

2.2 Graphical User Interface

The GUI of standard endoscopes mainly include the video recorded by the camera placed at the tool tip, or the result of the external imaging system, such as X-ray fluoroscopy images for intravascular interventions. The GUI of the new robotic devices do not differ significantly from the standard ones. However, there are few additional tools that are sometimes included in order to ease the procedure. In the case of the Monarch™ platform, pre-operative 3D reconstruction of the airways is shown online on the GUI, together with the current position of the endoscope, and the pre-planned path (both manually and automatically generated) [43]. The device localization is tracked with EM sensors. In addition, the CT scan images are reported on the lateral side of the interface (Figure 2.3.A). Similar systems for showing online the position of the endoscope inside a 3D reconstructed map of the organ were developed also for gastroenteroscopy and uteroscopy [54–56]. In order to help the clinician orienting the tool tip inside the lumen, both the Magellan™ and Sensei™ X2 Robotic System show a real-time animation of the catheter, reproducing the direction of deflection on top of anatomical images [41, 42, 58]. Both systems, also allow the visualization of pre-operative images, if required by the clinician. Other kind of information generally showed on the GUI are feedback about the status of the robotic system, the irrigation

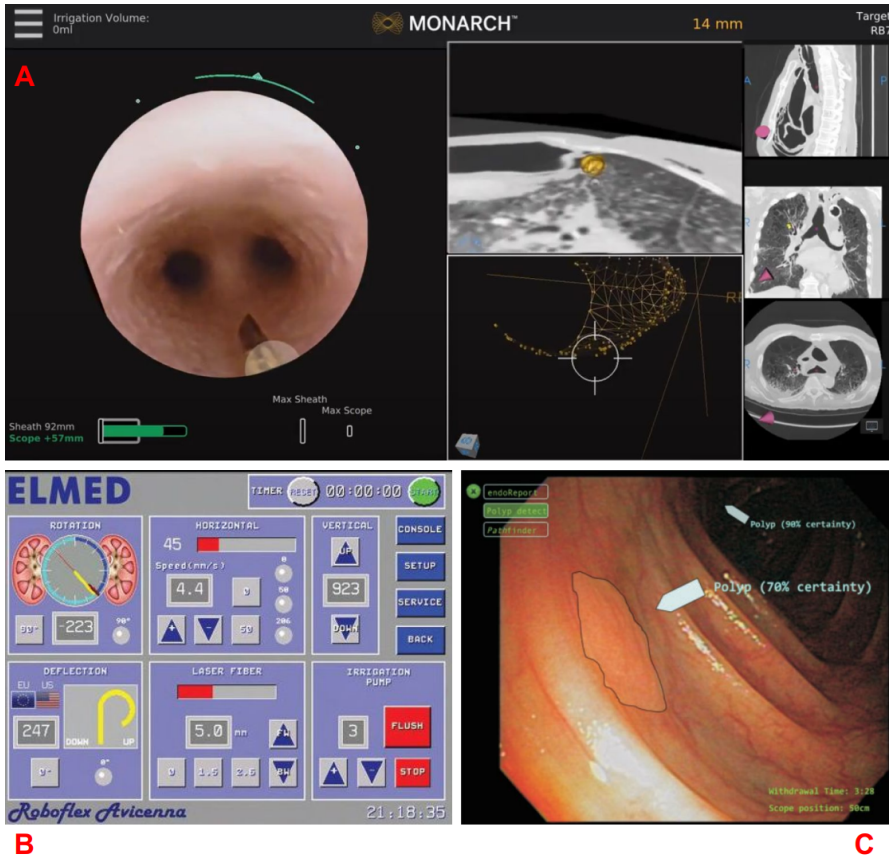

Figure 2.3. Examples of graphical User Interfaces for robot-assisted intraluminal devices. A: Monarch™ platform [43]; B: Roboflex Avicenna [52]; C: example of Augmented reality (AR) in colonoscopy [57].

volume or the length of scope already introduced inside the patient. Tool contact force information are also given through visual cues, updating the value on a virtual meter or providing a visual alarm when the magnitude exerts a certain limit [42, 54](Figure 2.3.B). In the gastrointestinal field, many researches are focused on the development of an online system to reconstruct a map of the tract of the visualized mucosa [59, 60]. These systems would allow the clinicians to localize the part of the mucosa not screened, in order to recover it. Among all the platforms mentioned, none of them exploit AR to deliver visual cues to the user. AR is the process of combining computer-generated objects and information with existing real-world images [61]. In this way, the real environment is augmented with virtual information. Thanks to the increasing trend of application of Artificial Intelligence (AI) to the medical field, many useful information can now be automatically extracted during a procedure,

in real time. These include polyp detection, classification (*e.g.*, neoplastic or non-neoplastic) and sizing [57]. Nowadays, there are also commercial systems using AI to focus users' attention on polyps, *i.e.,* GI Genius™ (Medtronic, Dublin, Ireland) [29], Caddie (Odin Vision, London, UK) [28]. This information could be automatically rendered on endoscopic images in form of labels, 3D rendering and shadow effects, as an assistance tool for the user (Figure 2.3.C shows an example of AR applied to colonoscopy images: the boundaries of a polyp, detected with AI, are highlighted and a label is inserted).

2.3 Haptic feedback

The application of robotics to the medical field allowed the introduction of the telemanipulation, which means that the robotic device, operating on the human body, can receive orders on how to move by a remote input device (*i.e.* master). In intraluminal procedures, decoupling the HMI from the robotic endoscope has allowed the construction of more complex and efficient interfaces. However, an intrinsic feature of the hand-held devices has been lost: force feedback. This is naturally provided by the friction between the endoscope and the surrounding tissues, and in many cases is an important cue for the user. Haptic interfaces have the potential to restore this information, by artificially constraining the movements of the master [62]. Three dimensional tactile interfaces are commercially available and have been adopted in robotic assisted intraluminal procedures (*i.e.* previously mentioned Touch™ haptic device and Omega x) [54, 63]. In addition, several research groups have built custom-made haptic interfaces [64]. The tactile feedback can convey different information. Firstly, it can restore a lost force feedback, by estimating the contact force between the device and the surrounding tissue. This information can be acquired (endowing the endoscope with extra sensors [65], or performing vision based force estimation [66]), filtered, scaled and finally given back to the user by increasing or decreasing the friction at the master interface. In the case of standard endoscopic devices, this means restoring the insertion force and the friction related to the rotating torque [64, 65]. Whereas, for active snake-like devices or endoscopic capsule, the information to be conveyed is the estimated contact force between the tool-tip and the lumen walls [54]. Secondly, virtual forces (*i.e.*, virtual fixtures) can guide the user along a certain path or avoiding restricted regions (See figure 2.4). More in detail, by applying regional constrains, the movement of the tool is restricted to a limited workspace (Figure 2.4.1.A). Whereas, implementing bilateral guidance constrains, the tool is attracted toward a specific path [66, 67] (Figure 2.4.2.B and 2.4.1.B). Finally, virtual fixtures can be implanted for providing extra information such as the singularities of the workspace of the specific robotic device to be controlled, reproduced as boundaries for the manipulation [63, 68].

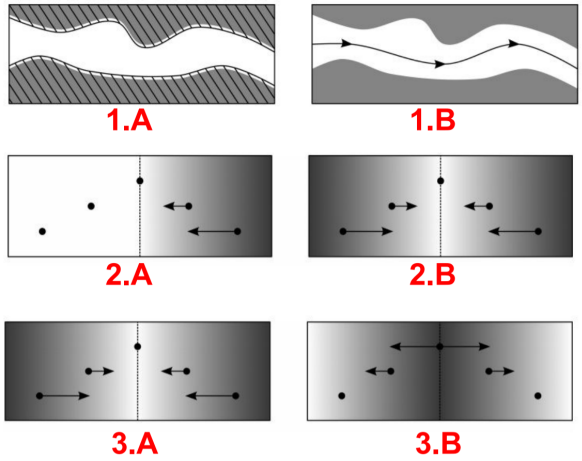

Figure 2.4. Classification of haptic constrains. Virtual constrains can be classified based on how the corrective force is applied. Here, the corrective force is represented with arrows.1: A – regional vs B: guidance constrains; 2: A - unilateral vs B – bilateral constrains; 3: A - attractive vs B - repulsive constrains.

2.4 Comparison studies between interfaces

As a result of the analysis of the literature related to the application of robotics in intraluminal procedures, no guidelines on the design of the related HMI has been outlined. As a matter of fact, several physical interfaces, control strategies, visual and haptic cues, have been developed and employed, but little space has been left to the comparison between each solution. However, some research works have centered their focus on the comparison of different human-machine interactions in order to understand the optimal paradigm for robotic-assisted endoscopic navigation [69–72]. Table 2.1 summarizes the contents of these works, which were all set in the colonoscopy environment. The experiments, involving either residents or novices, were adopting features related to the outcome of the procedure as metrics to be compared between each platform (*e.g.*, time spent for each task, a quality analysis of the trajectory run, number of contacts with the lumen walls, *etc.*). In addition, many studies administered questionnaires at the end of each experiment in order to estimate the perceived mental load. However, none of them measured in fact neither the mental nor the physical stress of the users while using each platform. This could be done by measuring biometrical parameters linked to the physical or cognitive load of the clinician (e.g. heart rate, skin conductance, pupillometry *etc.*) [73–75].

Study	Goal	HMI	Protocol	Outcome
E. Rozeboom *et.al.* (*Surg. Endosc.*, 2014)	**Test**: efficiency of a robotic system with intuitive UI in controlling the tip of the flexible endoscope. **Metrics**: time and tip trajectory.	1) Touchpad with position control algorithm; 2) joypad with linear rate control; 3) joypad with non-linear rate control; 4) conventional colonoscope handle;	- 14 novices; - 2 virtually simulated tests: navigation & fine targeting task.	Significantly faster in steering the endoscope tip when using robotic steering compared to the conventional steering method. **Fastest:** touchpad. **Shortest trajectory:** joypad with non-linear rate control. **Preferred:** joypad with non-linear rate control.
C. Fan *et.al.* (*Surg. Endosc.* 2015)	**Test:** effect of spatial disorientation in pathway surgery (control-display compatibility). **Metrics:** time, travel length, distance from center line, number of warnings, subjective workload, TLX scores.	1) Normal mapping with thumb control interface; 2) normal mapping with wrist control interface; 3) mirrored mapping with thumb control interface; 4) mirrored mapping with wrist control interface;	- 24 novices; - 10 successful trials with each platform in a virtually simulated environment (orientation tasks).	Normal mapping reduces the training time and the workload, improving the overall performances.
C. Fan *et.al.* (*Surg. Endosc.* 2015)	**Test:** effect of spatial local disorientation in pathway surgery. **Metrics:** time, travel length, distance from center line, number of warnings, subjective workload, TLX scores	1) egocentric view-point (immersive - the standard one); 2) tethered viewpoint (visible tip).	- 20 novices; - 10 testing sessions for each view-point: 10 successful trials for each session in a virtually simulated environment (navigation tasks).	The visible tip gives strong direction cues and reduces the time of the procedure but increases the number of collision errors.
G. Ciuti *et al.*, (*IEEE Trans. Robot*, 2012)	**Test:** comparison HMI for magnetic capsule endoscopy. **Metrics:** % identified markers, time, speed, travel length, smoothness of trajectory, metrics related to the magnetic link between the capsule and the external magnet;	1) Hand-held tool (human-robot cooperative control); 2) haptic device with serial architecture; 3) 3D mouse.	- 15 residents - 1 colonoscopy for each HMI using a physical simulator.	Robotic teleoperated control better than the human-robot cooperative control. **Fastest:** haptic device. **Smoothest trajectory**: haptic device.

Table 2.1. Summary of experimental studies comparing different HMI. Virtual Four research works comparing different HMI are reported. For each study, the table summarizes the goals, the types of platform compared, the methodology and experiments' outcomes. HMI: Human Machine Interface, UI: user interface.

2.5 Semi-autonomous systems

The advancement in technology and AI over the last twenty years has brought to the development of many innovative tools, from which the endoluminal procedures can potentially benefit. As a matter of fact, autonomous endoscopic navigation based on AI or on more traditional methods, tools and episode segmentation and anomalous tissue detection and classification have the potential to automatize many parts of a procedure [15, 76–81]. In addition, advanced tasks such as online or pre-operative organs' map reconstruction, intra-operative images registration, path planning, procedure metrics' tracking and user's physical and mental state measurement could really improve the quality of the surgical interventions [62, 82–84]. Accordingly, these features once combined in a comprehensive framework can assist the surgeon, reducing the risk of errors and easing the procedure. However, a comprehensive framework of this kind is still lacking [57]. Multi-level autonomy interfaces together with multi-layer shared control strategies need to be designed and extensively investigated. As a matter of fact, on one hand the introduction of too many inputs to the users might negatively affect their performance by providing an excessive amount of information to process. On the other hand, a high level of automation might leave the clinicians out of the loop and decrease their attention levels, risking to worsening their performance [85].

2.6 Conclusions

This overview on the state-of-the-art HMIs for robot assisted intraluminal procedures plays an important role on the design of the objectives of the thesis. Indeed, it is evident that many interfaces have been developed so far, which include several different characteristics, both hardaware and the software. However, there is a lack of common understanding about which are the features that an interface should have to be the optimal solution for its specific case, *i.e.,* to minimize the cognitive and physical load of the user and maximize the outcome of the procedure. At the same time, there is also a lack of guidelines, tools and methodologies to assess how to properly design "intuitive", "ergonomic" and "user-friendly" interfaces in the specific context of robot-assisted intraluminal devices. Therefore, this thesis, as better explained in the next chapter, mainly aims at closing this gap by providing a methodology to follow on the design and evaluation of HMIs for robotics intraluminal devices.

CHAPTER 3

Objective and contributions

The introduction of robotic technologies for intraluminal procedures, *e.g.* snake-like robots and endoscopic capsules, has resulted in notable improvements in terms of endoscopes flexibility and control stability. Nevertheless, it also introduced additional DOF to control and sensing information to process, posing the basis for a new framework of human-robot interaction and high-level telemanipulation control. Therefore, this PhD thesis aims to address the following research question:

which is the optimal HMI for robot-assisted intraluminal procedures, i.e., the one that minimizes the cognitive and physical load of the user and maximizes the outcome of the procedure?

To do so, this research focuses on the development of the first bio-engineering framework suited for the investigation, detailed analysis and comparison of the HMI for robot-assisted intraluminal procedures. The framework, named *HMI evaluation framework*, aims at enabling the extraction of metrics and guidelines for the design of the next generation HMI. The*HMI evaluation framework* is meant to be as open and modular as possible, to be used in different scenarios and be customized for the different needs and applications *e.g.,* medical procedures, HMI, *etc.* In this context, the different human-robot interaction paradigms can be designed and tested in terms of user's performance, mental stress and physical load using a purposely designed evaluation framework.

Consequently, the following additional outcomes will be provided by this thesis:

- the *know-how* for the development of an intuitive, user-friendly and ergonomic HMI for robot assisted intraluminal platforms;
- guidelines and methodologies for the design and development of an interface with the characteristics described above;
- flexible and open simulator of intraluminal procedures.

3.1 Research Workflow

To reach these goals, the thesis is gradually directed towards the investigation and development of the tasks reported below with respect to an intraluminal procedure (*i.e.*, colonoscopy).

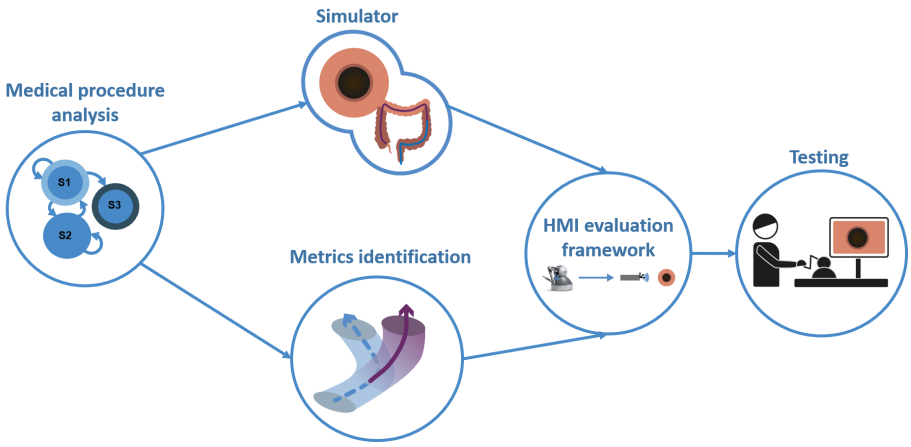

Figure 3.1. Research workflow: 1) analysis of the intraluminal procedure (*i.e.,* robotic colonoscopy), 2) extraction of metrics for optimal performance and control during the procedure, 3) Design of the *HMI evaluation framework*, 4) Deployment of comparative tests on the *HMI evaluation framework*.

- Analysis and decomposition of the medical procedure into tasks and sub-tasks to be replicated in the simulation platform. Therefore, identification of the sub-goals of each phase of the procedure to use as a basis for the identification of the metrics for evaluating the HMI.
- Analysis of the HMI available for the specific robot-assisted medical procedure, and of the needs to be addressed in terms of human-robot interaction.
- Design, development and validation of a modular, open and customizable simulator of the medical procedure to be used for testing the HMI.
- Identification of metrics for optimal performance and control during endoscopy for each state of the procedure, based on the literature and on a close collaboration with clinicians. Accordingly, for each sub-step the main tasks and goals are identified, and the related criticalities highlighted. Therefore, a set of metrics measuring the quality of the procedure and of control are identified. In

addition, metrics related to the cognitive and physical load of the user are also investigated.

- Design, development and testing of a *HMI evaluation framework* including the simulator and a data acquisition and analysis system tracking the metrics identified previously.
- Definition and implementation of a HMI to be evaluated with the framework.
- Deployment of comparative tests of the HMI with clinicians using the evaluation framework.

A visual summary of the workflow is available in figure 3.1.

3.2 Methodology: the HMI evaluation framework

The *HMI evaluation framework* is the main outcome of this thesis. It is a comprehensive platform suited to evaluate and compare different HMI or parts of them in a controlled simulation environment. It is composed of:

- an open, modular, interactive **virtual simulator of robotic colonoscopy**, allowing to freely connect different input devices, implement different control strategies and provide various feedback to the users; the simulator enables the acquisition of all relevant data related to the execution (*e.g.,* time, distance traveled, force exerted on organs *etc.)*;
- two **wearable sensors**, *i.e.,* heart rate band and eye trackers, to track the cognitive load of the users during the experiments;
- a **data collection and synchronization unit** able to gather all the data coming from the simulator (*i.e.,* metrics related to the performances on the medical procedure and quality of control) and from the sensors;
- a set of **questionnaires** to collect personal information about users, and their impressions in terms of preferences, cognitive and physical load, easiness to use, intuitiveness, and satisfaction regarding each device/system tested;
- **HMI** to be tested; these could be either the controller devices as the experiments reported in this paper or specific modules/features of the interface (*e.g.,* type of haptic feedback, control strategies, augmented reality *etc.*)

The tests conducted with this framework will give objective and subjective measures about (1) the performances in the clinical scenario, (2) the quality of control (3) the *intuitiveness*, (3) the *user-friendliness*, and (5) the *ergonomicity* of the HMI tested. Based on this information, the quality of the HMI tested with the framework is assessed. The design of the framework is as modular and flexible as possible to enable the testing and evaluation of different HMI or its different parts, both hardware and software.

The following part (part II) will extensively describe the two main components of the *HMI evaluation framework*: the virtual simulator of robotic colonoscopy and the metrics to evaluate the HMI.

Part II

Methodology

CHAPTER 4

Simulator of robotic colonoscopy

The first step of this research is the design of a simulator, used both as a development platform and a testing tool for the HMI. Therefore, firstly, the simulation environment is used for the connection of the different master controllers, implementation of the GUI, development of the different robot motion control strategies, feedback and autonomous tasks. Afterwords, the simulator is employed to perform tests with the final users (*i.e.,* endoscopists), as main core of the *HMI evaluation framework*.

This chapter describes the design and development of the simulator, starting from its design specification. Herein, the simulation platform is specifically intended to replicate the robotic colonoscopy procedure, which is the first medical application of this thesis. However, the design specification as well as the architecture of the platform imposes a modular approach to develop an open and flexible simulation platform, which can be used for different medical scenarios (*e.g.,* gastroscopy). Thanks to these characteristics, other research works related to the ATLAS project were validated using this simulator (chapter 9). In addition, a detailed state of the art on the simulators for colonoscopy is presented. The goal of this part is to demonstrate the need of creating a custom platform as part of the HMI evaluation framework. Indeed, none of the simulators available at the time of this thesis fully satisfied the design requirements of the research project. The content of this section was published as part of a review paper on training simulators for GI endoscopy: *Finocchiaro et al. (2021)* [86].

4.1 Specifications

The simulator is the core of the HMI evaluation framework and the fundamental software infrastructure used to compare the different HMI. Therefore, it presents the following design specifications:

- **openly and easily interfaceable** - able to connect, receive inputs and provide output to different devices and systems, and able to collect different data;

- **modular and scalable** - enabling the activation/deactivation of different modules and the development/integration of new modules without altering the basic simulation kernel;
- **realistic** in terms of visual and mechanical rendering - allowing a smooth online interactive simulation;
- **robust, controllable, reliable and repeatable** - to perform multiple user's tests obtaining robust and deterministic data.

Considering these specifications, the architecture of the simulator should aim at maximizing its modularity and ability to be customized for the different testing requirements. Therefore, the simulator should allow to easily load multi-anatomical models and robotic device models (*i.e.,* colonoscope), smoothly connect master devices for the guidance of the robot, implement diverse and multi-modal feedback and record multi-source data in a sincronized mode. The final goal is to have an open and flexible platform able to be easily customized for any needs related both to the medical procedure/scenario and to the HMI under evaluation. Indeed, the latter could include different master controllers, feedback modalities (*e.g.,* haptic, AR, auditory) or types of controls/levels of autonomy.

Additionally, the simulation should realistically reproduce the intraluminal procedure visually and mechanically, with real-time deformation of the organ caused by the interaction with the endoscope. Indeed, the simulator will be used as a basis platform for testing the different interfaces with the clinicians. Therefore, the users will need to feel the simulation as close as possible to the real medical procedure to act as if they would do in the Operating Room (OR).

4.2 State of the Art

This section summarizes the state of the art for simulators of GI endoscopy, including both the upper and lower GI tract. An extended version of the content presented here was published in [86]. Nowadays, the majority of simulators of GI endoscopy are designed for medical training. This is especially true for the commercial platforms. However, there are also few simulators at research stage that foresee the testing of new devices, or in particular the training and testing of AI algorithms (*e.g.,* autonomous navigation, Simultaneous Localization And Mapping (SLAM), lesion detection, episode segmentation *etc.*)

Medical simulators are artificial platforms which offer the opportunity to train clinical procedures in a non-patient care environment and to test new engineering devices and applications in safe scenarios. The first endoscopic simulator is dated back in 1969 and was made up of a simple mannequin for sigmoidoscopy training [87]. Over the following fifty years, the technology advancements led to the development of several artificial platforms, targeting a wide range of endoscopic procedures, including both the upper and lower gastrointestinal GI tract (Figure 4.1). Ranging from pure

mechanical systems to more complex mechatronic devices and animal-based models, nowadays a variety of options are available. Currently, there are several commercial and research platforms available for GI endoscopy simulation. The present review classifies them, based on the main characteristics, into three categories: (1) mechanical simulators, (2) computerized simulators, and (3) animal models, both *in-vivo* and *ex-vivo*.

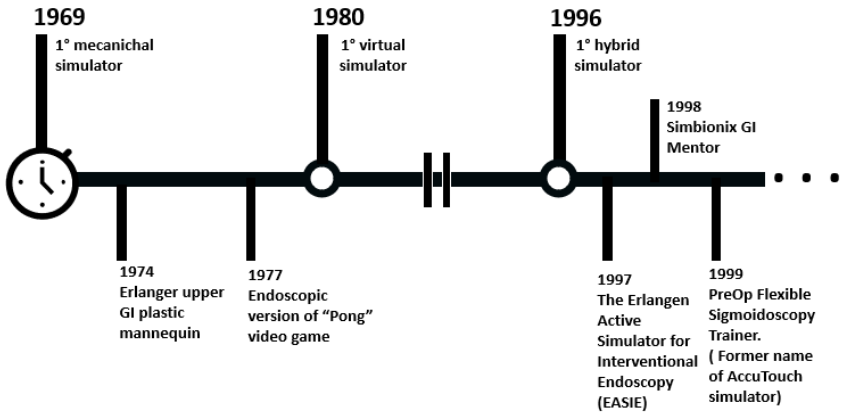

Figure 4.1. First steps of GI endoscopy simulators. Image from [86].

4.2.1 Mechanical simulators

Mechanical simulators (*i.e.*, physical simulators), reproduce anatomical organs using a combination of soft and hard materials (*e.g.*, silicone). In such cases, cavities inside the replicated phantoms allow the insertion of a standard endoscope, mimicking the endoscopic procedure. Consequently, the physical simulators aim at reproducing, with high fidelity, the mechanical and visual properties of the GI tract, focusing on an accurate selection of the appropriate materials, molds and surface textures. Even having the intrinsic advantage of providing natural tactile feedback, unfortunately, each platform offers only a limited set of procedures, since each scenario needs to be physically reproduced. Physical endoscopy simulators, mainly designed for training, have been developed before the computerized platforms. One of the first works in this field was published in 1974, reporting the design of the Erlanger plastic mannequin, a training simulator for the upper GI tract [87]. Over the years, mechanical trainers have not experienced drastic changes. As a matter of fact, the main components of the physical GI simulators, currently on the market, barely differ from those available in the Erlanger platform. These modules are listed below (Figure 4.2):

1. a replica of the anatomical lumen (*e.g.,* intestine) resembling the living organ in terms of visual appearance and tactile texture, made with soft plastic (*i.e.*, silicone rubbers);
2. an external rigid case containing the phantom, endowed with one or multiple cavities, allowing the insertion of the endoscope (*e.g.*, replicas of anal sphincter);
3. rigid or semi-flexible internal support for keeping the organs in place, in some cases allowing the partial deformation/movement of the lumen during the procedure;
4. optional adds-on replicas of pathological tissue (*i.e.*, polyps) to be attached to the main organ, allowing to practice multiple tasks (*e.g.*, biopsy).

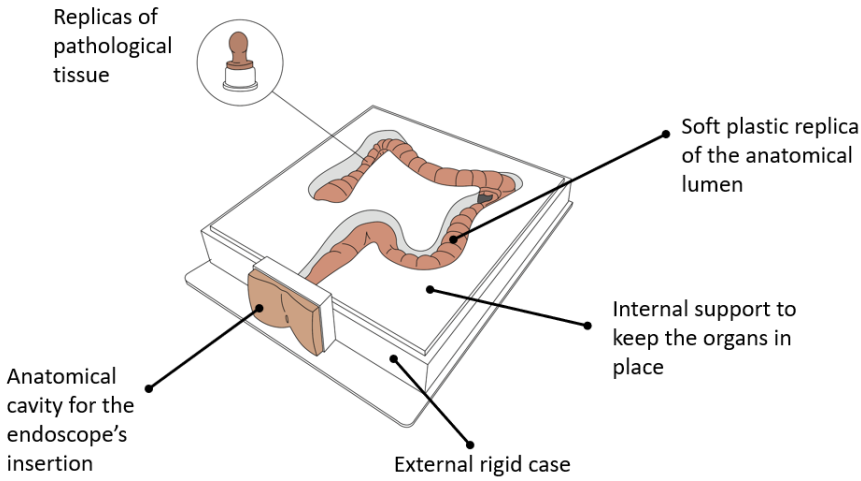

Figure 4.2. Mechanical simulators for gastrointestinal endoscopy: main components.Image from [86].

While virtual trainers simulate multiple procedures with the same platform, physical trainers provide each module separately. The only comprehensive platform, reproducing both the colonoscopy and gastroscopy is the EMS Trainer (Chamberlain Group LLC, Great Barrington, Mass) [88]. However, this system allows to reproduce only one scenario, has a rigid support which does not leave space for large deformation of the organs and replicates limited portions of the GItract. In addition, just like all the other physical simulators, it allows to provide any online suggestion, guidelines over the procedure or objective measurements of the performance at the end of the training. Currently, there are three main medical companies producing mechanical GI trainers: the Chamberlain Group (previously mentioned), the Koken Co., Ltd.

(Tokyo, Japan) [89] and the Kyoto Kagaku Co., Ltd. (Kyoto, Japan) [90] (Table 4.1). Besides the EMS Trainer (Figure 4.3.b), the Chamberlain Group produces also the Upper GITrainer, the Biliary Endoscopy Trainer, and three types of Colonoscopy Trainer. All these platforms do not provide insufflation or suction, allowing the insertion of the scope through patient cavities. One of the colon trainers (*i.e.*, Colonoscopy Trainer) replicates the shape of the colon and allows inserting a stricture and eight polyps in pre-selected locations. Whereas the other two platforms (*i.e.*, Colon Endoscopy Trainer with Flat Polyps and Colon Endoscopy Trainer with Raised Polyps) include a straight colon section, each featuring 25 polyps, respectively flat or raised, permanently embedded behind the replicated folds.

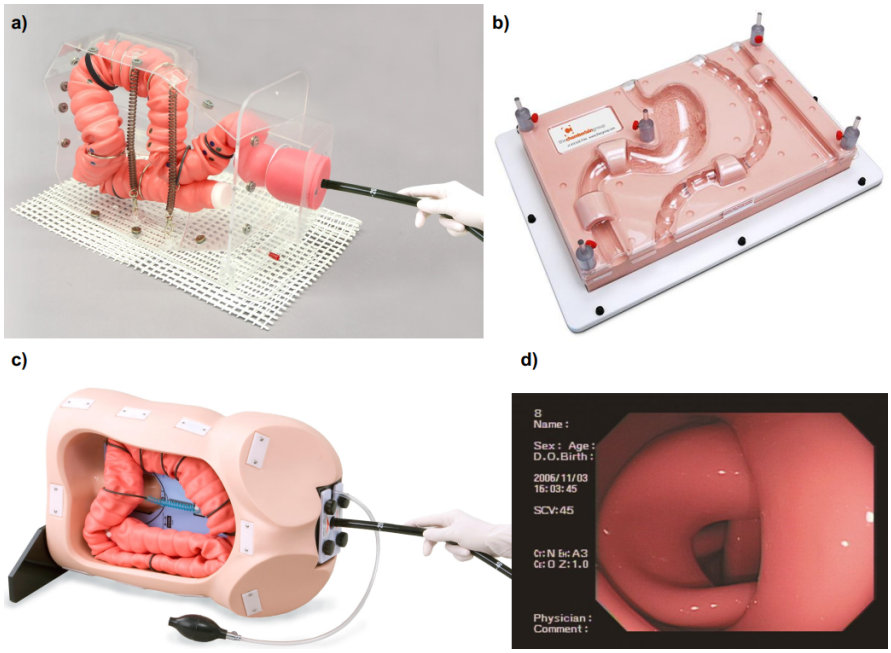

Figure 4.3. Mechanical simulators. a) MW24 NKS Colonoscope Training Simulator from Kyoto Kagaku Co.; b) EMS trainer from Chamberlain Group, LLC; c) M40 Colonoscope Training Simulator from Kyoto Kagaku Co.; d) Internal endoscopic view of M40 Colonoscope Training Simulator from Kyoto Kagaku Co. Image from [86].

A more realistic environment is provided by the two colonoscopy trainers of Kyoto Kagaku Co., Ltd..The first one, the Colonoscope Training Simulator (Figure 4.3.c-d), has the capability to make the colon tube air-tight and manipulate the anal sphincter opening using a hand air-pump. This system enables the air-insufflation and suction. Different cases can be reproduced by easily modifying the configuration of the intestine, and changing the colon fixtures, offering multiple levels of difficulties. The design of the colon tube and the support layout allows testing the loops formation,

	Endoscopic Trainer for the upper GI system Chamberlain Group LLC	**Biliary Endoscopy Trainer (ERCP)** Chamberlain Group LLC	**Colonoscopy Trainer** Chamberlain Group LLC	**EMS trainer** Chamberlain Group LLC	**Colonoscope Training Simulator** Kyoto Kagaku Co.	**3D Colonoscope Training Simulator NKS** Kyoto Kagaku Co.	**Colonoscopy Lower GI endoscopy simulator type II** Koken Co.	**EGD Simulator** Koken Co.
Modules								
Upper GI endoscopy	x			x				x
Lower GI endoscopy			x	x	x	x	x	
ERCP		x						x
GI Bleeding							x	x
Polypectomy/Biopsy							x	x
Key features								
Intestinal looping					x	x		
Multiple organ layouts					x	x		
Attachable polyps			x	x			x	x
Ulcerous replica				x				x
Suction/ insufflation					x	x		
Stricture replicas		x	x	x				
Multiple body position					x	x		
Anomalous tissue sites		x		x				
Lubricant gel		x			x			
Manual abdominal compression					x	x		
3D configuration						x		

Table 4.1. Comparative analysis of mechanical GIendoscopy simulators.
ERCP: Endoscopic Retrograde Cholangio-Pancreatography.

hence the task of loops avoidance or straightening. Finally, applying a skin cover over the organs, manual compression may be practiced together with changing the position of the body (*i.e.*, lateral or supine). The second platform produced by Ky-

oto Kagaku Co., Ltd. the 3D Colonoscope Training Simulator NKS (figure 4.3.a), is even more realistic than the first one since it offers a three-dimensional representation of the colon, based on an analytical study of CT Colonoscopy. This simulator includes loop formation avoidance and allows to pre-set the sigmoid colon to three different morphologies. The most suitable platform simulating the polyp detection and removal tasks are the Colonoscopy Lower GI endoscopy simulator type II and the Esophagogastroduodenoscopy (EGD) Simulator, both produced by Koken Co., Ltd.. As a matter of fact, they allow to attach different types of polyps on the surface of the phantom including laterally spreading tumors in the ascending colon, gastric ulcers and early gastric cancer in the stomach and duodenum. In addition, polypectomy and clipping techniques can be replicated, by attaching simulated tumors which bleeds once removed.

In addition to commercial platforms, there is a consistent number of simulators at a research level. A part of them presents similar characteristics to those available on the market, whereas others show distinctive features. In particular, several developed platforms aim at reducing the costs and the dimensions of the device, in order to ease their widespread distribution and promote the uptake of simulation among the endoscopy units. As a result, many researchers have focused on the development of mechanical simulators made with easy-to-find and inexpensive materials (*e.g.*, PVC hose, derange tubes, plastic sheaths, latex balloons, plastic boxes *etc.*). In these systems, the anatomical phantom is fixed to the desk mainly using rubber bands, and polyps or biopsy sites are replicated with small pieces of sponges, foam padding or snap fasteners. The construction of these platforms is meant to be easy, and achievable by many people without any technical background [91–93]. A more realistic, but still cost-effective system, was developed by exploiting the 3D-printing technology for the manufacturing of the upper GI tract replica [94]. The organs' 3D models are reconstructed from several CT images of neck, chest and gastrography using free software such as 3D Slicer (3D reconstruction) [95] and *Autodesk Meshmixer* (mesh modification). A more complex platform, recently developed by *Fuji et al.*, is based on a hybrid colonoscopy simulator. The system, called "Mikoto", is an advanced mechanical simulator endowed with motors, which allow the position change of the replicated abdomen. In addition, several functions are supported, such as the abdominal compression and repositioning of the diaphragm, simulating the deep inspiration. Pressure and optical sensors enable measuring the distensibility of the colon phantom, correlated with the potential pain experienced by the patient. This information, together with other metrics tracked online, is used to evaluate the user performance [96].

4.2.2 Computerized simulators

Computerized simulators (*i.e.*, Virtual Reality (VR) simulators) are mechatronic systems which combine standard endoscope handling, with virtual intraluminal scenarios. Using this approach, it is possible to simulate a wide variety of endoscopic procedures

and interventions (*e.g.*, gastroscopy, colonoscopy, polypectomy, bleeding control, *etc.*). Thanks to these platforms, the movements of a physical endoscope are mapped in a virtual environment, reproducing the endoluminal view with endoscopic images [97]. The first computerized simulators were developed in the 1980s as an adaptation of video games, reproducing EGD, colonoscopy, and Endoscopic Retrograde Cholangioppancreatography (ERCP) [98, 99]. At that time, the high cost of the technology did not facilitate their expansion into the clinical practice, which gradually arrived years later with the appearance of the GI Mentor (3D Systems, Littleton, Colorado, US) [100] and the CAE EndoVR Simulator (CAE Healthcare, Montreal, Quebec, Canada) [101], previously called Accutouch, and nowadays dismissed.

VR simulators for intraluminal procedures are characterized by a combination of hardware components, and software functionalities, aiming at training endoscopy beginners with the most realistic scenarios possible. Accordingly, the main physical modules included in these platforms are (Figure 4.4):

1. a mobile cart platform including one or two screens, a keyboard or/and a touchpad, a box with one or two anatomical plates (*i.e.*, holes) for inserting the endoscope, and a processing unit;
2. a set of scope heads and tubes for upper and lower GI tract endoscopy, with identical appearance and functionalities of those used in the clinical practice;
3. a collection of tools to insert in the endoscope operative channels (*e.g.*, forceps, electrodes for coagulation *etc.*);
4. optional pedals for extra functionalities.

Concerning the software components, the VR simulators may provide:

1. a GUI showing the simulated endoscopic environment, together with all the additional information and aids regarding the procedure;
2. biomechanical simulation of the organs, allowing to reproduce the expansion and collapse of the lumen under insufflation, or in the case of a colonoscopy, looping formation;
3. haptic feedback mimicking the tactile sensation normally felt by the endoscopists while navigating the endoscope throughout a lumen;
4. a repository of real patient cases, simulating diverse pathologies and anatomies, with different level of difficulty both for the upper and lower GI tract;
5. indications for performance metrics both real-time and as a summary at the end of each procedure;
6. didactic modules, providing online aids to the user, such as step by step instructions on how to perform the procedure or a 3D map of the scope inside the lumen.

Having a wide variety of simulated cases, in addition to the opportunity of reproducing the same scenarios many times, is a great advantage for standardizing training

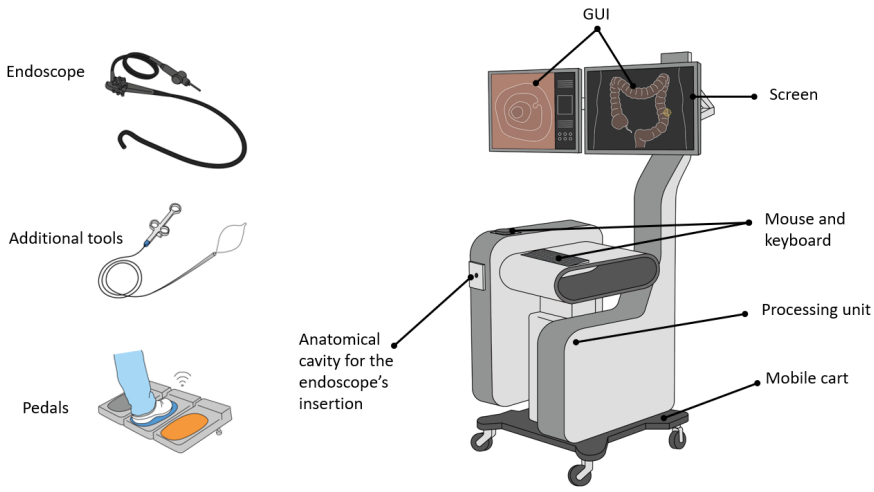

Figure 4.4. Computerized simulators for gastrointestinal endoscopy: main components. Image from [86].

of endoscopists or testing of the devices. All the commercial platforms mentioned provide objective measurements of the quality of the performance such as the patient's pain level, the percentage of mucosa visualized, the time of the examination and the amount of air insufflated. This information allows tracking the learning curve of the users, as well as customizing the benchmarks for the assessment of the capabilities of individuals. However, in order to have an immersive experience, the visual and tactile rendering should be as realistic as possible. Otherwise, the skills transfer from the simulator to real life (and the other way around) could be not an easy task. In this regard, the realism of the tactile cues is closely related to the quality of the organ's biomechanical model. As a matter of fact, a good approximation of the tissues' behavior enables a realistic force feedback computation.

Currently, in addition to the two aforementioned platforms (*i.e.* GI Mentor and CAE EndoVR Simulator), there are two more simulators commercially available for VR GI endoscopy training: (1) Endosim (Surgical Science, Gothenburg, Sweden) [102] and (2) Endo Vision STANDARD (MedVision, Nihonbashi Honcho, Chuo-ku, Tokyo) [103] (Table 4.2, Figure 4.5). In addition, a third platform called Endo-X (Medical-X, Rotterdam, Netherlands) was commercialized until 2017, but it is now out of production. However, the Endo-X features are reported in Table 4.2. Finally, Olympus (Olympus Keymed, Essex, UK) also developed a simulator for GI endoscopy training, *i.e.*, Endo TS-1, but it was never commercialized [104]. Each of these platforms integrates the basic hardware and software components previously listed in this section with few variations on the training modules (Table 4.2). Indeed, all the VR simulators include both upper and lower GI endoscopy. However, the GI Mentor provides a couple of training tasks in a non-anatomical environment, in order to learn

Figure 4.5. Computerized simulators: a) Simbionix GI Mentor from 3D Systems; b) EndoSim from Surgical Science; c) EndoVison system from MedVision; d) CAE EndoVR from CAE Healthcare. Image from [86]

the basics of the endoscope manipulation. Finally, it also comprises a didactic set of training for guiding the user in the learning of the deconstructed skills as defined by the Society of American Gastrointestinal and Endoscopic Surgeons (SAGES), *i.e.*, endoscopic navigation, mucosal evaluation, targeting, retroflexion, and loop reduction [105]. This application is performed with AR cues on simulated intraluminal scenarios and providing step by step instructions. Similar modules are offered by the Endo-X and Endosim simulators. The latter also allows recording the user's performance, to be able to rewind them as a learning tool. An additional interesting feature is offered

by CAE EndoVR, which provides online indications of the patient vitals (*i.e.*, heart rate, oxygen saturation, blood pressure) during a procedure simulation, and asks the users to manage the sedation. Doing so, it provides a more immersive experience. Finally, a distinctive feature of the GI Mentor worthy to report is the possibility to

	GI Mentor	CAE Endo VR	Endo-X	EndoSim	EndoVision
Modules					
Upper GI endoscopy	x	x	x	x	x
Lower GI endoscopy	x	x	x	x	x
Non-anatomical environments	x				x
ERCP	x	x		x	
Flexible sigmoidoscopy	x	x	x		
EUS	x				
GI Bleeding	x	x	x		x
EMR/ESD	x				
Polypectomy/Biopsy	x	x	x	x	x
Bronchoscopy	x	x		x	x
Basic skills	x	x	x	x	x
Key features					
Force feedback	x	x	x	x	x
Intestinal looping	x			x	
Virtual patients' cases	x	x			x
Patient vitals measurements	x				
Drugs management	x	x	x		
Online tips	x	x			x
3D Map of the organ	x			x	x
Recording the procedure	x			x	x
Trainee feedback	x	x	x	x	x

Table 4.2. Comparative analysis of computerized GIendoscopy simulators.
ERCP: Endoscopic Retrograde Cholangio-Pancreatography; EUS: Endoscopic Ultrasonography; EMR: Endoscopic Mucosal Resection; ESD: Endoscopic Submucosal Dissection.

have the simulator in a portable format called GI Mentor™Express. This simulator includes a box for inserting the endoscope, and it can be plugged in every laptop, which is used as a screen.

Regarding virtual simulators at research stage, the development efforts mainly focus on improving the realism of the systems and creating low-cost portable platforms. Trade-offs need to be found between realistic force feedback, organ and endoscope deformation, visual rendering, and computational cost [106–111]. A promising example of this kind of simulators is the one developed by the Australian Commonwealth Scientific and Industrial Research Organisation (CSIRO) for colonoscopy. In this system, the endoscope is inserted in a small box, which is easily connected to a laptop that is used as a monitor for the training. Realistic visual rendering and haptic feedback improve the quality of the training, still keeping the device's dimensions modest [112].

4.2.3 Animal models

Animal models have been and still are widely exploited for training medical procedures and testing medical devices. For endoscopic applications, the literature dates the first ERCP simulation on a live canine model in 1974 [113]. Overall, both live animals and explanted organs have been used for practicing and simulating GI endoscopic procedures. However, high costs and ethical concerns related to the *in-vivo* cases, and the logistic issues in collecting and storing *ex-vivo* specimens, limit their use. In addition, limited evidence is available on the literature regarding the use of cadavers for simulating GI endoscopy procedures. The main advantage reported is the quality of the tactile feedback [114], that overcomes the one of artificial simulation platform. However, cadaveric tissues present a different stiffness with respect to live bodies, sometimes making the procedure harder to perform [115].

4.2.3.1 *In-vivo* animal models

Endoscopic simulation in *In-vivo* models consist of practicing the whole procedure, or part of it, on anesthetized live animals. Specific clinical scenarios, such as targeted lesions, can be artificially reproduced before starting the practise [116]. According to the literature, large animals are the most used for training in endoscopy, since their GI tract dimensions most resemble the human ones. Among the animals, swine are the most commonly adopted for endoscopy training, both in the upper and lower GI tract. As reported, the adoption of live animal models for the training has been limited to the most complex procedures. Whereas, regarding the testing of medical devices, live animal simulation should be left for the latest stages of validation (even if this recommendation is not often applied). As a matter of fact, on one hand, *in-vivo* cases provide real haptic feedback, very close to the one experienced with human tissues, and high visual rendering. In addition, they allow to reproduce drug administration, replicating all the conditions of the real clinical intervention: secretions, respiratory movements and bleeding. With this regard, in case of tissue

damage or bleeding, it is possible to check the tissue recovery, eventually, in a second endoscopic procedure. However, on the other hand, there are evident anatomical differences between humans and animals, reducing the realism of this kind of models, and sometimes making them inadequate for the training. In addition, the need of on-site-care facilities and veterinary staff for performing the procedure significantly increases the costs of the whole process costs. Finally, ethical concerns regarding the sacrifice of animals conservatively limit their use. Indeed, endoscopic training, as part of animal experimentation, requires the careful approval of the planned protocol by specific independent institutions ensuring animal welfare, as well as the compliance with applicable regulations and standards [117]. In this regard, the World Organization for Animal Health (OIE) [118] refers to three key-elements to enable the use of animals for research and education purposes: (1) the existence of a project / training proposal review developed under a risk-based approach; (2) the identification of transparent inspections procedures of the facilities to ensure their suitability for the project/training, and (3) the ethical evaluation of the overall procedures involving animals (*e.g.*, methodologies, source of animals, staff's skills and competence, husbandry, transportation, *etc.*) [119]. The mentioned OIE key-elements are generally required in the documentation and procedures have to be submitted to the competent independent body/committee/authority in several jurisdictions, even though different approaches might address specific obligations/limits in a given legal system. Therefore, the conformity of the use of animals for our educational purposes shall be assessed case-by-case. For example, in the European Union, the Directive 2010/63/EU [120] established a series of principles and procedures that Member States had to regulate in the national implementations. In particular, it presents a structured methodological approach to be replicated in the national legislative initiatives in order to enable a compliant – and, therefore, ethically accepted - use of animals in education and training. To this end, specific guidelines have been drafted by the Experts Working Group (EWG) appointed by the EU Commission in order to properly address the interpretations of the Directive. In particular, the mentioned EU legal framework requires the researcher to provide a full exploration of alternative strategies through the identification of objectives and defined benefits within the request for the use of live animals. In our scenario, indeed, this would include a list of alternatives learning methods, *i.e.*, virtual simulators, physical trainers, *ex-vivo* models, and the reasons why they are inadequate for reaching the desired training goals. National implementations may, however, concern possible limits and procedures to assess the justification requirement for the use of animals, in general identified by applying the 3Rs criteria (Replacement, Reduction and Refinement). In addition, according to article 24 of the mentioned Directive, at least one person in the testing centre shall be appointed to take care of the animals and oversee their welfare. These activities shall include daily checks on animals and the development of strategies to increase awareness on the culture of animal care within the whole staff. The appointed staff member must also act as liaison between the training centre and institutional bodies and other professionals (*e.g.*, the Animal Care Body, the Veterinary Services, and experts able to recognize any variation on normal health and behavior) [121].

In light of the illustrated remarks, the *in-vivo* model shall be developed in specialized and certified structures, firstly identifying the applicable ethical-legal framework, then developing the procedures by addressing the binding requirements in light of the main benefits/risks assessment in each step of the procedures [121].

4.2.3.2 *Ex-vivo* animal models

Ex-vivo animal models for GI endoscopic training are combined systems, including a plastic frame and an explanted specimen. In this case, the desired lumen is inserted in a rigid case, which gives contains the soft tissues, mimicking the abdominal surrounding organs. These models are much easier to set up, with respect to live animals, and represent a slight improvement from an ethical standpoint. Indeed, the GI samples are supposed to come from the slaughter industry, where the animals are killed for the meat industry. The first simulator of this kind was developed in 1997, using porcine intestine's specimens. Initially, it was called the EASIE model (*i.e.*, The Erlangen Active Simulator for Interventional Endoscopy), while later it started to be commercially distributed as the Erlanger Endo-Trainer model (ECE-Training GmbH, Erlangen, Germany) [122]. The system includes a plastic structure reproducing a human head and torso, in which the explanted upper GI samples can be installed. Depending on the procedure to be simulated, the specimen undergoes different specific preparation (*e.g.*, recreation of polyps, small lesions, band ligation, tumors, varices, strictures). The rigid case, replicating the torso, can be rotated around the longitudinal axis, and can be fixed in any lateral position. Realistic bleeding is rendered with a perfusion device, endowed with an adjustable container and a stop-valve system. The blood circulation is regulated by an electric pump, simulating the heart rate of the patient and it is easily controlled by an assistant. A more compact version of the Erlanger Endo-Trainer was later developed, called the Erlangen compact EASIE/EASIE-R (EndoSim, LLC, Bolton, Mass) [123,124]. In this case, all the hardware parts are reduced to a small rigid frame for the fixation of the organ, and a roller pump for the hemostasis simulation. In spite of the reduced size, it allows to perform up to 30 different procedures. Nowadays, there are different variations of the compactEASIE commercially available. The most recent one, EASIE-R4, adapted for the upper GI tract, includes a torso-shaped tray with attachment clamps to fix the specimen in position. This device is endowed with a support for the esophagus, stomach and a portion of the duodenum. In addition, a specific frame called the COLOEASIE-2, suitable only for colonoscopy replicas, has been designed. In all these platforms, the biological specimens can be supplied by local butchers or by specialized companies with particular competences in harvesting and preparing the tissues. In this case, the animal organs may be frozen and delivered in order to be ready for the installation into the models, after thawing. Like the compactEASIE, other two types of combined simulators are available on the market: the Endo X Trainer (Medical Innovations International, Rochester, Minn) [125], and the DeLegge EndoExpert Tray (DeLegge Medical LLC, Awendaw, SC) [126] for training in the both upper and lower GI tract. Overall, *ex-vivo* animal models have the advantage

to provide a more realistic haptic and visual feedback, with respect to the mechanical and virtual simulators. However, using explanted organs, the tissue characteristics may change with respect to the live ones (*e.g.*, loss of elasticity), increasing the difficulty of endoscope navigation. As an advantage, the costs are moderate, especially in comparison with computerized simulators. Nevertheless, the tissues require long preparation and an appropriate disposal, and the number of training scenarios are intrinsically limited. Finally, as with mechanical simulators, no online guidelines or quality final metrics are provided during the training.

4.2.4 Strength and limitations

Overall, both mechanical and virtual simulators present advantages and disadvantages. Indeed, mechanical simulators and *ex-vivo* models can easily provide realistic tactile and visual feedback. However, they are unable to reproduce multiple procedures with the same platform, and they provide little information about quality metrics, *e.g.,* evaluation of the performances *etc.*. To this end, limited examples are available in the literature reporting cases of sensorized physical platforms used to collect measures (*e.g.*, contact forces) during the procedure [16, 127]. Similar consideration can be done for *in-vivo* animal models, which additionally have the potential of replicating realistically the clinical scenarios, but their use arises many ethical and economical concerns. To this end, nowadays, the use of live animals for experimentation/medical training is limited only to really complex procedures in the case that any other simulation cannot be used instead. However, the continuous technological progress has now the potential to strongly decrease, if not eliminate, the need to involve animals by enabling an everyday more accurate remotely and/or virtually reproduction of scenarios and tasks. On the other hand, virtual simulators allow to replicate the same procedure and conditions multiple times, while tracking evaluation metrics and customizing the environment as needed. In addition, the same platform can be used to reproduce different medical procedures and surgical tasks. Using a commercial virtual simulator rises important economic issues. Indeed, the cost of one platform varies from 50k $ for basic modules up to more then 150k for the most complicated ones [97]. Additionally, most of the simulators available lack visual and physics realism rendering. This represent a barrier against the user immersion during training/evaluation sessions and a gap between the simulated and the real scenarios. Physical computational simulations of tissue deformation, tool interaction, suture thread represent still open fields of research [86]. As a matter of fact, it is still not uncommon to observe physical breakages of rendered volumes due to excessive deformation; unrealistic dynamic behaviour due to the difficulty of modelling and calculating the behaviour of the tissues in real time, not realistic gravity simulation in suturing threads, *etc.* The continuous advances in parallel computing in graphical computer units (GPUs) with an affordable price are contributing to decrease this problem. The evolution of open-source physics computation libraries and packages is also contributing to increase the simulation realism. An example of this

software packages to compute and render physics is *SOFA (Simulation Open Framework Architecture)* [128]. In addition, high level graphical packages like *Unity* (Unity Technologies, San Francisco, CA, USA), have opened the possibility to develop realistic visual rendering. Table 4.3 summarizes the strength and limitations of each type of simulator.

	Mechanical	Computerized	Animal models	
			Ex-vivo	In-vivo
Visual realism	••	••	•••	•••
Mechanical realism	••	•	•••	•••
Repeatability	•	•••	•	•
Customizability	•	•••	•	•
Modularity	•	•••	•	•
Controllability	••	•••	••	•
Ability to track metrics	•	•••	•	•
Cost	•••	••	•	•
Availability	•••	•••	••	•
Legal and ethical issues	•••	•••	•	•

Table 4.3. Strength and limitations of the different types of simulators. The dots represent how good each type of simulator is with respect of each feature. Three green dots is the highest score while one red dot is the lowest.

Therefore, considering the specifications of the simulator to be embeded in the HMI evaluation framework (section 4.1), the use of a virtual simulator is recommended. In this way, the use of explanted tissues and live animal models is avoided for ethical issues, furthermore quantitative metrics for immediate evaluation and continuous monitoring and comparison of performance is guaranteed. Being the simulator the basis of the framework, it needs to be highly open to be interfaced with different HMI and to be customized as much as possible. This is now possible by creating a virtual platform using the mentioned libraries (*i.e.*, *SOFA* and *Unity*) which ensures a high level of realism both mechanically and visually.

4.3 Design of the new simulator

None of the simulators available in the literature satisfy the specific requirements listed in section 4.1. Therefore, a new simulation platform was designed and developed to be embedded in the *HMI evaluation framework*. Accordingly, the simulator was purposely conceived to maximize its modularity and ability to be customized for the different testing needs. The platform is a virtual simulator of robotic intraluminal procedures, specially focused on robotic colonoscopy. Both the colon and the robotic endoscope (modelled as a robotic capsule) are simulated. The colon is endowed with different types of polyps and has a realistic visual appearance and mechanical behaviour.

4.3.1 Architecture

The simulator was developed under *SOFA* [128], which is an open and modular development framework oriented to physics simulation. *SOFA* is the central module of the simulation platform architecture and contains the virtual workspace with the anatomical model and the robotic colonoscope. In *SOFA*, each object of the simulation can have a multi-modal representation. This means that the simulated objects, in this case the colon, can be represented using several models, each one of them optimized for a specific task, *e.g.,* the computation of internal forces, the collision detection, or the visual display of the object itself. Each one of these models is basically a representation of the object, and is synchronized with the rest through a mapping mechanism. These three models, commonly used to describe an object, are

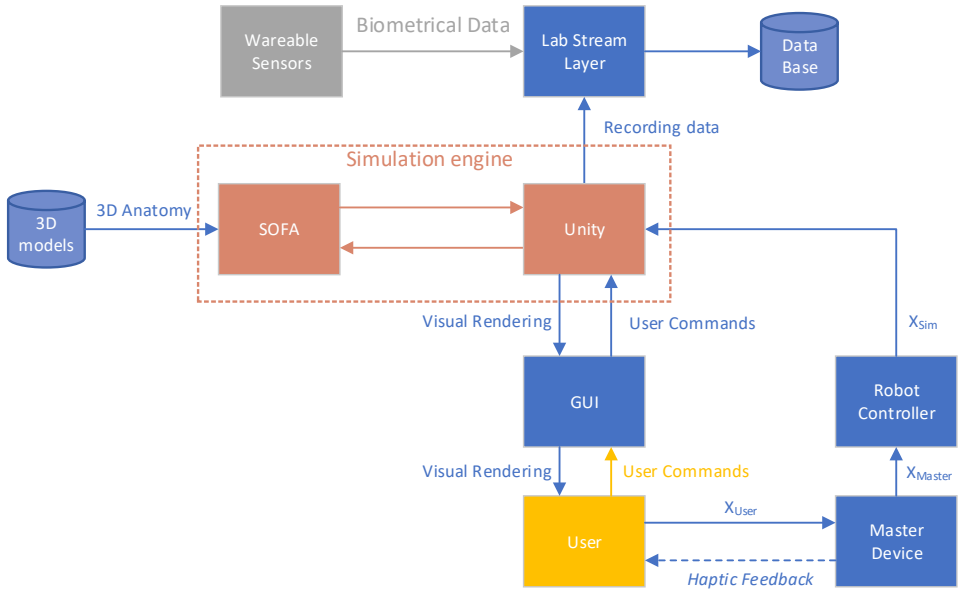

Figure 4.6. Architecture of the simulator: *SOFA* and *Unity* represent the main simulation engine. *SOFA* receives the 3D models of the organs and creates the simulation environment, whereas *Unity* provides the visual rendering displayed on the GUI (Graphical User Interface). The master device (*i.e.,* controller device) communicates with *Unity* by sending the user's commands, and the updated position of the robots. In addition, *Unity* sends the recorded data related to the simulation and to the users' performances to the Lab Streaming Layer. As part of the *HMI evaluation framework*, also the data recorded by the wearable sensors for tracking the user's cognitive load are sent to the Lab Streaming Layer, which works as a data synchronization and storage unit. X_{User} is the position of the robot sent by the user, X_{Master} is the position of the robot sent by the master device and X_{Sim} represents the position of the robot in the simulation frame of reference.

the (1) mechanical or deformation model, dealing with the computation of internal forces; (2) the collision model, dealing with the collision detection between objects; and (3) the visual model, allowing the visual display of the object in screen. These models are implemented hierarchically, where usually the mechanical model is the master, and the collision and visual models the slaves. This means, that any change that affects the master model (mechanical model) is transferred down to the slaves (collision and visual models). For instance, if the object is deformed in a certain area, this deformation will be observed too in the other models, especially in the visual representation. Each model can be represented with a different mesh, optimized for the specific needs. Therefore, the organ (*i.e.,* colons) were 3D reconstructed from real patients' images and represented with three different meshes: (1) a mesh representing the mechanical model; (2) a mesh for collision estimation and (3) a mesh for visual rendering.

SOFA physics engine computes collision, deformation and interaction forces between the colonoscope (herein simplified as a capsule with a camera on one side) and the simulated anatomy. The platform uses the *SOFA* plugin *SOFAAPAPI-UNITY3D* (InfinyTech3D, Nice, France) to replace the *SOFA* visual rendering module with the *Unity* game engine to increase the visual realism. In addition, *Unity* is used to interface with the proposed master devices to guide the virtual robotic colonoscope. The complete architecture of the simulator is presented in figure 4.6. The architecture scheme includes also the data collection and synchronization unit: *Lab Streaming Layer (LSL).* The LSL is an open-source networked middleware ecosystem to stream, receive, synchronize, and record data streams acquired from diverse sensors and devices [129]. It is used to collect and syncronize (1) any data measured during the simulation (*e.g.,* time spent to perform the procedure, trajectory of the robot *etc.* more information available in chapter 5), and (2) the data coming from external wearable sensors. The wearable sensors, as described in in chapter 5, are used to track the cognitive load of the users during the simulated procedure.

All the software modules and datasets used for the design of the simulator are open source, except for the *SOFAAPAPI-UNITY3D* plugin (connection between *SOFA* and *Unity*). The simulation frequency is 25Hz in *SOFA* and 20Hz in *Unity* under a laptop with Intel(R) Core(TM) i7-10750H processor, CPU of 2.60GHz, 32GB of RAM and NVIDIA GeForce RTX 2060 graphic card.

4.3.2 Generation of 3D anatomical models

The anatomy of the colon is complex and different among individuals. Therefore, the 3D models of the simulated colons were generated from computed tomography (CT) colonographies of real patients. The images were acquired from the public dataset *Cancer Imaging Archive* [130]. Figure 4.7 shows an example of CT) colonographies. The reconstruction pipeline started from a pseudo-automatic 3D segmentation of the CT images using the open-source software *3D Slicer* [95, 131].

Firstly, a segmentation by *thresholding* was applied since the colon, inflated with

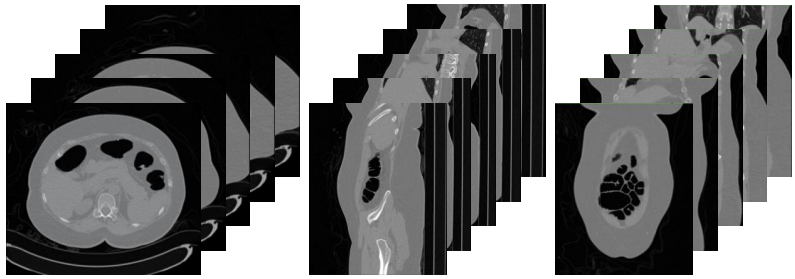

Figure 4.7. Tomographic colonographies (CT) images of one patient sourced from the *Cancer Imaging Archive* [130]

air, is visually detectable from the rest of the organs in the grey-scale image, as shown in figure 4.7. To do so, a range of pixel intensity corresponding to those of the colon was defined between (black) and a variable upper limit, set manually for each patient. Therefore, a first 3D model was generated only with the pixels (in 3D: voxels) having a color intensity value within the range. However, also the air around the body and other organs, *e.g.,* lungs and small intestine, fall into the defined pixel range. Therefore, a second volume segmentation was applied by means of a *region growing*

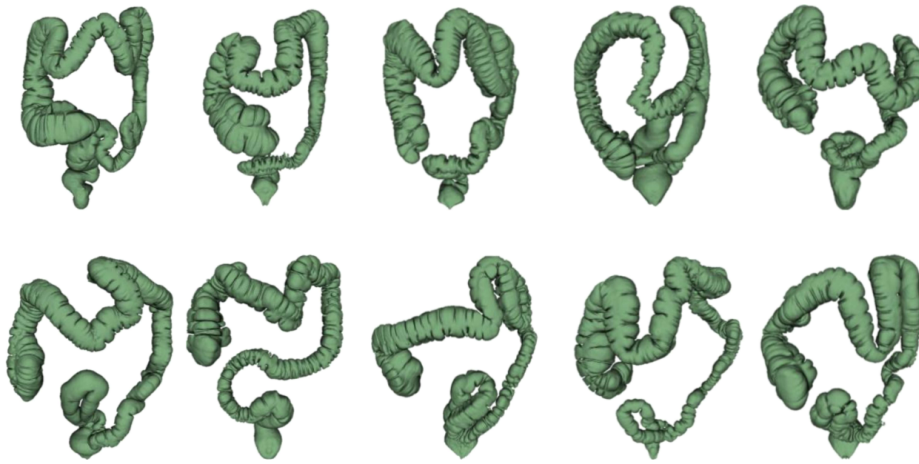

Figure 4.8. Colon models of 10 patients obtained from the 3D segmentation of CT colonography images.

algorithm, using a seed in one of the points that belong to the colon. Doing so, all those regions not connected to the colon were removed, *i.e,* only those voxels that are connected to the seed are classified as colon. It could happen that after the threshold was applied, some parts of the small intestine remained stuck to the colon. To remove those pieces, the connections between the colon and the bodies were manually deleted,

and the *region growing* operation was repeated. Examples of the 3D models obtained with this workflow are presented in figure 4.8, whereas a summary of the workflow is presented in figure 4.9. The colon models reconstructed were refined using *Autodesk*

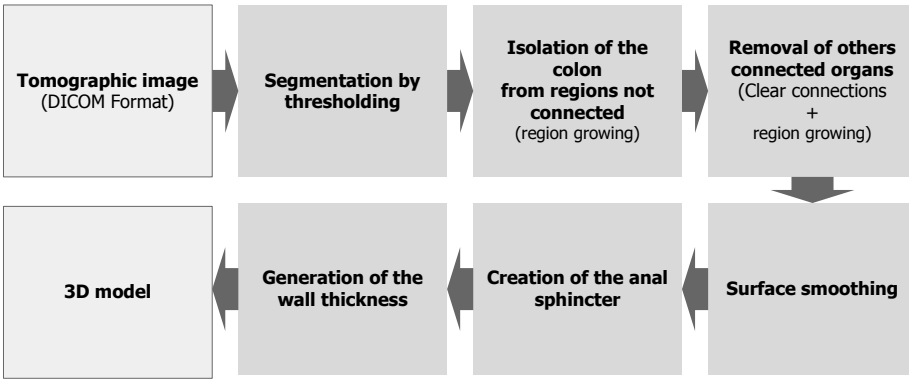

Figure 4.9. Summary of the steps for the reconstruction of the 3D colon models starting from CT colonography images.

Meshmixer (Autodesk, San Rafael, CA, USA) to (1) make the surface smoother, (2) create the anal sphincter and (3) generate a wall thickness of 2.5 mm (figure 4.10). This value approximates the thickness of the real colon, which usually varies along the length of the colon between 0 and 5 mm [132]. However, the realism of the deformation of the tissue perceived by the clinicians during the tests was not affected by this approximation, as demonstrated in the validation experiments described in Part III.

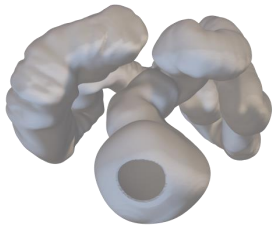

Figure 4.10. Inferior view of the a colon model after the post processing: generation of the anal sphincter and the colon with a wall thickness of 2.5 mm.

4.3.3 Generation of 3D models of polyps

The 3D models of polyps were generated separately with respect to the colon models. Doing so, the number of polyps inserted in each colon, as the type and the size, can be varied following the specific needs. The polyps were 3D reconstructed following the same procedure than for the colons models (section 4.3.2), starting from the CT colonography dataset [130]. The dataset informs about the presence of polyps in each

patient's colon, their approximate location and their size. This data facilitates their localization within the tomographic images and the subsequent extraction of the 3D model.

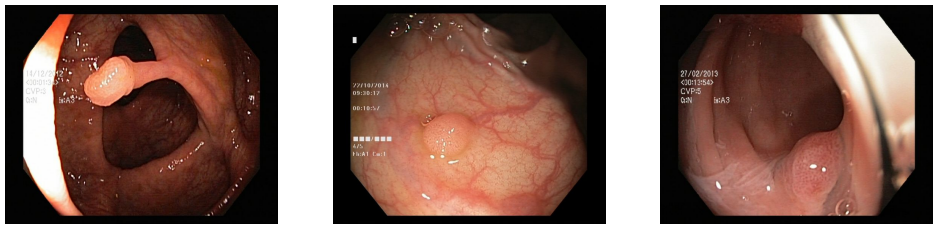

Figure 4.11. Examples of pedunculated (left), sessile (centre) and slightly elevated (right) polyps. Image courtesy of [133].

According to the Paris endoscopic classification of superficial neoplastic lesions, polyps can be classified in three types based on the morphology: peduncolated, elevated and sessiles [134] (figure 4.11). Therefore, one model of each type was reconstructed with *3D Slicer*. The morphology was slightly modified with the *Autodesk Meshmixer* to obtain a total of six polyps, two for each type (figure 4.12).

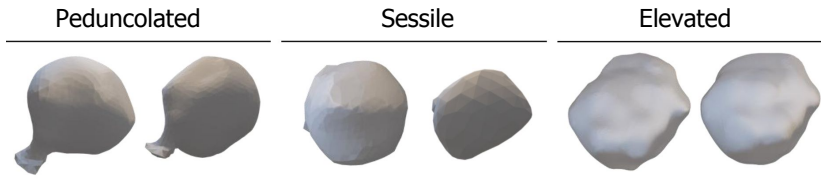

Figure 4.12. 3D reconstructed polyp models

Once the polyps are reconstructed, they can be placed in different spots of the lumen. The difficulty in detecting them during a colonoscopy depends mainly on two factors: the type of polyp and its location within the intestine. Therefore, three levels of difficulty associated with the type of polyp were established: pedunculate (easy), sessile (medium), elevated (difficult); and two levels of difficulty associated with its position within the colon: straight section (easy) and behind a bend (hard).

By combining these two criteria, the following levels of difficulty in polyps detection can be defined:

- a pedunculated polyp in a straight section (easy level);
- a flat polyp on a straight stretch (medium level);
- a sessile polyp behind a bend (difficult level);
- a flat polyp behind a bend (very difficult level).

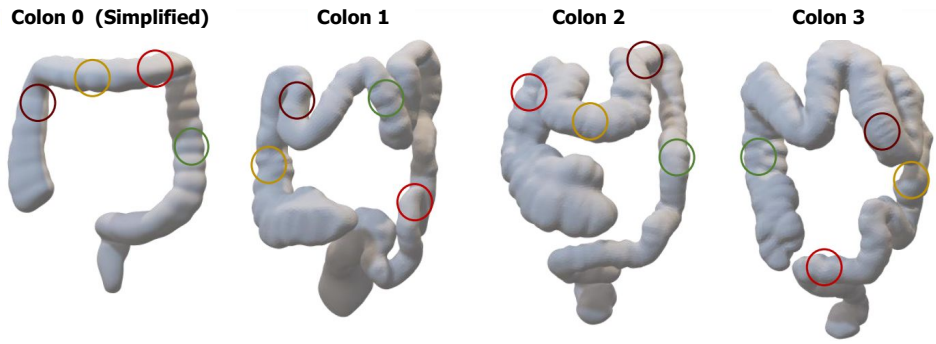

Figure 4.13. Example of placement of the polyps with four levels of difficulty: easy (green), medium (yellow), difficult (red) and very difficult (brown)

Figure 4.13 shows an example of the location of the polyps considering the different levels of difficulty for their detection in four colon anatomies (*i.e.,* colon anatomies used in the case study reported in chapter 8).

4.3.4 Anatomical model simulation

The physical properties of a colon are computed using the Finite Element Method (FEM) solvers provided by *SOFA*, generating realistic deformation of the tissue resulting from the interaction with the virtual endoscope tip. The colon tissue usually behaves as an hyperelastic anisotropic material. However, herein it was modelled as a linear elastic material with stiffness of 1.5 MPa and Poisson Coefficient of 0.3 [135]. This simplification was made since the non-linear FEM presents high computation cost. Hence its solution is hard to be computed during an online interactive simulation. Considering the specific application of this simulator, the accuracy of the forces and deformations computed does not have to be extremely precise as long as the clinicians feel that the environment behaves realistically. Therefore, the behaviour of the colon tissue was approximated to a linear elastic material and its realism was confirmed during the validation experiments described in part III. A second assumption was made regarding the direction of deformation of the tissue. Indeed, in the majority of the cases, the deformation of the colon tissue due to the contact with the endoscope occurs in the circumferential direction. According to [135], the yield strength of colon tissue in the circumferential direction occurs when the stress is 840 kPa and the strain is 0.59%. Therefore, assuming that the first section of the stress-strain curve is linear and must pass for this point and the origin of coordinates, the Young's modulus can be approximated to:

$$E = \frac{840 \text{ kPa}}{0,59} \simeq 1,5 \text{ MPa}.$$

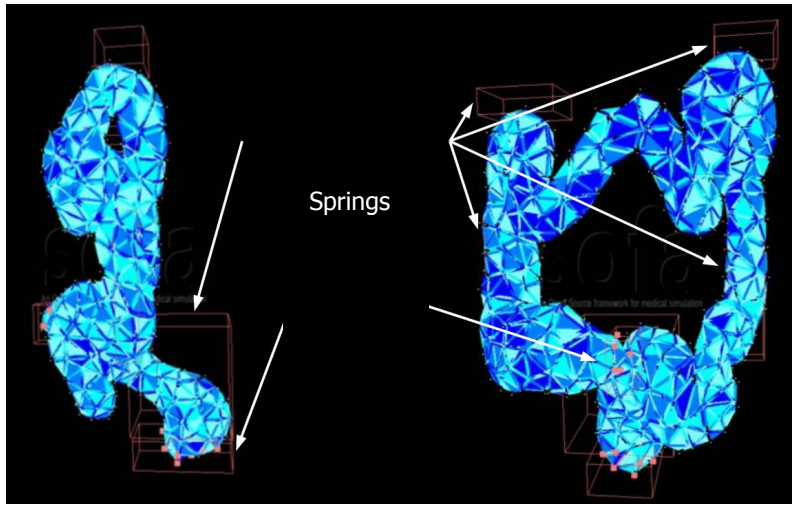

Figure 4.14. Side and front views of the mechanical model of a colon with the physical constrains modelled as springs.

The total mass of the colon was set to 500 g. Physical constraints, modeled as springs with one end in a fixed position and the other attached to a node of the tetrahedral mesh, were included to constrain the maximum colon deformations, generating a more realistic anatomy behaviour. The stiffness of the springs was fixed to 50 kN/mm following the recommendations of [136]. The deformations are computed using the *SOFA linear Conjugate Gradient solver*. The number of iterations was empirically set to 25 and was validated by experienced colonoscopists. The update frequency of the simulation was set to 25 Hz, which resulted in a good balance between realism and computer costs. The collision endoscope-colon is computed with the *SOFA default pipeline* (contacts solved with the *Lagrange Multiplier method*).

4.3.4.1 Mesh Generation

The anatomical models (*i.e.,* colon) were represented with three different meshes:

- a high-resolution triangular mesh for visual rendering.
- a volumetric tetrahedral mesh representing the mechanical model for deformation and interaction forces computation;
- a low-resolution triangular mesh for collision estimation.

The meshes were obtained using *Autodesk Meshmixer* (Autodesk, San Rafael, CA, USA) and the open source tool *Gmsh* [137]. *Gmsh* was employed to create the volumetrical meshes, whereas the superficial meshes were generated with *Autodesk Meshmixer*. The resolution of the meshes was chosen as a trade-off between simulation

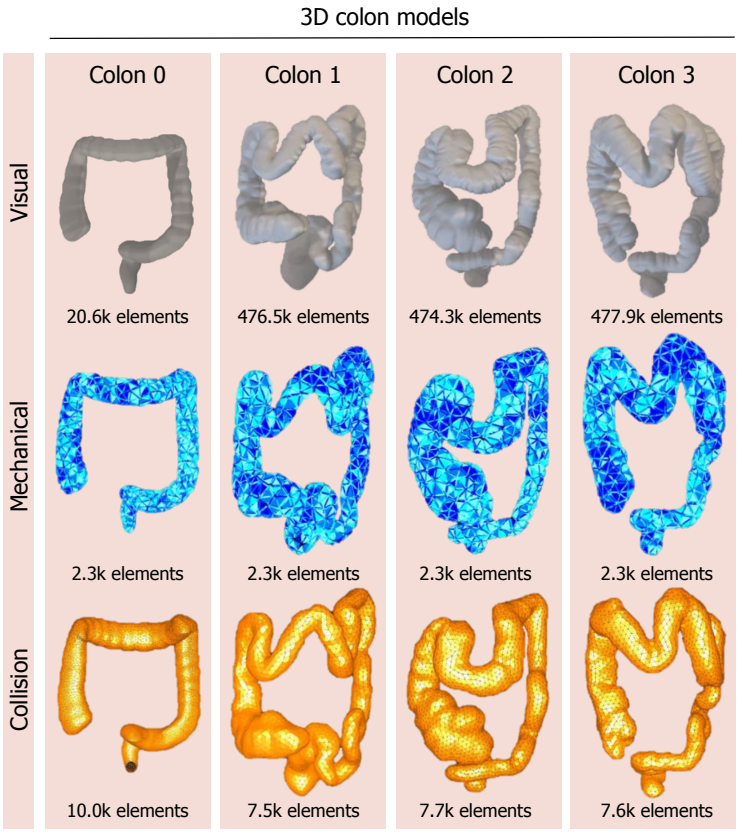

Figure 4.15. Meshes of the visual, mechanical and collision models in four colons. For each 3D colon, three meshes are generated respectively for the visual (high density triangular mesh), mechanical (low density tetrahedral mesh) and collision model(moderate density mesh).

accuracy and computational cost, obtaining a realistic visual and force feedback while preserving a real-time simulation. Accordingly, the mechanical mesh was set to approximately 2.3k tetrahedrons, the collision mesh to 7.5k triangles and the visual mesh to 75.0k triangles (see figure 4.15 representing the four colon models used during the experiments presented in 8). The resulting simulation models obtained from the simplified meshes were validated by expert endoscopists.

4.3.5 Visual properties

The visual rendering of the simulation is generated in *Unity*. Figure 4.16 shows real colonoscopy images. To replicate this type of visual effects several steps were needed. Firstly, generating realistic textures of the internal walls of the colon. These textures were obtained from real 2D endoscopic images from the KVASIR dataset [133] and applied to the high-resolution surface triangular mesh with the UV mapping technique (*i.e.,* 3D modeling process of projecting a 2D image onto a 3D model surface for

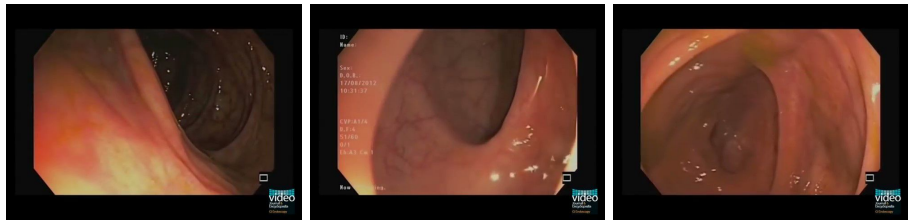

Figure 4.16. Endoscopic view of the colon from a real colonoscopy procedure [1].

texture mapping [138]). The process of adapting the 2D image to the 3D colon model was performed using the open-source software *Blender* [139].

Secondly, a *Unity normal mapping* image was generated and mapped onto the colon to create a three dimensional effect (*e.g.,* roughness, veins in relief). Normal maps are RGB-scaled images created from the overlap of three layers, which store information about the appearance of the surface based on the direction of light hitting it. Each of these layers corresponds to one of the three color channels, assigned following specific rules. Indeed, if the map lies on the X-Y plane, where X and Y are the horizontal and vertical axes respectively, then usually the red channel (R) corresponds to the layer containing the information about the shadow projection when the light came horizontally (shadows appear to the right or left); green (G), when the light came from a side perpendicular to the previous one and on the plane of the image (shadows appear above or below); and blue (B), when the light came in a direction perpendicular to the other two. Normal maps methodology was selected because it is less computationally expensive than other types of techniques adopted to render 3D effects (*e.g.,* height maps) and generates similar results. The maps were generated from the original endoscopic image adopted as a texture for the whole colon using the open-source *GIMP program (GNU Image Manipulation Program)* [140], a free program focused on editing and modifying images. To generate the normal map, the generic *GIMP Normal Map filter* was used with the following steps.

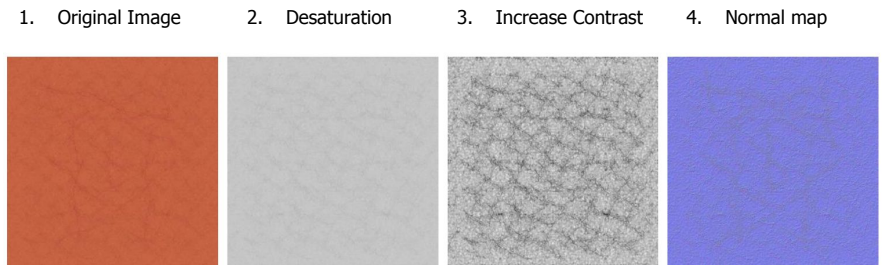

Figure 4.17. Steps to generate the *normal mappings* of the colon starting from the original 2D endoscopic image. From the increased contrast image, the normal map is obtained by applying the *GIMP Normal Map filter* (GNU Image Manipulation Program).

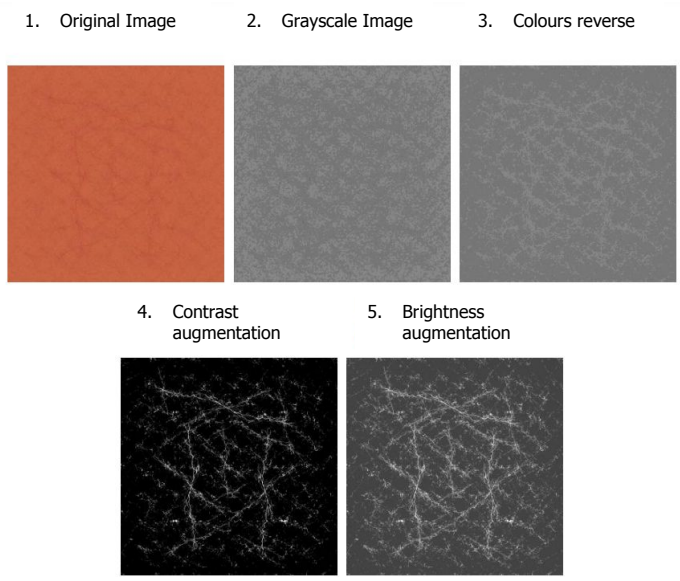

Figure 4.18. Steps to generate the *coat mask* image of the colon.

First, the original colon image was desaturated using the RGB to gray-scale Value (HSV) step mode. Secondly. the contrast was increased. Finally, the normal map filter was applied and the degree of definition and detail of the image was set through a scale parameter. Figure 4.17 shows the process followed to obtain the normal map.

Thirdly, a *Unity coat mask* was used to give the effect of light reflection due to the moisture inside the lumen. The coat mask is a grey-scale image which makes the surface look shiny by increasing the brightness of some areas of the image (*i.e.,* the lightest areas). To obtain the *coat mask* image, the same real endoscopic image from figure 4.17.1 was processed with the GIMP program. Figure 4.18 shows the steps followed. The goal of this process is to get an image where the veins and some details appear white and the rest of the background, gray. In this way, smaller and more concentrated reflections will be created when the light hits the areas where the image is white while, in the others, a slightly more opaque effect will appear. To segment the veins, the image was first gray-scaled. Following, the colors were inverted to make the veins appear lighter than the rest of the image, and the contrast was increased to emphasize more the veins. Finally, the brightness was increased to make the entire surface a little shiny. This is possible by setting the background gray while maintaining the veins white.

Additionally, *Unity* allows to adjust the light blur parameter (*Smoothness*), which can be used to define the smoothness of the objects. Figure 4.19 shows the visual effects obtained by varying the brightness of the *Coat mask* and the *smoothness* parameter, finally set respectively to 125 and 0.4. These values were selected by

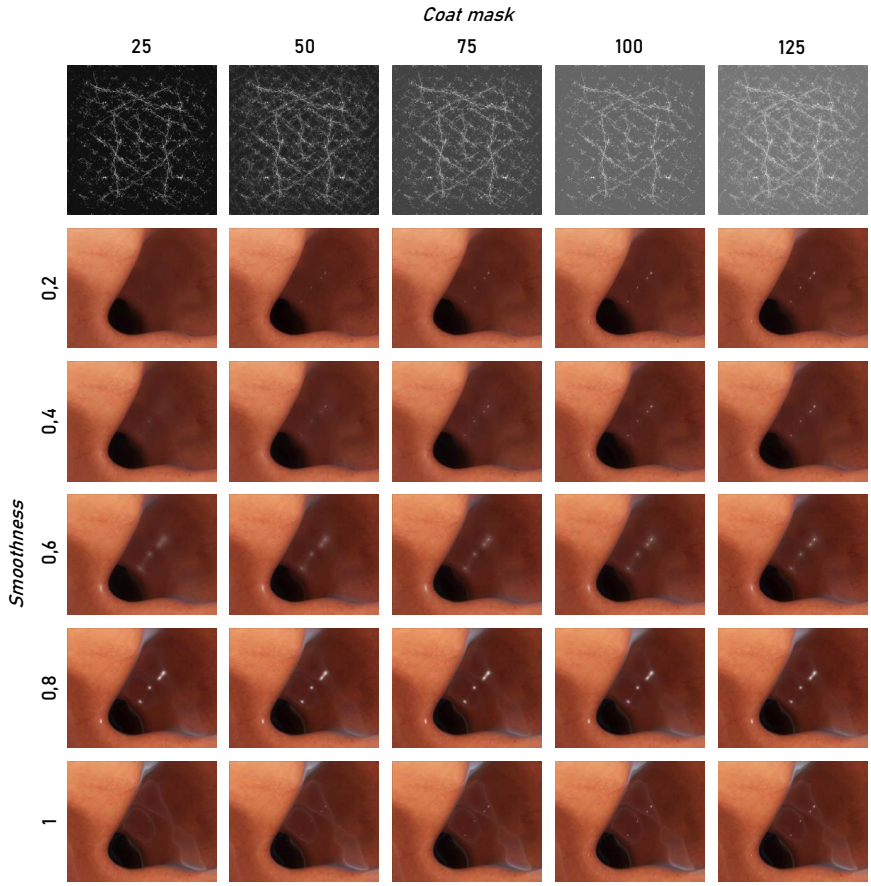

Figure 4.19. Visual effects obtained applying to the colon surface a *coat mask* with different levels of brightness and different levels of *smoothness*.

comparing their effects on the virtual colon with real endoscopic images, and were validated by expert endoscopists.

4.3.5.1 Lightening

In order to create a realistic visual rendering it is necessary to adapt the light conditions generated by the endoscope. The endoscopic lightening was rendered with a cone of white light of 140°, as in a real colonoscope. The intensity of the light was empirically set to 150 lux and its temperature to 7000 K. These values were obtained by comparing the simulation visual aspect with the real endoscopic images (figure 4.20).

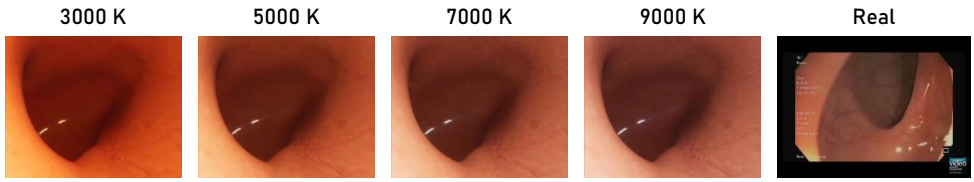

Figure 4.20. Visual rendering of different light temperatures compared with an images of a real colonoscopy [1].

4.3.5.2 Endoscopic Camera

The camera is attached to one of the endoscope extremes and provides a field of view of 120°. The final visual feedback is improved by adding the following visual effects, which increase the realism of the visual appearance of the colon.

1. **Vignetting effect**: darkening the edges of the image so that the centre is in focus and gradually blurs towards the sides.
2. **Lens distortion**: optical aberration appears mostly when using wide-angle lenses (*i.e.,* barrel lens distortion). As a result, straight lines become curved as they approach the edges of the image.
3. **Chromatic aberration**: optical distortion in which the lens is unable to make all colors converge to one point. The effect causes some blurring and the appearance of lines of different colors in areas where the colors change quickly from dark to light, *e.g.,*, those where light reflections appear.
4. **Blurring due to motion**: during the intervention, the endoscopic movements are not anyways continuous and fluid. In these cases, the camera does not have enough time to receive the light and motion blur is generated. The result is the production of momentary blurred images and effects that are especially noticeable in the brightest spots.

Figure 4.21 shows the different visual results obtained by changing the magnitude of the camera visual effects. The final parameters set in the simulation are shown in table 4.4. Figure 4.22 shows different images extracted from the simulator with the final visual rendering (the snapshots are extracted from the four colon models used in the user study presented in chapter 8).

Effect	**Value**
Vignetting	0,05
Lens distortion	0,30
Chromatic aberration	0,40
Blurring due to motion	10

Table 4.4. Selection of parameter values corresponding to the different camera effects.

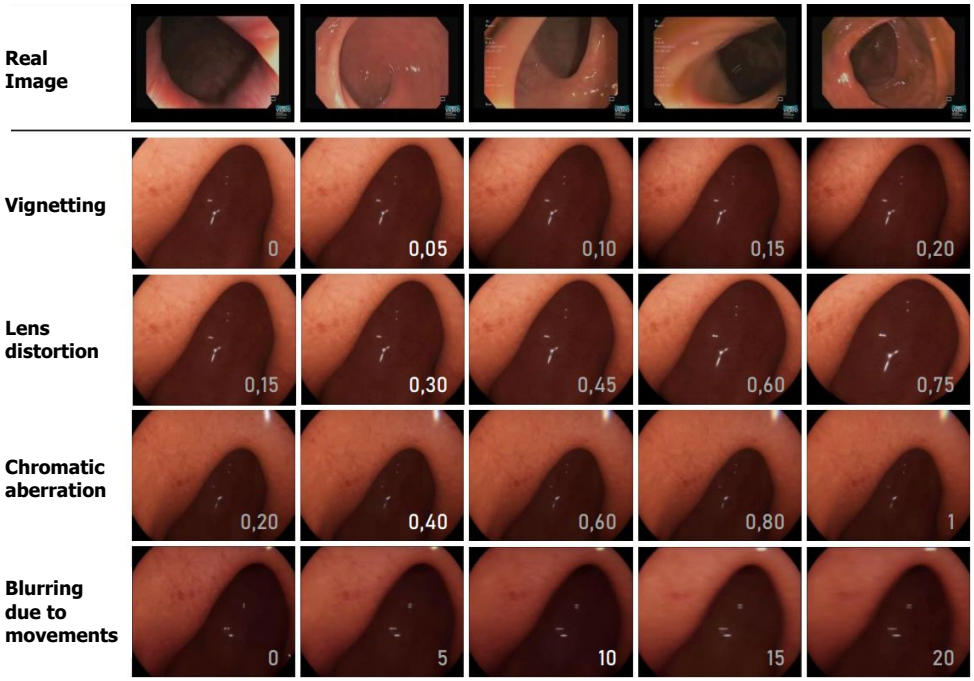

Figure 4.21. Comparison of the endoscopic images obtained by setting different intensities of each camera effect. The values chosen for each are marked in white.

4.4 Conclusions

This chapter presents the complete workflow followed to design a modular, flexible and open simulation platform of an intraluminal procedure. The specific simulator developed here replicates a robotic colonoscopy procedure. However, the same modular architecture can be adopted to simulate also other intraluminal scenarios. To this end, the anatomy, mechanical models and visual appearance will be changed in accordance to the procedure to replicate. In this case, the same workflow used to derive the different models (*i.e.,* 3D reconstruction of the organ, mechanical model, visual model *etc.)*, as well as the whole architecture can be adopted to create the new medical scenario.

Being open, the simulation platform allows to connect different interfaces, and implement a wide variety of additional modules related to both the medical procedure (*i.e.,* polyp removal, organ motility *etc.*) and to the robotic device including its HMI (*i.e.,* AR, haptic feedback *etc.*) In addition, the simulator allows to easily record different data related to the quality of the procedure, as better described in the next chapter. Doing so, it can be integrated in the *HMI evaluation framework* for analizing

and evaluating the performance of the users with the different HMI tested.

The simulator was clinically validated, as described in chapter 7. In addition, a complete user study testing the simulator as part of the *HMI evaluation framework* was conducted and is presented in chapter 8. Finally, the last part of this thesis, presents a new improved version of the simulator, including organ motility, *i.e.,* peristalsis and deformation of the colon due to air insufflation/suction.

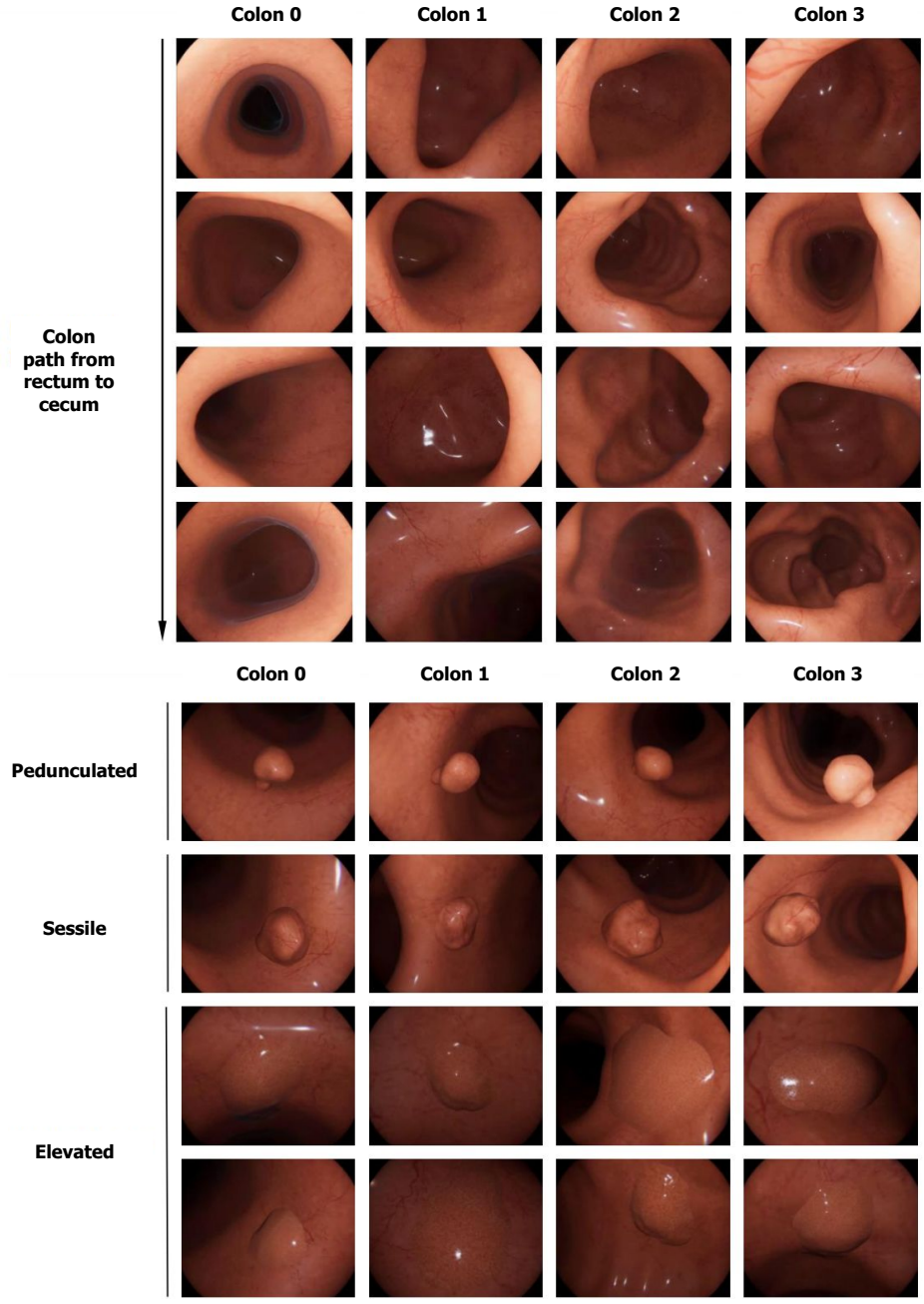

Figure 4.22. Snapshot from four different colon models.

CHAPTER 5

HMI oriented evaluation metrics

In order to compare the users' performances and experiences with the different HMI in the simulation environment, as part of the *HMI evaluation framework*, three types of data and metrics are recorded during and after the procedures:

- data correlated with the **clinical outcome** of the procedure (*e.g.,* percentage of total mucosa visualized during the withdrawal, force exerted on the mucosa during intubation, *etc.*);
- data related ewith the **cognitive and physical stress** experienced by the users (*e.g.,* gaze entropy, perceived mental demand *etc.*);
- data related with **the quality of control** of the endoscope with the HMI used (*e.g.,* smoothness of the trajectory, control intuitiveness *etc.*).

All the required information is collected through data recorded directly from the simulator, wearable sensors and questionnaires administered to the users before and after the experiments. The analysis of these metrics aims at providing objective and subjective measures about (1) the performances in the clinical scenario, (2) the quality of control (3) the *intuitiveness*, (4) the *user-friendliness*, and (5) the *ergonomicity* of the HMI tested. Based on this information, the overall quality of the HMI tested with the framework is assessed. The full list of objective metrics identified as relevant for the evaluation of the HMI, therefore included in the *HMI evaluation framework*, are reported in table 5.1. Additional metrics related to the subjective experience of the users with the HMI are collected with questionnaires.

All the execution data is collected from the simulation platform (20Hz) and the wearable sensors: eye tracking glasses (30Hz) and heart rate band (1Hz). The required multi-source data synchronisation is achieved with the *LSL* [129] and all data are stored into a single data base.

5.1 Clinical Performance

A list of relevant metrics correlated with the quality of the colonoscopy is derived during the simulated procedure (full list available in table 5.1). Indeed, during the

		Metric	Description
Clinical performances	Intubation	Time	Time spent to intubate the colon
		Lenght of trajectory	Length of the path followed by the endoscope during the intubation phase
		Deformation	Sum of the maximum deformation of all the elements of the mesh at any time step
	Withdrawal	Time	Time spent for the withdrawal of the endoscope
		Lenght of trajectory	Length of the path followed by the endoscope during the withdrawal phase
		% mucosa visualized	Percentage of mesh elements visualized during the withdrawal
Control	Fine movements	Time	Time spent for targeting the polyp from the first time it appears on the screen
		Error	Distance between the center of the target and the center of the polyp
	Overall	Fixations	Number of fixations of the device based on a dispersion-duration detection method (max dispersion = 3.0°, min time = 300ms)
		Rotations	Sum of 3D angles of rotation in absolute value
		Smoothness	Smoothness of the trajectory computed as the cumulative angular variation between consecutive segments of the spatial trajectories: $index_{smoothness} = \frac{1}{L}\sum_{i=1}^{L}\sum_{j=1}^{L}\Delta\alpha_j$ L = total number of segments of the trajectory; $\Delta\alpha_j$ = angular difference between two consecutive trajectory segments. * Lower values of the index → smoother trajectories
Physiological data	Gaze entropy	Intubation	Measure of the uncertainty over the gaze position at any point in time $H_g(X) = -\sum p(x,y)\cdot\log_2 p(x,y)$ p(x,y) is the probability that the gaze falls on a certain point of the screen
		Withdrawal	
		Whole procedure	
	Heart rate	Intubation	Heart rate mean
		Withdrawal	
		Whole procedure	

Table 5.1. List of all the objective metrics extracted from the simulation and from the wearable sensors to evaluate the HMI.

robotic colonoscopy, the clinician guides the robotic endoscope from the anal sphincter to the cecum (*i.e.,* intubation), minimizing the force exerted on the walls to avoid patients' pain and risks of generating lesions. Once reached the cecum, the endoscope is pulled back while carefully screening the whole mucosa to find any polyp or lesion (*i.e.,* withdrawal) [11]. Therefore, the extracted metrics are divided in these two phases, *i.e.*, (1) intubation, and (2) withdrawal. In the clinical practice, the time of withdrawal and Adenoma Detection Rate (ADR, percentage of time a clinician detects a precancerous polyp during screening colonoscopies) are the main objective metrics currently used to evaluate the quality of colonoscopy [141]. However, a simulated scenario allows to track more precise indicators of the performances. Therefore, during both, the intubation and the withdrawal, the total time and length of the trajectory is recorded. In addition, and only during the withdrawal phase, two specific metrics are obtained: the force exerted on the mucosa, obtained by summing the maximum deformation of the mesh at every time step; and the percentage of total mucosa visualized with the endoscope.

5.2 Quality of control

Besides the clinical outcome, the data recorded from the simulation are analysed to derive insights on the quality of control of the endoscope. The experiments reported in

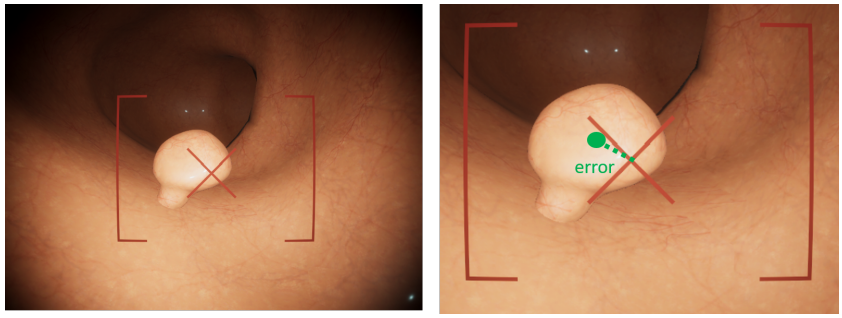

Figure 5.1. Targeting task: localise and focus each polyp in the middle of a superimposed marker (in the form of an X) over the endoscopic view. The right figure shows how the accuracy is computed: distance between the centre of the polyp and the centre of the marker.

this thesis included a polyp targeting task, which is a standard colonoscopy precision task during the withdrawal phase. Therefore, during the tests, the users were asked to localise and centre each polyp with a superimposed marker over the endoscopic view (*i.e.,* centring the marker represented with an X with the polyp). The performance is analysed in terms of time for completing the task and target focusing accuracy (*i.e.,* distance between the centre of the polyp and the marker, figure 5.1). In this way, the ability of performing fine movements with each interface device is evaluated.

In addition, the smoothness of the whole trajectory is computed as the cumulative angular variation between consecutive segments of the spatial trajectory (equation reported in table 5.1). Figure 5.2 shows the trajectories performed in the same colon with different levels of smoothness. Smoother trajectories are considered safer, in-

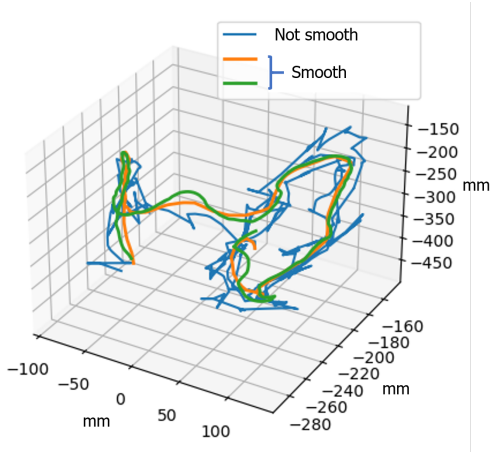

Figure 5.2. Example of trajectories on the same colon with different smoothness values

volving less risk of having the endoscope collide with the mucosa with brusque and uncontrolled movements which could cause perforations. Smooth trajectories are also a sign of positive and confident control over the endoscope through the controller device, therefore indicating a good relationship between the user and the interface itself. Finally, a more randomized path could indicate less proficiency and confidence in the tasks performed, having the user uncertainess about the direction to follow or the input control to provide to the endoscope.

Finally, the sum of rotations performed with the endoscope is also measured (*i.e.,* sum of 3D angles of rotation in absolute value). A high number of rotations made with the endoscope could be a sign of random exploration of the medical scene. This behaviour can be correlated with a failure of the user to master the procedure and/or the interface used.

5.3 Physiological data

Biometrical data is measured to objectively estimate the users' cognitive load during the execution of the trials (table 5.1). Accordingly, the mental stress imposed by each interface cannot be neglected when designing new human-machine interaction paradigms. From the analysis of the literature, the heart rate and gaze entropy represent a good combination for tracking mental overload [75, 142]. Indeed, studies have shown that the heart rate of surgeons increases during stressful tasks [143]. Similarly, the gaze entropy increases when the users perform more complex tasks [75], showing more random exploration patterns. Herein, the heart rate is measured with a Polar H10 chest strap (Polar, Kempele, Finland) at 1KHz, and its running average is transmitted via Bluetooth to the laptop at 1Hz with a dedicated program. The eyes movements are recorded at 30 Hz with a binocular wearable eye tracking glasses (Pupil Core, Pupil Labs GmbH, Berlin, Germany) [144]. Figure 5.3 shows the wearable sensors used to track the gaze entropy and the heart rate. Gaze entropy gives a measure of the average uncertainty over the direction of the gaze at an instant in time during the simulated tasks/procedures [145]. To compute the gaze entropy, the total visual field allowed by the eye tracker is divided into 80 x 54 degrees of visual angle (DVA), generating 4320 bins of 1x1 DVA. Gaze data with a confidence lower than 0.8 are discarded, following the *Pupil Labs* recommendations [146]. Therefore, the probabilities of the gaze falling on each bin is computed, and the gaze entropy is derived as in [75]. The gaze entropy is measured in bit and the formula to compute it is reported in table 5.1. Both gaze entropy and average heart rate are recorded for the whole procedure, and separately during the withdrawal and intubation phase. No reference value or normal range are provided for these measurements to be used as a threshold to determine when a state of cognitive overload has been reached. Most studies compare cognitive load in two or more situations. For this reason, the tracking of the cognitive load will always involve the comparison of two or more HMI.

The gaze analysis is also used to derive the number of fixations of specific parts of

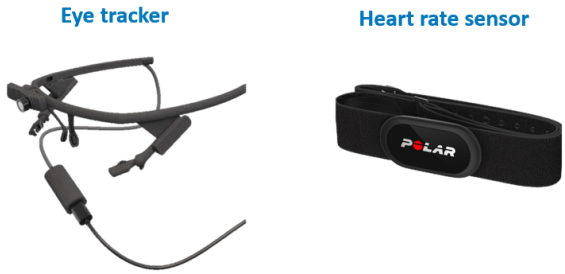

Figure 5.3. Wearable sensors used for tracking the cognitive laod: eye tracker and heart rate sensor

the HMI (*i.e.,* the controller device) [147, 148]. A fixation is counted when the gaze falls on a point of the controller for a minimum time of 300 ms [146]. The position of the controllers is constantly tracked during the procedure, using the *Pupil Labs Surface Tracking*. This plugin allows to define planar surfaces within the operational environment to track areas of interest. The surfaces to track (*e.g.,* controller device) are defined using printed Apriltag markers, which need to be placed in close proximity of the desired areas of interest.

5.4 Surveys

Three sets of questionnaires are used for the users' subjective evaluation of the HMI and the analysis of their usefulness/easiness. The first one, filled at the beginning of the experiments, examines the previous experience of the users concerning these aspects that can influence in the use of the HMI: (1) experience in colonoscopy, (2) experience with video games, simulators or musical instruments, and (3) level of tiredness at the moment of the experiments, *i.e.,* number of hours slept the night before the tests and the number of hours worked on the same day (full survey available in figure 5.4 - survey I). This information is relevant for the cognitive load analysis. The second set of questions investigates the subjective experience of the user with the HMI. Inspired by the NASA-Task Load Index [149] and the Borg rating of perceived exertion [150], the questions explore five different areas: (1) mental demand, (2) physical demand, (3) subjective impression on the own performance, (4) effort, (5) frustration. These questions are based on the Likert scale (1-5) and are administered right after having tested each HMI (figure 5.4 - survey II). As further explained in section 8, the order in which each HMI is tested is random. A final questionnaire is conceived to be delivered at the end of all the trials (having tested all the HMI in the study), and reviews the subjective mental and physical stress associated with each tested platform (figure 5.4 - survey III). In this way, the users are motivated to compare the HMI and provide a more informed opinion about their preferred one.

Survey I: administered at the beginning of the tests to collect general information on the subject.

1. Age	2. Sex	3. Dominant Hand		
4. Speciality:	○ Gastroenterologist	○ Colorectal surgeon	○ Others	
5. Education level:	○ Student	○ Resident	○ Specialist	○ Professor
6. Average number of colonoscopies performed in a week, during last 3 months			7. Years of experience in colonoscopy	
8. Do you usually play dynamic* videogames? (*shooters, races, sports simulators, etc. Non dynamic: puzzles or similar)				
9. Did you use to play dynamic* videogames? (*shooters, races, sports simulators, etc. Non dynamic: puzzles or similar)				
10. Have you ever used a simulator for colonoscopies before? If yes, which one?			11. Hours of sleep last night	
12. Average hours of sleep		13. Hours worked today	14. Average work shift length	

Survey II: administered after the test with each HMI.

Rate in a scale from 1 to 5 the following items	Scale	
	1 = very low	5 = very high
1 Easiness to control the movements of the endoscope	not easy	very easy
2 Intuitiveness of the input controls	not intuitive	very intuitive
3 Mental demand of the overall procedure	not demanding	very demanding
4 Mental demand of the mucosa visualization during the withdrawal phase	not demanding	very demanding
5 Mental demand of the navigation of the colon during the intubation phase	not demanding	very demanding
6 Mental demand of the targeting task	not demanding	very demanding
7 How insecure, discouraged, irritated, stressed and annoyed you were during the procedure	very low	very high
8 Physical demand of the procedure	not demanding	very demanding
9 Your success in performing what you were asked to do	not successful	very successful
10 How hard it was to achieve your level of performances	not hard	very hard
11 Satisfaction on your performances	not satisfied	very satisfied
Please, provide any additional comment to help us improve the platform		

Survey III: administered at the end of the tests (after having testes all the HMI).

Reply to the following questions	Answears	
1 Which HMI do you prefer? Why?	Videogame Joystick	Haptic device
2 Would you prefer it to the standard colonoscope handler? Why?	yes/maybe/no	
Rate in a scale from 1 to 5 the following items	Scale	
	1 = very low	5 = very high
3 Easiness to control the movements of the endoscope	not easy	very easy
4 Physical demand of the procedure	not demanding	very demanding
Please, provide any additional comment to help us improve the platform		

Figure 5.4. Surveys

5.5 Conclusions

This chapter describes four types of metrics to measure for the evaluation of *HMI* for robot-assisted intraluminal devices: (1) user's clinical performance, (2) user's quality of control of the endoscope, (3) user's cognitive and physical load and (4)

user's personal impressions. Herein, the metrics selected are optimized for a specific intraluminal procedure, *i.e.,* colonoscopy. This aspect is particularly true for the data related to the user's clinical performance during the medical procedure. Therefore, when evaluating interfaces for different intralumianl scenarios, some of these metrics might need to be changed and adjusted to the specific application. Other types of metric, *e.g.,* those related to the physical and mental load, can work for different scenarios without the need of modifications.

The set of metrics described in this chapter, together with the virtual simulator and the data collection and synchronization unit, represent the basic core of the *HMI evaluation framework*. Chapter 8 will describe the first user study conducted with the whole framework. In this case, all the metrics were measured from 42 clinicians in order to test two HMIs for teleoperated control in robotic colonoscopy. Therefore, chapter 8 will also report the analysis of the metrics and a discussion about their usefulness in defining the optimal interface.

Part III

Experiments and Results

CHAPTER 6

HMI screening Survey

A preliminary survey was conducted to perform a screening of all the HMI, and in particular the controller device, used for teleoperated control of robotic endoscopes. Its goal was:

1. understand the preferences of the final users (*i.e.,* endoscopists) in terms of features to be included in the HMI of robot-assisted colonoscopy devices;
2. select a set of device controllers with the most interesting features for the endoscopists to be tested with the *HMI evaluation framework*

To do so, all the controllers used for robotic intraluminal procedures were analyzed and their main features extracted [151]. Accordingly, a set of 38 questions were conceived to explore the main features of a HMI, with a special focus on the controller device. Therefore, the questions investigated four main areas: (1) type of control, (2) ergonomicity, (3) feedback modalities and (4) inclusion of autonomous/assistive tools.

6.1 Methods

A group of 71 endoscopists, both gastroenterologists and colorectal surgeons, with different levels of experience, filled an anonymous online survey comprising 38 questions [151]. The questionnaire required to rate with a 5-points Likert scale the level of agreement regarding the inclusion of several features on the next generation of HMI for robot-assisted colonoscopy. Therefore, the possible answers for each question could be "strongly disagree", " disagree", "neutral", "agree", "strongly agree". Figures 6.2 and 6.3 at the end of the chapter show the full survey. Explanatory graphics were provided to help understand the questions, which were conceived jointly by clinicians and engineers. The questions inquired about specific parts of each interface (*e.g.,* type of control, shape of the handler, presence of force feedback *etc.*). Each query was not directly linked to the controller itself to avoid biases and to allow participants not familiar with all the interfaces to give their valuable opinion. Consensus measure [152] was used to assess the dispersion of the clinicians' answers. Subjects' preferences were estimated comparing the distributions of the medians through the Wilcoxon signed rank test. Each test was considered significant for p-values < 0.05. The percentage of subjects agreeing with each statement was computed by summing all the *agree* and *strongly agree answers*.

In order to select the HMI to test with the *HMI evaluation framework*, four different controllers were evaluated. These controller devices were chosen as the ones most used for robot-assisted colonoscopy, and having configurations similar to most of the HMI used in the literature:

- haptic device with a spring-mass mechanism for the insertion/retraction and deflection/roll (proportional control), and extra functionalities controlled with the buttons on the controller;
- joypad using the two finger levers for insertion/retraction and deflection, and controlling the roll and the extra functionalities with buttons integrated into the controller;
- one-hand joystick for the control of all the movements of the endoscope and pedals for extra functionalities;
- 3D mouse enabling insertion/retraction by pressing the device inward/outward and extra functionalities by buttons.

See table 6.1 for better visualization of the mapping of DOFs in each controller and the related features. This classification covers most of the HMIs for robot-assisted colonoscopy presented in chapter 2. Indeed, each interface has similar features to one of the four options proposed. For instance, a controller like the touchpad has similar features to the videogame joypad. Sliders or buttons on the screen are used for controlling the insertion/retraction and deflection of the endoscope, and other buttons for activating the extra functionality. The ergonomy is slightly different but would imply still the use of two hands (no forearms), in particular two fingers, *i.e.,* two indices versus the thumbs used for the videogame joypad. For each HMI, a sum of all the scores obtained by a feature of the interface was computed. Scores were proportionally distributed between *absolutely disagree* = -2 and *absolutely agree* = 2, and summed for all the participants for each interface.

6.2 Results

Of the 71 participants, 80% were gastroenterologists, while the other 20% were colorectal surgeons. The clinicians had different levels of experience: 15% had less than 2 years, 58% had more than 10 years, and 27% were in the middle. The average consensus computed was 0.78 ± 0.04, indicating a high degree of agreement among the clinicians for each question. Figure 6.1 shows the distribution of answers, together with the p-values of the statistical significant tests. Accordingly, the subjects expressed their preference in controlling the endoscope with two hands without using pedals and activating the extra functionalities with buttons integrated in the controller. The clinicians prefer to control the insertion and retraction of the endoscope by moving a joystick placed on top of the controller with a thumb (up/down), instead of pushing/pulling a manipulator towards the monitor, pressing pedals, or

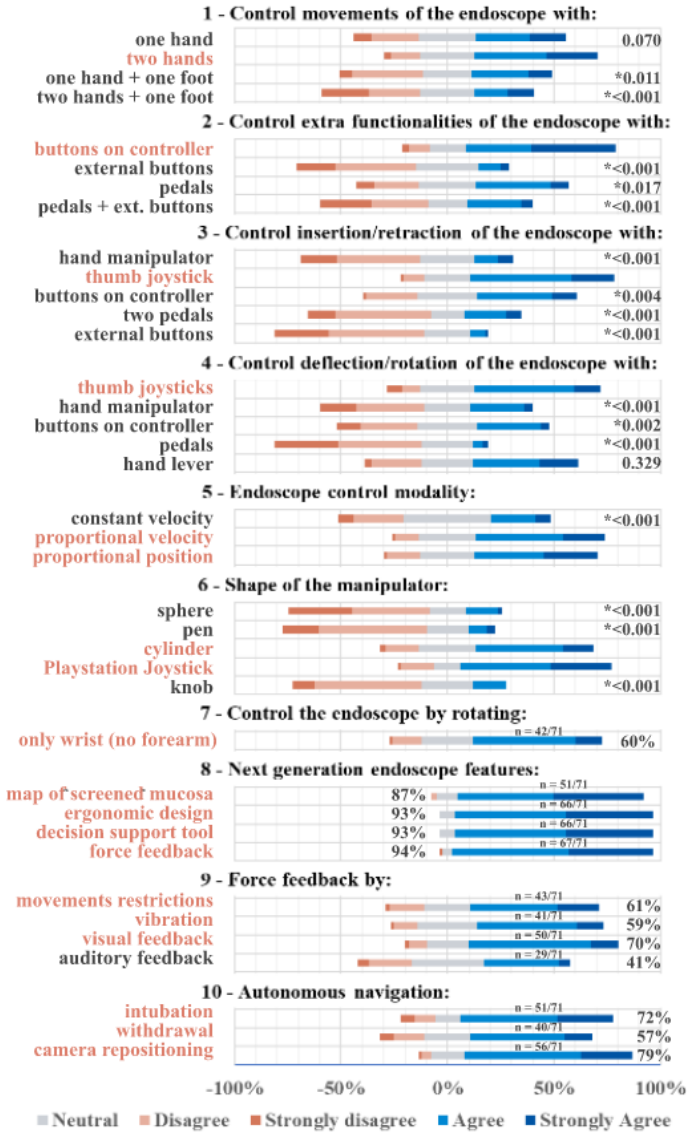

Figure 6.1. Summary of the questions and answers provided by 71 endoscopists using a 5-point Likert scale. From questions 1-6, the clinicians' preferred option is highlighted in pink, and the respective p-values (preferred option vs other option) of the Wilcoxon signed rank test are reported. For questions 7-10 the answers collecting a percentage of agreement (agree + strongly agree) $> 50\%$ are highlighted in pink. The number of subjects agreeing (n) and their percentage with respect to the total number of subjects interviewed is reported.

using buttons. Same preferences were expressed for controlling the deflection and rotation of the endoscope (*i.e.*, moving thumbs joystick up-down/right-left). Regarding the control strategy, similarly high rates were given to the proportional velocity control (*i.e.*, the velocity of the tip is proportional to the joystick displacement from its

			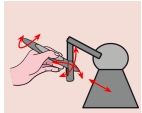		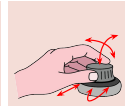
Control	Control movements of the endoscope	Two hands **+44**	One hand **+14**	One hand **+14**	One hand **+14**
	Control insertion/retraction of the endoscope	Move a lever placed on top of the controller with a thumb (up/down) **+53**	Push/pull the manipulator along a specific direction (in/out) **-34**	Press buttons integrated in the controller **+22**	Push/pull the manipulator along a specific direction (in/out) **-34**
	Control deflection/rotation of the tip of the endoscope	Move two levers placed on top of the controller with the thumbs (up/down - right/left) **+35**	Move a manipulator along its three main axes (up/down - right/left - in/out) and twist it **-23**	Move a lever along its two main axes (up/down - right/left) and rotate it around itself **+27**	Move a lever along its two main axes (up/down - right/left) and rotate it around itself **+27**
	Control of extra functionality	Buttons on the controller **+67**	Buttons on the controller **+67**	Pedals **+10**	External set of buttons **-40**
Ergonomy	Shape of the controller	Playstation style joypad **+57**	Cylindric device **+34**	Cylindric device **+34**	Knob **-39**
	Body parts involved in the control	Only wrist **+40**	Wrist and forearm **-40**	Wrist and forearm **-40**	Only wrist **+40**
Feedback	Modular force feedback	no **-93**	yes **+93**	no **-93**	no **-93**
	Type of force feedback	Vibration **+41**	Movement restriction **+43**	Vibration **+41**	Visual information **+51**
	Total	**+244**	**+154**	**+15**	**-74**

Table 6.1. Classification of the commercial controllers according to the preliminary survey. For each of the four configurations, and for each of the questions, the sum of the scores obtained is reported in blue (Likert scale where *absolutely disagree* is -2 and *absolutely agree is +2*). The joypad and the haptic device are the preferred controllers.

rest-position) and the proportional position control (*i.e.*, the whole deflection of the tip is proportionally mapped on the joystick range of motion), both p-value <0.001. The manipulator shape is preferred to be cylindrical or video game joypad style (*i.e.*, PlayStation® joystick style), and allowing manipulation by moving only the wrist, without involving the forearm. Force feedback (*e.g.*, to assist the navigation, provide contact forces, attract the camera towards important spots *etc.*) is highly requested (94%) either with haptic constrains (movement restriction and vibration) or with visual information. In addition, all the clinicians highly recommend the insertion of (1) optional autonomous navigation for intubation, withdrawal and tip repositioning, (2) an intelligent tool for decision support during the examination and diagnosis, and (3) a virtual map showing the parts of the mucosa not visualized during the screening. Finally, up to 93% of the clinicians interviewed agree on the need of a more ergonomic design with respect to the conventional colonoscope to reduce the physical load.

The result of the analysis shows that the characteristics of the joypad and the haptic devices are the most preferred by the users, collecting respectively +244 points and +154 points. Therefore, these two controllers were chosen to be tested with the *HMI evalutation framework*. Both the 3D mouse and the one-hand joystick were discarded because they reached low scores (-74, +15), and they were considered not worthy to test (figure 6.1). Indeed, the 3D mouse got a negative score while the hand cloche got +15 points (which is less than the 6% of the points collected by the joypad).

6.3 Discussion

Results show clear preferences of the clinicians for most of the questions, pointing the high consensus and the outcome of the statistical tests. Considering the inquiries related to the physical aspects of the HMI, the platform commercially available best fitting all the clinicians' desires are the videogame joypad style and the haptic device, which might increase the easiness of use of the controls and reduce the physical load. However, the information collected could also drive the design of new custom interfaces, best fitting all the requests. On the software side, clear interest has been shown in the adoption of intelligent tools assisting both navigation and decision making. Considering these results, the final interfaces chosen for the testing with the *HMI evaluation framework* are the videogame joypad and the haptic device with serial kinematics architecture.

1. I would control the endoscope movements using:

A - One hand
B - Two hands
C - One hand and one foot
D - Two hands and one foot

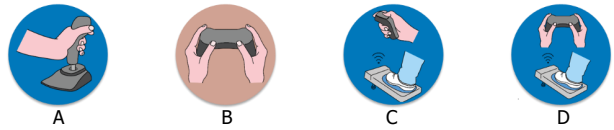

2. I would activate/deactivate the different functionalities (*e.g.* air insuflation) using:

A - Buttons on the controller
B - External set of buttons
C - Pedals
D - Pedals + external buttons

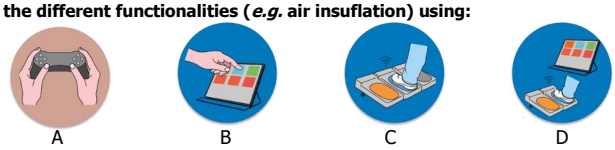

3. I would prefer to control the endoscope insertion/retraction by:

A - Pushing/pulling the manipulator towards the monitor (inwards/backwards)
B - Moving a joystick placed on top of the controller with a thumb (up/down)
C - Pressing two buttons placed on top of the controller (insertion/retraction)
D - Using two pedals
E - Pressing two buttons on an external interface

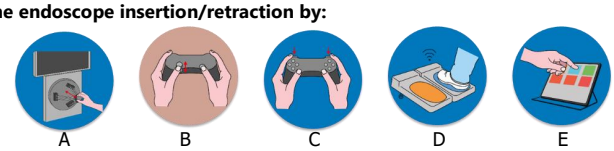

4. I would prefer to control the endoscope deflection and rotation by:

A - Moving two joysticks placed on top of the controller with the thumbs (up-down/right-left)
B - Moving the manipulator around two main axis (up-down/right-left) and rotating it
C - Pressing different buttons on the controller
D - Using only pedals
E - Moving a lever along its two main axes (up-down/right left) and rotating the manipulator around itself

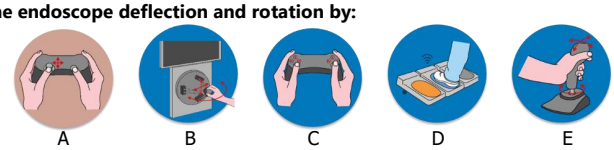

5. Imagine you are using a joystick to control the tip deflection. You would like that:

A - The velocity of the tip is constant when moving the joystick
B - The velocity of the tip is proportional to how much the joystick is moved from its rest-position (small movements give low rate, whereas large movements give higher rate)
C - The whole deflection of the tip is proportionally mapped on the joystick range of motion. When the joystick reaches its maximum range of motion, the tool tip reaches its maximum deflection as well

6. I would prefer the controller to have the shape of:

A - A sphere
B - A pen
C - A cylinder
D - A PlayStation style joystick
E - A knob

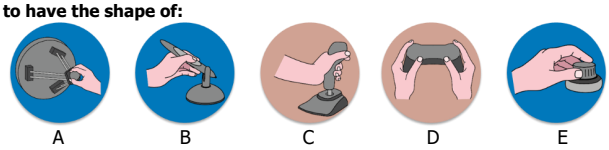

Figure 6.2. HMI screening survey (1/2), including the info-graphic provided to better understand the questions. Subjects were asked to rate on a 5-points Likert scale the level of agreement regarding the inclusion of each listed feature in the next generation of HMI for robot-assisted colonoscopy (from ”strongly disagree” to ”strongly agree”). The clinicians’ preferred option is highlighted in pink.

7. I would prefer to control the colonoscope by rotating only the wrist, instead of moving both the wrist and the forearm.

8. The next generation of colonoscope controller must be able to provide:
A - Virtual map showing the parts of the colon mucosa not visualized during the screening
B - More ergonomic design with respect to the standard colonoscope
C - Intelligent tools to support the clinician during the examination and diagnosis
D – Force feedback (*e.g.* assist navigation, provide contact forces, *etc.)*

8. The optimal way to convey the force feedback is:
A - Movements restriction
B - Vibration
C - Visual information
D - Auditive information

9. The procedure can benefit from a tool driving autonomously the colonoscope (considering that the navigation is totally safe, follows the same rules of an expert endoscopist, and can be activated and deactivated easily at any time) during:
A – Intubation
B – Withdrawal
C – Camera repositioning to a user desired spot

Figure 6.3. HMI screening survey, (2/2).

CHAPTER 7

Clinical validation of the simulator

An important aspect related to the introduction of any simulation platform in training programs, testing scenarios or more in general in the market, is their validation. In this regard, there are several studies that can be conducted to provide evidence of the performance of the simulators at different levels [86]. The first stage of assessment is the *face validity*, a type of study usually performed at the earliest phases of the development of the devices. In this context, a team of experts is asked to score the performances of the simulator in terms of ability to teach and evaluate what it is intended to teach and assess. Following, the *content validity* is a second subjective assessment in which experts evaluate the realism of the simulation with respect to the live one. In this case, each component of the simulator is analyzed in detail, and scored. Thirdly, the *construct validity* is performed to assess the ability of the device to discriminate the levels of expertise of the operators [86, 153].

This chapter describes the tests conducted to validate the use of the designed simulator of robotic colonoscopy for the *HMI evaluation framework*. Accordingly, *face* and *content validity* were assessed by 28 clinicians of two different hospitals in Italy and Spain.

7.1 Methods

The clinical validation of the simulation was assessed by a group of clinicians that took part to the first study case involving the *HMI evaluation framework*, described in chapter 8. All the participants had prior experience in colonoscopy: 28 subjects with an average of 10 years of experience in colonoscopy. The participants were asked to perform six simulated robotic colonoscopies: three controlling the endoscope with a Videogame Joypad, *i.e.,* DualShock 4 controller of PlayStation (Playstation, Tokyo, Japan) and three with the Haptic Device with serial architecture, *i.e.,* Touch (3D Systems, Rock Hill, South Carolina, USA). The first two medical procedures performed with each device were always the same (colon 0 and colon 1 of figure 7.1), whereas the last one was randomly assigned between two options (colon 2 or colon 3 of figure 7.1). Each experimental session took place in a dedicated training room (avoiding in-

terruptions and distractions during their execution) inside Hospital de la Santa Creu i Sant Pau (Barcelona, Spain) and A.O.U. Citta della Salute e della Scienza di Torino (Torino, Italy). Before starting the experiments, all the subjects were given the same clear instructions about the tasks to do: (1) perform a complete robotic colonoscopy starting from the rectum and reaching the cecum; (2) once reached the cecum, withdraw the endoscope looking for polyps; and (3) for each polyp found, take a picture by centring the lesion on a specific target (two brackets square on the side and a cross at the centre). A single experimental session lasted around 95 minutes. The subjects were allowed to take a short period of rest (less than 5 minutes) between subsequent experimental trials.

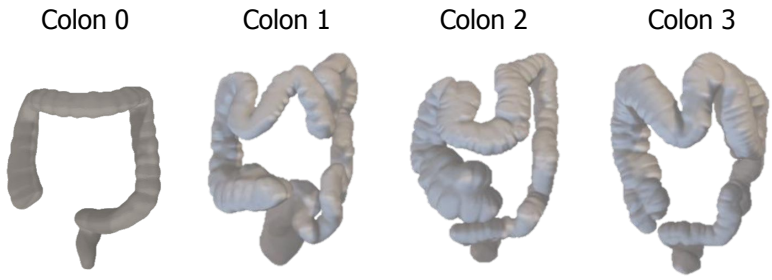

Figure 7.1. Colon models used for the clinical validation of the simulator

To evaluate *face* and *content validity*, at the end of the experimental session, the clinicians were asked to rate on a 5-points Likert scale the realism of different aspects of the simulation platform. Therefore, for each feature of the simulation, the possible subjects' rates were: "very unrealistic", "unrealistic", "neutral", "realistic", "very realistic". Figure 7.2 reports the full survey. The results were analyzed as follow: the consensus measure was used to assess the dispersion of the answers [152], whereas the mean value of each answer was used to assess the realism.

	Rate from 1 to 5 how realistic you think the following items are on the colonoscopy simulator	Scale 1 = very low	5 = very high
1	Overall simulation	very unrealistic	very realistic
2	Visual appearance of the internal view of the lumen	very unrealistic	very realistic
3	Endoscope illumination	very unrealistic	very realistic
4	Camera field of view	very unrealistic	very realistic
5	Visual appearance of polyps	very unrealistic	very realistic
6	Location of polyps	very unrealistic	very realistic
7	Colon anatomy	very unrealistic	very realistic
8	Colon deformation due to contact with the endoscope	very unrealistic	very realistic
Please, feel free to provide any further comment or suggestions			

Figure 7.2. Survey for the assessment of the face and content validity of the simulator.

Additionally, subjects' performances during the procedure in two colons with slightly different level of difficulty (colon 2 and colon 3 of figure 7.1) were compared. Indeed, colon 3 is longer than colon 2 (C2: 125 cm C3: 135 cm) and has more curvatures (sum of 3D angles of the trajectory: C2 = 48° and C3 = 63°), making the procedure slightly harder to perform. This evaluation was conducted to check whether a more difficult colon (*i.e.,* longer and more curved) implied significantly worse performances. To do so, the following metrics correlated with the outcome of the procedure, described in chapter 5, were measured: (1) time of intubation and (2) withdrawal, (3) length of trajectory of intubation and (4) withdrawal, (5) force exerted by the endoscope on the mucosa and (6) percentage of total mucosa visualized during the withdrawal phase, (7) time and (8) error of the polyps targeting task. The metrics measured in the two colons were compared by means of a separate unpaired Mann-Whitney U test. The test was considered statistically significant for p-values <0.05.

7.2 Results

Content and *face* validity were assessed by 28 clinicians, both gastroenterologists and colorectal surgeons. As shown in figure 7.3, all the questions got an average level of satisfaction ≥ 3 over 5. With a consensus always higher than 0.8, the survey shows a high level of agreement between the clinicians for each question. Further validation of the realism of the simulator was given by the fact that the performances on colon

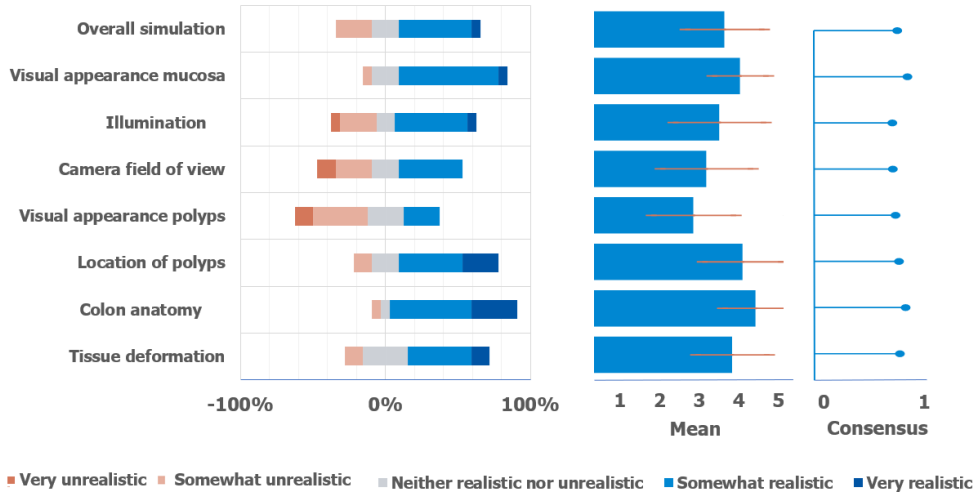

Figure 7.3. Content and phase validity of the virtual simulator. Distribution of the answers provided by 28 clinicians using the Likert scale (left), average score and standard deviation (centre), and consensus (right)

2 and colon 3 differed statistically. This was reflected in most of the clinical metrics, which got worse results in colon 3 (the most complex scenario). Figure 7.4 shows the boxplots of the metrics recorded in the two colons, whereas table 7.1 reports the mean values of each metrics and the p-values of the statistical tests. Accordingly, the time of intubation (C2: 1.5 ± 0.5 min vs. C3: 1.9 ± 0.6 min, p-value = 0.032) and withdrawal (C2: 4.5 ±1.8 min vs. C3: 6.0 ± 2.0 min, p-value = 0.001) were longer in C3 with respect to C2, the cumulative deformation of the intestinal walls was higher (C2: 2.6 ± 1.4 m vs. C3: 5.9 ± 1.4 m, p-value < 0.001), the trajectory of the withdrawal was longer (C2: 1.8 ± 0.4 m vs. C3: 2.1 ± 0.5 m, p-value < 0.001), the percentage of mucosa visualized was lower (C2: 75 ±6 % vs. C3: 68 ±7 %, p-value < 0.001) and the time to perform the targeting task was longer (C2: 9.3 ±3.8 s vs. C3: 11.8 ± 5.9 s, p-value = 0.039).

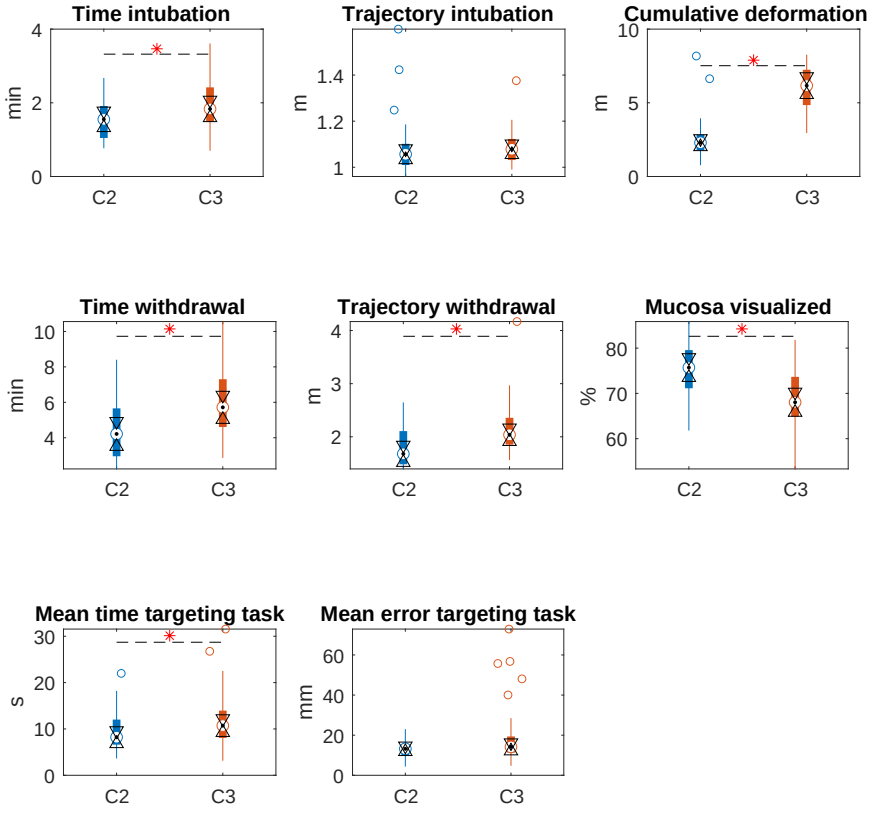

Figure 7.4. Boxplots of the metrics recorded during the validation experiments for colon 2 (C2) and colon 3 (C3). Statistical significance on the Mann-Whitney test is highlighted with the star (p-value < 0.05). The circle with the black point inside represents the median, with its confidence interval represented by the two triangles.

	Clinical performances						Control	
	Intubation			Withdrawal			Fine movements	
	Time [min]	Trajectory [m]	Deformation [m]	Time [min]	Trajectory [m]	Mucosa visualized [%]	Time [s]	Error [mm]
C2	1.57(0.54)	1.08(0.13)	2.56(1.41)	4.51(1.82)	1.81(0.38)	75.10(5.80)	9.35(3.84)	12.86(4.47)
C3	1.91(0.65)	1.09(0.08)	5.95(1.44)	6.02(1.97)	2.15(0.47)	68.44(7.34)	11.84(5.87)	19.60(15.35)
p-value	0,0318	0,1519	<0.001	0,0013	<0.001	<0.001	0,0389	0,0826

Table 7.1. Means and standard deviations of the metrics recorded during the validation experiments for colon 2 and colon 3 (C2 and C3). The last row shows the p-values of the unpaired Mann-Whitney test comparing the distributions of the medians between the two colons. Values < 0.05 are considered statistically significant and are highlighted in orange.

7.3 Discussion

Both *content* and *face* validity were assessed by 28 endoscopists with prior experience in colonoscopy. The construct validity of the robotic colonoscopy simulator could not be assessed due to the fact that there are not experts in robotic colonoscopy (all colonoscopic procedures are currently executed by manually handled colonoscopes). In consequence, experts in manual colonoscopy cannot be considered as experts in robotic colonoscopy. This hypothesis was also confirmed during the case study (chapter 8), in which no significant difference in terms of performance metrics was detected between novices and experts. This suggests that the use of two user-friendly interfaces and the easing of the procedure given by the control of a robotic device decreases the performance gap between experts and novices. However, an additional validation of the simulator was given by the fact that the metrics for all participants in the most complex procedures worsened.

CHAPTER 8

Case Study

Once the *HMI evaluation framework* was developed, and its most important piece, *i.e.,* virtual simulator, was clinically validated, a first case study for the evaluation of HMI was set-up. The *HMI evaluation framework* was tested for the first time by comparing two different teleoperated control modalities of the robotic endoscope. The experiments were designed to answer the following question: *which is the optimal controller for robot-assisted colonoscopy, i.e., the one minimizing the users' cognitive load and maximizing the outcome of the procedure?*

Although there are few examples in the literature of robotic devices driven by standard endoscope controllers [12], most of the innovative intraluminal systems introduce new control interfaces [15, 16, 40, 46, 48, 49]. These include both the physical manipulator and the system used to map the DOFs between the handler and the endoscope. Focusing on only the commercial controllers, the most used are: (1) thumb-driven videogame joypads, *i.e.*, DualShock 4 controller of PlayStation (Playstation, Tokyo, Japan); (2) haptic devices with serial architecture, *i.e.*, Touch (3D Systems, Rock Hill, South Carolina, USA); (3) 3D mouse-like interfaces, *i.e.*, 3Dconnexion SpaceMouse (3DConnexion, Munich, Germany); (4) hand joysticks with a cloche (different brands); and (5) Omega x haptic device with parallel architecture (Force Dimension, Nyon, Switzerland).

As a result of the *HMI evaluation survey* described in chapter 6, two controller devices were selected for the comparison with the *HMI evaluation framework*: the Video game Joypad (VJ), *i.e.,* DualShock 4 controller of PlayStation (Playstation, Tokyo, Japan) and Haptic Device (HD) with serial architecture, *i.e.,* Touch (3D Systems, Rock Hill, South Carolina, USA).

8.1 Generation of the virtual scenarios

To test and compare the HMI, it is important to balance the level of difficulty among the different simulated colonoscopy procedures involved in the experiments. The level of difficulty of the navigation and withdrawal tasks depend on the number of curves and length of the colon, whereas for the polyp detection/targeting task it follows the rules reported section 4.3.3, *i.e.,* location and type of lesion. In addition, it is also important to introduce some randomness to the order in which the polyps appear in each colon. In this way, the learning effects of the polyp location is minimized. Therefore,

to setup the experiments, three colon anatomies with similar level of difficulty, and one simplified colon, were selected. The simplified colon, as will be described later, serves to familiarize the user with the procedure. The polyps were placed in the colons in order to have one polyp for each level of difficulty as described in section 4.3.3 (total of four polyps for each colon). Figure 4.13 shows the four colon anatomies and the type and location of polyps inserted in each model based on on how difficult is their detection. The design choices described in this section were made in collaboration with two expert endoscopists (each one with more than 20 years experience).

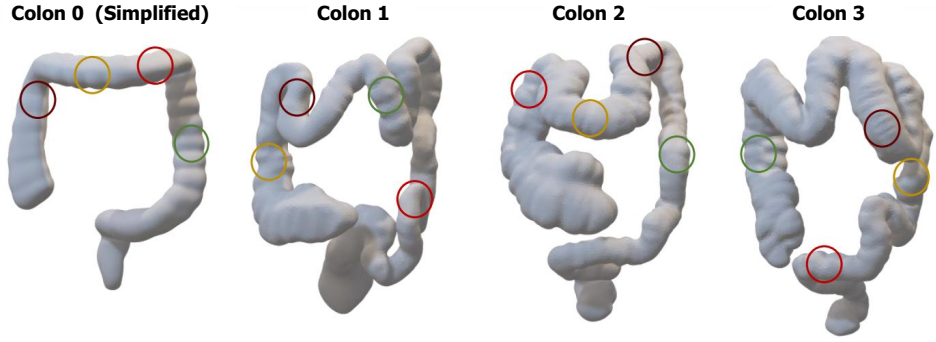

Figure 8.1. Colonoscopy cases administered to the endoscopists during the study case. The circles shows the location of the polyps with different levels of difficulty: easy (green), medium (yellow), difficult (red) and very difficult (brown)

8.2 Subjects, experimental design and procedure

A total of 42 endoscopists were enrolled for the experiments: 20 novices (less than 1 year of experience with colonoscopy) and 22 experts (more than 1 year of experience with colonoscopy). Considering the speciality, 21 were colorectal surgeons and 21 gastrointestinal endoscopists. The participants were asked to perform six simulated colonoscopies: three with one device (VJ, *i.e.,* DualShock 4 controller of PlayStation (Playstation, Tokyo, Japan)) and three with the other one (HD, *i.e.,* Touch (3D Systems, Rock Hill, South Carolina, USA)). The study followed a 2X2 mixed factorial design, considering (1) the two levels of experience in colonoscopy (novices vs. experts) and (2) the two devices (HD vs. VJ). For each device, the first two procedures were used as training phase, while the last one was considered as a valid trial (see figure 8.2). The training was performed always with the same two colons (figure 8.1: C0, C1), while the two testing trials were conducted with two different colons (C2 and C3). Potential practice/learning effects on the medical procedure were controlled by a Latin square design across (1) the device and (2) the colon used for the trial.

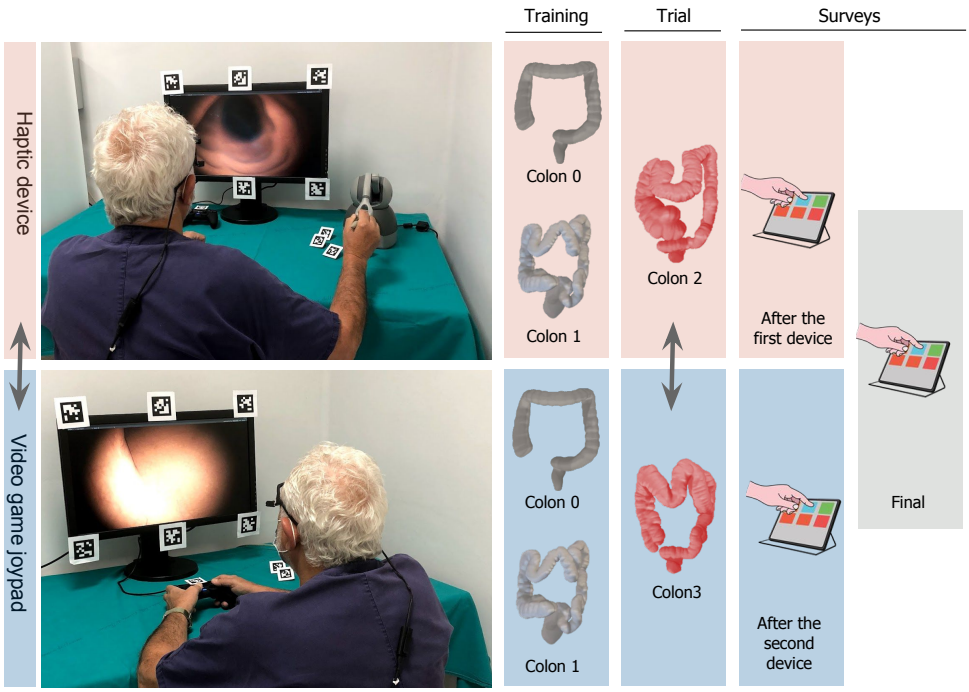

Figure 8.2. Experimental design: the users were required to perform three colonoscopies for each device: the first two procedures were for training, whereas the final one was the test. Surveys were administered after each trial and at the end of the whole experiment.

Therefore, (1) half of the participants started with the VJ and the other half with the HD), and (2) half of the participants performed the trial with the VJ in C2 and the trial with the HD in C3, while the second half followed the opposite sequence. This balance was ensured also among each group with the same level of experience, *i.e.,* novices and experts. Thus, the possible effects of confounding factors, including learning of series effects, and task-switching costs (*i.e.,* the costs associated with going from a complex task to an easy one) were minimized. In addition, the two training procedures before the trial ensure that all the subjects have the same level of experience with the simulator. Each experimental session took place in a dedicated training room inside Hospital de la Santa Creu i Sant Pau (Barcelona, Spain) and A.O.U. Citta della Salute e della Scienza di Torino (Torino, Italy). Before starting the experiments, all the subjects were given the same clear instructions about the tasks to do: (1) perform a complete colonoscopy starting from the rectum and reaching the cecum; (2) once reached the cecum, withdraw the endoscope looking for polyps; and (3) for each polyp found, take a picture by centring the lesion on a specific target (two brackets square on the side and a cross at the centre).

A single experimental session lasted around 95 minutes. The subjects were allowed

to take a short period of rest (less than 5 minutes) between subsequent experimental trials. Special care was dedicated to avoid any distraction that could interfere with the users' performance and mental stress (*i.e.,* silence, removal of mobile phones/smart watches or any source of notifications, stable light, forbidden entrance to any external person in the room). Surveys, described in section 5.4 and reported in figure 5.4 were administered at the beginning of the tests (survey I), after each trial (survey II) and at the end of the whole experiment (survey III). The experimental setup is available in figure 8.3).

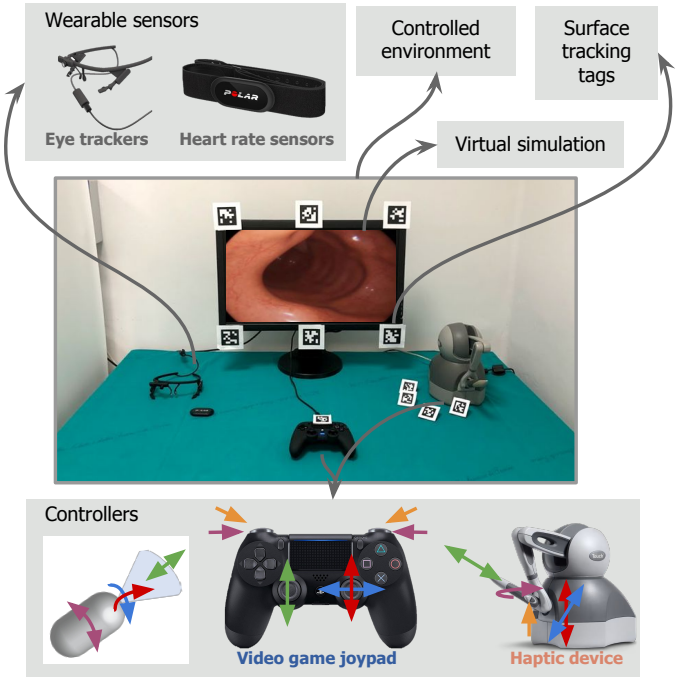

Figure 8.3. Experimental setup: the experiments were performed in a controlled environment (no external disturbances), using the colonoscopy virtual simulator, the eye trackers and chest band to track the cognitive load, and the two controllers: haptic device with serial architecture and video game joystick. The mapping of the degrees of freedom between the controllers and endoscope is shown at the bottom-left, where the yellow arrows represent the extra function of activating/deactivating the polyp target for the targeting task.

8.3 Data collection and analysis

All the data and metrics described in chapter 5 were collected from the surveys, the simulation platform (described in chapter 4, and the wearable sensors. Setup of the eye tracking systems, including the calibrations, and of the heart rate chest band preceded the start of the experiment. To analyze the effect of the device on the clinicians' performances, a series of separate unpaired Mann-Whitney U tests were conducted comparing the distribution of the medians for each metric between the two devices (HD vs. VJ) for (1) all the subjects, (2) only novices and (3) only experts. In addition, considering that one of the two colons used for the trials (C2) resulted to be slightly more difficult to navigate (longer and with more curves than C3), the tests were conducted also for each colon used in the trial: (4) all subjects, (5) novices and (6) experts in colon C2, and (7) all subjects, (8) novices and (9) experts in colon C3. Concerning the analysis of the surveys and the physiological data, a series of paired Mann-Whitney U tests were run, comparing the distributions of the differences of each subject's metric/answer for the two devices: VJ vs. HD for (1) all participants, (2) only novices and (3) only experts. Consensus measure as computed in [152] was used to assess the dispersion of the clinicians' answers to the questionnaires. Each test was considered significant for p-values < 0.05.

		Metric	VJ	HD
Clinical performances		% mucosa visualized	C3 N/All	
Control	**Fine**	Error	C3 E/All	
	Overall	Smoothness		All C N/All C3 N/E/All
		Fixations	All C N/E/All C3 N/All	
Physiological data	**Gaze entropy**	Withdrawal	N/All	
		Whole procedure	N/All	
	Heart rate	Intubation	E/All	
		Whole procedure	E/All	
Survey	**Mental demand**	5.Intubation		E/All
		9. Success		E
		10. Difficulty		All
		8. Physical demand	N/E/All	
Final survey		13. Physical demand	N/E/All	

Table 8.1. Summary of the metrics in which a statistical difference was found between the two devices during the case study: Videogame Joypad (VJ) vs. Haptic Device (HD). For each metric, the coloured cell under one of the two devices (blue for VJ and green for HD) shows that it performed statistically better than the other. The specific condition in which the statistical difference was found is reported inside each coloured cell (C: colon, N: novices, E: experts, All: both experts and novices, *e.g.,* novices performed statistically better in terms of percentage of mucosa visualized in colon 3 with the VJ with respect to the HD

8.4 Results

Of the 42 subjects that performed the experiments, 5 were discarded. Among them, 4 participants could not successfully complete one of the two trials, whereas for one subject there was a system failure during the collection of the data. The analysis shows that both of the interfaces selected (HD and VJ) represent a valuable solution for teleoperated control of a robotic colonoscope. However, few differences were detected between the two options, making the VJ the best option for teleoperated control of a robotic colonoscope. Indeed, the VJ (1) enabled better clinical performances (higher percentage of mucosa visualized in C3, the most complex colon to examine),

			All colons			Colon 2			Colon 3			Colon 2 vs Colon 3		
		Metric	Experts	Novices	All	Experts	Novices	All	Experts	Novices	All	Experts	Novices	All
Clinical performances	Intubation	Time	0,6168	0,8095	0,9311	0,7040	0,4079	0,8861	0,3233	0,2370	0,8143	0,3942	0,0473	0,0318
		Trajectory	0,7764	0,3015	0,6971	0,1106	0,2991	0,4354	0,0575	0,6334	0,0782	0,2184	0,5011	0,1519
		Deformation	0,5792	0,8633	0,6190	0,8792	1,0000	0,8610	0,7612	0,3154	0,5571	<0.001	<0.001	<0.001
	Withdrawal	Time	0,5609	0,2025	0,1801	0,0946	0,6065	0,0721	0,4941	0,1457	0,5184	0,1136	0,0068	0,0013
		Trajectory	0,9246	0,6794	0,7294	0,6485	0,3510	0,3316	0,7612	0,2031	0,2774	0,0155	0,0055	<0.001
		% mucosa visualized	0,1719	0,1579	1,0000	0,0946	0,4698	0,0625	0,9394	0,0021	0,0321	0,0011	0,0181	<0.001
Control	Fine movements	Time	0,6359	0,1386	0,1415	0,4941	0,3510	0,1760	0,9394	0,1728	0,2402	0,2977	0,0701	0,0389
		Error	0,2853	0,9451	0,5378	0,4474	0,6806	0,6444	0,0078	0,8286	0,0886	0,0720	0,4794	0,0826
	Overall	Fixations	0,0398	0,0093	<0.001	0,2665	0,1972	0,0685	0,2122	0,0133	0,0069	0,0503	0,2989	0,4949
		Rotations	0,5075	0,3179	0,2178	0,8197	0,3510	0,3642	0,1965	0,0085	0,0044	0,0098	0,0049	<0.001
		Smoothness	0,0962	0,0108	0,0051	0,0122	0,0311	0,0026	0,6485	0,1457	0,4453	0,1075	0,2206	0,0718
Physiological data	Gaze entropy	Intubation	0,5217	0,8900	0,6120							0,6742	0,0654	0,3542
		Withdrawal	0,3884	0,0110	0,0166							0,7285	0,6322	0,6247
		Whole procedure	0,5958	0,0079	0,0275							0,9854	0,4037	0,5601
	Heart rate	Intubation	0,0108	0,0479	<0.001							0,6226	0,8077	0,6088
		Withdrawal	0,1447	0,3303	0,0669							0,8288	1,0000	0,8739
		Whole procedure	0,0323	0,1876	0,0069							0,9217	0,9032	0,8462
Survey after tests		1. Easiness	0,4653	0,6279	0,8112									
		2. Intuitiveness	0,0551	0,6592	0,3264									
	Mental Demand	3. Overall	0,0963	0,4117	0,6251									
		4. Withdrawal	1,0000	0,2188	0,3938									
		5.Intubation	0,0165	0,6719	0,0152									
		6. Fine movements	0,6172	0,4824	0,3257									
		7. Insecureness, etc.	0,4117	0,9844	0,3961									
		8. Physical demand	0,0225	0,0225	<0.001									
		9. Success	0,0352	1,0000	0,1762									
		10. Difficulty	0,1565	0,1855	0,0275									
		11. Satisfaction	0,1289	0,5898	0,5324									
Final survey		12. Easiness	0,2958	0,2103	1,0000									
		13. Physical demand	0,0046	0,0039	<0.001									

Table 8.2. P-values of the unpaired and paired Mann-Whitney test comparing the distributions of the medians for each data collected between the two HMI (haptic device vs. videogame joypad) and the two colons (colon2 vs. colon 3). The paired test was used to compare the physiological data and the results of the surveys, whereas the unpaired test was used for the clinical performances and the quality of control. Values < 0.05 are considered statistically significant and are highlighted in orange. The first three columns (All colons, Colon 2 and Colon 3) refers to the comparison between the two HMI, whereas the last column refers to the comparison of the metrics between the two colons.

(2) facilitated the control (lower error in the targeting task in C3), (3) was objectively more user-friendly (less fixations, lower gaze entropy and mean heart rate) and (4) less physically demanding (expressed through the survey). Nevertheless, the HD (1) provided smoother trajectories and (2) was perceived as more user-friendly and intuitive by the users (rated in the survey as less difficult to use, less mentally demanding for the withdrawal phase and enabling better performances). In addition, (3) the majority of the users preferred the HD with respect to the VJ, especially among the experts, as expressed in the final questionnaire. A summary of the overall results is shown in table 8.1, whereas the results of the survey are presented in figure 8.4. All the p-values of the statistical tests are reported in table 8.2, the respective box plots in figure 8.5 and figure 8.6), and the mean and standard deviations of each data recorded in table 8.3 and table 8.4.

			Clinical performances						Control				
			Intubation			Withdrawal			Fine movements		Overall		
			Time [min]	Trajectory [m]	Deformation [m]	Time [min]	Trajectory [m]	Mucosa visualized [%]	Time [s]	Error [mm]	Fixations [n]	Rotations [rad]	Smoothness
All colons	E	HD	1.78(0.70)	1.09(0.14)	4.73(2.23)	5.37(2.28)	2.10(0.64)	71.21(6.19)	9.60(2.88)	14.44(5.06)	24.00(63.77)	240.12(76.38)	47.13(28.85)
		VJ	1.67(0.45)	1.06(0.07)	4.30(2.30)	5.79(1.99)	1.99(0.37)	73.99(7.19)	10.45(4.07)	22.04(15.56)	33.55(50.62)	221.35(59.67)	34.82(26.06)
	N	HD	1.71(0.58)	1.09(0.09)	4.04(2.04)	4.54(1.78)	1.94(0.42)	72.23(6.69)	10.14(6.22)	12.68(5.98)	7.35(18.41)	249.39(124.39)	77.32(31.64)
		VJ	1.83(0.76)	1.11(0.10)	4.07(2.41)	5.34(1.96)	1.88(0.34)	68.97(9.07)	12.54(6.74)	15.46(15.07)	28.76(35.50)	195.09(54.80)	47.31(30.27)
	All	HD	1.74(0.64)	1.09(0.12)	4.41(2.14)	4.99(2.08)	2.03(0.55)	71.68(6.36)	9.85(4.65)	13.63(5.49)	16.35(48.66)	244.38(99.89)	61.00(33.42)
		VJ	1.75(0.61)	1.09(0.09)	4.19(2.32)	5.58(1.96)	1.94(0.36)	71.68(8.39)	11.41(5.48)	19.02(15.48)	31.35(43.80)	209.28(58.22)	40.56(28.38)
Colon 2	E	HD	1.58(0.59)	1.13(0.19)	2.96(1.60)	4.12(1.99)	1.83(0.43)	73.63(5.09)	8.64(3.09)	14.41(5.37)	48.11(91.55)	194.01(50.60)	49.84(30.49)
		VJ	1.65(0.55)	1.03(0.06)	2.85(1.92)	5.61(1.78)	1.89(0.40)	78.03(4.74)	10.58(4.53)	13.46(4.99)	41.09(58.73)	208.07(63.35)	23.85(21.04)
	N	HD	1.61(0.49)	1.06(0.05)	2.21(0.74)	3.69(1.00)	1.63(0.30)	72.55(4.29)	7.87(2.83)	10.62(4.54)	2.43(4.39)	156.97(32.32)	71.09(25.32)
		VJ	1.45(0.61)	1.12(0.13)	2.08(0.68)	4.19(1.80)	1.81(0.38)	74.97(7.70)	9.73(4.33)	12.32(2.05)	18.56(26.25)	192.13(72.26)	38.92(27.68)
	All	HD	1.59(0.53)	1.10(0.15)	2.63(1.32)	3.93(1.60)	1.74(0.38)	73.16(4.63)	8.30(2.91)	12.75(5.24)	28.12(70.89)	177.81(46.30)	59.14(29.51)
		VJ	1.56(0.57)	1.07(0.10)	2.50(1.51)	4.97(1.89)	1.86(0.38)	76.65(6.26)	10.20(4.34)	12.95(3.90)	30.95(47.30)	200.90(66.16)	30.63(24.79)
		All	1.57(0.54)	1.08(0.13)	2.56(1.41)	4.51(1.82)	1.81(0.38)	75.10(5.80)	9.35(3.84)	12.86(4.47)	29.69(58.06)	190.64(58.57)	43.30(30.22)
Colon 3	E	HD	1.94(0.76)	1.05(0.05)	6.18(1.50)	6.39(2.05)	2.32(0.71)	69.23(6.53)	10.38(2.58)	14.46(5.05)	4.27(8.37)	277.85(74.55)	44.92(28.74)
		VJ	1.71(0.33)	1.10(0.07)	6.06(1.25)	6.00(2.31)	2.10(0.32)	69.06(6.72)	10.28(3.69)	32.53(17.87)	24.33(40.02)	237.57(53.87)	48.24(26.30)
	N	HD	1.77(0.66)	1.11(0.11)	5.33(1.61)	5.14(2.00)	2.16(0.35)	72.01(8.19)	11.73(7.52)	14.12(6.65)	10.80(23.62)	314.09(124.57)	81.68(36.06)
		VJ	2.26(0.71)	1.10(0.06)	6.31(1.37)	6.63(1.20)	1.95(0.29)	62.22(4.68)	15.70(7.79)	18.99(22.07)	40.25(42.53)	198.41(29.52)	56.74(32.05)
	All	HD	1.86(0.70)	1.08(0.08)	5.77(1.58)	5.79(2.08)	2.24(0.56)	70.55(7.32)	11.03(5.41)	14.30(5.71)	7.38(17.24)	295.10(100.53)	62.42(36.77)
		VJ	1.97(0.60)	1.10(0.06)	6.17(1.27)	6.30(1.84)	2.03(0.31)	65.84(6.68)	12.84(6.42)	26.15(20.53)	31.82(40.73)	219.14(47.31)	52.24(28.54)
		All	1.91(0.65)	1.09(0.08)	5.95(1.44)	6.02(1.97)	2.15(0.47)	68.44(7.34)	11.84(5.87)	19.60(15.35)	18.32(32.09)	261.12(88.86)	57.87(33.31)

Table 8.3. Means and standard deviations of the metrics recorded during the experiments for each controller device, type of colon and clinical expertise. Controller device - HD: haptic device, VJ: videogame joypad, all: both devices; type of colon - colon 1, colon2, all colons; clinical expertise - E: experts, N: novices, all: all participants.

8.4.1 Clinical Performances

During the intubation phase, no statistical significance was detected between the two devices. However, in the withdrawal phase, the clinicians performed better with the VJ in the most complex colon (*i.e.,* C3) having a higher percentage of mucosa visualized then with the HD (mean values for novices: 72 % vs. 62 %, and for all groups: 71 % vs. 66 %, p-value < 0.05). The percentage of mucosa visualized during the withdrawal as well as the cumulative deformation of the colon walls during the

intubation phase are considered the most important metrics to evaluate the quality of the clinical performances. Indeed, to maximize the diagnostic outcome of the colonoscopy, the mucosa visualized should be 100%. Whereas the force exerted on the walls should be minimized to avoid any discomfort for the patient and risk of lesions.

8.4.2 Precision movements control

The polyp targeting task showed that the VJ is slightly more precise than the HD, achieving lower mean errors in C3 (for experts: 14 mm vs. 33 mm and all participants: 14 mm vs 26 mm, p-values < 0.05). However, clinicians did not feel a difference in the difficulty of performing the required fine movements with the two devices (figure 8.4). Whereas, the results of the smoothness metric suggest that the HD enables smoother trajectories (All colon mean values for novices: 47 vs. 77, and all participants: 40 vs. 61; in C2 mean values for experts: 24 vs. 50, for novices: 39 vs. 71 and for all participants: 31 vs. 59; p-values < 0.05. Lower values of the index means higher smoothness levels).

8.4.3 Intuitiveness

No statistical differences were detected in the questions regarding the intuitiveness of the devices (figure 8.4). However, 11 of the 21 clinicians that preferred the HD device said it was due to its intuitiveness "feeling as they had the tip of the endoscope in their hand". In contrast, only 4 clinicians claimed they preferred the VJ for its intuitiveness. All of them have had previous experience with the VJ playing at video games, therefore feeling more familiar with it.

8.4.4 User-friendliness

The number of fixations of the HD was higher than the VJ suggesting that the HD was less easy-to-use, and required more visual supervision (mean values in all C for experts: 23 vs. 34, novices 7 vs. 29, and all participants 16 vs. 31; in C3 for novices: 10 vs. 40 and all participants: 7 vs. 31; p-values < 0.05). All the clinicians felt the HD was easier to use (Q10 Survey II, p-value < 0.05 for all participants) and less mentally loading in the intubation phase (Q5 Survey II, p-values < 0.05 for experts and all participants). However, these results were not confirmed by the final questionnaire in which both the devices were overall rated as they implied the same difficulty level. Additionally, the experts felt to be more successful with the HD (Q9 Survey II, p-value < 0.05 for experts) despite the clinical performances do not reflect this impression (figure 8.4). Regarding the objective measure of the cognitive load, both the gaze entropy and the heart rate suggest that the VJ is less cognitively stressful (figure 8.6, table 8.4 and 8.2). For the gaze entropy, the VJ implied an average reduction of 0.3 bit for novices and 0.2 bit for all participants during the withdrawal, and 0.3 bit

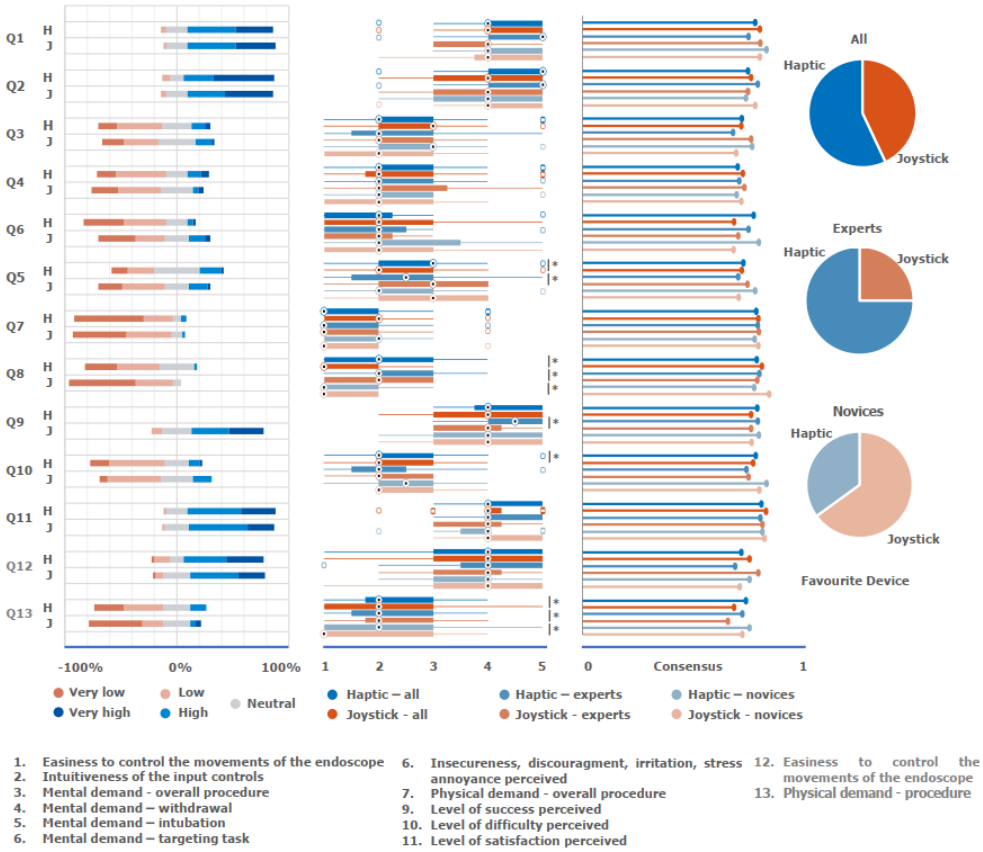

Figure 8.4. Summary of the questions and answers to the survey administered to the clinicians after each trial (1-11) and at the end of all the experiments (12-13): distribution of answers (right), boxplots divided by level of experience (centre-right), consensus (centre-left) and pie plot of the favorite device (right). Statistical significance on the paired Mann-Whitney test is highlighted with the star on the boxplot (p-value < 0.05).

for novices and 0.1 bit for all participants in the whole procedure (p-value < 0.05). Whereas, the mean heart rate was reduced by about 2 BPM for the experts and all the participants in both the intubation and the overall procedure (p-value < 0.05).

8.4.5 Ergonomics

The survey clearly reveals that the HD is less comfortable and ergonomic than the VJ, as assessed by both the questionnaires (Q8 Survey II and Q13 Survey III for all groups p-value < 0.05; see figure 8.4). However, during the experiments, the HD was fixed in a place for standardizing the experience, whereas the possibility to better

adjust its position for each person could have reduce the discomfort.

	Gaze entropy [bit]			Heart rate [BPM]		
	Intubation	Withdrawal	Whole	Intubation	Withdrawal	Whole
E	0.08(0.45)	-0.05(0.38)	-0.03(0.40)	-2.25(3.28)	-1.74(4.48)	-2.00(3.54)
N	0.02(0.43)	-0.34(0.46)	-0.26(0.33)	-2.09(3.71)	-1.49(4.49)	-1.79(3.96)
All	0.05(0.43)	-0.19(0.44)	-0.14(0.38)	-2.18(3.42)	-1.63(4.42)	-1.91(3.67)

Table 8.4. Means and standard deviations of the differences on gaze entropy and average heart rate for each participant when using videogame joypad (VJ) with respect to the haptic device (HD). The table shows the differences for each metric when using the VJ with respect to the HD for each group (E: experts, N: novices, all: all participants)

8.5 Discussion

The experiments described in this chapter represents the the first complete study investigating the optimal device for teleoperated control of robotic colonoscope. Herein, the *HMI evaluation framework* was used for the first time to evaluate two device controllers. Nevertheless, the proposed experimental protocol together with the *HMI evaluation framework* can be fully applied for testing different parts of the HMI: the usability of a new assistive tool (*e.g.*, autonomous polyp detection), the optimal way to convey a piece of information (*e.g.,* haptic feedback vs. augmented reality), the usefulness of autonomous navigation, *etc.* Indeed, the framework enables to analyze in detail the different aspects of the HMI and derive an informed idea about which is the optimal interface in terms of clinical outcome, intuitiveness, user-friendliness, and ergonomics.

Regarding the comparison between the two teleoperated modalities, *i.e.,* VJ and HD, no impressive differences were detected. However, both the HMI were selected after a preliminary screening survey involving the clinicians, therefore they had many of the characteristics requested by the users. Nevertheless, interesting results were observed from the experiments. The HD was preferred and generally felt as more intuitive, less hard to control, and more empowering, especially by the expert clinicians. However, the VJ allowed better clinical performances, finer control and lower objective cognitive load (measured through the sensors) and perceived physical load. Although many young clinicians might have been biased by their previous experience with the VJ, also the other participants (without prior experience with video games) obtained similar results. In the VJ the directional commands are decoupled between the two hands: one hand controls the rotation while the other one is in charge of the insertion/retraction. Although this paradigm might be seen as less intuitive, it could have eased the control of the movements of the endoscope. Additionally, the HD requires more physical effort to be controlled being less ergonomic than the VJ.

Therefore, the increasing fatigue during its use could have had a harmful impact on the users' performances.

The results obtained by the preliminary survey for the initial screening of the HMI to test (section 6.1) confirm those of the study conducted in [72]: haptic device performing better than the 3D mouse and hand-held control. However, our study introduces a controller not considered in [72], *i.e.,* the videogame joypad, which results to be the preferred one from the survey and the optimal one from the experiments. A commercial endoluminal robot using the joypad is the MONARCH® Platform (Johnson and Johnson, NJ, USA), designed for the bronchoscopy procedure. However, a similar configuration is also adopted by the Ion robot (Intuitive Surgical, Inc., CA, USA) and by the Corindus Vascular (Siemens Healthineers, Erlanger, Germany). Indeed, the Ion replaces the joypad with two spheres moved with two fingers (the indices of each hand). Whereas, the Corindus Vascular uses two hand cloches. In both the configurations there is a decoupling of the controls (*i.e.,* insertion/retraction is controlled with one hand/finger, while the deflection with the other) and the same type of inputs to control the endoscope (*i.e.,* movements of two "levers"). The drawback of the standard joypad is the impossibility to provide haptic constrains, which is the main advantage of the haptic device, and, as reported in the HMI evaluation survey, is highly requested by the endoscopist. Indeed, an excessive pressure on the colonic wall is the main cause of perforation, which is the most feared adverse event during a diagnostic colonoscopy. Force feedback is therefore important for preventing the surgeon to cause perforations. Therefore, future studies involving the *HMI evaluation framework* could focus on the optimal way to provide the force feedback (*i.e.,* haptic feedback, augmented reality, visual warnings, auditory alerts, *etc.*), and how to embed this feature on the "joypad-style configuration control".

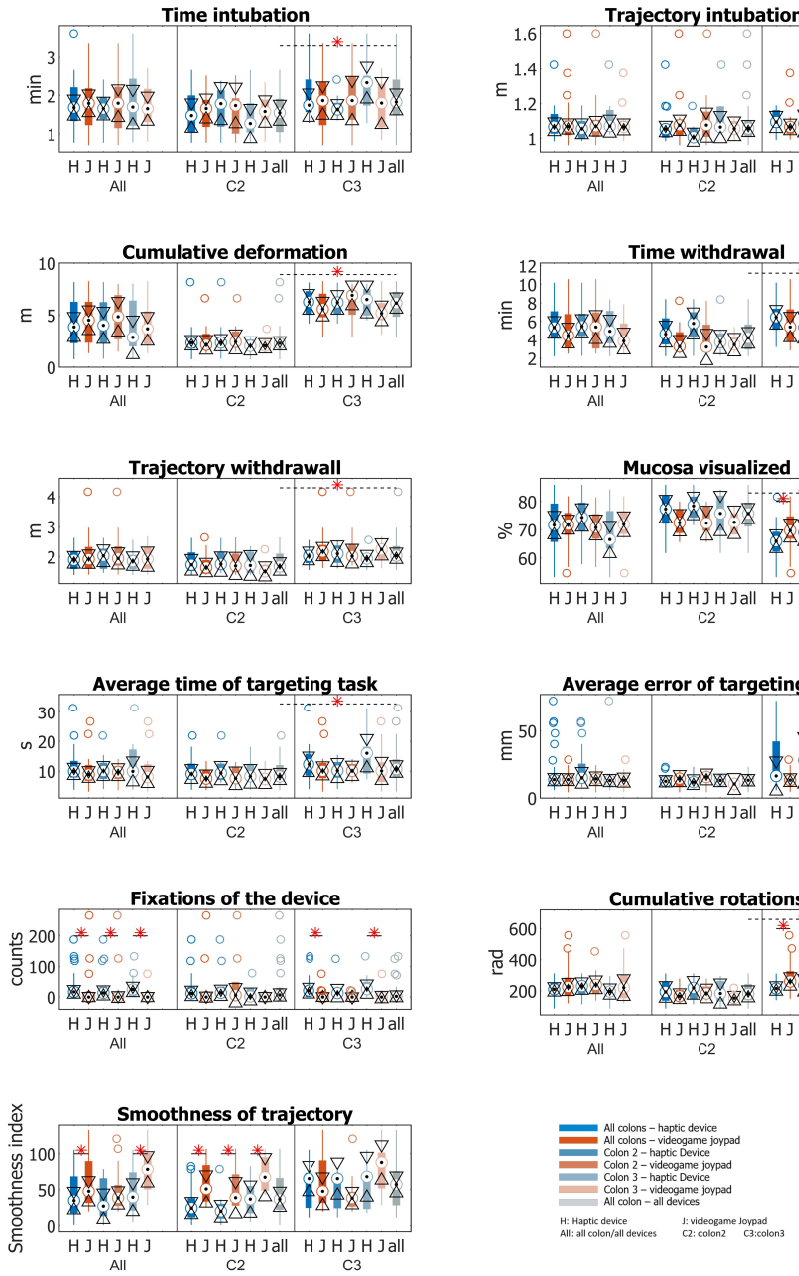

Figure 8.5. Metrics recorded during the experiments divided for controller device (H: haptic device, V: videogame joypad) colon (All colons, C2: colon 2, C3: colon 3) and level of expertise (All: all participants, E: experts, N: novices). Statistical significance on the Mann-Whitney test is highlighted with the star (p-value < 0.05).

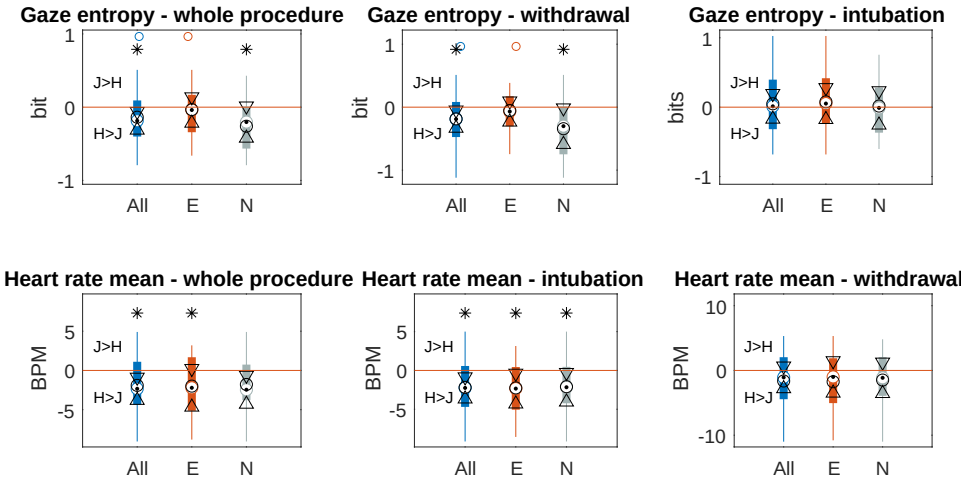

Figure 8.6. Differences on the metrics recorded during the experiments between the videogame joypad (V) and the haptic device (H) divided for colon (all: all colons, C2: colon 2, C3: colon 3) and level of expertise (all: all participants, E: experts, N: novices). Statistical significance on the paired Mann-Whitney test is highlighted with the star (p-value < 0.05). The data above the orange line shows higher values for the videogame joypad, whereas those under the line shows higher values for the haptic device.

Part IV

Additional Contributions

Introduction

This final part of the manuscript introduces four research studies conducted in collaboration with colleagues from the ATLAS project and/or from the Scuola Superiore Sant'Anna and Universitat Politècnica de Catalunya. Doing so, on one hand, the knowledge acquired during the development of this Ph.D. thesis has been applied to other medical scenarios or applications. On the other hand, new insights on HMI, medical simulations, and intraluminal robotic procedures have been acquired, expanding the final contribution of this thesis to the research field of interest. The first two research works presented here, respectively in chapter 9 and 10, refers to the development of new HMIs. In both cases, there is a special focus on the automation of the navigation task. Therefore, multi-level autonomy HMIs are explored, together with their impact on the user's clinical performance and perceived cognitive stress. Whereas, the last two research projects, reported respectively in chapter 11 and 12, show additional advancements made in the field of simulation for robotic colonoscopy. In the first case, the virtual simulator designed and validated within this thesis was enhanced with the inclusion of new features. In the second one, a mechanical simulator for colonoscopy was designed as an alternative physical solution to the virtual simulation platform.

More in details, in chapter 9, the virtual simulator developed within this thesis was exploited for the design, training and test of a control algorithm for autonomous navigation in the colon. The final HMI obtained with the integration of the autonomous tool was evaluated with a user study involving novice subjects. In this case, two types of autonomous control and the teleoperated one were compared. In this preliminary evaluation of the interfaces, the *HMI evaluation framework* was not adopted. However, a study with the complete framework involving expert clincians will be performed in the future.

Secondly, chapter 10 introduces a new medical intraluminal scenario: ureteroscopy. Herein, a multi-level autonomy robotic device was designed to overcome the challenges related to the procedures performed in the urinary tract. Therefore, the knowledge acquired within this thesis was applied in a new medical context to (1) design the HMI of the robotic device, including the different levels of autonomy, and (2) perform a preliminary user study to evaluate the overall robotic device. Likewise the previous case, also in this project a deeper evaluation of the proposed HMI will be performed in the future with the *HMI evaluation framework* involving expert clincians.

Thirdly, in chapter 11, a new enhanced version of the virtual simulator developed

and validated within this thesis was designed and tested. This new simulator of robotic colonoscopy simulates also the motility of the colon due to peristalsis and/or air insufflation/suction. In this case, a pilot validations study was conducted with a small group of clinicians. However, future work will focus on the set-up of a more complete validation test similar to the one performed for the first version of the simulator (chapter 7).

Finally, chapter 12 presents a new method for designing low-cost, highly customizable and modular mechanical simulators for colonoscopy. Mechanical simulators were explored in this thesis to find an alternative solution to the virtual simulation, in the cases where a physical platform is needed. Therefore, also in this simulator, the modularity of the design is maximized to have a platform customizable for the different testing needs. Future work will focus on the integration of this mechanical simulator in the *HMI evaluation framework* as an alternative to a physical platform for the evaluation of the interfaces.

CHAPTER 9

Autonomous navigation in robotic colonoscopy

Autonomous navigation in robotic colonosocpy represents represent a viable solution to reduce the workload of endoscopists and the training time while making the procedure safe and easier to perform [154]. Herein, an autonomous navigation algorithm for robotic colonoscopy was designed and tested in the simulation environment developed as part of this thesis, and extensively described in chapter 4. The autonomous navigation algorithm is based on an image-based control of the endoscope using Deep Reinforcement Learning, called Deep Visuomotor Control (DVC). Prior works on autonomous endoscope control use heuristic policies that limit their generalisation to the unstructured and highly deformable colon environment and require frequent human intervention. Whereas, DVC learns a mapping between the endoscopic images and the control signal of the endoscope.

The control algorithm was trained and tested with colon navigation data of 20 expert GI endoscopists performed on the virtual robotic colonoscopy simulator. As a result, DVC showed equivalent performance as that of expert clinicians on several assessment parameters (*i.e.,* metrics related to the clinical performance), while being safer. Moreover, a second user study with 20 novice participants was performed to demonstrate whether the autonomous controller allows (1) easier human supervision compared to a state-of-the-art heuristic control policy and (2) easier navigation with respect to teleoperated control. Indeed, in safety-critical areas, such as medical robotics, it is highly desirable to maintain human supervision to address ethical and legal concerns [155]. Hence, it is essential to consider human-in-the-loop for DVC deployment in realistic surgical scenarios. Therefore, this second user study demonstrated also that non-expert users can easily supervise autonomous navigation, and DVC reduces the need for human intervention compared to a state-of-the-art method.

This chapter presents a joint research work conducted in collaboration with University of Verona (Verona, Italy) and published in [26]. The main contributions of this thesis in the research are (1) the design of the whole virtual simulation platform,

extensively described in chapter 4, (2) the collection of the clinicians' navigation data used for training and testing the control algorithm, (3) the definition and analysis of the metrics used for evaluating the performances of both the autonomous control and clinicians, (4) the set-up of the final user study.

9.1 Introduction

The introduction of robotic solutions in colonoscopy, and in particular automation technologies, could enhance the human operator abilities. This is especially true for the navigation phase, which could be one of the most time-consuming step of a routine colonoscopy procedure [15]. Indeed, autonomous navigation would allow the endoscopists to focus on the clinical aspect of the procedure rather than the manual control of endoscope, potentially improving the overall procedure outcome and reducing the training time [36]. During the navigation phase, the clinician mainly uses visual feedback from the camera placed on the tip of the endoscope to advance through the lumen [156].

A common gesture observed by endoscopists during a colonoscopy procedure is to centralise the target direction of the endoscope towards the lumen centre. Prior works on autonomous endoscopic navigation have built rule-based controllers to replicate this gesture, by reducing the distance error between the image centre and the detected lumen centre [157]. These algorithms fail in situations when the tip of the endoscope approaches close to the colon wall. Such situations occur due to the highly deformable nature of the colon and the variable mobility introduced by patient

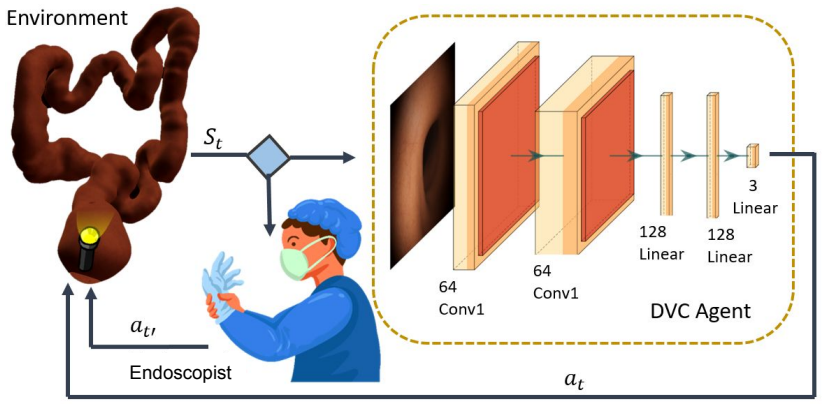

Figure 9.1. Deep Visuomotor Control (DVC) flow diagram. The environment provides a state observation S_t. The DVC agent uses the state input to generate an action a_t that is applied to the environment. During the training phase, DVC learns a task-conditioned policy to perform autonomous colonoscopy navigation. In the evaluation phase, the clinicians can supervise and override DVC decisions through action $a_{t\prime}$.

movements, peristalsis and breathing, which lead to changes in lumen diameter and haustral folds making lumen detection not trivial. These situations require human interventions to find the correct motion direction, or they can be handled by adaptive exploration methods, as proposed here.

Originally postulated rule-based controllers are being progressively replaced by data-driven approaches such as Deep Reinforcement Learning (DRL), since they are able to provide some degree of adaptability [158, 159]. However, the application of DRL in learning surgical task policies has been limited to low-dimensional physical state features such as robot kinematic data, which are widely accepted to be sample-efficient and trivial to learn [159,160]. This chapter reports the use of an image-based DRL approach for endoscopic control (figure 9.1) focusing on learning the navigation task by devising an end-to-end policy to map the raw endoscopic images to the control signal of the endoscope, referred henceforth as DVC.

This work presents an initial study towards generating adaptive control for the colonoscopy procedure by proposing a DVC control policy for autonomous navigation and providing its performance evaluation with expert GI endoscopists.

9.1.1 State of the Art

The advantages of autonomous navigation in colonoscopy have prompted several studies in this field. In [161], a screw-type colonic endoscope is developed, and motion adjustment is demonstrated using reinforcement learning. This study uses robot kinematics variables as state inputs; however, navigation through the straight segments was slow, and navigation through bends proved awkward due to the robot's size. Several studies have focused on magnetic guided endoscopes [15, 31, 36], where external actuating magnetic fields generated by electromagnetic coils or permanent magnets control the motion of the magnetic tip. In [31], navigation by following simple predefined trajectories is presented; hence extending this method to complex non-linear trajectories is challenging. Heuristic path planning algorithms are used in [36] to generate a feasible path in a colon map. This approach employs force-based real-time sensing to guide navigation. Force-based sensing is not yet widely available in existing endoscopic devices; moreover, the interpretation of robotic actions without scene visualisation is challenging, hence not suitable for human supervision. In [15], a static perception model is developed, which extracts the centre of the lumen from raw image observation. The control of endoscope position and orientation is imparted by a proportional controller that aligns the endoscopic image with the centre of the lumen. Similar rule-based controllers have been previously developed in [157]; however, they require significant manual tasking for non-linear components such as analytically computing image jacobian, and interaction matrix [162]. Moreover, lumen detection could be unstable and prone to errors due to the dynamic nature of the colon and its sharp bends. Such scenarios require a vision-based control system to improve during policy training which is limited with hand-engineered features for perception [162]. Learning end-to-end visuomotor representations for direct control using DRL over-

comes these limitations without separately designing perception and control models and offers the ability to improve model parameters while training [163, 164].

Some studies have proposed frameworks for training DRL policies to automate surgical tasks [158, 159, 165, 166] such as manipulation of rigid and deformable objects. These studies use simplified environments designed explicitly for robot-assisted surgery to learn the instrument control during the procedure. Recently, [167] proposed a DRL method for optimising the endoscopic camera viewpoint. These studies use low-dimensional state information for training DRL algorithms, such as kinematic values of the robot, the position of target *etc.* [158,159,165,167]. In a real colonoscopy scenario, it is challenging to accurately capture the endoscope kinematics due to limits on the sensing capabilities [36], and intra-operative guidance is solely based on visual feedback.

9.2 Design of the Deep Visuomotor control

The objective of this work was to develop end-to-end joint training for perception and control to learn navigation policies that map raw endoscopic image observations directly to the control signals of the robotised colonoscope (*e.g.*, motor torques). A medical scenario close to a magnetically guided robotic colonoscopy was assumed, where an external magnet control the motion of the magnetic capsule endoscope while a tether attached to the capsule follows the tip passively [31]. The DVC algorithm was trained and tested in the virtual simulator of robotic colonosocpy developed within this thesis and described in in chapter 4. Hence, in this preliminary simulator version, the effect of the endoscope tether due to multiple collision points with the colon model was neglected. The endoscope tip was modelled as a rigid capsule with weight, length and diameter of 20 g, 36 mm and 14 mm, respectively [168]. The endoscope tip embeds a camera and has four DOF for the motion as shown in Fig. 9.2, *i.e.*, translation (insertion/retraction), roll and bending in two perpendicular directions (pitch/yaw).

9.2.1 DRL background

The colon navigation problem is formalised into a Markov Decision Process (MDP) represented by a tuple $(\mathcal{S}, \mathcal{A}, \mathcal{R}, \mathcal{P}, \gamma, T)$, where $\mathcal{S}$ denotes the state space, $\mathcal{A}$ is the action space, $\mathcal{P}$ is the transition probability distribution, $\mathcal{R}$ is the reward space, $\gamma \in [0, 1]$ is the discount factor and T is the time horizon per episode. At each timestep t, the environment produces a state observation $s_t \in \mathcal{S}$. The agent then generates an action $a_t \in \mathcal{A}$ according to a policy $a_t \sim \pi(s_t)$, and applies it to the environment to receive a reward $r_t \in \mathcal{R}$ [169]. As a consequence, the agent transitions to a new state s_{t+1} sampled from the transition function $p(s_{t+1}|s_t, a_t)$, $p \in \mathcal{P}$ or terminates the episode at state s_T.

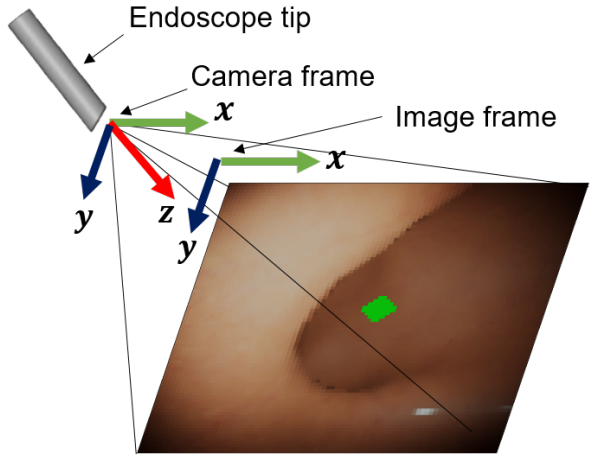

Figure 9.2. Representation of the local frame at the endoscope tip. The X-Y plane of the camera is parallel to the image frame, while the z-axis represents the direction of insertion. Tip bending is carried out on the X-Y plane while the roll is carried on the z-axis. DVC uses a low-resolution image as state input. The green region represents the detected lumen centre.

9.2.2 Learning algorithm

The goal of the agent is to learn a stochastic behaviour policy π parameterised by ϕ, $\pi_\phi : \mathcal{S} \rightarrow \mathcal{P}(\mathcal{A})$ to maximise the expected future discounted reward $E[\sum_{i=0}^{T-1} \gamma^i r_i]$. Proximal Policy Optimization (PPO) [170] was chosen as a consolidated DRL algorithm over other types of algorithms, *e.g.,* Soft-Actor Critic [171] and Deep deterministic policy gradient [172], due to overall returns in terms of wall-clock training time and hyper-parameter tuning. It was out of the scope of this work to propose a novel DRL method, while the main goal was to perform a user study to evaluate the performance of image-based DRL in colonoscopy navigation.

PPO consists of a value and a policy network that uses shared parameters to estimate the state value (V) and predict the action vector (a). PPO alternates between collecting new observations and improving the policy, while approximating the value function as well [170]. The update function for the PPO policy is the following:

$$L(s_t, a_t, \theta_k, \theta) = min\left(\frac{\pi_\theta(a_t|s_t)}{\pi_{\theta_k}(a_t|s_t)}\hat{A}^{\pi_{\theta_k}}(s_t, a_t), g(\epsilon, \hat{A}^{\pi_{\theta_k}}(s_t, a_t))\right) \tag{9.1}$$

where θ_k are the parameters of the old policy, and g is defined as:

$$g(\epsilon, \hat{A}) = \begin{cases} (1+\epsilon)\hat{A}_t, & \hat{A}_t \geq 0 \\ (1-\epsilon)\hat{A}_t, & \hat{A}_t < 0 \end{cases} \tag{9.2}$$

In the training session, the length of each episode was set to 10k iteration steps, $\gamma = 0.99$, and the batch size and the learning rate hyperparameters were 64 and 3e-4, respectively. The PPO clip ratio was 0.2 with 4 mini-batches per epoch and 4 epochs per iteration. A loss term proportional to negative policy entropy was added, with a coefficient of 0.01. Each training lasted for 1.5 million iteration steps, which was the measured time taken for the reward function to converge (figure9.6).

9.2.3 Action space

The preliminary teleoperated control of the endoscope revealed that if the endoscope is directed against the colon wall, especially at the sharp turns, the lumen is not visible. Hence, it is critical to avoid the translation of the endoscope in such scenarios. Therefore, an action strategy was developed, where a translation motion with a constant velocity of $v_{end} = 10$ mm/sec is carried out only when the lumen is detected. The action space consists of discrete angular rotation values in the three degrees of freedom at the endoscope tip, $\delta\theta_j = \alpha$, $\alpha \in \{0, -1, +1\}$ in the j^{th} spatial dimension. In the tip local reference frame, $j \in x, y, z$ corresponds to the orientation alignment in the horizontal and vertical directions in the image plane and the endoscope roll, respectively (figure 9.2). In cases when the lumen is not visible, the translation velocity of the endoscope is set to zero, and the agent carries out orientation changes to detect the lumen.

9.2.4 Observation space and policy

The sensory input to the DVC agent is composed of a downscaled endoscopic image. The RGB images rendered by the endoscopic camera (1024x1024 pixels) was downscaled to 128x128 pixels to reduce the computational complexity of the training DVC network. The policy π_ϕ is represented by a CNN architecture, consisting of two convolutional layers (figure 9.1) for encoding visual scene representations. The network details are publicly available on the project website[1]. The output of the convolutional layers are fed into a combination of fully connected layers and Long Short-Term Memory (LSTM) layer to represent time-dependent behaviour, each with 128 rectified units, followed by the linear connections to the output logits π_t for each action a_t and values estimate V_t. A softmax function transforms the logits to action probabilities. The complete network is trained end-to-end to acquire task-specific visual features.

9.2.5 Reward function

The goal of the navigation is to reach the end of the colon without any significant complication. Visuomotor control should be able to track the colon during the whole

[1] https://github.com/Ameyapores/DVC

procedure. Successful tracking requires the lumen centre P_L to be close to the image centre P_c. Hence, a dense reward $r_t(s_t, a_t)$ is designed as follows:

$$r_t(s_t, a_t) = \begin{cases} C(1 - (||P_L - P_c||_2 / D_{max})), & L = 1 \\ -1, & L = 0 \end{cases} \tag{9.3}$$

where $D_{max} = 1/2 * (Imagewidth) = 64$, is the normalisation factor which is the maximum distance possible, L represents the lumen detection flag, (1 denotes lumen detected, 0 denotes no lumen detected), the hyperparameter C is chosen as 1. Moreover, the agent is awarded a reward of +10 if the colon end is reached and -10 if it returns to the original starting point, to encourage the agent to move unidirectional towards the caecum. To detect the colon lumen in the endoscope image, a threshold segmentation algorithm was built that runs in real-time at 30 fps based on [173]. Therefore, the image is segmented to detect the darkest and most distinct region, with the presumption that this area contains the distal lumen with high probability (figure 9.3). The segmentation is performed by converting the RGB image to greyscale and cropping a circular region centred with the image and a diameter equal to the image width to remove the vignette effect on the corner.

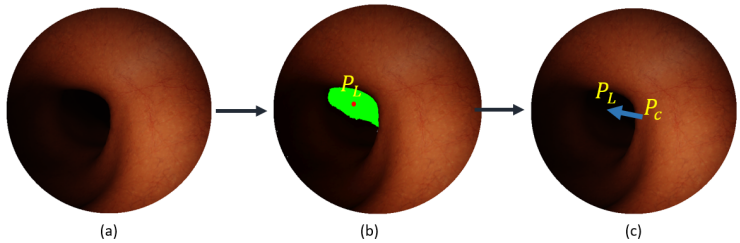

Figure 9.3. Proposed adaptive threshold segmentation pipeline for lumen detection. Each RGB frame captured by the endoscopic camera is passed through the adaptive filter to detect the dark pixels a) original RGB frame b) Image mask for the detected lumen (in green) c) distance vector between the image centre P_c and the centroid of the detected darkest regions P_L.

9.3 Experiments

The experimental goal was to compare the navigation performance of (1) the DVC agents, (2) the baseline method of rule-based control [15] and (3) the endoscopists. Hence, (1) the position and orientation values of the endoscope, (2) the distance between the endoscope and the lumen centre in the image space, (3) the deformation of the colon due to contact with the endoscope, and (4) the camera image were recorded within the developed simulator. This data was collected and synchronised using the *Lab Streaming Layer* software [174], as described in chapter 4.

9.3.1 Clinical data acquisition

A group of 20 expert *GI* endoscopists (each with more than four years of experience) were asked to make navigation attempts in the robotic colonoscopy simulation scene extensively described in chapter. 4. Four colon models were selected considering the opinion of domain experts to represent progressively more complex scenarios. The colon models are shown in figure 9.4. Before starting the experiments, all the subjects were given the same clear instructions about the tasks to do: perform a complete colonoscopy intubation starting from the rectum and reaching the cecum using a video game joypad DualShock 4 controller of PlayStation (Playstation, Tokyo, Japan). The colon model C_0 (where C stands for colon), which depicts a simplified colon model that conforms with the shape and size of the average human colon, was used to familiarise the endoscopists with the controls before initialising the trials. The trials started with endoscopist attempts on the C_1 colon, followed by randomised attempts on C_2 and C_3 colon. The randomness between C_2 and C_3 colon was introduced to identify performance bias based on the colon model. Each experimental session took place in a dedicated training room inside A.O.U. Citta della Salute e della Scienza di Torino (Torino, Italy).

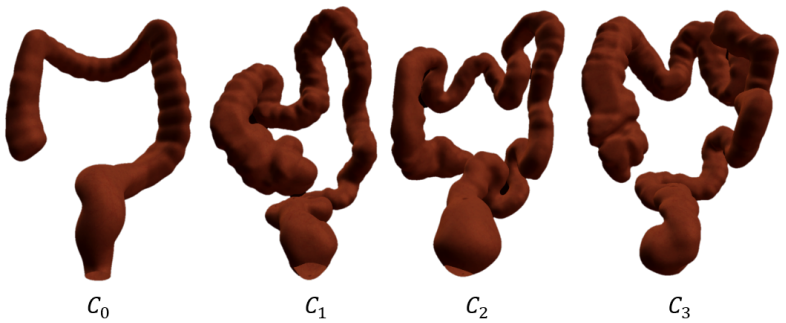

Figure 9.4. Colon models used in the experimental phase. (From left to right) ranked in increasing complexity order, C_0, C_1, C_2 and C_3 colon models. The model complexity is characterised by the centreline distance of the model from rectum to caecum, and the number of acute bending, *i.e.*, >90 degree, which is estimated through visual inspection.

9.3.2 Training of the DVC agents

Three experiments were conducted to validate the DVC. The aim of the first experiment was to determine the sample efficiency of training on different levels of colon complexity. Hence, the DVC agents were trained separately using the same models employed during the experiments with the endoscopists. Second, to establish a comparative analysis between the DVC and the endoscopists trials, a similar experimental workflow was followed as in the tests with the endoscopists, where the DVC

was only trained on C_0 (DVC_{C_0}) and tested on C_1, C_2 and C_3 colons. Third, the DVC was trained on the C_0 model followed by training on the C_1 ($DVC_{C_0+C_1}$) to test if training on a complex colon after a simple one improves performance. To keep the overall iteration steps for DVC training at 1.5 million, the training on C_0 was terminated after 1 million iteration steps and loaded back to train on C_1 for 500k iteration steps (Table 9.2).

9.3.3 User Study

A group of 20 novice participants (without any experience in colonoscopy) were asked (1) to supervise the performance of the rule-based controller agent and (2) the DVC agent, and (3) to perform teleoperated navigation. The experimental workflow consisted of three trials; for each trial, the participants attempted to navigate C_1, C_2 and C_3 colon models (figure 9.4). Each trial was characterised by one of the following control strategies:

1. **teleoperated control** - participants were instructed to exclusively control the endoscope using the videogame joypad during the entire duration of the procedure;
2. **rule-based baseline** - a proportional controller is generated for orientation control that aligns the image centre (P_c) to the detected lumen (P_L) [15], as follows:
$$\delta\theta = \beta \begin{bmatrix} P_{L_x} - P_{c_x} \\ P_{L_y} - P_{c_y} \end{bmatrix} \tag{9.4}$$
where the distance between P_L and P_c is the centreline distance ;
3. **DVC**- a fully trained DVC_{C_0} was deployed (*i.e.,* DVC trained in C_0).

In control strategy 2, the rule-based controller indicated the requirement of manual supervision when the lumen centre was not detected. This information was provided visually as shown in figure 9.5. In control strategy 3, the agent was given ($\Delta_t = 50$) iteration steps to search the lumen centre when the lumen was not detected. After Δ_t steps, the DVC notified the requirement of human supervision (as shown in figure 9.5), and teleoperated control was activated. In the two control strategies, the user had an override option to take control when unsafe behaviour was encountered, *e.g.*, collision with the colon wall or direction of motion reversed. Once the teleoperated control was active, the participants could navigate with the endoscope safely and give back the control to the DVC or the rule-based controller. During each attempt, the number of interventions by the participant was recorded. After all the trials, users were asked to complete a NASA Task Load Index (TLX) questionnaire [149], to score human-perceived workload.

Figure 9.5. Manual supervision through a videogame joypad while navigating by autonomous control strategies. The term *supervision* is printed on the screen, indicating the switch to teleoperated control. When the endoscope is oriented towards the lumen (green point), the user can give back the control to the autonomous agent. A low-resolution (128x128 pixels) image is displayed to facilitate interpretability of machine decisions, however users have the option to change to high resolution (1024x1024 pixel) display.

9.3.4 Data collection and Analysis

Four different metrics are used to score the navigation performance and compare the DVC with the rule-base control and the navigation of experts clinicians. The metrics are shown in table. 9.1. The intubation time and the number of colon perforations are qualitative assessment measures for colonoscopy procedures [175], while average lumen distance (*distance between the centre of the lumen and the image*) and the normalised trajectory length are two technical metrics devised in this study to measure the accuracy of the trajectories. When the user or DVC reversed its direction of

Metric	Description
Intubation Time	Time spent to intubate the colon: from the time point where the initial movement of the endoscope is detected to the time point when the caecum is reached
Number of perforations	Number of times excessive force is applied on the colon: deformation > 3 cm
Normalized lenght of trajectory	Length of the path followed by the endoscope during the intubation normalised by the centerline length of the colon model. Therefore, normalised length > 1 indicates a path distance longer than the centerline path
Average centerline distance	Distance between the center of the lumen and the center of the endoscopic image. This distance is normalised by the size of the image. Therefore, a value of 0 denotes that the image centre coincides with the detected lumen, and value 1 denotes that the detected lumen is at the farthest point

Table 9.1. Metrics correlation with the clinical performances used for validation

motion and returned to the rectum instead of moving towards the cecum or perforated the wall heavily to destabilise the colon model, it was considered a failed navigation attempt.

9.4 Results

The learning curves when DVC was trained on different levels of colon complexity are presented in figure 9.6. C_0 represents a simplistic model; hence, the DVC agent reaches high reward values in relatively fewer steps than in other colon models. A high reward indicates that the agent successfully learns to complete the navigation task. Whereas C_2 represents high complexity, the agent requires 1.2 million steps

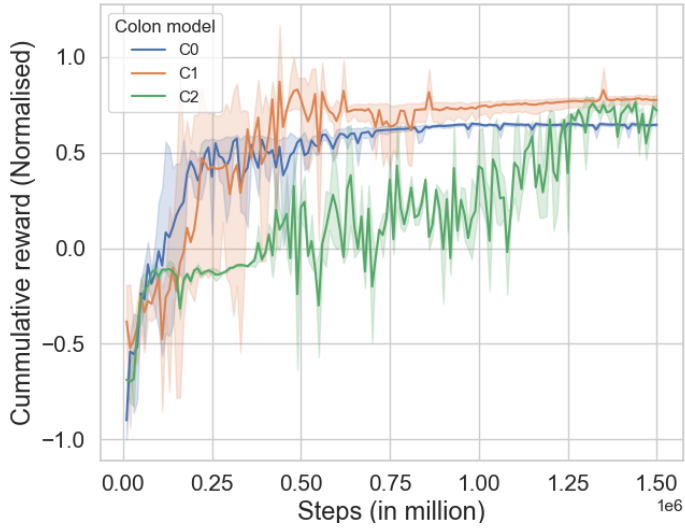

Figure 9.6. Learning curve of DVC trained on varying complexity of colon, using three colon models. Cumulative reward is normalised in the range $[-1, 1]$. The shaded area spans the range of values obtained when training the agent starting from five different initialisation seeds.

for high-reward convergence. The C_1 training curve lies between C_0 and C_2. This suggests that the training time is related to colon complexity. However, DVC_{C_0} can navigate other complex colon models, *i.e.,* it acquires task-specific features that can generalise to other colon models (Table. 9.2).

9.4.1 Comparative analysis

The performance data of 20 endoscopists was acquired while 10 different DVC agents were trained on the C_0 starting with a different random seed. Figure 9.7 shows the

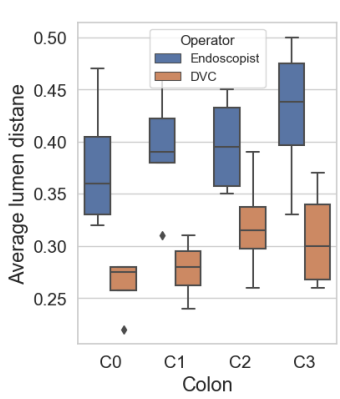

((a)) Distance between the centre of the image and the centre of the lumen

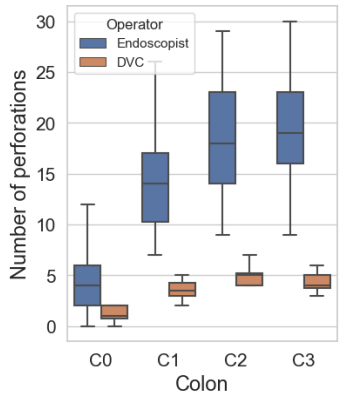

((b)) Perforations

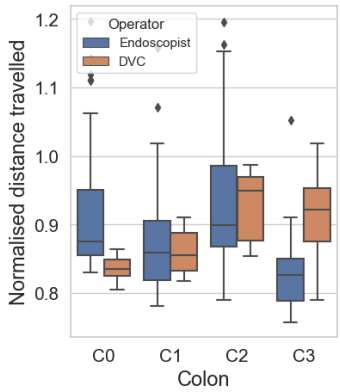

((c)) Normalised trajectory length

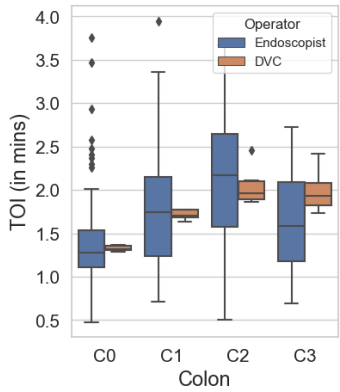

((d)) Time of intubation (TOI)

Figure 9.7. Navigation performance comparison plots between DVC (Deep Visuomotor control) and endoscopists: a) distance between the centre of the image and the centre of the lumen, b) number of perforations, c) normalised trajectory length, d) time of insertion.

comparison of (1) the average centreline distance, (2) the number of perforations, (3) the completion time and the (4) normalised distance travelled. There is a significant difference in the average centreline distance and the number of perforations between the endoscopists and the DVC. DVC shows precise tip centralisation and less number of perforations compared to endoscopists. One of the reasons for this difference is that clinicians tend to push the colon wall at acute bends of colon junctions. This is a gesture sometimes clinicians follow due to the rigid constraints of the clinically available flexible endoscopes. Whereas DVC is trained on reward feedback to minimise the

	DVC$_{C0}$				DVC$_{C0+C1}$			
	Intubation Time	Number of perforations	Normalized lenght of trajectory	Average centerline distance	Intubation Time	Number of perforations	Normalized lenght of trajectory	Average centerline distance
C0	0.27±0.01	0.5±0.25	1.37±0.05	0.84±0.02	0.24±0.02	1±1	1.32±0.03	0.84±0.02
C1	0.30±0.01	3.3±1.5$	1.74±0.04	0.88±0.08	0.25±0.01	3.3±0.5	1.70±0.07	0.82±0.03
C2	0.36±0.03	5±1	2.22±0.2	0.97±0.03	0.28±0.01	4.6±0.5	1.89±0.03	0.85±0.01
C3	0.35±0.02	4.6±0.5	2.15±0.23	0.92±0.08	0.29±0.03	3±1	1.78±0.05	0.89±0.09
Mean	0.31±0.04	5.0±1.2	2.20±0.75	0.90±0.04	**0.23±0.04**	**4.3±1.2**	**1.96±0.59**	**0.86±0.04**

Table 9.2. Comparison between DVC (Deep visuomotor control) algorithms trained only with C0 (DVC_{C_0}) and DVC trained with both C_0 and C_2 ($DVC_{C_0+C_1}$)

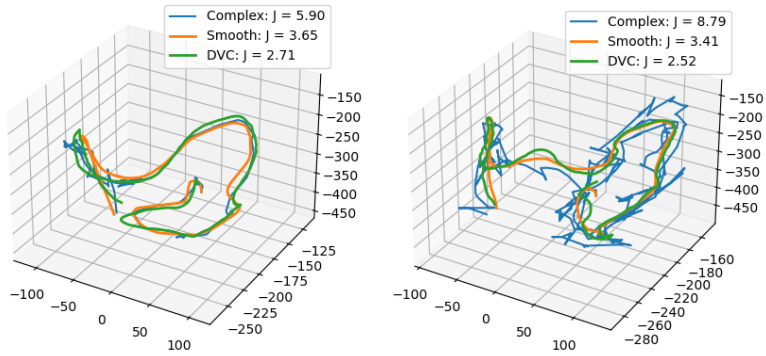

((a)) C_1 **((b))** C_2

((c)) C_3

Figure 9.8. Trajectory plot of DVC (Deep Visuomotor control), complex and smoothest endoscopist performance for a) C_1 b) C_2 3) C_3 models respectively.

distance from the centre of the lumen, it stays centralised to avoid contact with the wall. For the normalised trajectory length and the time of intubation, a substantial

difference is not noted. There is more variance observed in the performance of the endoscopists. Some endoscopists followed a convoluted trajectory that increased the normalised distance and time of insertion, while others followed smoother trajectories that resulted in the lower normalised distance and time. Figure 9.8 shows the most complex and smoothest trajectories demonstrated by the endoscopists and the trajectory executed by DVC_{C_0} for the C_1, C_2 and C_3 colons. The smoothness of a trajectory is estimated using a jerk index J (cm/sec^3) which characterises the average rate of change of acceleration in a movement [176]. Human operators tend to show wide variance in performing optimal trajectories, while DVC performance stays in the average range.

The result of splitting the training into two colon models $DVC_{C_0+C_1}$ and evaluating on other colon models are shown in Table. 9.2. There is an improvement in the lumen detection performance for $DVC_{C_0+C_1}$ in comparison to DVC_{C_0}. DVC_{C_0} reaches high rewards at 500k iteration steps; hence there is no additional feedback to improve the performance. We speculate that the agent reaches suboptimal local minima, while, when the DVC trained on C_0 is loaded to train on C_1, it encounters acute bends, offering the potential to maximise the cumulative reward. There is no considerable improvement on other navigation parameters, *i.e.,* perforation, time of intubation and normalised trajectory length.

9.4.2 Supervision

The human interventions are divided into two parts. First, where the user overrides the control due to unsafe behaviour and second, where the system demands human supervision. The average human intervention required for rule-based baseline was 5 ± 1.8 for human override and 2.5 ± 1.5 when the system demanded human control, while for DVC, the average number of human interventions were 0.1 ± 0.5 for human override and 0.05 ± 0.2 when the system demanded human control. This difference is attributed to the adptability of DVC to search for new insertion directions when the lumen is not easily detected, whereas the rule-based controller lacks this ability. The NASA TLX for each control strategy is shown in table. 9.3. Regarding ease of

	Teleoperated	Rule-based	DVC
Mental demand	63	33	18
Physical demand	65	38	9
Temporal demand	30	47	17
Performance	25	34	12
Effort	57	38	10
Frustration	42	41	12
Mean workload	47	38	13

Table 9.3. Mean values of the NASA Task Load Index of novice users for teleoperated control, rule-based control and DVC (Deep Visuomotor control) . Lower score indicates good user experience (scale 1-100).

use, participants found manual control and rule-based controller more demanding in all task load categories, while a substantial workload reduction is observed for DVC.

9.5 Discussion

Prior works on autonomous colonoscopy navigation use heuristic control policies that fail to adapt to situations where detecting lumen is not straightforward and requires frequent human intervention. This work proposes an end-to-end DVC that learns a mapping between the endoscopic images and the endoscope control signal, such as tip orientation. DRL has been applied in the surgical domain, however, these works use low-dimensional physical robotic state features that are challenging to obtain using robotic endoscopes.

The experimental validation showed an equivalent performance in terms of the time of insertion and the distance travelled between the DVC and the navigation of 20 experts endoscopists. However, DVC reduced the number of perforations and showed efficient lumen tracking and improved safety. Furthermore, the second novice user study demonstrated that supervision of DVC significantly reduces the user workload with respect to teleoperated control.

As demonstrated here, autonomous navigation offers potential for increased human productivity and off-loading cognitive and physical tasks. However, using human technical expertise and maintaining accountability is highly desirable. Moreover, in safety-critical areas such as medical robotics, there is a high cost associated to poor performance of an autonomous system, compounded by ethical and regulatory concerns [155]. Hence, it is essential to consider human-in-the- loop for the deployment of DVC in realistic surgical scenarios. This work is an initial demonstration that autonomous navigation with human supervision is possible, and overall reduces the cognitive stress of the clinicians while having a positive effect on the clinical outcomes. The next step foresees the performance of a larger user study involving experts clinicians and adopting the complete *HMI evalutation framework*. This will enable more objective tracking of both cognitive load and users' performance.

Finally, there are some limitations of this work worth to discuss. First, it is not straightforward to know the direction of motion of the endoscope. Hence, the newer version of the virtual scene will simulate the endoscope body dynamics, providing also the insertion length. Second, if the robot needs to learn from raw image observations, it also needs to evaluate the reward function from raw image observations, which itself requires a hand-designed perception system. This can be mitigated by using online user interaction through human-in-the-loop reinforcement learning [177].

CHAPTER 10

Multi-level-assistance robotic platform for applications in the urinary tract

Ureteroscopy is the gold standard procedure for treatment and diagnosis of upper urinary tract diseases [178, 179]. Performing ureteroscopy is a non trivial task and mastering it requires an extensive training. Current challenges related to navigation with traditional instruments inside the urinary tract could turn into a highly complex task due to the limited intuitiveness in controlling the endoscope movements, the poor visual feedback, and the absence of any type of guidance or assistance in current endoscopic systems [180]. In addition, considering that the localization of the endoscope inside the urinary tract relies mainly on fluoroscopic images taken intraoperatively, the procedure imply health risks for both the patient (especially children) and clinicians. Therefore, the number of x-ray images taken is usually minimized, making the localization and the navigation task even harder. In this context, robotic flexible ureteroscopy offers an opportunity to overcome the mentioned challenges, by reducing the stress of the clinicians [181] and offering safer treatments for patients. The advantages provided by the robotic systems include the use of an ergonomic and intuitive HMI which (1) reduces the physical and mental stress of the clinicians, (2) ease the implementation of more precise and smoother movement of the tools and (3) give the possibility to operate the robot remotely at a safer distance from radiation.

This chapter describes a joint research project oriented to develop a robotic assisted ureteroscopy platform. The research and development was conducted in collaboration with other Early Stage Researchers of the Marie Curie ATLAS project from KU Leuven (Leuven, Belgium), TU Delft (Delft, Netherlands), Politecnico di Milano (Milan, Italy), University of Strasburg (Strasburg, France) and published in [182] as part of the joint doctoral program. Herein, the resulting multi-level-assistance robotic

platform for navigation in the urinary tract is presented. The main contributions of this thesis in the project are: (1) participation in the definition of the robotic system requirements and specifications, driven by multiple discussions with the clinicians; (2) definition of the different level of autonomy of the robot; (3) implementation of the HMI with focus on the GUI, including the definition of the elements to be displayed and the communications with the different modules (*e.g.,* endoscopic camera, robotic device, sensors, *etc.*); and (4) execution and evaluation of the validation tests.

10.1 Ureteroscopy

Uretheroscopy is an intraluminal procedure to explore the upper urinary tract which allows the diagnosis and treatment of different conditions, *e.g.,* kidney stones, urothelial carcinoma of the upper urinary tract *etc.* [179]. Kidney stones are crystalline aggregates of one or more components, that may occur anywhere in the urinary tract. Most commonly they appear in the kidneys, and they are removed with ureteroscopy. Whereas, tumors can be found at any point in the renal pelvis, renal calyces and ureters [178].

Ureteroscopy involves the passage of a ureteroscope (*i.e.,* long flexible endoscope with the camera at the tool tip, with a diameter of about 2.5 mm) through the urethra and bladder, up the ureter and to the kidney or the point where the lesions/stones are located (figure 10.1)

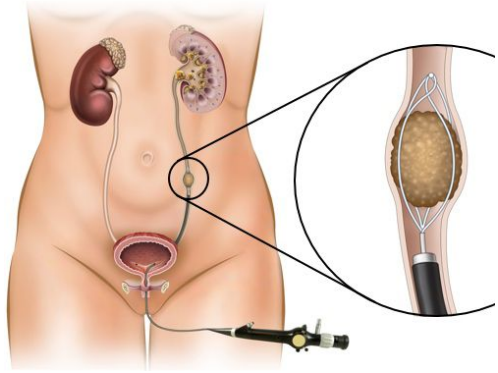

Figure 10.1. Ureteroscopy procedure and kidney stone removal. Image from [183]

In the case of kidney stones removal, once the endoscope is inside the kidney, exploration of the renal pelvis is carried out in order to identify all stones. The exploration is performed by first analysing the upper calices, followed by the middle ones, and finishing with the lower calices. Once the stones are identified, several options can be used for their removal [179].

Finally, once the stones have been removed, or the tumor has been ablated, a careful exploration of the ureter needs to be carried out to retrieve the endoscope as

well as to detect possible lesions that may have occurred during the procedure [184]. In cases in which injuries during the ureteroscopy are detected, or in cases were ureteral structure or other anatomical impediments to stone fragment clearance are identified, guidelines recommend the placement of an ureteral stent. Localization of the ureteroscope inside the urinary tract is performed via multiple fluoroscopic images [179].

10.2 State of the Art

Since the first reported clinical use of a robotic ureteroscope, the *Sensei Magellan* system (Hansen Medical, Mountain View, California), no longer commercially available [185], few other robotic platforms have been tested for urological applications. The *Magellan* robotic catheter system is composed of an active catheter (tip bending and insertion being robotically controlled), controlled by the clinician through a telemanipulation console placed a few meters away in the operating room. Although its approved use was for cardiac interventions, an off-label use for ureteroscopy was reported in 2008 [185]. The Magellan system was used as an ureteral access sheath, allowing enhanced renal access to the ureteroscope. After a series of 18 patients, ergonomic problems prompted the users to stop the trial [181].

A second robot designed for ureteroscopy is the *Avicenna Roboflex* by ELMED Medical Systems (Ankara, Turkey). It consists of robotic control and interface that is docked with a standard flexible fiberoptic ureteroscope. Therefore, the surgeons are still limited within the confines of the existing ureteroscope movement. Nevertheless, being able to stand further back from the radiation source and not having to contort their hands, wrists, or limbs are accompanying advantages of the robot [181].

Finally, the Auris Health, Inc. (Redwood City, CA, USA) *Monarch Platform*, already approved for bronchoscopy [18], it has been adjusted and tested in endourology procedures [186]. The ergonomic and easy-to-understand videogame joypad offers an additional range of motion, reducing the difficulty and improving the learning curve for the novice ureteroscopist.

All these platforms, although they ease the procedure, do not really provide great assistance to the operator (*e.g.*, haptic feedback, augmented reality, autonomous navigation, non harmful localization technique *etc.*). Therefore, their benefit and their actual use in the clinical practise are limited compared to manual approaches.

10.3 Design of the robotic platform

The innovative robotic platform developed in this research work aims at addressing the current challenges related to navigation in the urinary tract: (1) difficulty in steering the endoscope inside narrow lumen with a variety of shapes, especially for novices, (2) difficulty in localizing the endoscope inside the organ due to the poor

visual feedback from the camera and the lack of an online map of the organ and the localization of the endoscope tip on the map, (3) need of reducing the X-rays images taken for localizing the endoscope due to the health risks for both the patient and the clinician, (4) non ergonomic and intuitive controller device which makes the tasks physically and cognitively stressful for the clinician. The proposed system solution is depicted in figure 10.3 and it includes three main components:

- A **Visual-Servoing Module**, based on [187], comprising (1) a cable-driven soft robotic endoscope which has a backbone and a helical structure with two bending directions. The steerable segment of the soft robotic endoscope is 70 mm long which is similar to the one in a ureteroscope; (2) an actuation robotic platform to bend in two directions and to insert the robotic endoscope. In total, there are 3 DOF in Visual-Servoing Module. A multi-proposal microcontroller (based on Arduino ATmega2560) is used to implement two PID controllers and served as a bridge between high-level commands and all the actuators. The Visual-Servoing Module aims at enabling autonomous guidance having the tip of the catheter always pointing towards the centre of the ureter. A deep learning based visual servoing high-level controller is used to autonomously segment the lumen from the camera images, as presented in [188], and compute the centre of the ureter. The information from the detected centre is used to calculate the error and bring the tip of the endoscope towards the detected centre point. The average centre detection time is 0.15 s deployed on a NVIDIA GeForce RTX 2080 GPU. A close-up of the robotic platform is presented in figure 10.2.

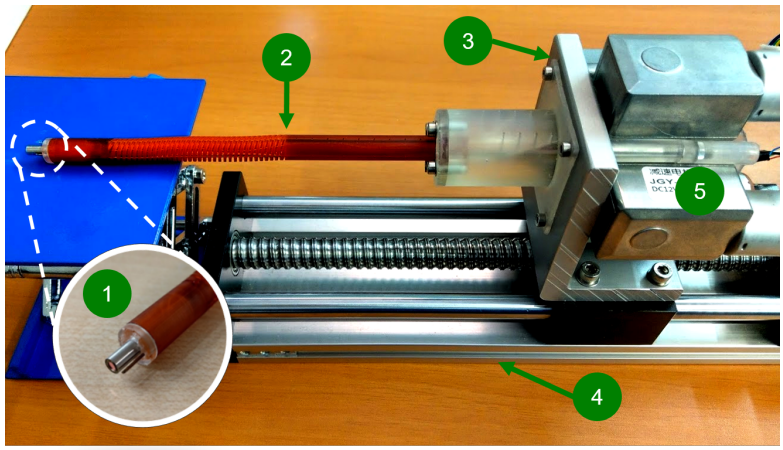

Figure 10.2. Assembly of the *Robotic Ureteroscope Platform*: 1) Endoscopic camera and EM tracking sensor; 2) Soft robotic arm; 3) Support for actuation system; 4) Linear stage; 5) DC motors;

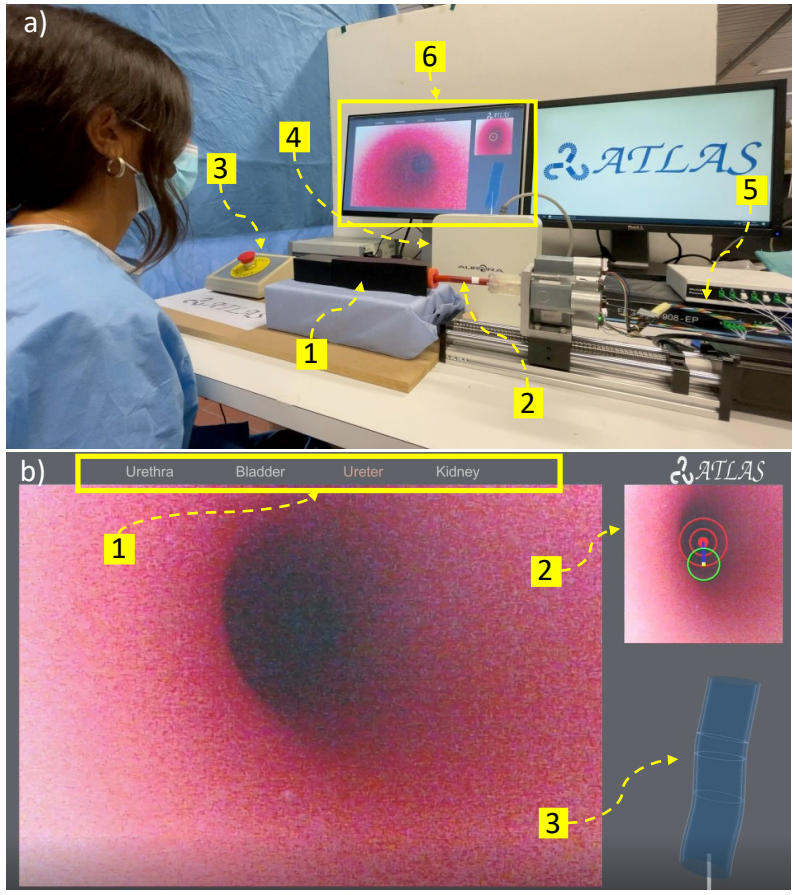

Figure 10.3. a) General perspective of the Multi-level-assistance robotic platform including: 1) ureter phantom, presenting the visual conditions of a real ureter; 2) built robotic endoscope; 3) emergency stop button; 4) EM tracking system; 5) FBG interrogator and 6) Human Machine Interface. b) The Graphical User Interface: 1) current phase of the procedure; 2) processed output (centre of the ureter) of our visual-servoing module and 3) 3D shape of the endoscope relative to the phantom expressed in the EM coordinate frame.

- A **Shape Sensing Module** adapted from [189] includes a multicore Fiber Bragg Grating (FBG)) (FBGS, Geel, Belgium) embedded in the centre channel to sense the 3D shape of the soft robotic endoscope. Two Electromagnetic (EM) tracking sensors (NDI, Waterloo, Canada) are attached to the tip and to the base of the robotic scope to localize the 3D reconstructed shape in the EM coordinate frame.
- **A multi-level autonomy HMI** including a GUI implemented in *Unity* (Unity Technologies, San Francisco, CA, USA) and a videogame joypad, *i.e.*, Dual-

Shock 4 controller of PlayStation (Playstation, Tokyo, Japan), for controlling the endoscope during teleoperated control. The GUI shows: (1) the endoscopic image recorded by the camera, (2) the position and deformation of the endoscope registered in the pre-operative and intra-operative images, (3) the image with higher level features such as computed by the visual-servoing module, and (4) the phase of the procedure.

Three different levels of assistance are considered.

1. **Teleoperated** - The operator can see the endoscopic images recorded by the camera and the information regarding the position and deformation of the endoscope obtained from the shape sensing module. The operator controls the 3 DOF of the endoscope through the master device (*i.e.,* videogame joypad).

2. **Visual assistance** - In addition to the information mentioned in the manual scenario, information regarding the detected centre of the lumen and the clinical phase is shown on the GUI. In this operation mode, the navigation is still performed by the user using the master device.

3. **Autonomous** - During fully automated intraluminal navigation, the visual servoing module drives the endoscope inside the lumen, *i.e.*, the two DOF bending and the insertion/retraction, following the centre-line detected with the computer vision module. The clinician supervises the procedure and, in case there is any concern, they can halt immediately the process by pressing the emergency stop button and recover full manual control of the endoscope. In case that the computer vision system fails on detecting the lumen, the robot halts its movement.

10.4 Preliminary Experiments

Preliminary validation phase was composed of two different experiments. First, the fully autonomous navigation was successfully tested in a 20 cm curved silicon ureter phantom. Second, a pilot user study was conducted to test the capabilities of the integrated robotic platform when using the different levels of autonomy. A group of 10 novice subjects (with no prior experience in endoscopy) were enrolled for the experiments. The subjects were asked to perform a lumen centring task, *i.e,* bend the tip of the robot in order to reach the centre of the lumen. Each participants was allowed to get familiar with the system for five minutes before performing the task in order to exclude possible learning effects. The participants had only one chance and were asked to perform the task with both the teleoperated control scheme and the visual assistance. In the visual assistance scheme, the information regarding the detected centre of the lumen was shown to the users.

The performance metrics taken into account were the settling time and the Steady State Error (SSE). The settling time is defined as the first time the endoscope reaches

a distance within less than 20% of the initial distance with respect to the centre of the lumen. A condition was herein that this position is maintained for more than one second. The SSE is defined as the distance between the theoretical detected lumen centre and the centre of the camera frame when the participants or the robot finished the tasks. The performances of the users in the two tasks were compared against the autonomous control. In this case, the robot performed the task with aid of the visual servoing high-level controller for 10 times.

10.5 Results

As a first result, the fully autonomous navigation was successfully demonstrated in the ureter phantom. Secondly, the performances of the autonomous control were compared with those of the 10 novice users that participated to the experiments in both teleoperated and assisted control. All the participants successfully performed the robotic procedure with both control strategies. In the case of settling time, the median values obtained were 39.47, 30.37 and 15.36 s for the teleoprated, visual assistance, and autonomous control respectively and the values obtained for SSE were 21.35, 30.37 and 15.36 pixels, respectively. In both metrics the autonomous modality obtained the best performance. In the case of settling time, the autonomous modality reached the goal in half the time that is required with visual feedback and was 2.5 times faster than in the case when there is no feedback. For the case of SSE metric the values obtained with visual feedback and manual mode were twice and four times higher than the autonomous mode. The Boxplots comparing the results between each of the modalities are shown in figure 10.4.

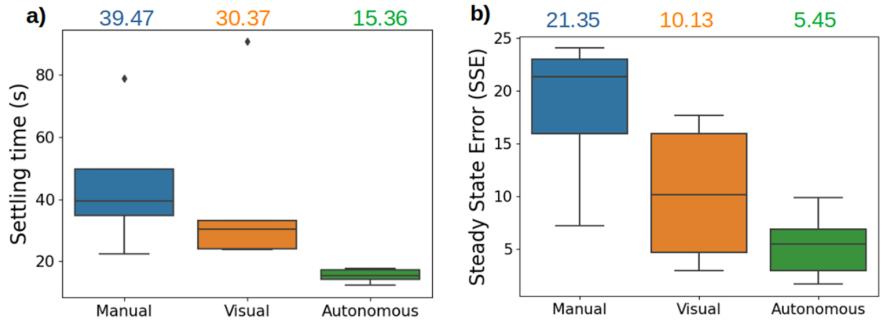

Figure 10.4. Boxplots comparison of a) Steady State Error (pixels) and b) settling time between the three modalities of the system (manual control, visual feedback, autonomous) tested for the lumen centring task. The median value for each setting is presented on the top.

10.6 Discussion

Robot-assistance catheters represent an opportunity to reduce the risks and difficulties related to ureteroscopy. This work presents an integrated robotic platform aiming at easing the endoscopic procedure inside the urinary tract. The mechanical properties of the developed active robotic catheter together with its autonomous and semi-autonomous abilities can help clinicians prevent perforations and get support during the procedure. Furthermore, thanks to the integrated tracking system, the real-time position of the ureteroscope together with its shape mapped inside the patient's anatomy may become available during the whole surgery, reducing the need to use X-rays for localization.

The preliminary study conducted shows that the proposed integrated robotic platform, including its sensors, robotic catheter and multi-level autonomy HMI, successfully allow the navigation inside a ureter phantom. In addition, the integration of the autonomous navigation demonstrates its advantages with respect to the teleoperated control, even if assisted with visual cues, in terms of time to complete the task and precision of control.

Future work will include testing the whole system in a multi-organ phantom and conducting user studies with expert endoscopists using the *HMI evaluation framework*.

CHAPTER 11

Virtual simulator of robotic colonoscopy with intestinal motility

The realism of a simulator is a key point for a correct translation of the results obtained in simulation to the real case scenario for both (1) the testing of new biomedical devices and (2) the training of clinicians. This chapter presents the integration of two important features in the virtual simulator for robotic colonoscopy developed and validated within this thesis, and described in chapter 4. Both features are related to the deformation of the colon, which affect the robotic colonoscopy procedure: (1) peristalsis and (2) expansion/contraction of the colon walls due to air insufflation/suction. Air insuflation is commonly used during colonosocopy to facilitate the insertion of the probe and to stretch the colon walls for better visualization of the lumen. Emulating the behaviour of the colon related to peristaltic motion and air insufflation is necessary to increase the realism of the platform and helps to face the possible situations that occur during real colonoscopy procedures. Therefore, the simulator presented in this chapter represents a new and more realistic version of the previous simulation platform integrated in the *HMI evaluation framework*. In this context, the peristalsis is implemented as continuous pressure waves travelling along the whole length of the colon. Whereas, air insufflation/suction is performed by applying a surface pressure to the walls of the colon close to the tip of the colonoscope. Its magnitude can be regulated by the doctor as in the standard colonoscopy. The integrated simulation platform including the two new features was validated by a medical team. In particular, the degree of realism achieved by the simulator and the truthfulness of the models were assessed.

This work was performed in collaboration with a M.Sc. student from Università di Pisa (Italy), as part of her M.Sc. thesis in biomedical engineering. The author of this thesis' main contributions are: (1) the set-up of the project including definition of objectives, requirements, research workflow and expected results, (2) close supervision of the whole work and (3) organization and management of the clinical validation.

11.1 Introduction: peristalsis

The peristalsis is an involuntary contraction of smooth muscles that occurs in the GI tract. The result is a wave movement that allows the substances, contained in the GI organs, to proceed in a certain direction. Peristalsis was observed for the first time in 1902 in dogs [190]. Ten years after, the same wave motion was identified in humans [191]. Carlson discriminated three phases during motor activity [192] and in 1969 Szurszewski described the electric activity of the small bowel in dogs [193]. During peristalsis propulsion, the longitudinal muscles contract while circumferential muscles relax [194]. The contractions of the muscles are modulated by the Intestinal Cells of Cajal (ICC). The ICC act like an electrical pacemaker and generate spontaneous electrical slow waves in the GI tract [195]. The frequency of ICC pacemaker changes according to the intestinal region [196]:

- 3 per minute in the stomach
- 11-12 per minute in the duodenum
- 8-9 per minute in the ileum
- 3-4 per minute in the colon

As shown in figure 11.1, the GI motion can be divided into 4 phases [195], [197]:

1. quiescence, a period without contractions (40-60% of the cycle);
2. irregular and intermittent contractions with a low amplitude (20-30% of the cycle);
3. regular contractions with high amplitude that propagate caudally (5-10 minutes);
4. short transition from contraction to quiescent period.

The third phase occurs every 1,5-2 hours and the frequency of peristalsis in the colon is equal to 3-12 minute^{-1}.

Shifting the attention to engineering aspects, many studies were conducted to model and assess the characteristics of the peristaltic wave. *Bassotti* and *Gaburri* [198] described the peristaltic motion using a colonoscopically positioned manometric probe and an infusion system. The manometric prove can estimate the pressure variations [199], related to peristalsis. The study revealed the trend of pressure in several sections of the colon in 20 healthy people for 24 hours.

Sometimes in medical practice, sedation can be necessary. It is usually administrated to reduce (1) colon motion artifacts during tomography and (2) probability of injuries due to peristaltic motion in colonoscopy procedures. Drugs such as *Motilin* and *Erythromycin*, for instance, can regulate the contractions during phase three [200]. In addition, some studies show that drugs such as *butylscopolamine, glucagone* and *dicyclomine chlorhydrate* reduce peristaltic contractions thanks to their myorelaxant effect, *i.e.,* produce a relaxation of the smooth muscles [201], [202]. The result is a decrease in the amplitude of the pressure wave.

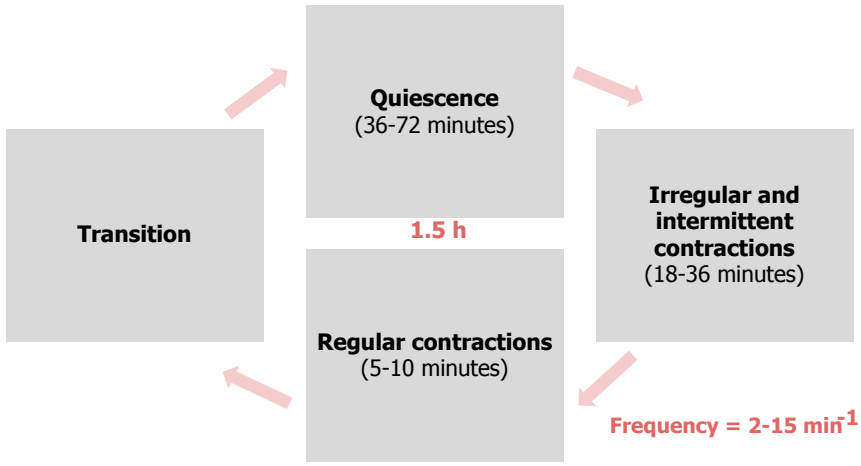

Figure 11.1. Peristaltic activity in the GI tract.

11.1.1 Models of peristalsis

In the literature, a virtual simulation of the peristalsis of the colon has been modelled in two different ways. The two ways differ in relation to the complexity and characteristics of the 3D model of the colon considered.

- **Fluid-Structure Interaction (FSI) Model**: the peristaltic wave is not an input of the simulator but is predicted from the fluid-structure interaction and muscular control [203]. The nodes of the mechanical mesh are connected using a linear spring model and, peristaltic wave is implemented on a cylinder by varying the intra-luminal pressure and muscular contraction forces. Relaxation and contraction are recreated changing the dimension of each elastic element. Nevertheless, the introduction of intestinal contents and the FSI increase the computational cost of the simulation and make it suitable only on simpler geometries.

- **Wave-like Motion Model**: the colon is divided into discrete segments and peristalsis is generated estimating the difference between the final and initial position of each segment [133]. Each vertex of the mechanical mesh is moved in a sine wave-like motion to provide contraction and expansion of the colon. However, the resulting movement of the wall does not consider the mechanical characteristics of the real tissue. The peristalsis is related to the displacement of each point of the mesh given by a sine function.

11.2 Generation of collapsed 3D models of the lumen

Both peristalsis and air insufflation/suction causes an expansion or contraction of the colon. The colon models 3D reconstructed in chapter 4 for the virtual simulator are already inflated since they come from CT colonography images, which are taken insufflating air in the lumen. Therefore, the first step was to derive collapsed colon models. Therefore, starting from from the completely insufflated 3D colon model of each patient, an external pressure was applied to the entire structure by means of simualtion run in *SOFA*. The collapse of the model on itself involve a lot of complications related to the self-collision and interpenetrations. So, the best solution was to create a cylinder inside the colon and let the model collapse on it. Indeed, while self-collision is still not best optimized in *SOFA*, the collision between two different objects is very realistic and efficient. Given the centreline of the colon, the CAD model of the cylinders were made in *Autodesk Fusion 360* (Autodesk, Mill Valley, CA, USA). This program allows the upload of the spline containing the points of the cetreline and makes a sweep extrusion of a given sketch along a predetermined path. Finally, the mesh of the obtained cylinder can be extracted and saved. In this way, it is possible to create a series of cylinders, extruded from the centreline, with several diameters (figure 11.2).

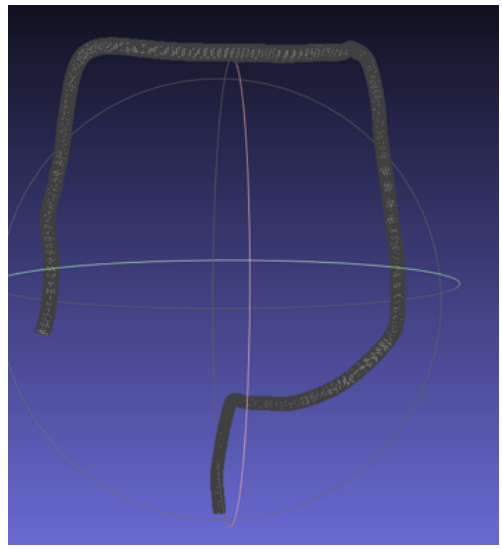

Figure 11.2. Cylinder mesh example obtained from the colon centreline.

Once these cylinders were obtained, they were used in *SOFA* to collapse the initial insufflated model by running a simulation in which a uniform pressure was applied on the entire colon. *SOFA* allows to save the colon mesh at different time steps, therefore several models of the lumen with different levels of collapse were saved during the

application of the pressure. All the models were collected in a repository and are shown in the figures 11.3 and 11.4 from the most insufflated to the most collapsed, from 1 to 9 respectively. The visualization of the obtained models is provided both from the outside and from the inside, exploiting the endoscopic camera of the tip of the colonoscope. These images were shown to the doctors to understand which model is closer to a normal (*i.e.*, without insufflation) and insufflated colon.

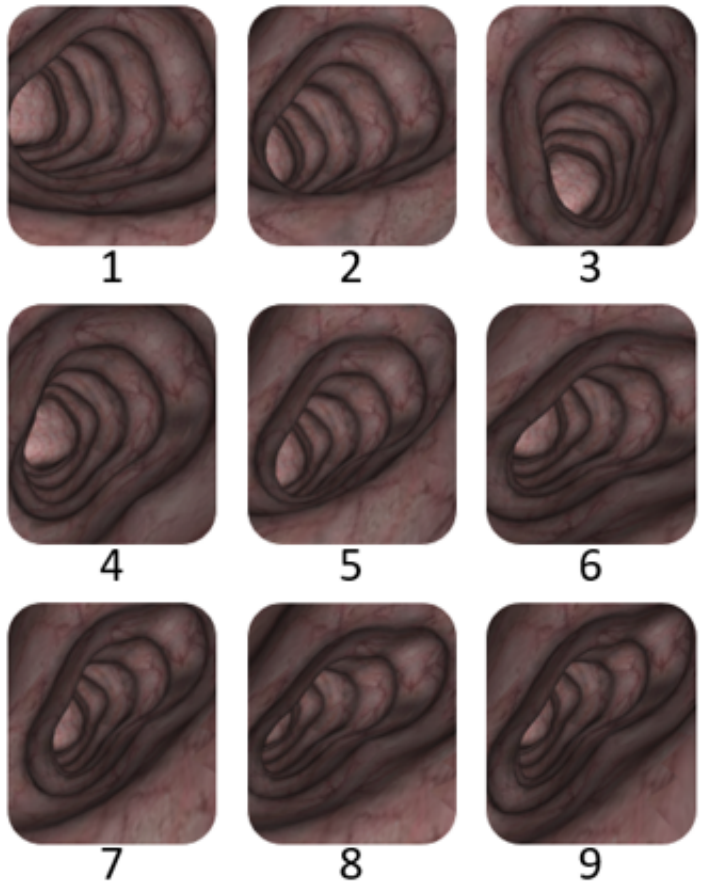

Figure 11.3. Endoscopic view of the colon models with different levels of collapse

The detailed meshes obtained with this process were used for the visualization model. Whereas, in order to create the collision model and the mechanical model used to implement both the peristalsis and the insufflation, the mesh was simplified through the *quadric edge collapse decimation algorithm*. In addition, for all the models, the

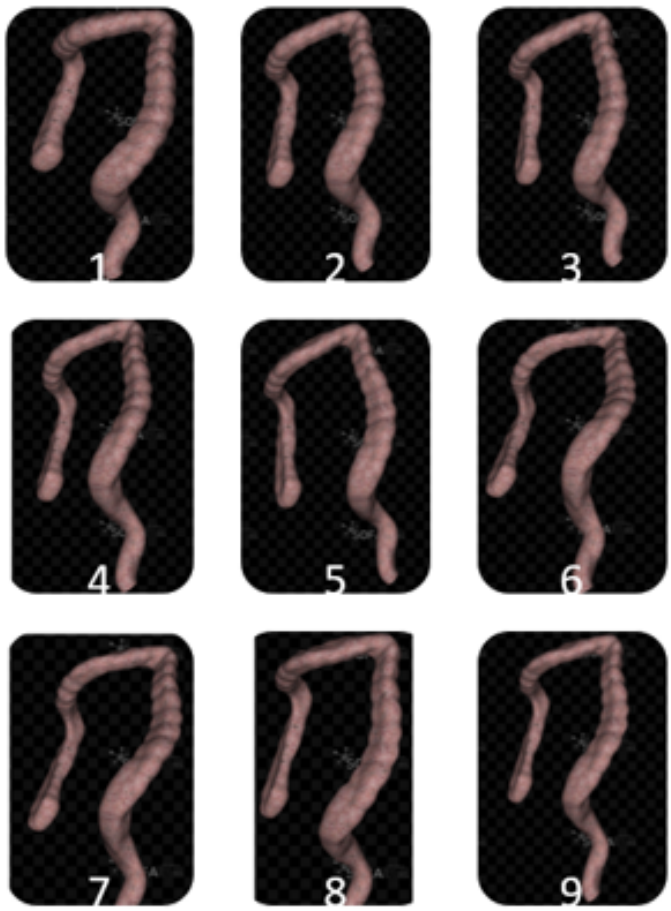

Figure 11.4. Colon 3D models with different levels of collapse.

"problematic" regions (*i.e.*, triangles with a low aspect ratio) were subjected to a standard *Laplacian smoothing*.

11.2.1 Mechanical properties

The previous simulator, introduced in chapter 4, uses the FEM to estimate the mechanical behaviour of the colon. In this new version, a mass-spring model is adopted to mimic the deformation of the tissues due to peristalsis and air insufflation/suction and contact with the colonoscope. Indeed, comparing the two methods, the mass-

spring model results more suitable to adjust the response of the tissue during the application of a surface pressure and allows the model to come back to the original shape once the colon (or a segment of it) is no longer subject to a pressure. This method requires a value of stiffness to estimate the restoring force of the spring and this must be lower than a threshold to let the tissue deforming under the action of a pressure. In addition, although the FEM is more accurate in terms of force-deformation estimation, it implies a high computational cost. This can be reduced by using the mass-spring model without having a noticeable impact in the mechanical realism of the simulation. Although, the force-deformation estimation might be less accurate, the overall simulation results as realistic as the FEM based model, as also confirmed by the clinicians.

The model parameters, *i.e.,* the elastic modulus, the Poisson coefficient, and the mass of the lumen were maintained the same as those set in the previous simulator version: respectively 1.3 MPa, 0.3 and 500 g. Also, the same physical constrains as those of the previous simulator version were applied.

11.3 Peristalsis model

To model the peristalsis the characteristics of the real peristaltic wave, *e.g.,* the amplitude, the velocity of propagation, the duration and the frequency, were extracted from the literature. Table 11.1 shows the characteristics of the peristalsis according to the study presented in [198]. Considering that these characteristics do not vary

	Duration (s)	**Amplitude** (mmHg)	**Velocity** (cm/s)
Ascending	15.9 ± 0.9	114.7 ± 6	1.8 ± 0.1
Transverse	14.6 ± 0.8	109.5 ± 6	1.1 ± 0.1
Descending	13.9 ±0.7	117.6 ± 7	1 ± 0.1
Sigmoid	13 ± 0.7	95.3 ± 5	0.8 ± 0.1

Table 11.1. Characteristic of peristaltic wave in different regions of the colon [198].

a lot across the different tracts, the respective average values were adopted in this study and set for the whole colon. Therefore, the peristalsis was implemented as a pressure wave that travel along the whole colon, from the cecum to the rectum, with a constant frequency and amplitude, that can be adjusted by the user. Each segment of the colon undergoes a progressive contraction and expansion in 14 seconds and the velocity of propagation is fixed and equal to 1.1 cm/s. In order to apply this pressure wave to each segment of the 3D model, the colon is divided in several regions and the triangles of each surface are extracted and saved in a list. The idea is to mimic the deformation of the tissue during peristalsis by applying a pressure, with a specific pattern, to the triangles of the model. Indeed, in *SOFA* there is a function that takes as an input a value of pressure and the indices of the triangles of a surface, and assigns this pressure value to each triangle along its normal direction

(*SurfacePressureForceField*). Therefore, given the triangle indices of each region and the values of pressure, the wave timing is made using two vectors:

- a position vector that identifies the regions in which the peristaltic wave is located;
- a pressure vector that contains the value of pressure that must be applied to each region (this value is different from zero in the areas where the peristalsis is).

Thus, for each time step these two vectors are used to assign the input of the previous function in the *SOFA* simulation.

Thus, the first step is to subdivide the 3D colon model to extract the indices of the triangles associated to each region. The triangles of each area can be obtained using another function in *SOFA*, that allows the selection of all the component contained inside a box (*i.e., BoxRoi*). The dimension of the selected area is carefully chosen in order to consider all the triangles of the region of interest and reduce the computational costs. The advantages and disadvantages related to the box size are summarized in the table 11.2.

Box size	Big	Small
Advantages	- less boxes - less computational costs - select a bigger area	- finer selection - apply the pressure only in the desired region
Disadvantages	- might select wrong triangles - might overlap another box	- might loss triangles - more boxes - higher computational costs

Table 11.2. Advantages and disadvantages according to the box size.

Therefore, in order to balance all these factors, a large number of tests was performed. Finally, the length of the boxes was set to 4 cm. Therefore, according to this dimension, the colons were divided into several regions with a constant length by creating the boxes along the entire model. The boxes were created in *SOFA* by defining a plane using three points and an extension along the orthogonal direction.

Thus, the indices of triangles of each region of the colon falling in each box were collected in a text file, so the list of triangles can be easily load at the beginning of the scene, reducing the computational costs of the simulation. Indeed, the other option would have been to compute the indices of the triangles in runtime, computationally more expensive. The data are stored in a variable and the indices of the each area are uploaded according to the region in which the wave is located. This information is provided by the position vector that contains a number of elements equal to the number of regions extracted from the model of the colon. In this way, the peristalsis will be located in the regions in which the position vector presents a value different from zero. In addition, the propagation of the peristaltic wave (from the cecum to the rectum) is modelled with a shift of the elements inside the position vector. This shift occurs every 4 seconds because each region has a length of 4 cm and the velocity of

propagation of the wave is about 1 cm/s. So, when the position vector assume a value different from zero, the corresponding region will be activated, loading all the indices of the triangles in the function in *SOFA* (*SurfacePressureForceField*). This function will take as an input also a value of pressure and this data will be provided by a pressure vector. Finally, in order to reduce the computational costs of the simulation, the deformation of the tissues related to peristalsis is performed only if the tip of the colonoscope is located in a region in which the peristaltic wave is. Indeed, for each time step, before the activation of a certain region, the peristalsis location will be compared with the position of the tip of the colonoscope. The region will be activated only if the instrument tip is in the region in which the peristaltic wave is or close to this area.

Once the region is correctly selected, a pressure must be applied to each triangle of the surface along the normal direction in order to mimic the behaviour of the colon related to the peristaltic motion. Thus, during peristalsis the tissue undergoes two main deformations: a strong contraction that has a duration of 7 seconds and a slow relaxation that takes more or less other 7 seconds. So, the pressure applied to the triangles of the model is modelled using the sine-wave pattern shown in figure 11.5. The maximum value reached by this curve can be modify by the doctor, changing the amplitude in the simulation environment. The value of the amplitude represents a scale factor that is multiplied by the current value of pressure, extracted from this curve.

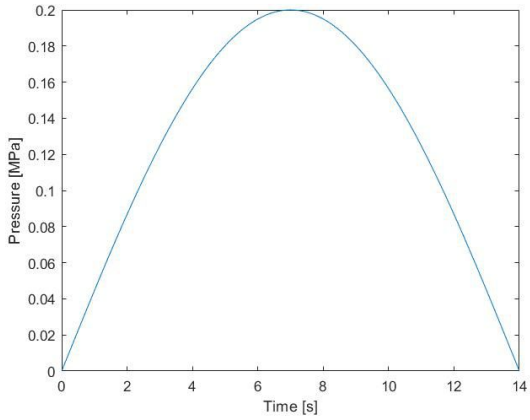

Figure 11.5. Chart of the pressure trend in 14 seconds for each colon section.

Similar to the position vector, the pressure vector contains the value of pressure of each region of the colon. So, the number of element of this vector is proportional to the number of regions extracted from the colon model and the value is different from zero only in the districts in which the peristaltic wave is. The values of pressure inside the pressure vector are updated, every time step, following this sine-wave pattern. Then, if the tip of the colonoscope is located in a region in which the peristaltic wave

is, the values of pressure are given as an input, with the triangles' indices, to the *SurfacePressureForceField SOFA* function.

11.3.1 Implementation

After the the definition of the two previous vectors, position and pressure, the mechanical model of the region must be created in *SOFA* to apply the pressure on a specific district. Indeed, the function, that allows the application of a constant value of pressure along the normal direction of each selected triangles, needs the association with a mechanical object inside the *SOFA* framework. A mechanical object in *SOFA* is a component which contains the mechanical state of an object, namely the DOF, their associated velocity, acceleration and the forces applied on the simulated body. Therefore two options are available:

- associate to all the regions, extracted from the colon model, a mechanical object in the simulation environment and apply the pressure to the district in which the peristaltic wave is;
- create only few mechanical object and update the indices of the triangles and the pressure in the SOFA function, according to the position of the wave.

The second solution is adopted in order to decrease the costs of the simulation. Indeed, as mentioned in the mechanical properties section, the computational costs are mostly related to the mechanical model. Thus, the minimum number of mechanical object that must be created to implement the peristaltic wave is equal to 4 because the wave travels with a constant velocity of propagation v = 1 cm/s, each region has a length (l) equal to 4 cm and the wave spends a time (t) equal to 14 seconds in each region. The integer value is calculated as following:

$$MechanicalObjects = \frac{t}{v * l} = \frac{14}{1 * 4} = 3.5 \tag{11.1}$$

Since it must be an integer, the value is rounded to 4.

Thus, the function, used to apply the pressure in *SOFA*, is implemented in four different mechanical objects in the simulation environment. This allows the independent activation of each region according to the location of the peristaltic wave. As a result, the peristaltic wave is performed by:

- evaluating the position of the instrument in the colon model,
- estimating the position of the peristaltic wave along the colon;
- comparing the position of the instrument with the location of the peristalsis: if the capsule is in an active region (*i.e.*, presents the peristaltic wave), the values of pressure, contained in the pressure vector, and the indices of the triangles of the active regions, supplied by the position vector, are given as an input to the function (*SurfacePressureForceField*) in *SOFA*.

Finally, parameters, such as the amplitude of the peristaltic wave and the frequency between two consecutive waves, can be adjusted by the user. The following figures 11.6 and 11.7 show the peristalsis performed in the final simulation environment.

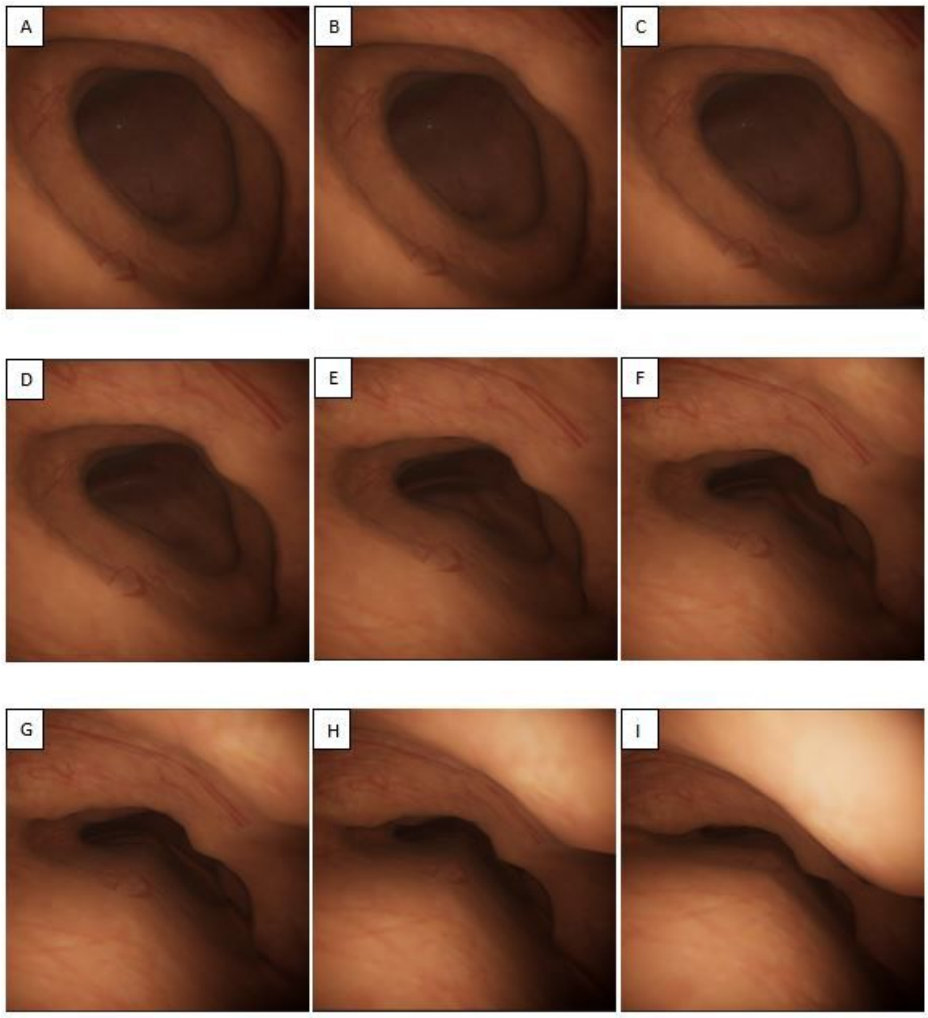

Figure 11.6. Contraction of the colon (from A to I) due to the peristaltic wave.

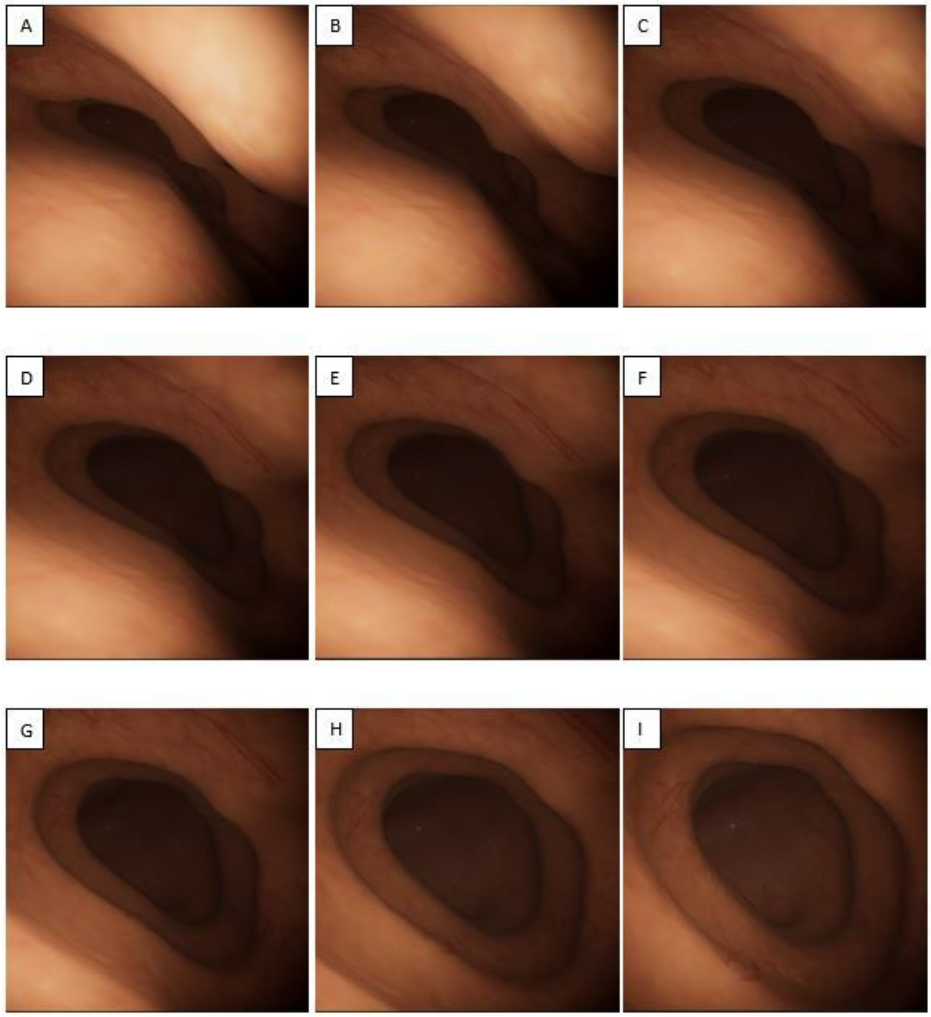

Figure 11.7. Relaxation of the colon (from A to I) due to the peristaltic wave.

11.4 Air insufflation model

The other important feature integrated in the simulator is the deformation of the colon during the air insufflation/suction. Since the colon is normally collapsed, the insufflation of air is necessary to expand the wall of the colon to allow both the navigation with the colonoscope, and to improve the polyps detection. However, the

pressure must be extremely controlled to avoid the over-distension of the colon that generates pain and discomfort to the patient.

Unlike peristalsis, there are few studies that consider the value of pressure applied during air insufflation. In general the deformation of the colon wall, induced by the air, must be controlled by the doctor to avoid damages of the mucosa and perforation of the colon, but there are no recommendation about the maximum pressure value that can be applied to the tissues. There is only a suggested range in which the pressure should stand and it is between 9 and 57 mm Hg [111].

The air insufflation/suction is modelled as a homogeneous surface pressure applied to the segment of the colon close to the tip of the colonoscope with the same *SOFA* function used to mimic the peristaltic motion (*SurfacePressureForceField*). As with peristalsis, the collapsed model of the colon is divided into many regions to inflate only the section where the endoscope tip is located. Also in this case, the list that contains the indices of the triangles is useful and will be loaded at the beginning of the simulation to reduce the computation costs.

First of all, every time that the user activate the insufflation or the suction, the position of the instrument along the centreline is estimated. Then, knowing the point of the centreline closer to the tip of the colonoscope, the surrounding portion of colon of about 12 cm is selected as a region of interest. The indices of the triangles of the region are provided by the text file loaded at the beginning of the simulation. In the same way, the triangles of the adjacent regions are selected. As shown later, these three region will be deformed with different values of pressure. The pressure has two starting values according to the function that the user wants to activate between insufflation and suction:

- for the insufflation the pressure values are set equal to -0.01 MPa for the region in which the instrument is and -0.005 MPa for the two adjacent segments,
- for the suction the pressure values start from 0.01 MPa for the region in which the tip of the colonoscope is and 0.005 MPa for the adjacent sections.

These values are set to provide a rapid initial expansion/collapse of the colon when the user activate the function to mimic the rapid and visible deformation of the tissues as in a real colonoscopy. The control of the air insufflation/suction should be proportional, as in standard colonoscopy. Indeed, the conventional colonoscope provides two buttons respectively for insufflating and desufflating the air.

Therefore, the values of pressure are decreased during the air insufflation as follows:

$$P_{\mathrm{i}} = P_{\mathrm{i\text{-}1}} - P_{\mathrm{dec}} \tag{11.2}$$

where the new value of pressure $\mathrm{P_i}$ is calculated from the previous value ($\mathrm{P_{i\text{-}1}}$) minus the $\mathrm{P_{dec}}$=0.005 which represent the decrement in terms of pressure when the user presses the corresponding button. In the same way, the value of pressure are increased during suction as follows:

$$P_{\mathrm{j}} = P_{\mathrm{j\text{-}1}} + P_{\mathrm{inc}} \tag{11.3}$$

where the new value of P_j is calculated from the previous value (P_{j-1}) plus the P_{inc}=0.005, which represent the decrement in terms of pressure when the user presses the button. The P_{dec} and P_{inc} are equal both in the region in which the capsule is and in the segments close to it. In addition, two maximum pressure values are determined to avoid the generation of instabilities in the simulation. Examples of these instabilities are the interpenetration of the colon walls caused by an excessive suction and the explosion of the colon model due to a huge pressure value reached with the air insufflation. Therefore, the maximum values of pressure are set as follow:

- during insufflation -0.1 MPa and -0.08 MPa, respectively for the region in which the instrument is and the adjacent segments;
- during suction 0.03 MPa and 0.015 MPa, respectively for the region in which the capsule (or the tip of the colonoscope) is and the adjacent segments.

A negative pressure corresponds to an expansion of the colon walls while a positive pressure entails a contraction of the intestinal tissues. This is because the function (*SurfacePressureForceField*) in *SOFA* applies a scalar value of pressure along the direction of the normals of each selected triangle. Indeed, given the colon model with the normals shown in figure 11.8, the expansion of the colon is implemented using a negative pressure while the contraction is implemented with a positive pressure.

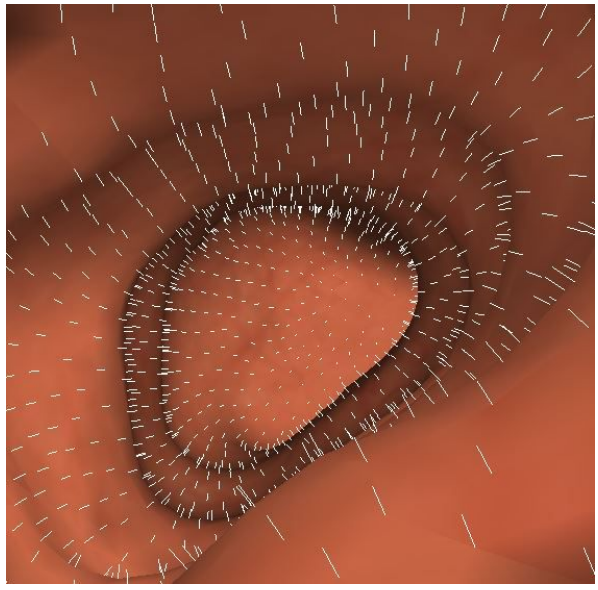

Figure 11.8. Direction of the normals in the colon model.

11.4.1 Implementation

At the beginning of the simulation the indices of the triangles are loaded from the text file. In addition, as with the peristalsis, the mechanical objects are created in order to use the function *SurfacePressureForceField* in *SOFA*. In this case, only three mechanical objects are needed: one to deform the region where the endoscope tip is located, and the other two for the regions close to it (the one on the front and the one on the back). Indeed, for each section, a different value of pressure will be assigned in order to achieve a realistic deformation of the intestinal tissues. Therefore, whenever the air insuflation/suction is activated by the user, the indices of the triangles of the region where the endoscope tip is located and the adjacent sections are selected. Those data are given as an input to the*SurfacePressureForceField* function and the values of pressure are assigned following the details given in the previous section. Indeed, a starting value of pressure is given when the insufflation is activated for the first time in a certain region, then the value is updated incrementally or decrementally, according to the equation above. Hence, the pressure value is increased or decreased respectively to mimic suction and insufflation until the established maximum values are reached. This allows clinicians to progressively control the expansion and the collapse of the colon walls as in a colonoscopy procedure.

The figure 11.10 shows the deformation of the colon due to air insufflation in two different tract of the colon. In the same way, the collapse of the colon due to suction is presented in figure 11.9.

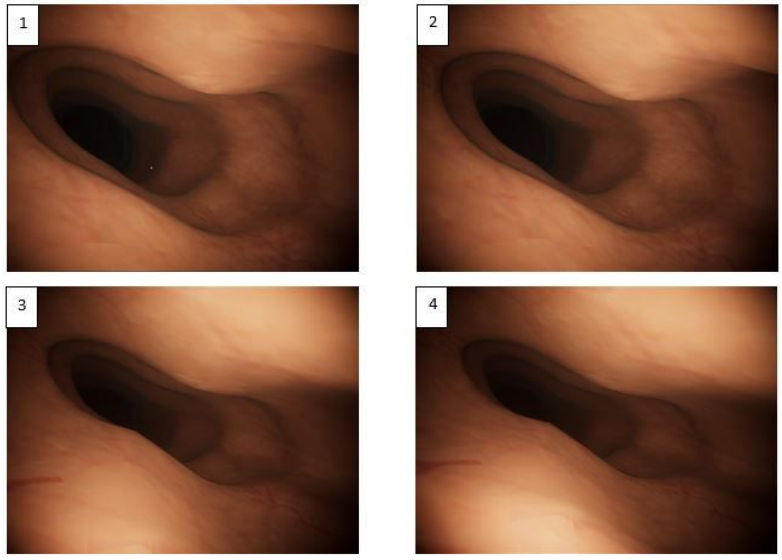

Figure 11.9. Progressive contraction of the colon due to air suction.

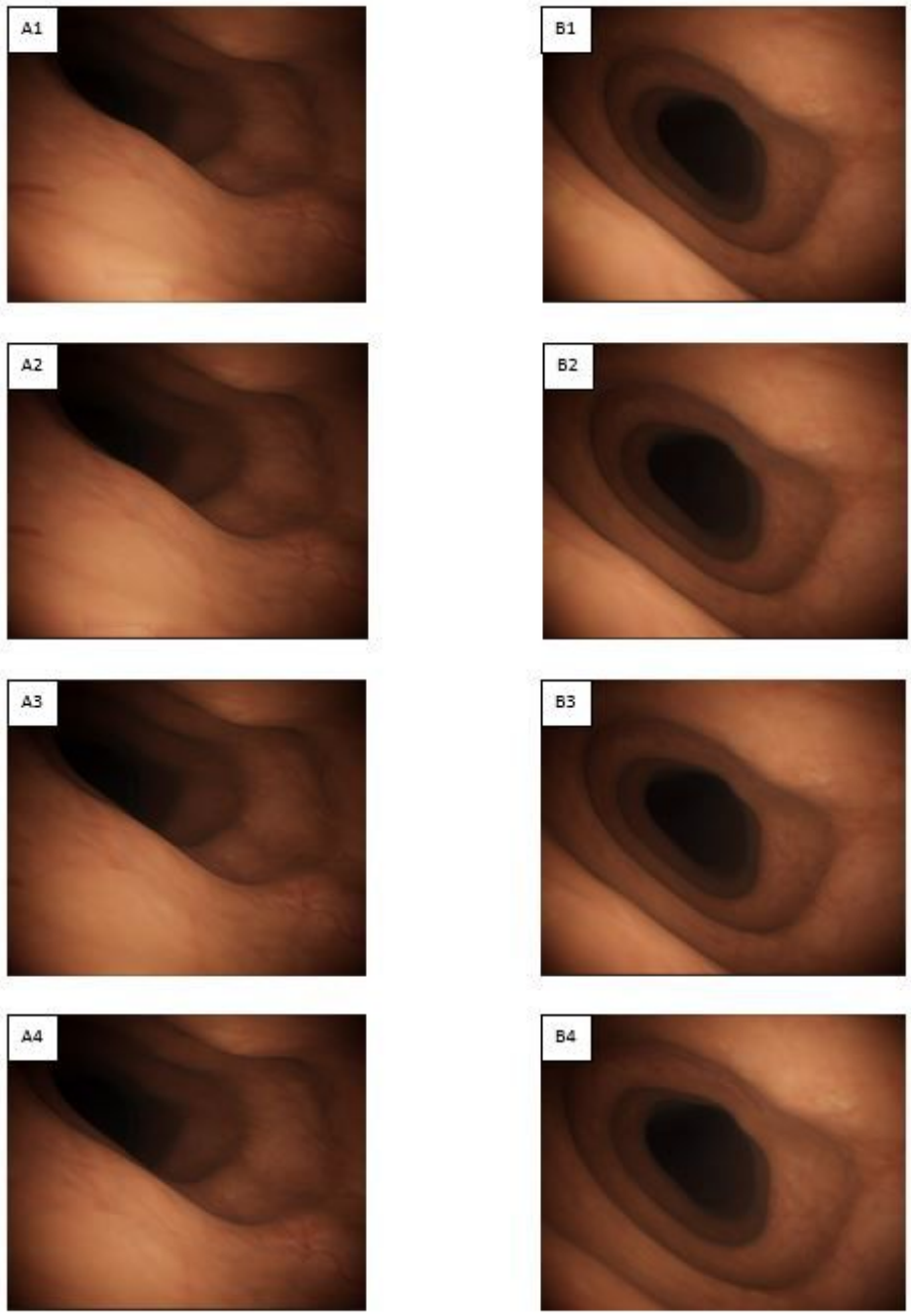

Figure 11.10. Progressive insufflation of the colon (from 1 to 4) in two different regions.

11.5 Clinical Validation

The realism of the overall simulation environment, including the effect of the peristalsis and of the air insufflation, were evaluated with four expert gastroenterologists. The subjects were asked to (1) perform a complete robotic colonoscopy starting from the rectum and reaching the cecum; (2) once reached the cecum, withdraw the endoscope looking for polyps. The movements of the robotic endoscope were controlled by a videogame joypad. During the procedure, the peristalsis was automatically generated. The value of amplitude and the frequency were assessed with an expert gastroenterologist during a preliminary evaluation. The doctors could control the air insufflation and suction, and they were asked to use it as the would do in a standard colonoscopy procedure (*e.g.,* to better visualize the lumen). The insufflation and suction could be controlled incrementally by pressing two buttons on the device controller.

Each experimental session took place in a dedicated training room (avoiding interruptions and distractions during their execution) inside Hospital de la Santa Creu i Sant Pau (Barcelona, Spain). Each participants was allowed to get familiar with the system for five minutes before performing the task.

At the end of the test, the clinicians were asked to evaluate the realism of the overall simulation environment and the new added features (*i.e.,* peristalsis movements and air insufflation/suction) during both intubation and withdrawal. Thus, the subjects were asked to rate on a 5-points Likert scale the realism of the following items: (1) overall simulation enviroment, (2) peristaltic motion, (3) air insufflation, (4) mechanical deformation of the colon when in contact with the endoscope. Finally, they were asked to rate (5) the usefulness of the simulator for training porpoises.

Concerning the analysis, the consensus measure as computed in [152] was used to assess the dispersion of the clinicians' answers to the questionnaires. Whereas, the mean and standard deviation values of the rate given for each question were used to assess the realism of each evaluated feature.

11.6 Results

The final simulator could smoothly operate on a laptop with Intel(R) Core(TM) i7-10750H processor, CPU of 2.60GHz, 32GB of RAM and NVIDIA GeForce RTX 2060 graphic card. The simulation environment was updated every 0.02 seconds, and no delays were reported. All the four participants could successfully complete the tests. Regarding the analysis of the survey, the consensus for each question was greater than 0.8. This shows a high level of agreement between doctors for each question. As reported in figure 11.11, all the five questions got an average rate greater than 3.5 points, assessing a high level of realism for each the features.

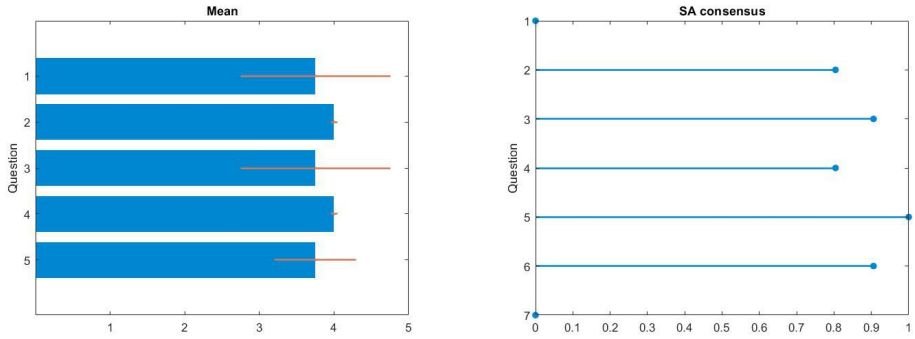

Figure 11.11. Mean and standard deviation (left) and consensus measure (right) of the five questions assessing the realism of (1) the overall simulation enviroment, (2) the peristaltic motion, (3) the air insufflation, (4) the mechanical deformation and (5) the usefulness of the simulator for training porpoises.

11.7 Discussion

This work successfully demonstrated the integration of two important features related to the motility of the colon on the virtual simulator developed and tested within this thesis. The realism of the final simulator is corroborated by the validation test made with the clinicians. However, future work will focus on improving even further the new features: peristalsis and air insufflation. For instance, a more realistic deformation of the intestinal tissues due to the peristaltic wave can be obtained by generating a more concentric contraction of the colon walls. In addition, the velocity of collapse of the colon related to the suction, was considered slow by the doctors. Indeed, during real colonoscopy procedures, the suction rapidly produces a completely closure of the lumen. This aspect can be improved by increasing the pressure of the suction and tuning the parameters of the simulator to avoid the generation of instability in the simulation environment. In addition, the future perspectives will include the simulation of the intestinal content and the capability to treat and remove the polyps.

CHAPTER 12

Modular mechanical simulator of colonoscopy

Although virtual simulators have many advantages with respect to the mechanical ones, there are some cases in which a mechanical simulation platform is preferred. For instance, when testing new devices, physical simulators avoid the need and related difficulties of modelling the medical device in a computational environment. As described in chapter 4, current physical simulators, especially those in the market, often show scarce visual realism, limited variability of the anatomical configurations and high costs. Therefore, this chapter presents an innovative and low-cost workflow for designing and fabricating silicone-made colon simulators with a modular and versatile approach. The simulator fabricated following this method represents an alternative mechanical solution to the virtual simulator developed within this thesis (chapter 4). The ultimate goal, indeed, will be its integration in the *HMI evaluation framework*.

The production line of the mechanical simulators envisages free customization of molds, that are supposed to be 3D printed and arranged according to the desired colon configuration to be replicated. Afterward, fabrication and connection of modular colon segments are realized through silicone molding, enabling the choice of any compatible silicone rubber. For demonstration, FEM analysis was performed to address silicone selection aiming to qualitatively mimic the colon biomechanics. A complete colon simulator was fabricated and equipped with assorted magnetic polyps. The content and face validity of the designed simulator were judged by expert GI endoscopists.

The research presented in this chapter was conducted in collaboration with the Scuola Superiore Sant'Anna of Pisa, as part of a M.Sc. student's thesis in bionics engineering. The main contributions provided by the author of this Ph.D. thesis are (1) know-how regarding simulators for robotic colonoscopy, (2) supervision of the design choices and, more in general, of the overall project, and (3) close support for the set-up of the clinical validation, including the analysis of the results.

12.1 Introduction

The ability to perform efficient and safe endoscopy procedures is a core element of GI endoscopy practice. Mastering a complex procedure as colonoscopy requires experienced physicians to show cognitive and technical competencies, *e.g.,* subtle control of the endoscope navigation, high-level of visual-motor coordination, and looping avoidance techniques. In this context, simulation-based education offers a low-risk teaching and assessment tool aimed at providing repetitive and low-stress training in a non-patient care environment [86]. Extensive use of simulation is beneficial not only for the independent and self-confident acquisition of skills, but also for the prevention of skills decay, shortening the learning curve, and for enhancing patient safety and quality of health care [204]. In addition, realistic simulation platforms endowed with robust data collection systems are highly needed for accurate design and testing of new innovative technologies, *e.g.,* robot-assisted colonoscopes, in controlled and repeatable environments. The tests conducted with the *HMI evaluation framework* reported in chapter 8 are a demonstration of this application.

12.1.1 State of the Art

As reported in section 4.2, over the past ten years, several simulation solutions have been developed for acquiring competences in lower GI endoscopy, varying in affordability, anatomical realism, targeting different tasks and expertise levels. Among all the solutions (*e.g.,* virtual, mechanical, animal models), the strengths of the mechanical simulators remain (1) the level of immersive interaction they offer to the users given their physical consistency, (2) their natural integration in the standard clinical layout with the ordinary instrumentation, (3) the reliability of the scope navigation, and tactile sensation. In addition, in terms of testing new medical devices, they avoid the need and related difficulties of modelling the devices in a computational environment. Nevertheless, according to the medical experience [205], they often lack several features such as detailed visual realism, the possibility of selecting different anatomical configurations, and the inclusion of objective feedback on the performance, besides their limited affordability.

Recent research-oriented simulators [93, 96] have been developed in view of offering a wider range of realistic cases and reducing the costs of the simulator. This is obtained by embedding inexpensive materials and exploiting 3D-printing manufacturing, paving the way for adaptable and easy-to-fabricate phantoms. One research group [92] has designed and fabricated a colon simulator via a serial assembling of common and inexpensive material, *e.g.,* plastic hamster tubing, rubber bands, and vacuum extension hoses. Although clinical validation highlighted the ability of this platform to distinguish trainees and experts, this solution cannot incorporate the use of insufflation and it cannot transmit the true haptic feedback of a real endoscope interaction. *Formosa et al.* [206] proposed the innovative Modular Endoscopy Simulation Apparatus (MESA) relying on both 3D printed molds and open steel piping

components and designed to be the negative of the colon geometry. Even though the model was scaled to twice the average colon size and silicone selection was guided by ease of casting and pigmenting, mold-by-mold stacking paves the way for a modular conjunction of shorter sections, offering a simplified fabrication process.

12.2 Design

The aim of this work is the development of a standardized methodology for the envisage and straightforward fabrication of a low cost custom-made physical colon simulator. Given the extreme variability in configurations, length, and tortuosity of the human colon, a versatile and easy-to-use strategy for the replication of its anatomy is given by the modular conjunction and assembly of printable molds for silicone pouring. Silicone rubbers are popular materials of choice for lightweight compliant systems. This is due to their high power to weight ratios, the relatively small input air pressures needed to induce large deformations, and the ease of modeling and shaping at substantially low costs [207].

12.2.1 Model of the colon

The first step is the definition and design of a model to be used for reproducing the lumen cross-section, and its peculiar shape. Indeed, the complexity of the human colon mostly arises from the presence of haustra[1], semilunar folds[2], and taenia coli[3] which may occlude structural abnormalities during endoscopy. Inspired by the three-folds topology presented by *Langer et al.,* [208], a symmetrical and triadic configuration was defined, the *clover-like section*, as the nominal lumen cross-section of the model.

Sizing of this configuration was performed referring to both the latest findings on colon morphology from the analysis of CT colonography data [209] and *ad-hoc* measurements. The latter were retrieved on eight real 3D colonic models collected from colonography examinations of the *Cancer Imaging Archive* [130]. Three qualitative haustral loops were analyzed for each model, by means of three planes intersecting the lumen section in ascending, descending and transverse segments in order to highlight three different geodesics. Incident planes were chosen appropriately to identify sections that were clearly correspondent to the *Langer* model and inscribed triangles were sketched to distinguish the three haustral pockets. Specifically, the width (a) and height (b) of each haustra was quantified. A dimensionless parameter R, *i.e.,* the ratio between height and width (a and b), was defined to represent the extent of the fold bulge. A graphical clarification of these parameters is shown in figure 12.1

[1]Haustra: wall protrusions of the colon that are delimited by their corresponding semilunar folds.
[2]Semilunar folds: visible circumferential folds of the mucosa resulting from the circumferential contraction of the inner muscles between stiffened taeniae.
[3]Taenia coli: three outer longitudinal bands of the gut tunica muscularis, creating a three-helix structure of strong cables upon contraction.

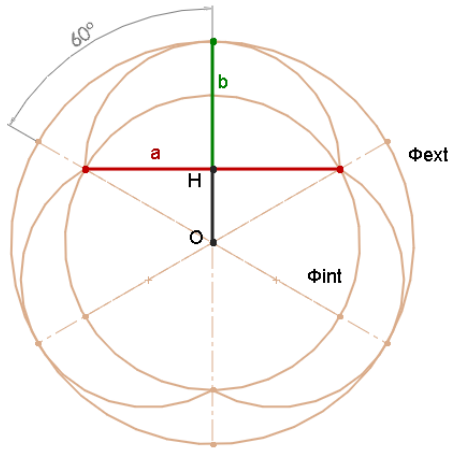

Figure 12.1. Colon section design.

. A total of 24 measurements for both a and b parameters was retrieved and outliers were removed from the distribution of R coefficients. Main features of retrieved data are reported in table 12.1. To reproduce the oscillatory appearance of the colon

Ratio R	Average	Min	Max	Std
	0.372	0.203	0.668	0.077

Table 12.1. Descriptors of R coefficient derived from eight colonographies. R is the ratio between height and width.

haustra along the longitudinal direction, the average R was used for sections that are coplanar with the semilunar folds (*i.e.,* terminal), and the maximum value of R for the in-between sections (*i.e.,* middle), in which the colon lumen shows the typical bumped shape. In terms of average external diameter, the choice relied on *Alazmani et al.* findings [209]:

- 34,5 mm, the mean of the average diameter measured on each colonic tract weighted for the tract length, in terminal sections;
- 41 mm, the average between the total colonic diameters on supine and prone position, in middle sections.

Given these parameters and assuming that non-inflated colonic wall thickness ranges between 0.2 and 2.5 mm [132], the nominal colonic thickness was taken as the average, hence 1.35 mm. An additional dimension was needed to complete the design of the *clover-like cross-section*, namely the internal diameter delimiting the attachments of the taeniae coli. For this reason, simple trigonometric relationships were deployed referring to the triadic model of figure 12.1:

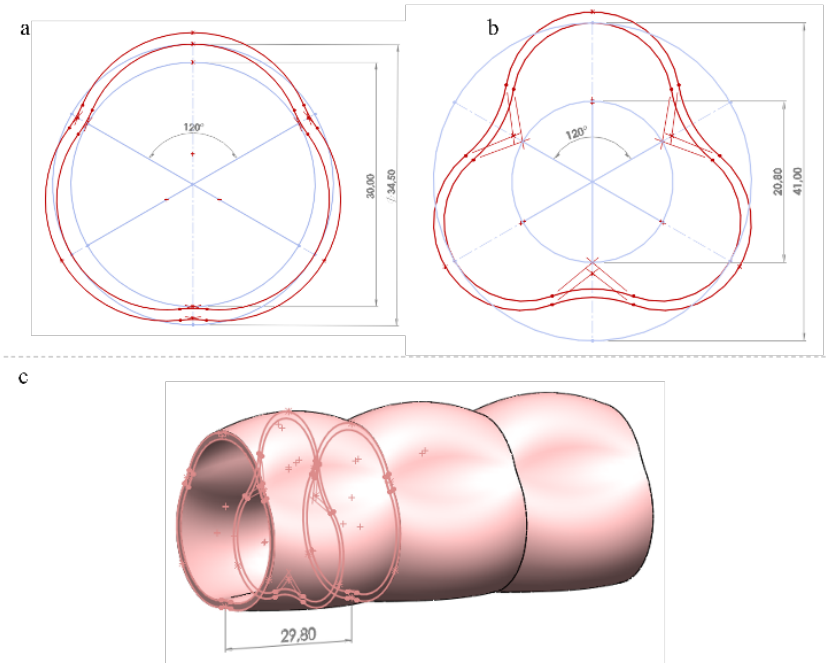

Figure 12.2. Colon sections (a,b) and conceptual module (c).

$$R = \frac{b}{a} \tag{12.1}$$

$$b + OH = \frac{\varphi_{ext}}{2} \leftrightarrow \varphi_{int} = \frac{\varphi_{ext}}{\sqrt{3}R + 1/2} \tag{12.2}$$

Equation 12.2.1 provides a unique descriptor to formulate the set of cross-sections which will define a complete colon unit. Specifically, table 12.2 summarizes all the essential parameters for designing the final cross-sections reported in figure 12.2, where haustral geodesics are sketched with an offset equal to the average thickness. Finally, according to further suggestions given by medical expertise, 8 mm bevels were applied in correspondence to the three clover "edges" to simulate the presence of the outer taeniae bands.

As a second step, the envisage of a modular assembling system requires the selection of the minimum fabrication length, according to a "building blocks" concept. In this regard, differently from the haustral fold height, that was introduced by *Thompson et al.* [210], here we refer to taeniae unit as the distance on the longitudinal direction of the lumen between each triad of semilunar folds. Taken as reference an average colonic length of 185 cm [209], we considered the number of haustral loops identified by a team of experienced clinicians, against an haustral loop extraction

	Terminal	Middle
φ_{ext} (mm)	34.50	41.00
φ_{int} (mm)	30.00	20.80
b (mm)	2.61	1.80
a (mm)	0.97	1.20

Table 12.2. Terminal and middle cross sections parameters.

algorithm [211], and we considered the taeniae unit as the mean of the ratios between colon length and number of extracted loops, *i.e.,* 29.8 mm. At this point, the design of the final colon module results from filling the sequential arrangement of the clover-like sections in parallel, at a reciprocal distance of half of the taeniae unit, so that a 1-unit colon is composed of two terminal sections and one middle section in-between. The minimum colon module can be further expanded (figure 12.2.c) to envisage longer straight colonic tracts, which are essentially constituted by the replication of N (*e.g.,* three) identical units along the longitudinal axis. The three-unit module was chosen as the modular straight base for realizing a complete colon simulator.

12.2.2 Molds

With the intention of proposing a modular, reusable, personalized fabrication method compatible with any anatomical configuration, a set of mechanical molds dedicated to silicon pouring was developed. The molds should enable both a customizable arrangement in the 3D space and a versatility of design modifications. Assuming one *taeniae-unit* as the smallest module that can be manufactured, a series of *ad-hoc* molds were designed in *SolidWorks* (Dassault Systèmes, Vélizy-Villacoublay, France). All ensembles share a common configuration: interlocking of an inner mold and three outer molds to comply with the clover triadic symmetry, without any screw mechanism. The upper outer mold is equipped with a cylindrical hollow reservoir for accommodating silicone pouring and a pair of 4 mm holes for enabling airflow.

The minimum set of molds for developing a complete colon simulator consists of (1) segment molds, devoted to fabricating standalone straight colonic segments of N units (*e.g.,* N=3) and (2) connection molds, meant to fuse several modular colon units. Figure 12.3, shows the molds. The connection molds can be of two kind: straight and curved. Straight connectors generate a straight single-unit link between two colonic segments (figure 12.3.c). Instead of developing a specific mold set for each module length that the user would like to recreate, a straight connector is a versatile tool suitable to bond two colon segments, either straight or curved. Curved connectors are a flexion of a straight connection mold of either two or three units by any desired angle. Given the limited set of angles offered by the flexion of a single unit, two-units and three-units curves where selected in order to offer a range of flexion of 0

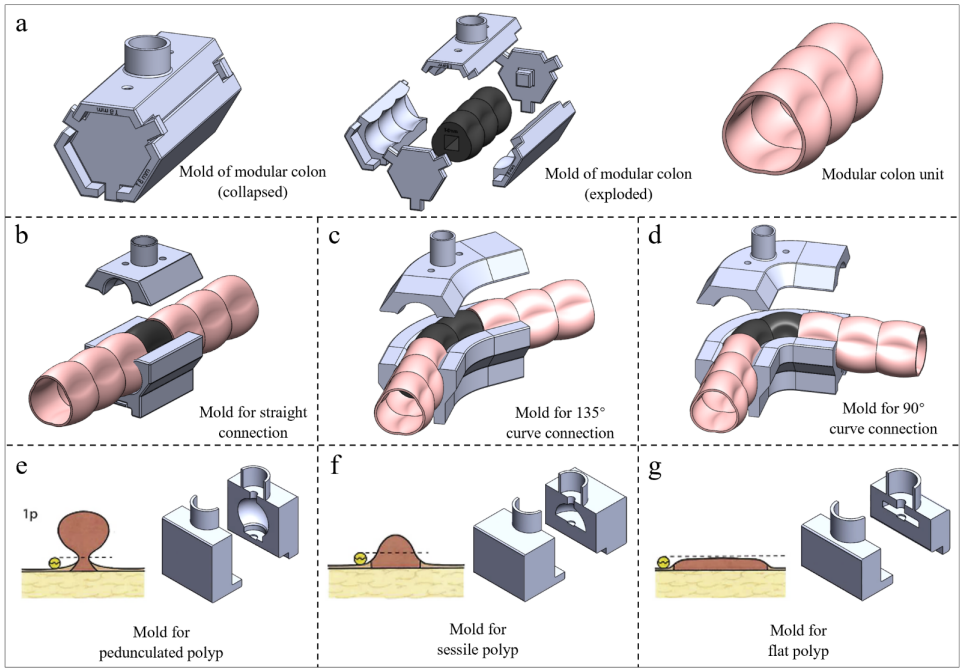

Figure 12.3. Design of molds for fabrication of colon simulator: (a) mold design of one modular colon unit and the corresponding modular colon unit; mold set for straight (b), 135° curve (c), and 90° curve (d) connection, respectively; mold design of pedunculated (e), sessile (f), and flat (g) polyps.

- 140° and 0 - 180°, and minimum radius of curvature of 24,39 mm and 28,45 mm, respectively. This choice allows to obtain sharper or smoother curvatures. Mold sets for connecting two colonic segments by adding double-unit links of 135° and 90° are shown in figure 12.3.c-d.

As a complementary feature of the colon simulator, artificial polyps were also implemented to simulate polypectomy. Three types of polyps, *i.e.*,, pedunculated, sessile, and flat were considered, and their corresponding molds were designed as shown in figure 12.3.e-g. For the purpose of making these pathological extensions modular also in their arrangement along the simulator, a magnetic connection was devised as a suitable and simple technique for repositioning polyps after removal. This was obtained by integrating a cylindrical magnet (diameter 3 mm, height 1 mm) within the stalk channel before silicone pouring. Therefore, the polyp is suitable for being installed in any location of the inner lumen by placing an equivalent external magnet on the outer surface of the synthetic colon.

12.2.3 Modular Fabrication concept

The fabrication of a complete simulator required to choose a reference model to be replicated. From the *Cancer Imaging Archive* [130], a 3D colon model was reconstructed from a CT colonography using *3D Slicer* [95, 131]. The centreline was also extracted with *3D Slicer* as shown in figure 12.4.a. Dimensional analysis of the reference model was performed in *SolidWorks*, in order to retrieve (1) the lengths of each colonic tract along the centreline and (2) the inter-segmental angles between adjacent segments, sketched along the centreline considering a length equal to the *taeniae-unit*. The centreline was simplified and parameterized for reasons of simplicity and ease of fabrication. Therefore, curved connection molds of 135° were designed to reproduce angles greater than 120°, whereas molds of 90° curve for angles lower than 120°. However, after curing, silicone softness enables to adapt and further modify the curvature. Finally, a global 3D spline was derived using *SolidWorks* to have a complete overview that summarized the lengths, curvatures, and orientation of each colonic tract to be reproduced in the simulator (figure 12.4.b). This trace was the main reference for identifying the number of equivalent straight segments and connections that were needed and to be assembled in a modular way, as shown in figure 12.4.c.

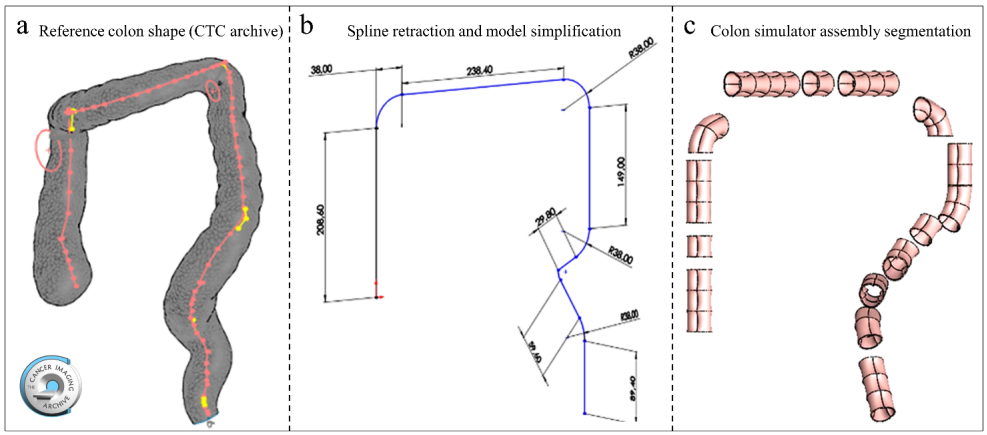

Figure 12.4. Modular fabrication concept: (a) take reference colon geometry from a CT colonography; (b) extract and simplify the geometry to a spline; (c) based on the spline, retrieve the curve and length information of each section to segmentize the whole colon assembly.

This approach provides a general pipeline for modularization and production concept, which readily transfers to other users depending on their different needs (*e.g.*, different choice of anatomical configuration, material, color, molds arrangement etc.).

12.3 Experiments

12.3.1 Material Analysis

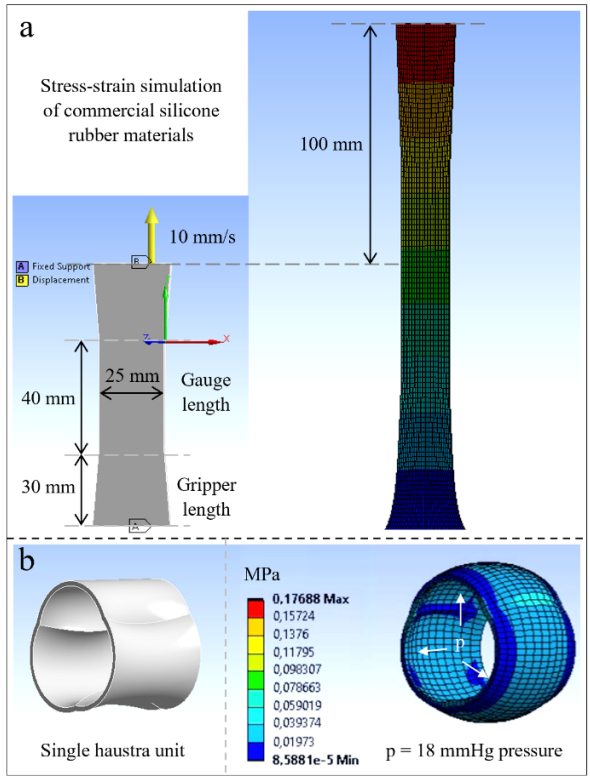

Figure 12.5. Material simulations: (a) stress-strain evaluation of silicone rubber specimen under quasi-static loading condition; (b) deformation evaluation of single haustra unit made of *Ecoflex 00-50*.

FEM simulations were performed using *Ansys* (Ansys, Canonsburg, PA, USA) to detect the stress-strain behavior of each available and affordable silicone rubber material (Smooth-On Inc., Macungie, PA, USA). The purpose of the simulations was to compare the performance of the different silicones against the human colon response. Specimen dimension and loading conditions had been collected by [212], where uniaxial stress-strain tests were performed on human colonic samples. Therefore, bone-shaped specimens were modeled according to the same dimensions specified by the [212], namely a gauge length of 40 mm, a width of 25mm, and a total sample length of 100 mm. Samples were subjected to the uniaxial quasi-static loading

condition, which consists of a tensile load of 10 mm/s up to 100 mm of displacement applied on one grip edge with a fixed support on the opposite grip edge. Intermediate or dynamic loading speeds were not evaluated, given that they are less representative of true interaction between the colonoscope and the colonic tissue. Eight materials including *Ecoflex series 00-10, 00-30, 00-50, 5*, *Dragon Skin series 10M, 20, 30*, and *Smooth-Sil 940* were selected and examined. Constitutive hyperelastic models of the aforementioned silicones were retrieved from the mechanical characterization conducted by *Marechal et al.* [213]. The boundary conditions and the deformed specimen after 100 mm displacement are shown in figure 12.5.a. As better described in section 12.4.1, a preliminary assessment drove to the selection of Ecoflex 00-50 as the potential candidate for fabrication. Consequently, with the goal of selecting a material that replicates not only the mechanical properties of the human colon, but also its viscoelastic behavior, the validation of Ecoflex 00-50 as the potential candidate was completed performing a simulation under insufflation conditions. The simulation entails the assessment of deformation and stress performance of a one-unit colon model, instead of a three-unit module, in order to minimize the computational cost of the solver. The test protocol follows the prescriptions reported by [214] concerning the quasi-static loading condition: controlled inflation from 0 mmHg to 44 mmHg is applied linearly at a speed of 5,3329 Pa/s (equivalent to 4 mmHg every 100 s). For simplicity, a single average equilibrium time of 100 s for each pressure incremented was chosen. Displacement of terminal delimiting sections of the model was impeded by fixed supports. Figure 12.5.b shows the single haustra unit and the color map of equivalent Von Mises stress at 18 mmHg pressure.

12.3.2 Fabrication

Once molds sets had been completed and the silicone had been selected, the next step was the fabrication of the complete simulator. Every mold was manufactured by means of *Zortrax M200* 3D printer (Zortrax, Olsztyn, Poland) with a nozzle diameter of 0.4 mm. Employed materials for printing were chosen according to the availability and affordability of rigid plastic filaments, specifically: *Z-HIPS* and *Z-GLASS*. The general fabrication steps for the colon simulator is: (1) deposition of mold release, *Ease Release™ 200* (Smooth-On Inc.) on the inner surfaces of the mold (figure 12.6.a); (2) assembling and sealing of the mold (additional parafilm and hot glue were applied to mitigate the leakages of silicon through the gaps between the mold pieces) (figure 12.6.b); (3) addition of calculated weight of *Ecoflex 00-50* agent A in a container (with translucent white color) and mix with a drop of pink and a drop of red colored pigment (figure 12.6.c); (4) Addition of the same amount of Ecoflex 00-50 agent B in the container as agent A and stirring evenly the mixed solution with a stick (figure 12.6.d); (5) Placement of the mixed solution in the *Heraeus VTR5022* vacuum machine for degassing to avoid bubble formation in the final prototype (figure 12.6.d); (6); pouring the mixed solution into the mold through the dedicated inlet port (figure 12.6.f); (7) curing the silicon at room temperature for the three hours after filling

all the mold(figure 12.6.g); (8) removal of the silicon made colon segments from the molds (figure 12.6.h). The above fabrication steps can be repeated for fabricating several modular colonic segments, that can be joined together to achieve a complete colon simulator. After joining all the modular colonic segments, the final complete

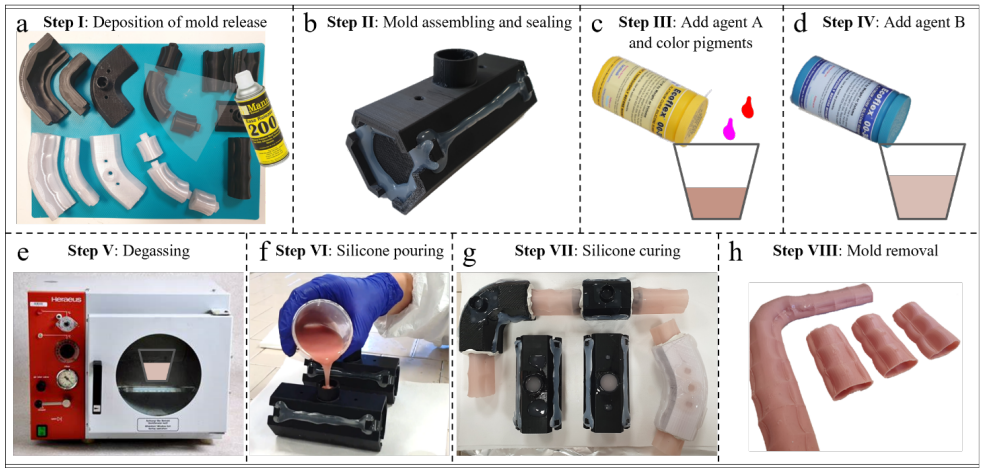

Figure 12.6. Colon fabrication steps: (a) Deposition of *Ease Release™ 200* on the inner side of molds; (b) Molds assembly and closing: addition of parafilm and hot glue; (c) *Ecoflex 00-50* part A mixed with 1 drop of pink, 1 drop of blood pigments; (d) *Ecoflex 00-50* part B added to the mixture; (e) Vacuum-chamber degassing (5-8 min); (f) Pouring of the product in the central reservoir (pot life: 18 min); (g) Wait for curing time: 3 h; (h) Delicate removal of molds and silicone residuals.

colon simulator prototype, named the Modular Colon Simulator (MCS), was realized (figure 12.8.a). Various types of polyps with different sizes are also fabricated as shown in figure 12.8.b. Each of them is cured together with a small permanent magnet, in order to realize an easy yet robust integration with the simulator at any location. An integrated sessile polyp into the simulator is shown in figure 12.8.c.

12.3.3 Clinical validation

A group of 17 colorectal surgeons (*i.e.,* 8 experts colonoscopists and 9 novices) were enrolled for validating the appropriateness and grade of usefulness of the colon simulator fabricated trough the steps mentioned above, *i.e.,* MCS. To this end, after the recording of personal and professional information, the clinicians were asked to perform one complete colonoscopy (cecum intubation and withdrawal) in both the Kyoto Kagaku Colonoscope Training Model (Kyoto Kagaku Co. Ltd., Kyoto, Japan) [90] and the MCS (Figure 12.7.a). The Kyoto Kagaku is a commercial and validated simulator, used in this study as the gold standard for physical colonoscopy simulator, and as a mean of comparison of our MSC. More information about the Kyoto Kagaku

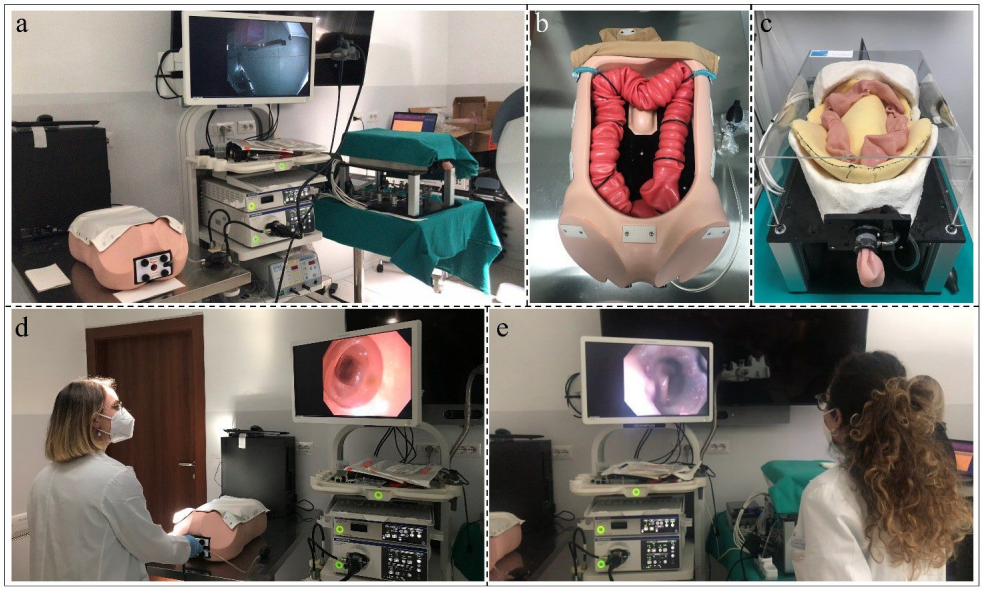

Figure 12.7. Pilot study comparing the Modular Colon Simulator and Kyoto Kagaku simulator. (a) Test setup with both simulator platforms and the colonoscopy system. Detailed view of the Kyoto Kagaku simulator (b) and the Modular Colon Simulator (c). Endoscopist performing the colonoscopy training with Kyoto Kagaku simulator (d) and the Modular Colon Simulator (e).

simulator are available in section 4.2.1. The procedures were performed using a clinical colonoscope with the associated equipment (Olympus GIF-HQ190 and connected modules, Olympus Corporation, Tokyo, Japan). Prior to the test, five minutes for each clinician were dedicated to acquiring confidence and familiarity with both simulators. The Kyoto Kagaku Colonoscope Training Model was mounted and prepared according to the Instruction Manual (Kyoto Kagaku Co. Ltd., Kyoto, Japan). Accessories such as rubber bands, guide frame, and sphincter were employed (figure 12.7.b). Total procedural time (1), cecum intubation time (2), and withdrawal time (3) were recorded. The MCS was installed in a custom-made abdominal simulator embedding 5 monoaxial strain gauge cells (OMEGA LCL-005, OMEGA Engineering Inc., Karvina, Czech Republic). This abdominal platform, used in [16], allows to acquire the force exerted on the colon walls during the procedure in five regions of interest, *i.e.,* rectum, splenic flexure, hepatic flexure, and cecum (figure 12.7.c) The arrangement of the colon lumen through the prefixed path was obtained through custom silicon-made rings, and fishing wires were used for the connection with the load cells eyelets. In addition, a pedunculated polyp was magnetically connected to the inner surface of the colon lumen in the cecum region. Therefore, the clinicians were asked to remove any detected polyp with the most appropriate polypectomy tool (*e.g.,* basket, snare,

grasping forceps, *etc.*) through the endoscope channel, during the withdrawal phase. To this end, the clinicians were not aware of either the number, the shape, or the presence of any polyps. In this case, in addition to the time for intubation, withdrawal and overall procedure, also the force exerted on the mucosa walls (4) and the polyp detection (5) and removal (6) was recorded. Before performing the colonoscopy, both simulators were lubricated with the dedicated solutions provided by the package of Kyoto Kagaku simulator platform and were covered to avoid any biases due to appearance or visual cues. Following the testing, the clinicians were asked to fill a custom-made survey expressing their opinion on a 5-point Likert scale for both the simulators tested regarding (1) the overall simulation setup, (2) the anatomical realism of each part of the colon simulator, (3) the mechanical and haptic response, (4) the complexity of the procedure, (6) the simulator appropriateness and usefulness in a real training.

Data from the surveys and recorded endpoints were extracted and analysed using *MATLAB* (MathWorks, Inc., Portola Valley, CA, USA) to assess the overall realism of the MCS platform (*i.e.,* content, phase and construct validity). The Wilcoxon Paired test was used to compare the two simulators both in terms of performances (*i.e.,* data acquired during the experiments) and clinicians' opinions expressed in the survey. Additionally, Wilcoxon Unpaired test was performed to evaluate any differences in performances between the experts and the novices (construct validity), and among the results of the survey on the MCS. Finally, the consensus measure [152] was used to assess the dispersion of the clinicians' answers to the survey.

12.4 Results

12.4.1 Material Selection

Equivalent Von Mises stress-strain curves were acquired from the central 3D element of each bone-shaped silicone sample and plotted against deformation. As first approximation, silicone selection was driven by Young modulus metric to comply, qualitatively, with the tensile response of human colon samples when loaded quasi-statically in the circumferential direction, *i.e.,* 0.63±1.25 MPa [106], assuming that stronger interactions between the colonoscope and colon walls occur mainly along this trajectory. The approximated elastic modulus of each silicone was computed by linearizing the stress-strain curves reported above. In particular, *Dragon Skin 10 Medium* and *20*, showed the nearest linearized values, 0.427 MPa, and 0.894 MPa respectively. Nevertheless, neither of these two candidate silicones was suitable for filling homogeneously all the molds cavities, because of their high viscosity (23000 and 20000 cps). In this regard, taking a step back along the elastic response, *Ecoflex 00-50* was assumed as the optimal trade-off in terms of elastic modulus order of magnitude (0.224 MPa) but also feasibility of fabrication thanks to its sufficient pot life (18 minutes), lower viscosity (8000 cps), and relatively short curing time (3 hours). FEM insufflation entails

the validation of *Ecoflex 00-50* as the potential material for fabrication: maximum pressure before high distortion without convergence was 39.6 mmHg, which was considered acceptable compared to the reference bound of 44 mmHg in the human colon. This is further supported by *Sosna et al.* [215], explaining how rectal pressures, in the supine and prone position, stand around ranges of 38.3-40.07 mm Hg and 38.3-32.25 mm Hg respectively.

12.4.2 Complete Integrated Colon Simulator

The complete MCS, resulting from the execution of sequential conjunctions, is shown in figure 12.8.a. The final prototype is suitable to be mounted and adjusted in commercial abdominal simulators as the Kyoto Kagaku abdominal case. This can be

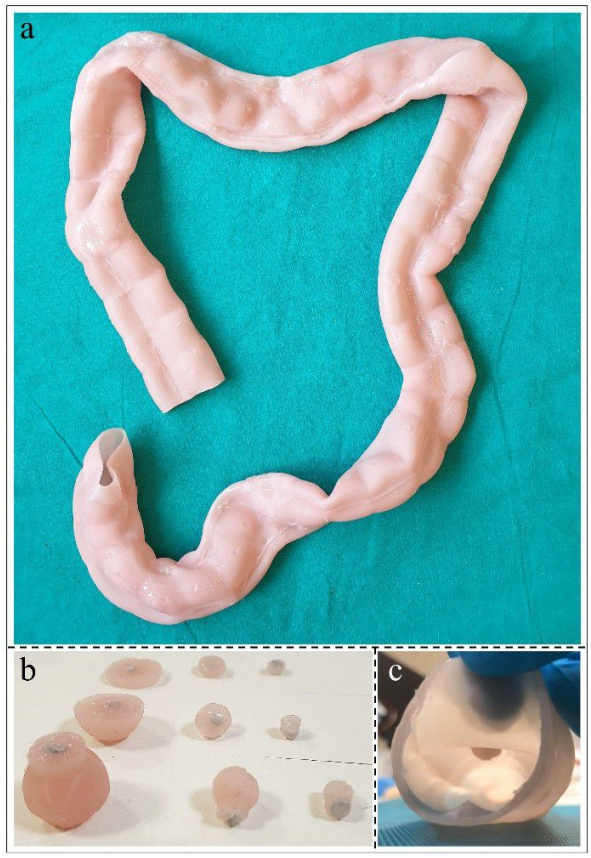

Figure 12.8. Fully integrated colon simulator: (a) complete colon simulator; (b) magnetic-based artificial polyps with various geometry; (c) artificial polyp attached to the inner wall of the colon simulator.

achieved with the aid of either supplied rubber bands or custom-made silicone bands, cut from fabrication residuals, to offer softer support, especially at the splenic and hepatic flexures. The entire silicone lumen is naturally collapsed under gravity, which is consistent with the behavior of a non-insufflated human colon. The MCS includes a set of nine magnetic polyps with different morphologies and dimensions available, assuring a safe, stable, and ready-to-use installation. In addition, they can be re-used once removed. Consequently, modularity is accomplished not only through the fabrication methodology but also in the connection of the additional pathological modules.

12.4.3 Clinical Validation

All the 17 participants enrolled in the experiments were able to successfully complete the colonoscopy procedure in both simulators. The distribution of the answers to the validation survey are shown for both the simulators in figure 12.10 for all the questions except the last 8, which were only related to the MCS (polypectomy and usefulness). Ratings for the MCS were higher than 2.5 for all the questions (both for all the participants and for only the experts), confirming the face and content validity. The MCS simulators got higher average score for all the questions, with respect to the Kyoto Kagaku platform, with statistical difference confirmed by the Wilcoxon paired test for most of the aspects inquired (p-value < 0.05, table 12.3). The average consensus for all the questions was greater than 0.6, suggesting a high level of agreement between the clinicians. Regarding the construct validity, the Wilcoxon unpaired test

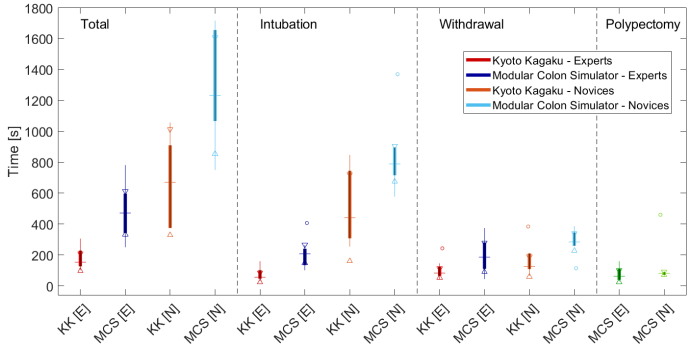

Figure 12.9. Boxplots of time metrics for both the simulator and the different clinicians' expertise

reveals that the MCS simulator is able to discriminate between experts and novices in terms of intubation time and total time, as the Kyoto Kagaku one (table 12.3 and figure 12.9). Whereas, from the force analysis, no significant difference was detected between novices and experts (figure 12.11) considering five selected metrics: mean force, minimum force, maximum force, cumulative force, and force range. Finally,

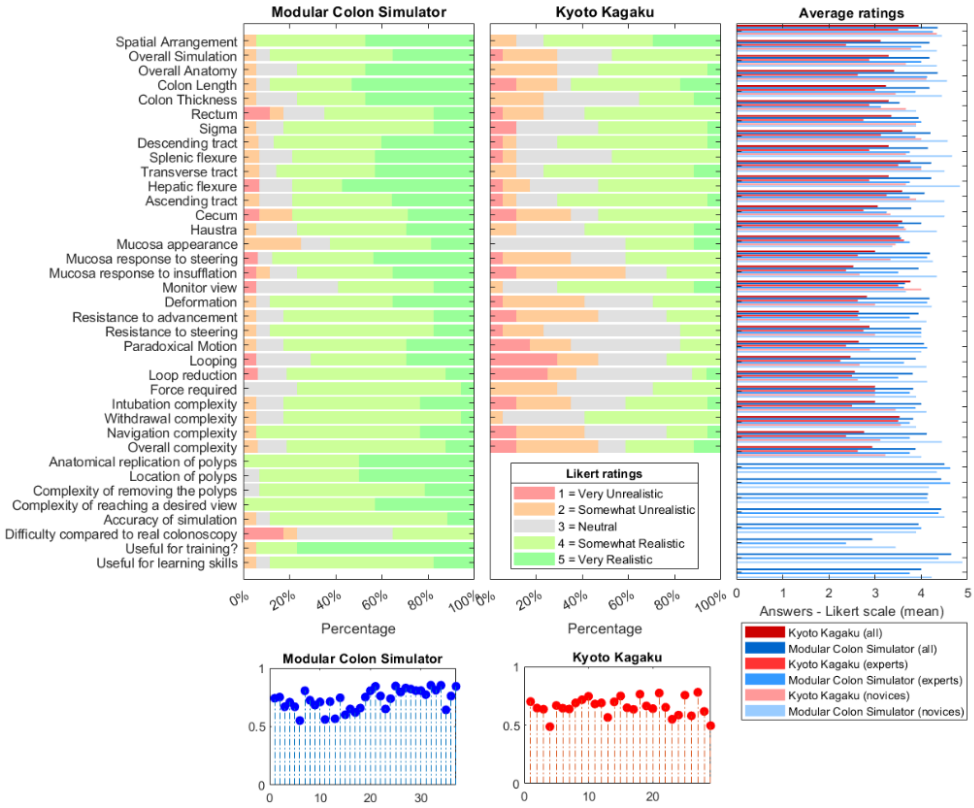

Figure 12.10. Results of the validation tests. At the top-left, summary of the 37 questions and answers provided by 74 endoscopists using a 5-point Likert scale for the Modular Colonoscopy Simulator (top left) and the Kyoto Kagaku (top centre). On the top right, average rating for all the questions related to both simulators, divided per experience level. At the bottom, consensus values for all the question, in both simulators.

a statistical difference was detected for the time of intubation (1), withdrawal (2) and overall procedure (3) between the two simulators for all the participants and for the expert groups. Indeed, the time spent to perform a procedure with the MCS was higher than with the Kyoto Kyoto Kagaku platform (table 12.3 and figure 12.9), suggesting the major complexity of the MCS, probably as a natural consequence of choosing a real anatomical configuration for the whole development.

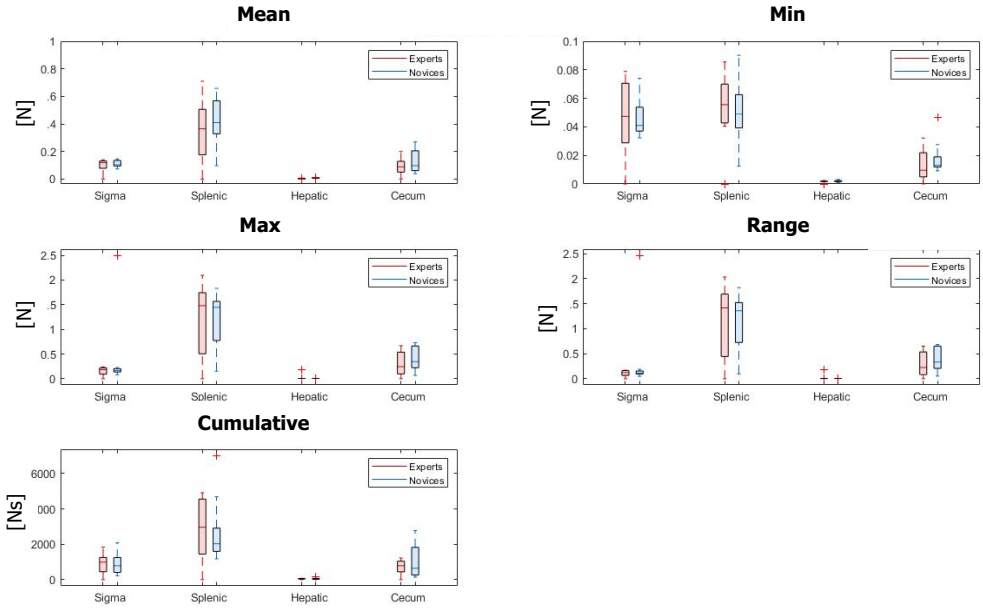

Figure 12.11. Boxplots of force metrics (mean, minimum, maximum, range, cumulative) acquired on the the Modular Colon Simulator platform, highlighted the different clinicians' expertise.

12.5 Discussion

This work shows a modular, reproducible, and adaptable approach for fabricating customized physical colon simulators, with a successful replication of colon geometry. Modularity is maximized thanks to (1) the straightforward design of the molds, requiring few and simple commands (number of units and angle of flexion) for modifying curvatures and connections; and (2) the installation of the magnetic polyps, that enables a prompt reuse and reinsertion at any location. Therefore, any user equipped with a 3D printer can easily fabricate colon simulators of different anatomies, either referring to existing models or random configurations. Moreover, the FEM analysis conducted in this study demonstrate that a low-cost silicon (*i.e., Ecoflex 00-50*) can be used to reproduce the colon, for satisfying both affordability and biomechanical similarity. Indeed, the only expenses associated with the production of the simulator are the cost of the printed material and the silicon. Overall, the simulator fabricated in this study costed 102,74 € (printed plastic filaments, sealing material and silicone), although, both the anatomy and the silicon can be changed, having an impact on the final costs. Finally, face, content, and construct validity tests have assessed the level of anatomical realism, teaching content, and capability of identifying different

levels of gastroenterologists' expertise of the simulator fabricated. Hence, the colon fabricated with the method proposed can be used for the training of endoscopists, especially at an early stage. However, here it is presented only one possible anatomy of the many that can be developed with this method. Indeed, the strength of the system relies on the modularity of materials and anatomies that can be generated depending on the final use.

Survey			
	All	Experts	Novices
Spatial Arrangement	0.1093	0.1250	1.000
Overall Simulation	<0.001	0.0078	0.0625
Overall Anatomy	0.0072	0.0312	0.1875
Colon Length	0.0083	0.0156	0.4062
Colon Thickness	0.0039	0.2500	0.0312
Rectum	0.3593	0.7500	0.6250
Sigma	0.0458	0.0156	1.000
Descending tract	0.0039	0.0625	0.1250
Splenic flexure	0.0019	0.0625	0.0625
Transverse tract	0.1562	0.5000	0.2500
Hepatic flexure	0.0019	0.0625	0.0625
Ascending tract	0.0312	0.2500	0.2500
Cecum	0.0156	0.2500	0.1250
Haustra	0.1289	1.000	0.1562
Mucosa appearance	1.000	0.8828	1.000
Mucosa response to steering	0.0029	0.03125	0.1250
Mucosa response to insufflation	<0.001	0.0625	0.0078
Monitor view	0.6699	0.9375	0.4531
Deformation	<0.001	0.0156	0.0078
Resistance to advancement	<0.001	0.0625	0.0156
Resistance to steering	<0.001	0.0625	0.0156
Paradoxical Motion	<0.001	0.0156	0.0156
Looping	0.0019	0.0625	0.0625
Loop reduction	0.0039	0.2500	0.0078
Force required	0.0078	0.2500	0.0312
Intubation complexity	0.0019	0.0312	0.1250
Withdrawal complexity	0.1875	1.000	0.3750
Navigation complexity	<0.001	0.0156	0.0156
Overall complexity	0.0053	0.0859	0.0625
Timings			
	All	Experts	Novices
Intubation time	0.0052	0.0078	0.0937
Withdrawal time	0.0039	0.0234	0.0937
Total time	0.0017	0.0078	0.0937
Insertion length	0.2297	0.4375	0.3437
Construct validity			
	KK	MCS	
Intubation time	<0.001	<0.001	
Withdrawal time	0.2358	0.1711	
Total time	<0.001	0.0013	
Insertion length	0.1341	0.9183	
Polypectomy	N.A.	0.3449	
Snare width	N.A.	1.000	

Table 12.3. P-values of the Wilcoxon paired test between the Kyoto Kagaku (KK) and the Modular Colonoscopy Simulator (MSC). P-values for each question of the validation survey and for the timings grouped on the different level of expertise (*i.e.,* all, only experts and only novices). At the bottom, p-values of the Wilcoxon unpaired test between the performances of novices and experts with the KK and the MCS. Statistical significance is highlighted in orange (p-values < 0.05).

Conclusions and future work

The HMI of medical robots has a relevant impact on the outcome of the procedure. Ideally, (1) it supports the user with the correct amount of information provided in a non-invasive way and (2) it enables precise movements while maintaining the highest transparency possible to ease the transfer of input controls from the user to the device. Intraluminal robots, in particular [20, 21], *i.e.,* multisteerable snake-like devices or endoscopic capsule, can benefit from an intuitive and user-friendly HMI [57,154]. Indeed, intraluminal procedures are complex to master due to a series of factors [2]. Among others, the most challenging are the limited workspace, the indirect view over the surgical scene mediated by the camera, requiring high-level hand-eye coordination, the high deformability of both the environment and the endoscope, and finally the fragility of the lumen which increases the risk of perforation [5, 11]. In this context, the HMI can aid the clinician with (1) intuitive, ergonomic and easy to use controller devices, (2) different levels of assistance and autonomy in both navigation, diagnosis and decision-making, (3) extra sensory information about the both device and surgical scene. However, it is important to acknowledge, and to test, that both the HMI input acceptance methods from the user (*i.e.,* controller device, type of control *etc.*) and the HMI output provision to the user (*i.e.,* sensory information, lesion detection, computer assisted diagnosis) have an impact on the physical and cognitive stress of the clinician, and eventually on the outcome of the procedure [70, 71, 76]. Indeed, receiving additional information about the procedure could have the negative effect of overloading or distracting the clinicians from their main tasks. Autonomy in terms of lesion detection or navigation have proved to be a powerful tool for assisting the clinicians, especially the less experienced ones [57, 76]. However, pre-clinical or clinical trials that prove the superiority of these systems as an assistance tool to the user in real-case scenarios are limited. Therefore, there is a lack of knowledge about the characteristics of the optimal HMI for robot assisted intraluminal procedures. A variety of HMI have been developed, and little space have been given to their comparison to get guidelines about the useful features [72]. There is also a lack of a controllable, and safe, pre-clinical scenario where is possible to properly test new HMI features, eventually deriving an informed idea about how an innovative solution can really have a positive impact in the real case scenario [86]. In

addition, few studies have been conducted to comprehensively assess which are the characteristics to form an optimal HMI.

As a general goal, this thesis aims at providing new knowledge, insights and inspiration for the design of the next generation HMI for intraluminal procedure. The thesis explores the field of HMI for robot-assisted intraluminal devices by developing and validating the first open, modular and versatile framework for the evaluation of HMI. The *HMI evaluation framework* allows to design and evaluate different HMI in a controlled environment in order to derive insights about the optimal solution. The framework does not include only the physical platform, *i.e.,* simulator and physiological sensors, but also the surveys exploring the subjective experience of the user, the objective metrics recorded to evaluate the HMI, and the whole protocol implemented for the testing. The *HMI evaluation framework* allows to study the performance of the interfaces both at the execution and physiological level, and combine all these metrics in a multi-parametric analysis. The framework is designed to maximize its modularity and scalability. It allows to test and analyze different aspects of the HMI, both hardware and software: the usability of a new assistive tool (*e.g.,* autonomous polyp detection), the optimal way to convey a piece of information (*e.g.,* haptic feedback vs. AR), the usefulness of autonomous navigation, *etc.* The framework has been tested in this thesis with a first case example: the study on the design of an optimal HMI for robot-assisted colonoscopy.

Another important contribution of this thesis is the development of a simulation platform for robotic colonoscopy, allowing to test the HMI in a controlled and safe pre-clinical environment. The simulator was designed with a modular and flexible architecture, in order to be adaptable to different simulation and evaluation requirements. It has been successfully validated by 28 endoscopists and resulted to provide realistic visual and mechanical rendering. For this reason, it can be also exploited for designing and testing new control algorithms, and training AI driven autonomous tasks as shown in chapter 9. Finally, the designed simulator could be exploited as an endoscopists' training tool for robotic colonoscopy.

The thesis also present two important mechanical features for the colonoscopy simulator related to the motility of the intestine: peristalsis and air insufflation (chapter 11). Both characteristics, which have an important positive impact on the final realism of the simulation, are not easy to find, neither in commercial platforms nor in the simulators at research stage. Future work will involve an extensive clinical validation of these new features, and the integration of the new simulator in the HMI evaluation framework.

Nevertheless, there are also situations in which a physical simulator is preferred [86]. To address these scenarios, a physical simulator of the colonoscopy procedure has been designed and reported in chapter 12. Future work will focus on embedding such a modular and customizable simulator in the HMI framework. To this end, it will be important to be able to create repeatable scenarios, and to track metrics to quantify the outcome in terms of performance and control quality. Therefore, including additional sensors to control the simulation environment will be essential.

This thesis mainly focuses on one medical scenario, *i.e.,* robotic colonoscopy, even

though other procedures could benefit from the insights derived. To support this, the work presented in chapter 10 shows a second application, *i.e.,* robot-assisted multi-steerable device for the urinary tract related procedure. Herein, the use of a multiple level assistance HMI is investigated and tested with novice users. Potential following works will focus on testing the new medical scenario with clinicians using the *HMI evaluation framework*.

Going back to the beginning, the initial objective of this thesis was to reply to the following research question:

which is the optimal HMI for robot-assisted intraluminal procedures, i.e. the one that minimizes the cognitive and physical load of the user and maximizes the outcome of the procedure?

After a deep analysis of the literature and of the HMIs of robotic platforms developed in the last decades, we can conclude that there is not a unique answer or solution to this question. Neither there is evidence nor guidelines available regarding how to design an "ergonomic", "intuitive", "user-friendly" interface for robot-assisted intraluminal procedures. These terms (*e.g.,* ergonomic, intuitive *etc.*) are used across several scientific articles with different meaning, and referring to different characteristics of the final interface. Therefore, the main contribution of this thesis is to give a rigorous protocol and established workflow to follow to design HMI by making informed decisions about the features to include in the interface. The thesis does not provide specific answers nor guidelines, but present a method to follow for the design of the HMI, based on objective and quantifiable measures of the "intuitiviness", "ergonomy", "userfriendliness", and more in general of the quality of the interface.

At the beginning of this journey, the objective of the Ph.D. project was to design a HMI for robot assisted intraluminal procedure. At that time, I wish I could have read a research like the one reported in this manuscript to guide that design process. Eventually, the lack of information and guidelines regarding the design of optimal interfaces was the first input to the development of the research work described here. Therefore, I hope that the methods and tools provided in this thesis will inspire and guide the new generation of Ph.D. students, and more general the research community, to finally design "optimal" HMI for robot-assisted intraluminal devices.

List of Publications

Journal papers:

- **Finocchiaro, Martina**; Cortegoso Valdivia, Pablo; Hernansanz, Albert; Marino, Nicola; Amram, Denise; Casals, Alicia; Menciassi, Arianna; Marlicz, Wojciech; Ciuti, Gastone; Koulaouzidis, Anastasios; Training simulators for gastrointestinal endoscopy: Current and future perspectives, Cancers, 13, 6, 1427, 2021, MDPI.

- Del Bono, Viola; Peine, Joseph; **Finocchiaro, Martina**; Price, Karl D; Mencattelli, Margherita; Chitalia, Yash; Ko, Victoria H; Yu, Lumeng; Secor, Jordan; Pan, Amy; Non-Surgical Removal of Partially Absorbable Bionic Implants, IEEE Transactions on Medical Robotics and Bionics, 4, 2, 530-537, 2022, IEEE.

Under review:

- **Finocchiaro, Martina**; Banfi, Tommaso; Donaire, Sonia; Arezzo, Alberto; Guarner-Argente, Carlos; Menciassi, Arianna, Casals, Alicìa; Ciuti, Gastone *; Hernansanz, Albert*; A bio-engineering framework for the evaluation of Human Machine Interfaces of robot-assisted intraluminal devices, under review for IEEE Transactions on Robotics (submitted in December 2022).

In preparation:

- Zabban, Clara; **Finocchiaro, Martina**; Huan, Yu; Mazzotta, Alessandro; Casals, Alicia; Hernansanz, Albert; Menciassi, Arianna; Arezzo, Alberto; Ciuti, Gastone; A Novel Modular Approach for the Design of Physical Simulators for Colonoscopy, in preparation for the Journal of computational design and engineering, Oxford Academic (expected date of submission February 2023).

- **Finocchiaro, Martina**; Damone, Angelo; Irardi, Roberta; Melillo, Tommaso; Giosuè, Cristina; Drago, Gaspare; Cibella, Fabio; Sprovieri, Fabio; Ciuti, Gastone, A magnetically-driven ingestible capsule for the sampling of the microbiota in the small bowel, in preparation for IEEE Transactions on Biomedical Engineering (expected date of submission March 2023).

Conference papers:

- **Finocchiaro, Martina**; Giosuè, Cristina; Drago, Gaspare; Cibella, Fabio; Menciassi, Arianna; Sprovieri, Mario; Ciuti, Gastone; Design of a magnetic actuation system for a microbiota-collection ingestible capsule, 2021 IEEE International Conference on Robotics and Automation (ICRA 2021), 6905-6911, 2021, IEEE.

- Chiurazzi, Marcello*; Damone, Angelo*; **Finocchiaro, Martina***; Farnesi, Francesca; Secco, Giacomo Lo; Forcignanò, Edoardo; Arezzo, Alberto; Ciuti, Gastone; Small bowel to closest human body surface distance calculation through a custom-made software using CT-based datasets, 2021 43rd Annual International Conference of the IEEE Engineering in Medicine & Biology Society (EMBC 2021), 2903-2909, 2021, IEEE.

- Pore, Ameya; **Finocchiaro, Martina**; Dall'Alba, Diego; Hernansanz, Albert; Ciuti, Gastone; Arezzo, Alberto; Menciassi, Arianna; Casals, Alicia; Fiorini, Paolo; Colonoscopy Navigation using End-to-End Deep Visuomotor Control: A User Study, 2022 IEEE/RSJ International Conference on Intelligent Robots and Systems (IROS 2022).

Posters:

- **Finocchiaro, Martina***; Xuan Thao, Ha*; Lazo, Jorge*; Lai, Chun-Feng*; Ramesh, Sanat*; Hernansanz, Albert; Borghesan, Gianni; Dall'Alba, Diego; Tognarelli, Selene; Rosa, Benoit; Multi-level-assistance Robotic Platform for Navigation in the Urinary System: Design and Preliminary Tests, Conference on New Technologies for Computer/Robot Assisted Surgery, 90-91 (CRAS 2022).

- **Finocchiaro, Martina**; Arezzo, Alberto; Menciassi, Arianna; Casals, Alicia; Hernansanz, Albert; Ciuti, Gastone; Human Machine Interfaces for Robot-Assisted Colonoscopy: a Clinical Survey, Hamlyn Symposium on Medical Robotics 2022.

- **Finocchiaro, Martina**; Arezzo, Alberto; Gordillo, Jordi; Concepción, Mar; Romero, Cristina; Menciassi, Arianna ; Casals, Alicìa; Ciuti, Gastone; Hernansanz, Albert; Guarner-Argente, Carlos; Estudio comparativo de diferentes interfaces hombre-máquina para la optimización de la colonoscopia robótica en un simulador virtual, XXXII Congrés de la Societat Catalana de Digestologia, 2023.

- **Finocchiaro, Martina**; Arezzo, Alberto; Murzi, Marianette; Romito, Raffaella; Menciassi, Arianna ; Casals, Alicìa; Ciuti, Gastone; Hernansanz, Albert; Guarner-Argente, Carlos; Validación de un sistema de simulación virtual de colonoscopia robótica, XXXII Congrés de la Societat Catalana de Digestologia, 2023.

Book chapters:

- **Finocchiaro, Martina**; Banfi, Tommaso; Vissani, Matteo; Mazzoni, Alberto; Ciuti, Gastone; Healthcare (Data Science in), Elgar Encyclopedia of Law and Data Science, 192–198, 2022, Elgar.

*Authors sharing equal contribution

Bibliography

[1] V. Jayasekeran, B. Holt, and M. Bourke, "Normal adult colonic anatomy in colonoscopy," *Video Journal and Encyclopedia of GI Endoscopy*, vol. 1, no. 2, pp. 390–392, 2013, special Issue: Expert Encyclopedia – Lower GI Tract, Bile Duct and Ampullary Region. [Online]. Available: https://www.sciencedirect.com/science/article/pii/S2212097113701730

[2] V. Vitiello, S.-L. Lee, T. P. Cundy, and G.-Z. Yang, "Emerging robotic platforms for minimally invasive surgery," *IEEE reviews in biomedical engineering*, vol. 6, pp. 111–126, 2012.

[3] D. E. Yung, T. Banfi, G. Ciuti, A. Arezzo, P. Dario, and A. Koulaouzidis, "Musculoskeletal injuries in gastrointestinal endoscopists: a systematic review," *Expert Review of Gastroenterology & Hepatology*, vol. 11, no. 10, pp. 939–947, 2017.

[4] A. K. Shergill and K. R. McQuaid, "Ergonomic endoscopy: An oxymoron or realistic goal?" *Gastrointestinal Endoscopy*, vol. 90, no. 6, pp. 966–970, 2019.

[5] B. J. Spier, M. Benson, P. R. Pfau, G. Nelligan, M. R. Lucey, and E. A. Gaumnitz, "Colonoscopy training in gastroenterology fellowships: determining competence," *Gastrointestinal endoscopy*, vol. 71, no. 2, pp. 319–324, 2010.

[6] J. P. Desai, R. V. Patel, A. Ferreira, and S. K. Agrawal, *Encyclopedia of Medical Robotics*. World Scientific, 2017, vol. 1075.

[7] NCI, "Nci dictionary of cancer terms," https://www.cancer.gov/publications/dictionaries/cancer-terms, Últim accés: 01-05-2021.

[8] F. Bray, J. Ferlay, I. Soerjomataram, R. L. Siegel, L. A. Torre, and A. Jemal, "Global cancer statistics 2018: Globocan estimates of incidence and mortality worldwide for 36 cancers in 185 countries," *CA: a cancer journal for clinicians*, vol. 68, no. 6, pp. 394–424, 2018.

[9] M. Niederreiter, L. Niederreiter, A. Schmiderer, H. Tilg, and A. Djanani, "Colorectal cancer screening and prevention—pros and cons," *memo-Magazine of European Medical Oncology*, vol. 12, no. 3, pp. 239–243, 2019.

[10] A. B. Knudsen, A. G. Zauber, C. M. Rutter, S. K. Naber, V. P. Doria-Rose, C. Pabiniak, C. Johanson, S. E. Fischer, I. Lansdorp-Vogelaar, and K. M. Kuntz, "Estimation of benefits, burden, and harms of colorectal cancer screening strategies: modeling study for the us preventive services task force," *Jama*, vol. 315, no. 23, pp. 2595–2609, 2016.

[11] S.-H. Lee, Y.-K. Park, D.-J. Lee, and K.-M. Kim, "Colonoscopy procedural skills and training for new beginners," *World Journal of Gastroenterology: WJG*, vol. 20, no. 45, p. 16984, 2014.

[12] A. Eickhoff, J. Van Dam, R. Jakobs, V. Kudis, D. Hartmann, U. Damian, U. Weickert, D. Schilling, and J. F. Riemann, "Computer-assisted colonoscopy (the neoguide endoscopy system): results of the first human clinical trial ("pace study")," *Official journal of the American College of Gastroenterology| ACG*, vol. 102, no. 2, pp. 261–266, 2007.

[13] P. Berthet-Rayne, G. Gras, K. Leibrandt, P. Wisanuvej, A. Schmitz, C. A. Seneci, and G.-Z. Yang, "The i2snake robotic platform for endoscopic surgery," *Annals of biomedical engineering*, vol. 46, no. 10, pp. 1663–1675, 2018.

[14] A. De Donno, L. Zorn, P. Zanne, F. Nageotte, and M. de Mathelin, "Introducing stras: A new flexible robotic system for minimally invasive surgery," in *2013 IEEE International Conference on Robotics and Automation*. IEEE, 2013, pp. 1213–1220.

[15] J. W. Martin, B. Scaglioni, J. C. Norton, V. Subramanian, A. Arezzo, K. L. Obstein, and P. Valdastri, "Enabling the future of colonoscopy with intelligent and autonomous magnetic manipulation," *Nature machine intelligence*, vol. 2, no. 10, pp. 595–606, 2020.

[16] M. Verra, A. Firrincieli, M. Chiurazzi, A. Mariani, G. Lo Secco, E. Forcignanò, A. Koulaouzidis, A. Menciassi, P. Dario, G. Ciuti *et al.*, "Robotic-assisted colonoscopy platform with a magnetically-actuated soft-tethered capsule," *Cancers*, vol. 12, no. 9, p. 2485, 2020.

[17] G. A. Formosa, J. M. Prendergast, S. A. Edmundowicz, and M. E. Rentschler, "Novel optimization-based design and surgical evaluation of a treaded robotic capsule colonoscope," *IEEE Transactions on Robotics*, vol. 36, no. 2, pp. 545–552, 2019.

[18] "The monarch™ platform - auris health, inc." accessed: 2022-10-04. [Online]. Available: https://www.aurishealth.com/monarch-platform

[19] M. R. Lehto and S. J. Landry, *Introduction to human factors and ergonomics for engineers*. Crc Press, 2012.

[20] A. Blackler, V. Popovic, and D. Mahar, "Intuitive interaction applied to interface design," in *New Design Paradigms: Proceedings of International Design Congress (IDC) 2005*. International Design Congress, 2005, pp. 1–10.

[21] M. Soegaard and R. F. Dam, "The encyclopedia of human-computer interaction," *The encyclopedia of human-computer interaction*, 2012.

[22] A. K. Shergill, K. R. McQuaid, and D. Rempel, "Ergonomics and gi endoscopy," *Gastrointestinal endoscopy*, vol. 70, no. 1, pp. 145–153, 2009.

[23] S. O.-R. A. V. S. Committee *et al.*, "Taxonomy and definitions for terms related to on-road motor vehicle automated driving systems," *SAE Standard J*, vol. 3016, pp. 1–16, 2014.

[24] G.-Z. Yang, J. Cambias, K. Cleary, E. Daimler, J. Drake, P. E. Dupont, N. Hata, P. Kazanzides, S. Martel, R. V. Patel *et al.*, "Medical robotics—regulatory, ethical, and legal considerations for increasing levels of autonomy," p. eaam8638, 2017.

[25] P. E. Dupont, B. J. Nelson, M. Goldfarb, B. Hannaford, A. Menciassi, M. K. O'Malley, N. Simaan, P. Valdastri, and G.-Z. Yang, "A decade retrospective of medical robotics research from 2010 to 2020," *Science Robotics*, vol. 6, no. 60, p. eabi8017, 2021.

[26] A. Pore, M. Finocchiaro, D. Dall'Alba, A. Hernansanz, G. Ciuti, A. Arezzo, A. Menciassi, A. Casals, and P. Fiorini, "Colonoscopy navigation using end-to-end deep visuomotor control: A user study," in *2022 IEEE/RSJ International Conference on Intelligent Robots and Systems (IROS)*, 2022.

[27] W. Tavanapong, J. Oh, M. A. Riegler, M. Khaleel, B. Mittal, and P. C. De Groen, "Artificial intelligence for colonoscopy: Past, present, and future," *IEEE journal of biomedical and health informatics*, vol. 26, no. 8, pp. 3950–3965, 2022.

[28] "Caddie cloud based ai for endoscopy by odin vision," accessed: 2023-01-31. [Online]. Available: https://odin-vision.com/caddie-2/

[29] "Gi genius™ intelligent endoscopy module by medtronic," accessed: 2023-01-31. [Online]. Available: https://www.medtronic.com/covidien/en-us/products/gastrointestinal-artificial-intelligence/gi-genius-intelligent-endoscopy.html#:~:text=The%20GI%20Genius%E2%84%A2%20intelligent,through%20enhanced%20visualization%20during%20colonoscopy

[30] J. J. G. Rodríguez, J. M. Montiel, and J. D. Tardós, "Tracking monocular camera pose and deformation for slam inside the human body," in *2022 IEEE/RSJ International Conference on Intelligent Robots and Systems (IROS)*. IEEE, 2022, pp. 5278–5285.

[31] A. Z. Taddese, P. R. Slawinski, K. L. Obstein, and P. Valdastri, "Nonholonomic closed-loop velocity control of a soft-tethered magnetic capsule endoscope," in *2016 IEEE/RSJ International Conference on Intelligent Robots and Systems (IROS)*. IEEE, 2016, pp. 1139–1144.

[32] Y. Xu, K. Li, Z. Zhao, and M. Q.-H. Meng, "Autonomous magnetic navigation framework for active wireless capsule endoscopy inspired by conventional colonoscopy procedures," *IEEE Robotics and Automation Letters*, vol. 7, no. 2, pp. 1729–1736, 2022.

[33] P. R. Slawinski, A. Z. Taddese, K. B. Musto, K. L. Obstein, and P. Valdastri, "Autonomous retroflexion of a magnetic flexible endoscope," *IEEE Robotics and Automation Letters*, vol. 2, no. 3, pp. 1352–1359, 2017.

[34] J. W. Martin, L. Barducci, B. Scaglioni, J. C. Norton, C. Winters, V. Subramanian, A. Arezzo, K. L. Obstein, and P. Valdastri, "Robotic autonomy for magnetic endoscope biopsy," *IEEE Transactions on Medical Robotics and Bionics*, vol. 4, no. 3, pp. 599–607, 2022.

[35] Q. Zhang, J. M. Prendergast, G. A. Formosa, M. J. Fulton, and M. E. Rentschler, "Enabling autonomous colonoscopy intervention using a robotic endoscope platform," *IEEE Transactions on Biomedical Engineering*, vol. 68, no. 6, pp. 1957–1968, 2020.

[36] H.-E. Huang, S.-Y. Yen, C.-F. Chu, F.-M. Suk, G.-S. Lien, and C.-W. Liu, "Autonomous navigation of a magnetic colonoscope using force sensing and a heuristic search algorithm," *Scientific reports*, vol. 11, no. 1, pp. 1–15, 2021.

[37] J. M. Prendergast, G. A. Formosa, M. J. Fulton, C. R. Heckman, and M. E. Rentschler, "A real-time state dependent region estimator for autonomous endoscope navigation," *IEEE Transactions on Robotics*, vol. 37, no. 3, pp. 918–934, 2020.

[38] "Force dimension - omega.x," accessed: 2022-10-04. [Online]. Available: https://www.forcedimension.com/

[39] T. B. Cengiz, S. R. Steele, and E. Gorgun, "Implementation of novel robotic systems in colorectal surgery," in *Handbook of Robotic and Image-Guided Surgery*. Elsevier, 2020, pp. 147–158.

[40] M. Morino, E. Forcignanò, and A. Arezzo, "Initial clinical experience with a novel flexible endoscopic robot for transanal surgery," *Techniques in Coloproctology*, vol. 26, no. 4, pp. 301–308, 2022.

[41] "The magellan™ robotic system, hansen medical - youtube." accessed: 2022-10-04. [Online]. Available: https://www.youtube.com/watch?v=4xyAl966Qns

[42] "Sensei™ x2 robotic system, hansen medical - youtube." accessed: 2022-10-04. [Online]. Available: https://www.youtube.com/watch?v=PjXQLkiq8io

[43] S. D. Murgu, "Robotic assisted-bronchoscopy: technical tips and lessons learned from the initial experience with sampling peripheral lung lesions," *BMC pulmonary medicine*, vol. 19, no. 1, pp. 1–8, 2019.

[44] "The ion endoluminal system - intuitive," accessed: 2022-10-04. [Online]. Available: https://www.intuitive.com/en-us/products-and-services/ion

[45] "The corindus vascular - intuitive," accessed: 2022-10-04. [Online]. Available: https://www.corindus.com/

[46] T. Iwasa, R. Nakadate, S. Onogi, Y. Okamoto, J. Arata, S. Oguri, H. Ogino, E. Ihara, K. Ohuchida, T. Akahoshi *et al.*, "A new robotic-assisted flexible endoscope with single-hand control: endoscopic submucosal dissection in the ex vivo porcine stomach," *Surgical endoscopy*, vol. 32, no. 7, pp. 3386–3392, 2018.

[47] M. Hwang and D.-S. Kwon, "K-flex: a flexible robotic platform for scar-free endoscopic surgery," *The International Journal of Medical Robotics and Computer Assisted Surgery*, vol. 16, no. 2, p. e2078, 2020.

[48] L. Zorn, F. Nageotte, P. Zanne, A. Legner, B. Dallemagne, J. Marescaux, and M. de Mathelin, "A novel telemanipulated robotic assistant for surgical endoscopy: Preclinical application to esd," *IEEE Transactions on Biomedical Engineering*, vol. 65, no. 4, pp. 797–808, 2017.

[49] Y. Huang, W. Lai, L. Cao, J. Liu, X. Li, E. Burdet, and S. J. Phee, "A three-limb teleoperated robotic system with foot control for flexible endoscopic surgery," *Annals of Biomedical Engineering*, vol. 49, no. 9, pp. 2282–2296, 2021.

[50] J. Ruiter, G. M. Bonnema, M. C. van der Voort, and I. A. M. J. Broeders, "Robotic control of a traditional flexible endoscope for therapy," *Journal of robotic surgery*, vol. 7, no. 3, pp. 227–234, 2013.

[51] K. Kume, N. Sakai, and T. Ueda, "Development of a novel gastrointestinal endoscopic robot enabling complete remote control of all operations: endoscopic therapeutic robot system (etrs)," *Gastroenterology Research and Practice*, vol. 2019, 2019.

[52] R. Saglam, A. Y. Muslumanoglu, Z. Tokatlı, T. Çaşkurlu, K. Sarica, A. İ. Taşçi, B. Erkurt, E. Süer, A. S. Kabakci, G. Preminger *et al.*, "A new robot for flexible ureteroscopy: development and early clinical results (ideal stage 1–2b)," *European urology*, vol. 66, no. 6, pp. 1092–1100, 2014.

[53] W. He, S. Bryns, K. Kroeker, A. Basu, D. Birch, and B. Zheng, "Eye gaze of endoscopists during simulated colonoscopy," *Journal of robotic surgery*, vol. 14, no. 1, pp. 137–143, 2020.

[54] G. Tay, H.-K. Tan, T. K. Nguyen, S. J. Phee, and N. G. Iyer, "Use of the endomaster robot-assisted surgical system in transoral robotic surgery: A cadaveric study," *The International Journal of Medical Robotics and Computer Assisted Surgery*, vol. 14, no. 4, p. e1930, 2018.

[55] H. F. Talari, R. Monfaredi, E. Wilson, E. Blum, C. Bayne, C. Peters, A. Zhang, and K. Cleary, "Robotically assisted ureteroscopy for kidney exploration," in *Medical Imaging 2017: Image-Guided Procedures, Robotic Interventions, and Modeling*, vol. 10135. SPIE, 2017, pp. 279–284.

[56] F. Martina, T. H. Xuan, L. Jorge, L. Chun-Feng, R. Sanat, H. Albert, B. Gianni, D. Diego, T. Selene, R. Benoit, C. Alicia, P. Nicolas, F. Paolo, D. Jenny, V. P. Emmanuel, M. Arianna, and D. M. Elena, "Multi-level-assistance robotic platform for navigation in the urinary system: Design and preliminary tests," in *Conference on New Technologies for Computer/Robot Assisted Surgery (CRAS)*, 2022, pp. 90–91. [Online]. Available: https://re.public.polimi.it/bitstream/11311/1216641/1/CRAS22_proceedings_90-91.pdf

[57] N. Mahmud, J. Cohen, K. Tsourides, and T. M. Berzin, "Computer vision and augmented reality in gastrointestinal endoscopy," *Gastroenterology report*, vol. 3, no. 3, pp. 179–184, 2015.

[58] M. M. Desai, M. Aron, I. S. Gill, G. Pascal-Haber, O. Ukimura, J. H. Kaouk, G. Stahler, F. Barbagli, C. Carlson, and F. Moll, "Flexible robotic retrograde renoscopy: description of novel robotic device and preliminary laboratory experience," *Urology*, vol. 72, no. 1, pp. 42–46, 2008.

[59] M. A. Armin, G. Chetty, H. De Visser, C. Dumas, F. Grimpen, and O. Salvado, "Automated visibility map of the internal colon surface from colonoscopy video," *International journal of computer assisted radiology and surgery*, vol. 11, no. 9, pp. 1599–1610, 2016.

[60] R. Ma, R. Wang, S. Pizer, J. Rosenman, S. K. McGill, and J.-M. Frahm, "Real-time 3d reconstruction of colonoscopic surfaces for determining missing regions," in *International Conference on Medical Image Computing and Computer-Assisted Intervention*. Springer, 2019, pp. 573–582.

[61] S.-L. Tang, C.-K. Kwoh, M.-Y. Teo, N. W. Sing, and K.-V. Ling, "Augmented reality systems for medical applications," *IEEE engineering in medicine and biology magazine*, vol. 17, no. 3, pp. 49–58, 1998.

[62] S. A. Bowyer, B. L. Davies, and F. R. y Baena, "Active constraints/virtual fixtures: A survey," *IEEE Transactions on Robotics*, vol. 30, no. 1, pp. 138–157, 2013.

[63] T. Vrielink, Y. Pang, M. Zhao, S.-L. Lee, A. Darzi, and G. P. Mylonas, "Surgical task-space optimisation of the cyclops robotic system," *arXiv preprint arXiv:1712.03720*, 2017.

[64] K. Kume, N. Sakai, and T. Goto, "Haptic feedback is useful in remote manipulation of flexible endoscopes," *Endoscopy International Open*, vol. 6, no. 09, pp. E1134–E1139, 2018.

[65] J. Woo, J. H. Choi, J. T. Seo, T. I. Kim, and B.-J. Yi, "Development of a robotic colonoscopic manipulation system, using haptic feedback algorithm," *Yonsei medical journal*, vol. 58, no. 1, pp. 139–143, 2017.

[66] M. Mura, Y. Abu-Kheil, G. Ciuti, M. Visentini-Scarzanella, A. Menciassi, P. Dario, J. Dias, and L. Seneviratne, "Vision-based haptic feedback for capsule endoscopy navigation: a proof of concept," *Journal of Micro-Bio Robotics*, vol. 11, no. 1, pp. 35–45, 2016.

[67] R. Reilink, S. Stramigioli, A. M. Kappers, and S. Misra, "Evaluation of flexible endoscope steering using haptic guidance," *The International Journal of Medical Robotics and Computer Assisted Surgery*, vol. 7, no. 2, pp. 178–186, 2011.

[68] G. P. Mylonas, V. Vitiello, T. P. Cundy, A. Darzi, and G.-Z. Yang, "Cyclops: A versatile robotic tool for bimanual single-access and natural-orifice endoscopic surgery," in *2014 IEEE international conference on robotics and automation (ICRA)*. IEEE, 2014, pp. 2436–2442.

[69] C. Fan, D. Dodou, P. Breedveld, and J. Dankelman, "Spatial orientation in pathway surgery," *Surgical endoscopy*, vol. 29, no. 9, pp. 2705–2719, 2015.

[70] C. Fan, F. Jelínek, D. Dodou, and P. Breedveld, "Control devices and steering strategies in pathway surgery," *journal of surgical research*, vol. 193, no. 2, pp. 543–553, 2015.

[71] E. Rozeboom, J. Ruiter, M. Franken, and I. Broeders, "Intuitive user interfaces increase efficiency in endoscope tip control," *Surgical endoscopy*, vol. 28, no. 9, pp. 2600–2605, 2014.

[72] G. Ciuti, M. Salerno, G. Lucarini, P. Valdastri, A. Arezzo, A. Menciassi, M. Morino, and P. Dario, "A comparative evaluation of control interfaces for a robotic-aided endoscopic capsule platform," *IEEE transactions on robotics*, vol. 28, no. 2, pp. 534–538, 2011.

[73] K. Georgiou, A. Larentzakis, and A. G. Papavassiliou, "Surgeons' and surgical trainees' acute stress in real operations or simulation: A systematic review," *The Surgeon*, vol. 15, no. 6, pp. 355–365, 2017.

[74] W. C. Dobbs, M. V. Fedewa, H. V. MacDonald, C. J. Holmes, Z. S. Cicone, D. J. Plews, and M. R. Esco, "The accuracy of acquiring heart rate variability from portable devices: a systematic review and meta-analysis," *Sports Medicine*, vol. 49, no. 3, pp. 417–435, 2019.

[75] L. L. Di Stasi, C. Díaz-Piedra, J. F. Ruiz-Rabelo, H. Rieiro, J. M. S. Carrion, and A. Catena, "Quantifying the cognitive cost of laparo-endoscopic single-site surgeries: Gaze-based indices," *Applied Ergonomics*, vol. 65, pp. 168–174, 2017.

[76] O. F. Ahmad, A. S. Soares, E. Mazomenos, P. Brandao, R. Vega, E. Seward, D. Stoyanov, M. Chand, and L. B. Lovat, "Artificial intelligence and computer-aided diagnosis in colonoscopy: current evidence and future directions," *The lancet Gastroenterology & hepatology*, vol. 4, no. 1, pp. 71–80, 2019.

[77] J. M. Prendergast, G. A. Formosa, C. R. Heckman, and M. E. Rentschler, "Autonomous localization, navigation and haustral fold detection for robotic endoscopy," in *2018 IEEE/RSJ International Conference on Intelligent Robots and Systems (IROS)*. IEEE, 2018, pp. 783–790.

[78] O. F. Ahmad, D. Stoyanov, and L. B. Lovat, "Human-machine collaboration: Bringing artificial intelligence into colonoscopy," pp. 198–199, 2019.

[79] Y. Gong, D. Hu, B. Hannaford, and E. J. Seibel, "Toward real-time endoscopically-guided robotic navigation based on a 3d virtual surgical field model," in *Medical Imaging 2015: Image-Guided Procedures, Robotic Interventions, and Modeling*, vol. 9415. SPIE, 2015, pp. 76–83.

[80] G. N. Khan and D. F. Gillies, "Vision based navigation system for an endoscope," *Image and vision computing*, vol. 14, no. 10, pp. 763–772, 1996.

[81] S. Ali, F. Zhou, B. Braden, A. Bailey, S. Yang, G. Cheng, P. Zhang, X. Li, M. Kayser, R. D. Soberanis-Mukul *et al.*, "An objective comparison of detection and segmentation algorithms for artefacts in clinical endoscopy," *Scientific reports*, vol. 10, no. 1, pp. 1–15, 2020.

[82] F. Mahmood and N. J. Durr, "Topographical reconstructions from monocular optical colonoscopy images via deep learning," in *2018 IEEE 15th International Symposium on Biomedical Imaging (ISBI 2018)*. IEEE, 2018, pp. 216–219.

[83] G. Ciuti, M. Visentini-Scarzanella, A. Dore, A. Menciassi, P. Dario, and G.-Z. Yang, "Intra-operative monocular 3d reconstruction for image-guided navigation in active locomotion capsule endoscopy," in *2012 4th IEEE RAS & EMBS International Conference on Biomedical Robotics and Biomechatronics (BioRob)*. IEEE, 2012, pp. 768–774.

[84] R. D. Dias, M. C. Ngo-Howard, M. T. Boskovski, M. A. Zenati, and S. J. Yule, "Systematic review of measurement tools to assess surgeons' intraoperative cognitive workload," *Journal of British Surgery*, vol. 105, no. 5, pp. 491–501, 2018.

[85] A. Johnson and R. Proctor, *Neuroergonomics: A cognitive neuroscience approach to human factors and ergonomics*. Springer, 2013.

[86] M. Finocchiaro, P. Cortegoso Valdivia, A. Hernansanz, N. Marino, D. Amram, A. Casals, A. Menciassi, W. Marlicz, G. Ciuti, and A. Koulaouzidis, "Training simulators for gastrointestinal endoscopy: Current and future perspectives," *Cancers*, vol. 13, no. 6, p. 1427, 2021.

[87] H. D. Markman, "A new system for teaching proctosigmoidoscopic morphology." *American Journal of Gastroenterology (Springer Nature)*, vol. 52, no. 1, 1969.

[88] "Ems trainer (2068) – the chamberlain group," accessed: 2022-10-04. [Online]. Available: https://www.thecgroup.com/product/ems-trainer-2068/

[89] "Koken co., ltd." accessed: 2022-10-04. [Online]. Available: https://www.kokenmpc.co.jp/english/index.html

[90] "Kyoto kagaku," accessed: 2022-10-04. [Online]. Available: https://www.kyotokagaku.com/en/

[91] J. Y. Ahn, J. S. Lee, G. H. Lee, J. W. Lee, H. K. Na, K. W. Jung, J. H. Lee, D. H. Kim, K. D. Choi, H. J. Song *et al.*, "The efficacy of a newly designed, easy-to-manufacture training simulator for endoscopic biopsy of the stomach," *Gut and Liver*, vol. 10, no. 5, p. 764, 2016.

[92] N. King, A. Kunac, E. Johnsen, G. Gallina, and A. M. Merchant, "Design and validation of a cost-effective physical endoscopic simulator for fundamentals of endoscopic surgery training," *Surgical endoscopy*, vol. 30, no. 11, pp. 4871–4879, 2016.

[93] D. A. Walczak, M. Grajek, P. A. Walczak, M. Tuliszka-Gołowkin, R. Massopust, D. Pawełczak, Z. Pasieka, Ł. Krakowczyk, and A. Maciejewski, "The first homemade colonoscopy trainer," *Zeitschrift für Gastroenterologie*, vol. 55, no. 10, pp. 1004–1008, 2017.

[94] S. Lee, J. Y. Ahn, M. Han, G. H. Lee, H. K. Na, K. W. Jung, J. H. Lee, D. H. Kim, K. D. Choi, H. J. Song *et al.*, "Efficacy of a three-dimensional-printed training simulator for endoscopic biopsy in the stomach," *Gut and Liver*, vol. 12, no. 2, p. 149, 2018.

[95] R. Kikinis, S. D. Pieper, and K. G. Vosburgh, "3d slicer: a platform for subject-specific image analysis, visualization, and clinical support," in *Intraoperative imaging and image-guided therapy*. Springer, 2014, pp. 277–289.

[96] M. Fujii, T. Onoyama, Y. Ikebuchi, K. Uehara, A. Koga, M. Ueki, and H. Isomoto, "A novel humanoid-robot simulator for colonoscopy," *Endoscopy*, vol. 53, no. 08, pp. E291–E292, 2021.

[97] K. Triantafyllou, L. D. Lazaridis, and G. D. Dimitriadis, "Virtual reality simulators for gastrointestinal endoscopy training," *World journal of gastrointestinal endoscopy*, vol. 6, no. 1, p. 6, 2014.

[98] M. Noar, "Robotics interactive endoscopy simulation of ercp/sphincterotomy and egd," *Endoscopy*, vol. 24, no. S 2, pp. 539–541, 1992.

[99] C. Williams, J. Baillie, D. Gillies, D. Borislow, and P. Cotton, "Teaching gastrointestinal endoscopy by computer simulation: a prototype for colonoscopy and ercp," *Gastrointestinal endoscopy*, vol. 36, no. 1, pp. 49–54, 1990.

[100] "Gi mentor | simbionix," accessed: 2022-10-04. [Online]. Available: https://simbionix.com/simulators/gi-mentor/

[101] "Cae healthcare," accessed: 2022-10-04. [Online]. Available: https://www.cae.com/healthcare/

[102] "Endosim vr laparoscopic | endosim® | surgical science," accessed: 2022-10-04. [Online]. Available: https://surgicalscience.com/simulators/endosim/

[103] "Endovision vr laparoscopic | medvision," accessed: 2022-10-04. [Online]. Available: https://www.medvisiongroup.com/endovision.html

[104] A. Haycock, A. D. Koch, P. Familiari, F. van Delft, E. Dekker, L. Petruzziello, J. Haringsma, and S. Thomas-Gibson, "Training and transfer of colonoscopy skills: a multinational, randomized, blinded, controlled trial of simulator versus bedside training," *Gastrointestinal endoscopy*, vol. 71, no. 2, pp. 298–307, 2010.

[105] J. W. Hazey, J. M. Marks, J. D. Mellinger, T. L. Trus, B. Chand, C. P. Delaney, B. J. Dunkin, R. D. Fanelli, G. M. Fried, J. M. Martinez *et al.*, "Why fundamentals of endoscopic surgery (fes)?" pp. 701–703, 2014.

[106] C. Kühl and G. Dumont, "Coloscopy simulation: towards endoscopes improvement," *Computer Methods in Biomechanics and Biomedical Engineering*, vol. 8, no. 4, pp. 251–257, 2005.

[107] S. Yi, H. Woo, W. Ahn, J. Kwon, and D. Lee, "New colonoscopy simulator with improved haptic fidelity," *Advanced Robotics*, vol. 20, no. 3, pp. 349–365, 2006.

[108] H. De Visser, J. Passenger, D. Conlan, C. Russ, D. Hellier, M. Cheng, O. Acosta, S. Ourselin, and O. Salvado, "Developing a next generation colonoscopy simulator," *International Journal of Image and Graphics*, vol. 10, no. 02, pp. 203–217, 2010.

[109] S. Chakravarthy, M. V. Balakuntala, A. M. Rao, R. K. Thakur, and G. Ananthasuresh, "Development of an integrated haptic system for simulating upper gastrointestinal endoscopy," *Mechatronics*, vol. 56, pp. 115–131, 2018.

[110] W.-B. Cheng, Y.-Y. Di, E. M. Zhang, M. A. Moser, S. Kanagaratnam, L. Y. Korman, N. Sarvazyan, and W.-J. Zhang, "Modeling and in vitro experimental validation for kinetics of the colonoscope in colonoscopy," *Annals of biomedical engineering*, vol. 41, no. 5, pp. 1084–1093, 2013.

[111] C. Welch and J. Reid, "Looping formation during colonoscopy a simulation," in *Proceedings of the 14th International LS-Dyna Users Conference, Dearborn, MI, USA*, 2014, pp. 8–10.

[112] C. M. Zupanc, G. M. Wallis, A. Hill, R. Burgess-Limerick, S. Riek, A. M. Plooy, M. S. Horswill, M. O. Watson, H. de Visser, D. Conlan *et al.*, "Assessing colonoscopic inspection skill using a virtual withdrawal simulation: a preliminary validation of performance metrics," *BMC medical education*, vol. 17, no. 1, pp. 1–10, 2017.

[113] D. Falkenstein, R. Abrams, R. Kessler, B. Jones, G. Johnson, and D. Zimmon, "Endoscopic retrograde cholangiopancreatography in the dog: a model for training and research," *Gastrointestinal endoscopy*, vol. 21, no. 1, pp. 25–26, 1974.

[114] A. B. Balekuduru, A. K. Dutta, and S. B. Subbaraj, "Endoscopy on a human cadaver: a feasibility study as a training tool," *Journal of Digestive Endoscopy*, vol. 9, no. 03, pp. 103–108, 2018.

[115] N. Eleftheriadis, H. Inoue, H. Ikeda, M. Onimaru, A. Yoshida, T. Hosoya, R. Maselli, and S.-e. Kudo, "Training in peroral endoscopic myotomy (poem) for esophageal achalasia," *Therapeutics and clinical risk management*, vol. 8, p. 329, 2012.

[116] M. S. Bhutani, M. Aveyard, and H. F. Stills Jr, "Improved model for teaching interventional eus," *Gastrointestinal endoscopy*, vol. 52, no. 3, pp. 400–403, 2000.

[117] A. Parra-Blanco, N. González, R. González, J. Ortiz-Fernández-Sordo, and C. Ordieres, "Animal models for endoscopic training: do we really need them?" *Endoscopy*, vol. 45, no. 06, pp. 478–484, 2013.

[118] "Oie - world organisation for animal health," accessed: 2022-10-04. [Online]. Available: https://www.woah.org/en/home/

[119] O. W. O. for Animal Health, "Terrestrial animal health code, 28th ed." 2019.

[120] "Directive 2010/63/eu of the european parliament and of the council of 22 september 2010 on the protection of animals used for scientific purposes," 2010.

[121] "Project evaluation and retrospective assessment directive 2010/63/eu on protection of animals used for scientific purposes caring for animals aiming for better science national competent authorities for the implementation of directive 2010/63/eu on the protection of animals used for scientific purposes working document on project evaluation and retrospective assessment." 2010.

[122] J. Hochberger, M. Neumann, W. Hohenberger, and E. Hahn, "Easie-erlangen education simulation model for interventional endoscopy–a new bio-training model for surgical endoscopy," *Biomedizinische Technik. Biomedical engineering*, vol. 42, pp. 334–334, 1997.

[123] J. Hochberger, K. Matthes, J. Maiss, C. Koebnick, E. G. Hahn, and J. Cohen, "Training with the compacteasie biologic endoscopy simulator significantly improves hemostatic technical skill of gastroenterology fellows: a randomized controlled comparison with clinical endoscopy training alone," *Gastrointestinal endoscopy*, vol. 61, no. 2, pp. 204–215, 2005.

[124] "Gastrointestinal endoscopy specimen models and simulators — endosim evidence-based simulation," accessed: 2022-10-04. [Online]. Available: https://endosim.com/gastroenterology

[125] "Medicalinnovations – speciality medical device manufacturer and commercialization contractor medical," accessed: 2022-10-04. [Online]. Available: https://www.medicalinnovations.com/#products

[126] "Endoscopy training models | delegge medical design," accessed: 2022-10-04. [Online]. Available: https://www.deleggemedicaldesign.com/endoscopy-models

[127] C. Ho, S. Schostek, and D. Kalanovic, "Experimental testbed for measuring forces during gastrointestinal endoscopy," *Biomed. Tech*, vol. 50, no. 6, 2005.

[128] F. Faure, C. Duriez, H. Delingette, J. Allard, B. Gilles, S. Marchesseau, H. Talbot, H. Courtecuisse, G. Bousquet, I. Peterlik, and S. Cotin, "SOFA: A Multi-Model Framework for Interactive Physical Simulation," in *Soft Tissue Biomechanical Modeling for Computer Assisted Surgery*, ser. Studies in Mechanobiology, Tissue Engineering and Biomaterials, Y. Payan, Ed. Springer, Jun. 2012, vol. 11, pp. 283–321. [Online]. Available: https://hal.inria.fr/hal-00681539

[129] "Lab streaming layer," 2022. [Online]. Available: https://github.com/sccn/labstreaminglayer

[130] K. Clark, B. Vendt, K. Smith, J. Freymann, J. Kirby, P. Koppel, S. Moore, S. Phillips, D. Maffitt, M. Pringle *et al.*, "The cancer imaging archive (tcia): maintaining and operating a public information repository," *Journal of digital imaging*, vol. 26, no. 6, pp. 1045–1057, 2013.

[131] "3d slicer image computing platform," 2022. [Online]. Available: https://www.slicer.org/

[132] W. Wiesner, K. J. Mortelé, H. Ji, and P. R. Ros, "Normal colonic wall thickness at ct and its relation to colonic distension," *Journal of computer assisted tomography*, vol. 26, no. 1, pp. 102–106, 2002.

[133] K. İncetan, I. O. Celik, A. Obeid, G. I. Gokceler, K. B. Ozyoruk, Y. Almalioglu, R. J. Chen, F. Mahmood, H. Gilbert, N. J. Durr *et al.*, "Vr-caps: A virtual environment for capsule endoscopy," *Medical image analysis*, vol. 70, p. 101990, 2021.

[134] R. Lambert, "The paris endoscopic classification of superficial neoplastic lesions: esophagus, stomach, and colon: November 30 to december 1, 2002," *Gastrointest Endosc*, vol. 58, pp. S3–S43, 2003.

[135] M. B. Christensen, K. Oberg, and J. C. Wolchok, "Tensile properties of the rectal and sigmoid colon: a comparative analysis of human and porcine tissue," *Springerplus*, vol. 4, no. 1, pp. 1–10, 2015.

[136] A. J. Loeve, P. Fockens, and P. Breedveld, "Mechanical analysis of insertion problems and pain during colonoscopy: why highly skill-dependent colonoscopy routines are necessary in the first place... and how they may be avoided," *Canadian Journal of Gastroenterology*, vol. 27, no. 5, pp. 293–302, 2013.

[137] Geuzaine, Christophe and Remacle, Jean-Francois, "Gmsh." [Online]. Available: http://http://gmsh.info/

[138] T. Mullen, *Mastering blender*. John Wiley & Sons, 2011.

[139] B. O. Community, *Blender - a 3D modelling and rendering package*, Blender Foundation, Stichting Blender Foundation, Amsterdam, 2018. [Online]. Available: http://www.blender.org

[140] T. G. D. Team, "Gimp." [Online]. Available: https://www.gimp.org

[141] A. H. Calderwood and B. C. Jacobson, "Colonoscopy quality: metrics and implementation," *Gastroenterology Clinics*, vol. 42, no. 3, pp. 599–618, 2013.

[142] A. Rieger, R. Stoll, S. Kreuzfeld, K. Behrens, and M. Weippert, "Heart rate and heart rate variability as indirect markers of surgeons' intraoperative stress," *International archives of occupational and environmental health*, vol. 87, no. 2, pp. 165–174, 2014.

[143] K. I. Jones, F. Amawi, A. Bhalla, O. Peacock, J. P. Williams, and J. N. Lund, "Assessing surgeon stress when operating using heart rate variability and the state trait anxiety inventory: will surgery be the death of us?" *Colorectal Disease*, vol. 17, no. 4, pp. 335–341, 2015.

[144] M. Kassner, W. Patera, and A. Bulling, "Pupil: an open source platform for pervasive eye tracking and mobile gaze-based interaction," in *Proceedings of the 2014 ACM international joint conference on pervasive and ubiquitous computing: Adjunct publication*, 2014, pp. 1151–1160.

[145] L. L. Di Stasi, C. Diaz-Piedra, H. Rieiro, J. M. Sanchez Carrion, M. Martin Berrido, G. Olivares, and A. Catena, "Gaze entropy reflects surgical task load," *Surgical endoscopy*, vol. 30, no. 11, pp. 5034–5043, 2016.

[146] "Pupil labs documentation," 2022. [Online]. Available: https://docs.pupil-labs.com/core/

[147] V. K. Dik, I. T. Hooge, M. G. van Oijen, and P. D. Siersema, "Measuring gaze patterns during colonoscopy: a useful tool to evaluate colon inspection?" *European journal of gastroenterology & hepatology*, vol. 28, no. 12, pp. 1400–1406, 2016.

[148] M. J. Edmondson, P. H. Pucher, K. Sriskandarajah, J. Hoare, J. Teare, G.-Z. Yang, A. Darzi, and M. H. Sodergren, "Looking towards objective quality evaluation in colonoscopy: analysis of visual gaze patterns," *Journal of Gastroenterology and Hepatology*, vol. 31, no. 3, pp. 604–609, 2016.

[149] S. G. Hart and L. E. Staveland, "Development of nasa-tlx (task load index): Results of empirical and theoretical research," in *Advances in psychology*. Elsevier, 1988, vol. 52, pp. 139–183.

[150] G. Borg, *Borg's Perceived Exertion and Pain Scales*. Human Kinetics, 1998. [Online]. Available: https://books.google.es/books?id=MfHLKHXXlKAC

[151] M. Finocchiaro, A. Arezzo, A. Menciassi, A. Casals, A. Hernansanz, and G. Ciuti, "Human machine interfaces for robot-assisted colonoscopy: a clinical survey," in *Hamlyn Symposium on Medical Robotics 2022*, 2022, pp. 2903–2909.

[152] W. J. Tastle and M. J. Wierman, "An information theoretic measure for the evaluation of ordinal scale data," *Behavior Research Methods*, vol. 38, no. 3, pp. 487–494, 2006.

[153] C. M. Walsh, J. Cohen, K. L. Woods, K. K. Wang, D. K. Andersen, M. A. Anderson, B. J. Dunkin, S. A. Edmundowicz, D. O. Faigel, J. K. Law *et al.*, "Asge endovators summit: simulators and the future of endoscopic training," *Gastrointestinal endoscopy*, vol. 90, no. 1, pp. 13–26, 2019.

[154] G. Ciuti, K. Skonieczna-Żydecka, W. Marlicz, V. Iacovacci, H. Liu, D. Stoyanov, A. Arezzo, M. Chiurazzi, E. Toth, H. Thorlacius *et al.*, "Frontiers of robotic colonoscopy: a comprehensive review of robotic colonoscopes and technologies," *Journal of Clinical Medicine*, vol. 9, no. 6, p. 1648, 2020.

[155] E. Parliament and C. of the European Union, "Artificial intelligence act: Regulation laying down harmonised rules on artificial intelligence and amending certain union legislative acts," *Proposal for Regulation COM/2021/206 final, Brussels, Belgium*, 2021.

[156] D. Kragic, H. I. Christensen *et al.*, "Survey on visual servoing for manipulation," *Computational Vision and Active Perception Laboratory, Fiskartorpsv*, vol. 15, p. 2002, 2002.

[157] N. v. d. Stap, C. H. Slump, I. A. Broeders, and F. v. d. Heijden, "Image-based navigation for a robotized flexible endoscope," in *International Workshop on Computer-Assisted and Robotic Endoscopy*. Springer, 2014, pp. 77–87.

[158] F. Richter, R. K. Orosco, and M. C. Yip, "Open-sourced reinforcement learning environments for surgical robotics," *arXiv preprint arXiv:1903.02090*, 2019.

[159] E. Tagliabue, A. Pore, D. Dall'Alba, E. Magnabosco, M. Piccinelli, and P. Fiorini, "Soft tissue simulation environment to learn manipulation tasks in autonomous robotic surgery," in *2020 IEEE/RSJ International Conference on Intelligent Robots and Systems (IROS)*. IEEE, 2020, pp. 3261–3266.

[160] Y. Tassa, Y. Doron, A. Muldal, T. Erez, Y. Li, D. d. L. Casas, D. Budden, A. Abdolmaleki, J. Merel, A. Lefrancq *et al.*, "Deepmind control suite," *arXiv preprint arXiv:1801.00690*, 2018.

[161] G. Trovato, M. Shikanai, G. Ukawa, J. Kinoshita, N. Murai, J. Lee, H. Ishii, A. Takanishi, K. Tanoue, S. Ieiri *et al.*, "Development of a colon endoscope robot that adjusts its locomotion through the use of reinforcement learning," *International journal of computer assisted radiology and surgery*, vol. 5, no. 4, pp. 317–325, 2010.

[162] A. Saxena, H. Pandya, G. Kumar, A. Gaud, and K. M. Krishna, "Exploring convolutional networks for end-to-end visual servoing," in *2017 IEEE International Conference on Robotics and Automation (ICRA)*. IEEE, 2017, pp. 3817–3823.

[163] J. Ibarz, J. Tan, C. Finn, M. Kalakrishnan, P. Pastor, and S. Levine, "How to train your robot with deep reinforcement learning: lessons we have learned," *The International Journal of Robotics Research*, vol. 40, no. 4-5, pp. 698–721, 2021.

[164] S. Levine, C. Finn, T. Darrell, and P. Abbeel, "End-to-end training of deep visuomotor policies," *The Journal of Machine Learning Research*, vol. 17, no. 1, pp. 1334–1373, 2016.

[165] J. Xu, B. Li, B. Lu, Y.-H. Liu, Q. Dou, and P.-A. Heng, "Surrol: An open-source reinforcement learning centered and dvrk compatible platform for surgical robot learning," in *2021 IEEE/RSJ International Conference on Intelligent Robots and Systems (IROS)*. IEEE, 2021, pp. 1821–1828.

[166] P. M. Scheikl, B. Gyenes, T. Davitashvili, R. Younis, A. Schulze, B. P. Müller-Stich, G. Neumann, M. Wagner, and F. Mathis-Ullrich, "Cooperative assistance in robotic surgery through multi-agent reinforcement learning," in *2021 IEEE/RSJ International Conference on Intelligent Robots and Systems (IROS)*. IEEE, 2021, pp. 1859–1864.

[167] Y.-H. Su, K. Huang, and B. Hannaford, "Multicamera 3d viewpoint adjustment for robotic surgery via deep reinforcement learning," *Journal of Medical Robotics Research*, vol. 6, no. 01n02, p. 2140003, 2021.

[168] Y. Wang, Y. He, X. Deng, Z. Lei, Y. Chen, and M. Li, "Learning friction model for tethered capsule robot," in *2021 6th International Conference on Robotics and Automation Engineering (ICRAE)*. IEEE, 2021, pp. 280–285.

[169] R. S. Sutton and A. G. Barto, *Reinforcement learning: An introduction*. MIT press, 2018.

[170] J. Schulman, F. Wolski, P. Dhariwal, A. Radford, and O. Klimov, "Proximal policy optimization algorithms," *arXiv preprint arXiv:1707.06347*, 2017.

[171] T. Haarnoja, A. Zhou, K. Hartikainen, G. Tucker, S. Ha, J. Tan, V. Kumar, H. Zhu, A. Gupta, P. Abbeel *et al.*, "Soft actor-critic algorithms and applications," *arXiv preprint arXiv:1812.05905*, 2018.

[172] T. P. Lillicrap, J. J. Hunt, A. Pritzel, N. Heess, T. Erez, Y. Tassa, D. Silver, and D. Wierstra, "Continuous control with deep reinforcement learning," *arXiv preprint arXiv:1509.02971*, 2015.

[173] D. Wang, X. Xie, G. Li, Z. Yin, and Z. Wang, "A lumen detection-based intestinal direction vector acquisition method for wireless endoscopy systems," *IEEE Transactions on Biomedical Engineering*, vol. 62, no. 3, pp. 807–819, 2014.

[174] M. Merino-Monge, A. J. Molina-Cantero, J. A. Castro-García, and I. M. Gómez-González, "An easy-to-use multi-source recording and synchronization software for experimental trials," *IEEE Access*, vol. 8, pp. 200 618–200 634, 2020.

[175] M. F. Kaminski, S. Thomas-Gibson, M. Bugajski, M. Bretthauer, C. J. Rees, E. Dekker, G. Hoff, R. Jover, S. Suchanek, M. Ferlitsch *et al.*, "Performance measures for lower gastrointestinal endoscopy: a european society of gastrointestinal endoscopy (esge) quality improvement initiative," *Endoscopy*, vol. 49, no. 04, pp. 378–397, 2017.

[176] R. Shadmehr and S. Wise, "Supplementary documents for "computational neurobiology of reaching and pointing"," 2005.

[177] S. Chen, J. Gao, S. Reddy, G. Berseth, A. D. Dragan, and S. Levine, "Asha: Assistive teleoperation via human-in-the-loop reinforcement learning," *arXiv preprint arXiv:2202.02465*, 2022.

[178] K. C. Latchamsetty and C. R. Porter, "Treatment of upper tract urothelial carcinoma: a review of surgical and adjuvant therapy," *Reviews in urology*, vol. 8, no. 2, p. 61, 2006.

[179] B. K. Somani, O. Aboumarzouk, A. Srivastava, and O. Traxer, "Flexible ureterorenoscopy: tips and tricks," *Urology Annals*, vol. 5, no. 1, p. 1, 2013.

[180] V. De Coninck, E. X. Keller, B. Somani, G. Giusti, S. Proietti, M. Rodriguez-Socarras, M. Rodríguez-Monsalve, S. Doizi, E. Ventimiglia, and O. Traxer, "Complications of ureteroscopy: a complete overview," *World journal of urology*, vol. 38, no. 9, 2020.

[181] J. Rassweiler, M. Fiedler, N. Charalampogiannis, A. S. Kabakci, R. Saglam, and J.-T. Klein, "Robot-assisted flexible ureteroscopy: an update," *Urolithiasis*, vol. 46, no. 1, 2018.

[182] M. Finocchiaro, X. T. Ha, J. Lazo, C.-F. Lai, S. Ramesh, A. Hernansanz, G. Borghesan, D. Dall'Alba, S. Tognarelli, B. Rosa *et al.*, "Multi-level-assistance robotic platform for navigation in the urinary system: Design and preliminary tests," in *Proceeding of the 11th Joint Workshop on New Technologies for Computer/Robot Assisted Surgery*, 2022, pp. 90–91.

[183] "Brisbane urology clinic," accessed: 2022-10-04. [Online]. Available: https://brisbaneurologyclinic.com.au/procedures-we-perform/ureteroscopy/

[184] O. Traxer and A. Thomas, "Prospective evaluation and classification of ureteral wall injuries resulting from insertion of a ureteral access sheath during retrograde intrarenal surgery," *The Journal of urology*, vol. 189, no. 2, pp. 580–584, 2013.

[185] M. M. Desai, R. Grover, M. Aron, A. Ganpule, S. S. Joshi, M. R. Desai, and I. S. Gill, "Robotic flexible ureteroscopy for renal calculi: initial clinical experience," *The Journal of Urology*, vol. 186, no. 2, 2011.

[186] B. H. Chew, T. Chi, M. Monga, and M. Humphreys, "Robotic ureteroscopy: The future of stone management?" *Urology Times*, 2020.

[187] J. F. Lazo, C.-F. Lai, S. Moccia, B. Rosa, M. Catellani, M. de Mathelin, G. Ferrigno, P. Breedveld, J. Dankelman, and E. De Momi, "Autonomous intraluminal navigation of a soft robot using deep-learning-based visual servoing," 2021.

[188] J. F. Lazo, A. Marzullo, S. Moccia, M. Catellani, B. Rosa, M. de Mathelin, and E. De Momi, "Using spatial-temporal ensembles of convolutional neural networks for lumen segmentation in ureteroscopy," *International Journal of Computer Assisted Radiology and Surgery*, 2021.

[189] X. T. Ha, M. Ourak, O. Al-Ahmad, D. Wu, G. Borghesan, A. Menciassi, and E. Vander Poorten, "Robust catheter tracking by fusing electromagnetic tracking, fiber bragg grating and sparse fluoroscopic images," *IEEE Sensors Journal*, vol. 21, no. 20, 2021.

[190] W. Boldyreff, "Periodic wave phenomena in the secretory function of the digestive tract," *Gaz Hop Botkine*, vol. 34, pp. 1529–1542, 1902.

[191] W. B. Cannon and A. Washburn, "An explanation of hunger," *American Journal of Physiology-Legacy Content*, vol. 29, no. 5, pp. 441–454, 1912.

[192] A. J. Carlson, "Contributions to the physiology of the stomach.—i. the character of the movements of the empty stomach in man," *American Journal of Physiology-Legacy Content*, vol. 31, no. 3, pp. 151–168, 1912.

[193] J. H. Szurszewski, "A migrating electric complex of canine small intestine," *American Journal of Physiology-Legacy Content*, vol. 217, no. 6, pp. 1757–1763, 1969.

[194] J. D. Huizinga, "Chapter 13 - the physiology and pathophysiology of interstitial cells of cajal: Pacemaking, innervation, and stretch sensation," in *Physiology of the Gastrointestinal Tract (Sixth Edition)*, sixth edition ed., H. M. Said, Ed. Academic Press, 2018, pp. 305–335. [Online]. Available: https://www.sciencedirect.com/science/article/pii/B978012809954400013X

[195] J. Feher, "8.3—intestinal and colonic chemoreception and motility," *Quantitative Human Physiology. 2nd ed. Boston, MA: Elsevier*, pp. 796–809, 2017.

[196] G. Pocock, C. D. Richards, and D. A. Richards, *Human physiology.* Oxford university press, 2013.

[197] T. Takahashi, "Mechanism of interdigestive migrating motor complex," *Journal of Neurogastroenterology and Motility*, vol. 18, no. 3, p. 246, 2012.

[198] G. Bassotti and M. Gaburri, "Manometric investigation of high-amplitude propagated contractile activity of the human colon," *American Journal of Physiology-Gastrointestinal and Liver Physiology*, vol. 255, no. 5, pp. G660–G664, 1988.

[199] J. Christensen, "Motility of the colon. physiology of the gastrointestinal tract. edited by leonard r," 1981.

[200] E. Deloose, P. Janssen, I. Depoortere, and J. Tack, "The migrating motor complex: control mechanisms and its role in health and disease," *Nature reviews Gastroenterology & hepatology*, vol. 9, no. 5, pp. 271–285, 2012.

[201] L. Marti-Bonmati, M. Graells, and C. Ronchera-Oms, "Reduction of peristaltic artifacts on magnetic resonance imaging of the abdomen: a comparative evaluation of three drugs," *Abdominal imaging*, vol. 21, no. 4, pp. 309–313, 1996.

[202] J. F. Bruzzi, A. C. Moss, D. D. Brennan, P. MacMathuna, and H. M. Fenlon, "Efficacy of iv buscopan as a muscle relaxant in ct colonography," *European radiology*, vol. 13, no. 10, pp. 2264–2270, 2003.

[203] M. D. Sinnott, P. W. Cleary, J. W. Arkwright, and P. G. Dinning, "Investigating the relationships between peristaltic contraction and fluid transport in the human colon using smoothed particle hydrodynamics," *Computers in biology and medicine*, vol. 42, no. 4, pp. 492–503, 2012.

[204] K. Siau, J. Hodson, P. Neville, J. Turner, A. Beale, S. Green, A. Muruganantan, P. Dunckley, and N. D. Hawkes, "Impact of a simulation-based induction programme in gastroscopy on trainee outcomes and learning curves," *World journal of gastrointestinal endoscopy*, vol. 12, no. 3, p. 98, 2020.

[205] A. Hill, M. S. Horswill, A. M. Plooy, M. O. Watson, R. Karamatic, T. A. Basit, G. M. Wallis, S. Riek, R. Burgess-Limerick, and D. G. Hewett, "Assessing the realism of colonoscopy simulation: the development of an instrument and systematic comparison of 4 simulators," *Gastrointestinal endoscopy*, vol. 75, no. 3, pp. 631–640, 2012.

[206] G. A. Formosa, J. M. Prendergast, J. Peng, D. Kirkpatrick, and M. E. Rentschler, "A modular endoscopy simulation apparatus (mesa) for robotic medical device sensing and control validation," *IEEE Robotics and Automation Letters*, vol. 3, no. 4, pp. 4054–4061, 2018.

[207] D. Steck, J. Qu, S. B. Kordmahale, D. Tscharnuter, A. Muliana, and J. Kameoka, "Mechanical responses of ecoflex silicone rubber: Compressible and incompressible behaviors," *Journal of Applied Polymer Science*, vol. 136, no. 5, p. 47025, 2019.

[208] P. Langer and Á. Takács, "Why are taeniae, haustra, and semilunar folds differentiated in the gastrointestinal tract of mammals, including man?" *Journal of Morphology*, vol. 259, no. 3, pp. 308–315, 2004.

[209] A. Alazmani, A. Hood, D. Jayne, A. Neville, and P. Culmer, "Quantitative assessment of colorectal morphology: Implications for robotic colonoscopy," *Medical engineering & physics*, vol. 38, no. 2, pp. 148–154, 2016.

[210] A. Thompson, R. Jones, S. Banerjee, P. Poullos, and L. Shin, "Taller haustral folds in the proximal colon: A potential factor contributing to interval colorectal cancer?: 2069," *Official journal of the American College of Gastroenterology| ACG*, vol. 108, p. S628, 2013.

[211] Y. Liu, C. Duan, J. Liang, J. Hu, H. Lu, and M. Luo, "Haustral loop extraction for ct colonography using geodesics," *International journal of computer assisted radiology and surgery*, vol. 12, no. 3, pp. 379–388, 2017.

[212] D. Massalou, C. Masson, S. Afquir, P. Baqué, P.-J. Arnoux, and T. Bège, "Mechanical effects of load speed on the human colon," *Journal of Biomechanics*, vol. 91, pp. 102–108, 2019.

[213] L. Marechal, P. Balland, L. Lindenroth, F. Petrou, C. Kontovounisios, and F. Bello, "Toward a common framework and database of materials for soft robotics," *Soft robotics*, vol. 8, no. 3, pp. 284–297, 2021.

[214] A. E. Bharucha, R. D. Hubmayr, I. J. Ferber, and A. R. Zinsmeister, "Viscoelastic properties of the human colon," *American Journal of Physiology-Gastrointestinal and Liver Physiology*, vol. 281, no. 2, pp. G459–G466, 2001.

[215] J. Sosna, J. Bar-Ziv, E. Libson, M. Eligulashvili, and A. Blachar, "Ct colonography: positioning order and intracolonic pressure," *American Journal of Roentgenology*, vol. 191, no. 4, pp. W175–W180, 2008.